

**EXAMINING THE ROLE OF NITRATE AND NITRITE ANIONS  
IN OXIDATIVE C–H BOND FUNCTIONALISATION AT  
PALLADIUM**

**PHILIPPA KATE OWENS**

**MSc (by Research)**

**THE UNIVERSITY OF YORK**

**CHEMISTRY**

**DECEMBER 2013**

## Abstract

The synthesis of a range of palladacyclic complexes with C<sup>^</sup>N ligand backbones is described in this thesis. Novel palladium complexes containing anionic nitrite and nitrate ligands have been prepared and characterised, and the geometry and linkage isomerism at Pd have been examined. Density Functional Theory calculations have been used to rationalise the experimentally observed characteristics of the complexes.

Several novel palladium complexes prepared were found to be highly active precatalysts for oxidative C–H bond functionalisation co-catalysed by nitrate, achieving yields superior to Pd(OAc)<sub>2</sub> at low loadings of co-catalyst. In the model reaction of the acetoxylation of 8-methylquinoline, a novel C<sup>^</sup>N complex containing NO<sub>3</sub><sup>-</sup> and CH<sub>3</sub>CN ligands was found to catalyse the reaction in the absence of a sodium nitrate additive, showing that the complex can act as a source of catalytically relevant nitrite/nitrate. Preliminary substrate scope investigations have shown that this complex is able to catalyse the functionalisation of sp<sup>2</sup> C–H bonds, representing a significant improvement on the literature conditions.

Detailed mechanistic investigations have been conducted into the role played by nitrate in the catalytic cycle and the intermediates involved. Isotopic labelling experiments (<sup>18</sup>O) have been used to elucidate the source of the oxygen in the acetoxyated product, which is proposed to derive from acetic acid (solvent). Stoichiometric experiments have shown that reductive elimination of functionalised products from Pd<sup>II</sup> is not favorable, and thus high oxidation state intermediates are likely to be implicated in catalysis. Through a series of NMR experiments, several transient species were observed, and structures have been assigned to three proposed catalytic intermediates. Based on these results, a bimetallic Pd<sup>III/III</sup> mechanism is proposed. Work is ongoing to isolate and characterise the high oxidation state intermediates that result from the presence of NaNO<sub>3</sub> and identify their specific role in the catalytic cycle.

# Contents

<b>Abstract</b> .....	<b>1</b>
<b>Contents</b> .....	<b>3</b>
<b>Acknowledgements</b> .....	<b>5</b>
<b>Author's Declaration</b> .....	<b>6</b>
<b>Chapter 1: Introduction</b> .....	<b>7</b>
Pd-Catalysed C–H Bond Functionalisation.....	7
Pd-Catalysed C–O Bond Formation.....	11
Redox Co-Catalysis in C–H Bond Functionalisation.....	13
The Role of Nitrite in Pd-Catalysed Processes.....	16
Mechanistic Aspects of Oxidative C–H Bond Functionalisation.....	20
Proposed Work.....	31
<b>Chapter 2: Synthesis and Characterisation of Cyclopalladated C<sup>^</sup>N Complexes</b> .....	<b>33</b>
C <sup>^</sup> N Palladacyclic Complexes of 2-Phenylpyridine .....	33
Geometry and Linkage Isomerism in Pd–NO <sub>2</sub> and Pd–ONO Species.....	36
C <sup>^</sup> N Palladacyclic Complexes of 8-Methylquinoline.....	39
C <sup>^</sup> N Palladacyclic Complexes of 2-(2-Pyridyl)benzo[ <i>b</i> ]furan .....	44
<b>Chapter 3: C<sup>^</sup>N Palladacyclic Complexes as Precatalysts for Oxidative C–H Bond Functionalisation Processes</b> .....	<b>49</b>
C–H Acetoxylation of 8-Methylquinoline .....	49
Substrate Scope .....	58
<b>Chapter 4: Mechanistic Studies into Pd-catalysed C–H Bond Functionalisation Processes</b> .....	<b>66</b>
Reductive Elimination from Pd <sup>II</sup> Species.....	66
Isotopic Labelling Studies .....	73
Direct Observation of High Oxidation State Pd Intermediates.....	75
<b>Chapter 5: Conclusions and Future Work</b> .....	<b>94</b>
Conclusions .....	94
Future Work .....	97

<b>Chapter 6: Experimental</b> .....	<b>101</b>
General Experimental Details .....	101
Synthesis of C <sup>^</sup> N Ligands.....	103
Synthesis of C <sup>^</sup> N Palladacyclic Complexes.....	104
Synthesis and C–H Bond Functionalisation of Organic Substrates.....	116
Mechanistic Experiments.....	122
<b>Appendices</b> .....	<b>125</b>
Appendix A: Full Table of Data for the Pd-Catalysed C–H Acetoxylation of Organic Substrates .....	125
Appendix B: NMR Spectra .....	132
Appendix C: X-Ray Crystallography Data (on CD)	
Appendix D: XYZ Coordinates Calculated by Density Functional Theory (on CD)	
<b>Abbreviations</b> .....	<b>156</b>
<b>References</b> .....	<b>159</b>

## Acknowledgements

I'd firstly like to thank my supervisors, Prof. Ian Fairlamb and Dr Jason Lynam, for their invaluable guidance, patience and encouragement over the last year.

All members of the Fairlamb and Lynam groups past and present should be thanked for their support and advice, and particular thanks go to team #fairlambfun for providing much-needed distractions from work and generally making each day in the lab so enjoyable. I promise to keep up the ridiculous baking traditions!

I am especially grateful for the excellent technical support at York from Heather Fish and Dr Pedro Aguiar (NMR), Dr Karl Heaton (Mass Spectrometry), Dr Adrian Whitwood (X-Ray Crystallography), and in particular Dr Charlotte Elkington, without whom life in E114 would be infinitely more stressful.

Lastly, I'd like to thank the Kerr group at Strathclyde for putting up with a stressed-out new girl trying to juggle starting a PhD in a new city with writing up a Master's thesis; their patience is greatly appreciated.

## **Author's Declaration**

I declare that the work presented in this thesis is my own, and that any material not my own is clearly referenced or acknowledged. The work in this thesis was carried out between October 2012 and October 2013.

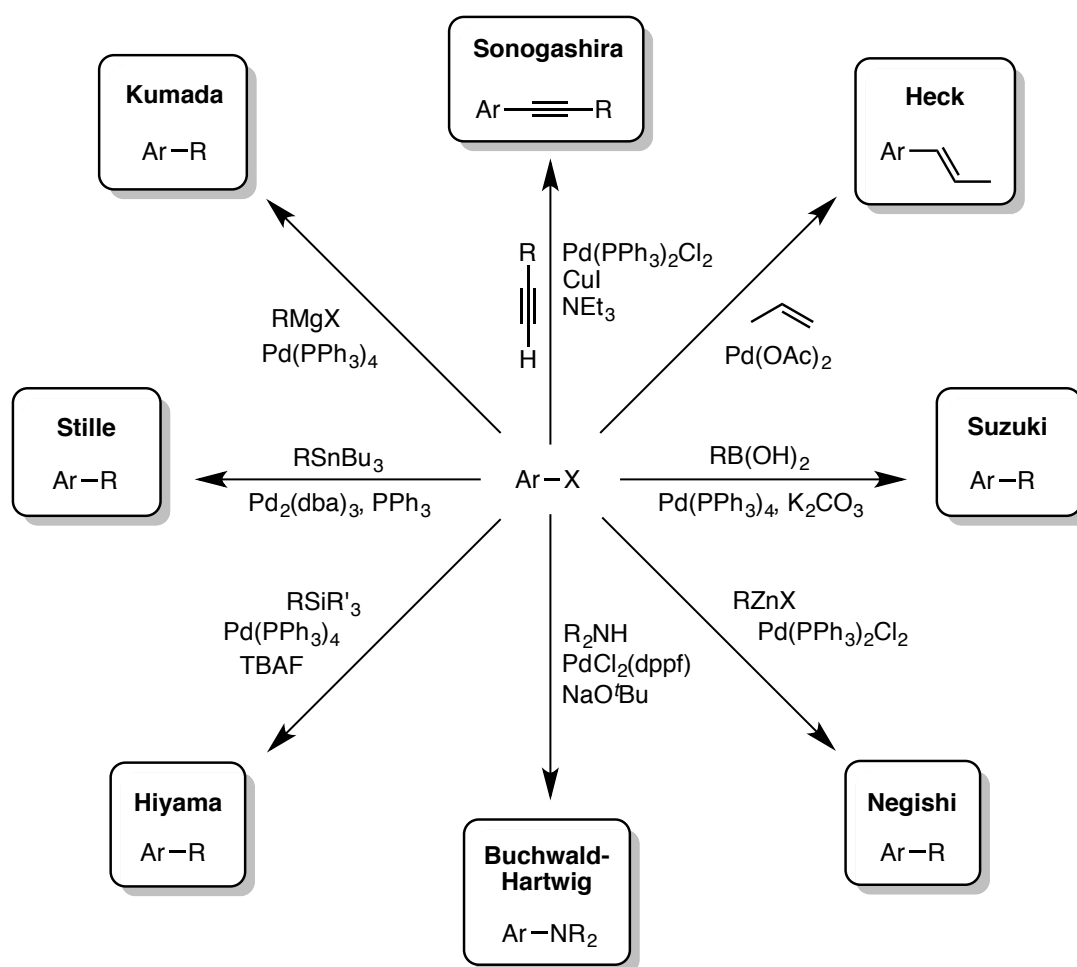
Philippa Kate Owens

December 2013

# Chapter 1: Introduction

## Pd-Catalysed C–H Bond Functionalisation

Palladium-catalysed C–C or C–heteroatom bond-forming reactions are among the most widely used transformations in modern organic synthesis, with applications in the synthesis of complex natural products and biomolecules of commercial interest.<sup>1,2</sup> During the last few decades, the advent of Pd-catalysed cross-coupling methodology has revolutionised the synthesis of complex organic molecules, allowing C–C or C–heteroatom bond formation to be achieved under mild conditions and from a range of prefunctionalised starting materials.<sup>3</sup> Several cross-coupling strategies are highlighted in Scheme 1, including the reactions that won Heck, Suzuki and Negishi the 2010 Nobel Prize in Chemistry.



**Scheme 1:** Classical Pd-Catalysed Cross-Coupling Strategies





reviewed in recent years.<sup>5-9</sup> In the late stages of complex molecule synthesis, the functionalization of unactivated C–H bonds is an attractive goal; the substrates are often compounds which already contain several potentially sensitive functional groups. It remains a significant challenge in synthetic organic chemistry to find conditions that favour C–C or C–heteroatom bond formation without affecting neighbouring groups or requiring either protection or deprotection steps to an already long synthesis.

The ubiquity of C–H bonds means that selectivity is difficult to control, with many organic molecules having multiple potential functionalisation sites. In comparison, the need for prefunctionalised starting materials in cross-coupling reactions (*e.g.* boronic acids or aryl halides) means that selectivity is typically easy to control, although their synthesis is not necessarily so straightforward. In order for C–H bond functionalisation methodology to be of use in the synthesis or modification of complex molecules, strategies must be developed to overcome this problem and allow the selective functionalisation of one C–H bond in the presence of others. There are several key strategies that have been adopted to achieve selectivity in catalytic C–H bond functionalisation processes.<sup>10</sup> One of the most commonly used is directing group control, where part of the substrate, for example a nitrogen atom, is able to act as a coordinating ligand, resulting in cyclometalation *via* stoichiometric C–H activation and dictating the site of C–H bond activation.<sup>11-13</sup> In compounds **1–3**, for example, the presence of coordinating directing groups causes C–H activation to occur at the positions labeled with an asterisk.

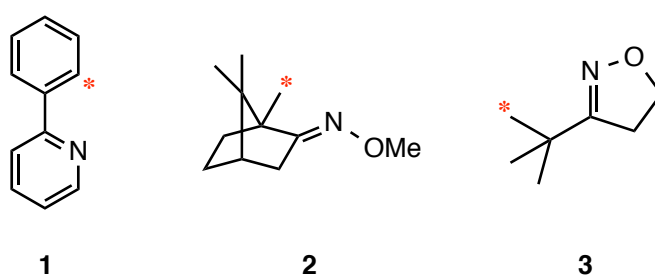
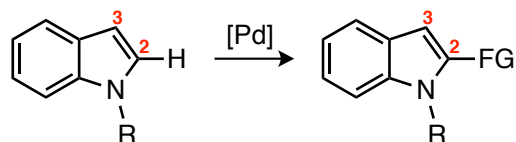


**Figure 1:** Directing Group-Assisted Site Selectivity in C–H Bond Functionalisation

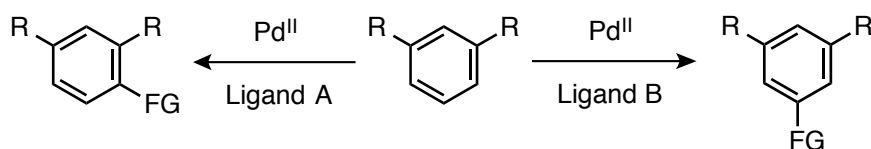
Substrate-based control is also observed in strategies relying on electronic control, where substrates containing a heteroatom, for example, show a bias towards cyclopalladation at a specific site, such as the C2 position in indole derivatives (Scheme 3).<sup>14</sup> The selective functionalisation of  $sp^3$  C–H bonds in the presence of  $sp^2$  and  $sp$  bonds remains a particular

challenge, and over the past decade heteroatom-directed C–H functionalisation has frequently been employed to achieve the conversion of  $sp^3$  C–H bonds.<sup>15–17</sup>



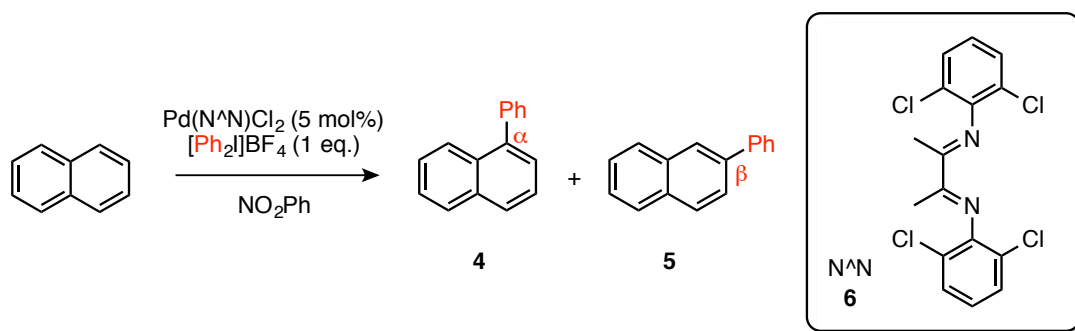
**Scheme 3:** Site Selectivity in C–H Bond Functionalisation Dictated by Electronic Effects

For substrates that lack a directing or activating group, site selectivity can also be achieved through ligand-accelerated catalysis, where the addition of a coordinating ligand to the reaction can affect the site of C–H bond functionalisation (Scheme 4).<sup>18,19</sup>



**Scheme 4:** Ligand-Directed Site Selectivity in C–H Bond Functionalisation

In the Pd-catalysed arylation of naphthalene, for example, Sanford and co-workers have shown that modification of the N<sup>^</sup>N ligand allows control of site selectivity, with ligand **6** affording the  $\alpha$ -substituted product **4** in good yield with 71% selectivity.<sup>18</sup>

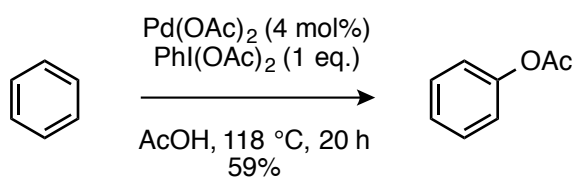


**Scheme 5:** Site Selectivity in the Arylation of Naphthalene

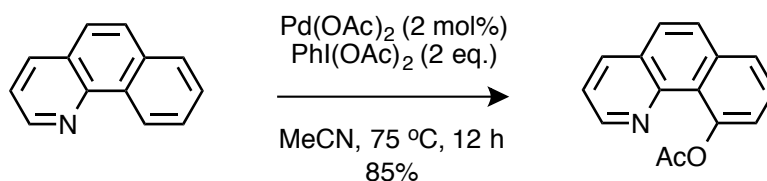
## Pd-Catalysed C–O Bond Formation

C–O bond-forming reactions remain some of the most useful examples of C–H bond functionalisation processes, due to the high prevalence of oxygen-containing groups in biologically-relevant compounds. In recent years, much work has been conducted into the use of Pd<sup>II</sup> complexes in the catalytic oxidation of C–H bonds.<sup>20,21</sup> Several promising results have been achieved using Pd catalysis in combination with a strong oxidant.

In 1996, Crabtree and co-workers reported the first use of PhI(OAc)<sub>2</sub> as an oxidant in the Pd-catalysed acetoxylation of unactivated arenes (Scheme 6).<sup>22</sup> In order to increase selectivity, Sanford applied this methodology to substrates containing pyridine derivatives as directing groups, achieving selective *ortho*-acetoxylation of several substrates in good to excellent yields (Scheme 7).<sup>21</sup> This methodology was also successfully employed in the first reported Pd-catalysed oxidation of unactivated sp<sup>3</sup> C–H bonds.<sup>23</sup>

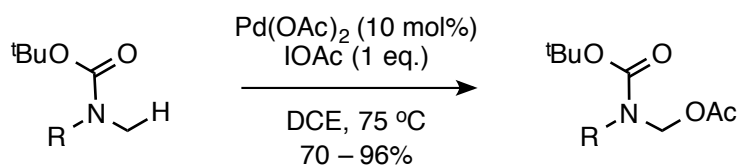


**Scheme 6:** Crabtree's Catalytic Acetoxylation of Unactivated Arenes<sup>22</sup>



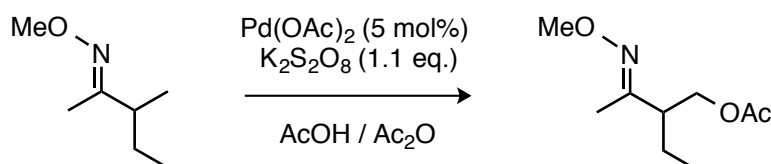
**Scheme 7:** Sanford's Acetoxylation of Pyridine Derivatives<sup>21</sup>

Iodine(III) complexes are now widely used in Pd-catalysed oxidation processes, but recent years have seen the use of alternative oxidants, such as those based on iodine(I) or peroxide groups, reported. Iodine(I) oxidants such as IOAc have been shown by Yu and co-workers to allow the oxidation of C–H bonds *ortho*- to a Boc-protected amine, where the carbonyl oxygen in the Boc group is able to act as a directing group (Scheme 8).<sup>24</sup> Interestingly, PhI(OAc)<sub>2</sub> was found not to work as an oxidant in this system.



**Scheme 8:** Iodine(I) as an Oxidant

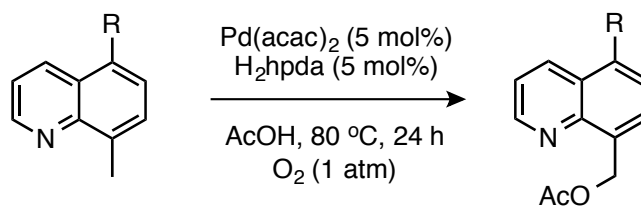
The use of inorganic peroxides, such as  $\text{K}_2\text{S}_2\text{O}_8$ , as terminal oxidants, provides a cheaper alternative to costly iodine reagents, and has been shown to work well in systems containing oxime ether directing groups, which induce selective C–H functionalisation at the  $\beta$ -carbon through the formation of a 5-membered palladacyclic intermediate (Scheme 9).<sup>25</sup>



**Scheme 9:** Inorganic Peroxides as Oxidants

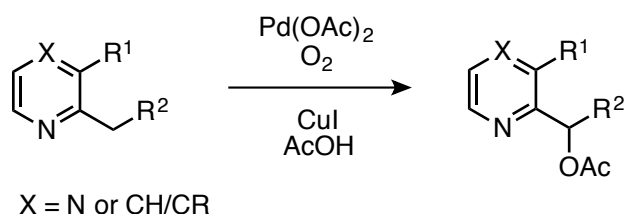
Despite the successful applications of iodine and peroxide reagents to oxidative C–H functionalisation processes, these reagents have their disadvantages; they often provide poor atom economy and lead to the formation of unwanted by-products. Moreover, the high cost of iodine reagents, typically needed in stoichiometric or super-stoichiometric quantities, can be a significant drawback in the widespread use of this methodology. From both cost and environmental perspectives, it remains an attractive goal to develop methods that employ dioxygen as the terminal oxidant.

Aerobic oxidation at Pd has been reported in the oxidation of secondary alcohols to ketones, catalysed by cyclopalladated complexes prepared from pyridine derivatives, but the widespread use of these processes has been hampered by the slow kinetics often observed.<sup>26,27</sup> In 2008, Vedernikov described the Pd-catalysed  $\text{sp}^3$  C–H acetoxylation of substituted 8-methylquinolines using oxygen in the air as the terminal oxidant (Scheme 10).<sup>28</sup> While this was an important breakthrough, the narrow substrate scope once again provided an obstacle to the application of this methodology to more complex systems.



**Scheme 10:** Vedernikov's Aerobic Oxidation of Substituted Quinolines<sup>28</sup>

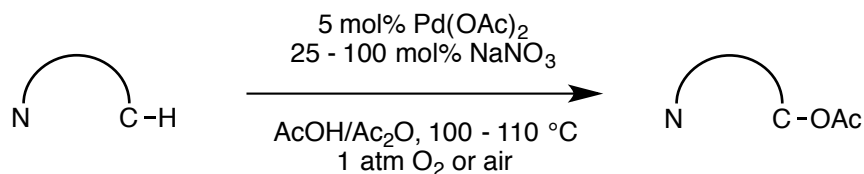
Similar methodology has also been used by Jiang and co-workers in the aerobic acetoxylation of 2-substituted pyridines and pyrazines, which proceeds in good to excellent yield across a range of substrates when a copper(I) iodide salt is used as an additive (Scheme 11).<sup>29</sup>



**Scheme 11:** Jiang's Aerobic Acetoxylation of Substituted Pyridines and Pyrazines<sup>29</sup>

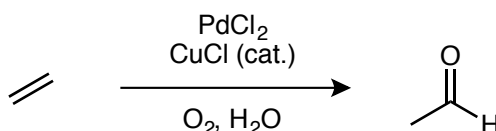
## Redox Co-Catalysis in C–H Bond Functionalisation

Recently, Sanford and co-workers reported the aerobic acetoxylation of C–H bonds with Pd(OAc)<sub>2</sub> in conjunction with NaNO<sub>3</sub>, which acts as a redox co-oxidant.<sup>30</sup> A series of substrates containing either pyridine or oxime ether groups were successfully oxidised using loadings of between 10 and 100 mol% of either NaNO<sub>2</sub> or NaNO<sub>3</sub> (Scheme 12).



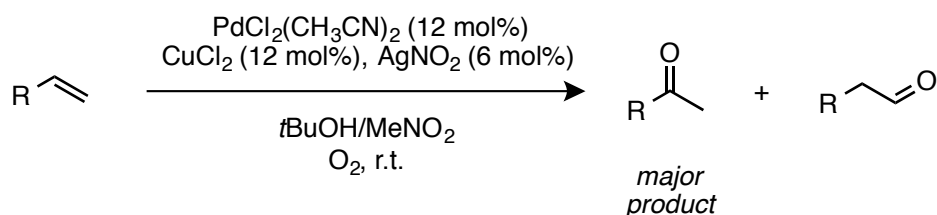
**Scheme 12:** Sanford's Aerobic Oxidation with Nitrate as a Co-Catalyst<sup>30</sup>

While this was the first reported example of the use of nitrate as a co-catalyst, the concept of co-catalysis in transition metal-mediated oxidation processes is not novel. The Wacker oxidation, in which ethene is oxidized to produce acetaldehyde *via* a Pd<sup>0/II</sup> pathway, utilizes O<sub>2</sub> as the terminal oxidant, and copper as a redox co-catalyst which regenerates the catalytically active Pd<sup>II</sup> species (Scheme 13).<sup>31</sup>



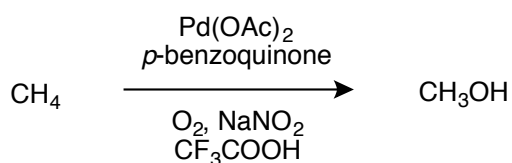
**Scheme 13:** The Wacker Oxidation of Alkenes

Recently, Grubbs and co-workers have reported the use of nitrite as a redox co-catalyst in a Wacker-type alkene oxidation, allowing the synthesis of anti-Markovnikov products in an interesting reversal of selectivity from the traditional Wacker process (Scheme 14).<sup>32</sup>



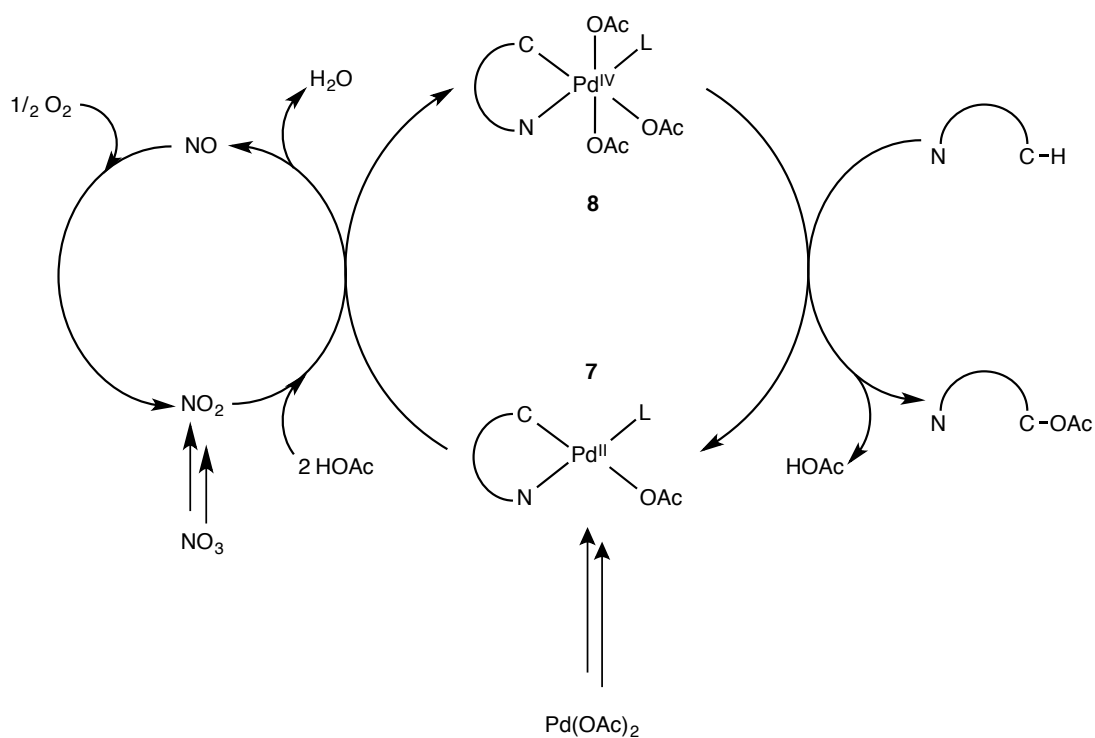
**Scheme 14:** Nitrite as a Co-Catalyst in the Wacker Oxidation of Alkenes

The use of redox couples in catalysis has also been reported in the oxidation of methane or benzene, where systems involving a Pd catalyst, benzoquinone and a heteropolyacid, such as molybdovanado-phosphoric acid, have been shown to oxidise methane to methanol under mild conditions.<sup>33,34</sup> Bao and co-workers successfully employed the NO/NO<sub>2</sub> redox couple in the aerobic oxidation of methane to methanol (Scheme 15).<sup>35</sup>



**Scheme 15:** Aerobic Oxidation of Methane Reported by Bao

The NO/NO<sub>2</sub> redox couple was successfully used in Sanford's work, where the NaNO<sub>3</sub> used is proposed to be a source of NO<sub>2</sub>, which has previously been shown by Campora and co-workers to oxidize Pd<sup>II</sup> to Pd<sup>IV</sup> (containing NO ligands, *vide infra*).<sup>36</sup> Sanford proposed the reaction mechanism shown in Scheme 16. Upon reaction with the Pd(OAc)<sub>2</sub> catalyst, the C<sup>N</sup> substrate forms the cyclometalated complex **7**, which is the catalytically active species. The oxidation of the Pd<sup>II</sup> complex **7** to Pd<sup>IV</sup> intermediate **8** with the addition of two acetic acid ligands is facilitated by the simultaneous reduction of NO<sub>2</sub> to NO. C–O bond-forming reductive elimination from **8** then releases the oxidation product, and the NO is oxidized by molecular oxygen to regenerate NO<sub>2</sub>. Although no mechanistic experiments have proved the nature of the intermediates, Sanford proposes that the coordinating ligands (L) at Pd could be either acetate or NO<sub>3</sub>/NO<sub>2</sub>/NO ligands.



**Scheme 16:** Proposed Catalytic Cycle for Sanford's Oxidation Conditions<sup>30</sup>

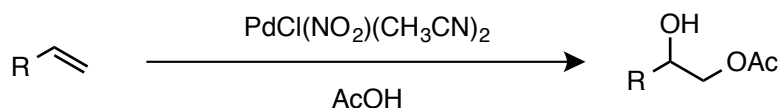
Isotopic-labelling experiments conducted in an atmosphere of <sup>18</sup>O<sub>2</sub> showed no incorporation of <sup>18</sup>O into the acetoxyated product, and thus Sanford concluded that the acetic acid is the source of the acetate oxygen in the product. The addition of 2,6-di-*tert*-butyl-4-methylphenol (BHT), which is known to react readily with NO,<sup>37</sup> to the reaction mixture

resulted in a significant decrease in yield (>95% to 12%) compared to standard conditions, supporting the idea that NO is a key intermediate in the reaction.

While the recent work on the use of NO/NO<sub>2</sub> redox chemistry indicates that it can play a significant role in oxidation reactions, the reaction mechanisms that have been proposed so far are somewhat tentative. In order to exploit the redox chemistry of anions such as NO<sub>2</sub><sup>-</sup> or NO<sub>3</sub><sup>-</sup> it is essential to fully understand their role in the catalytic cycle, *i.e.* whether their role is that of an oxidant which facilitates a change in Pd oxidation state, as proposed by Sanford, or whether they are able to act as ligands at Pd<sup>II</sup> or Pd<sup>IV</sup>; these could either be passive spectator ligands or active non-spectator ligands.

### The Role of Nitrite in Pd-Catalysed Processes

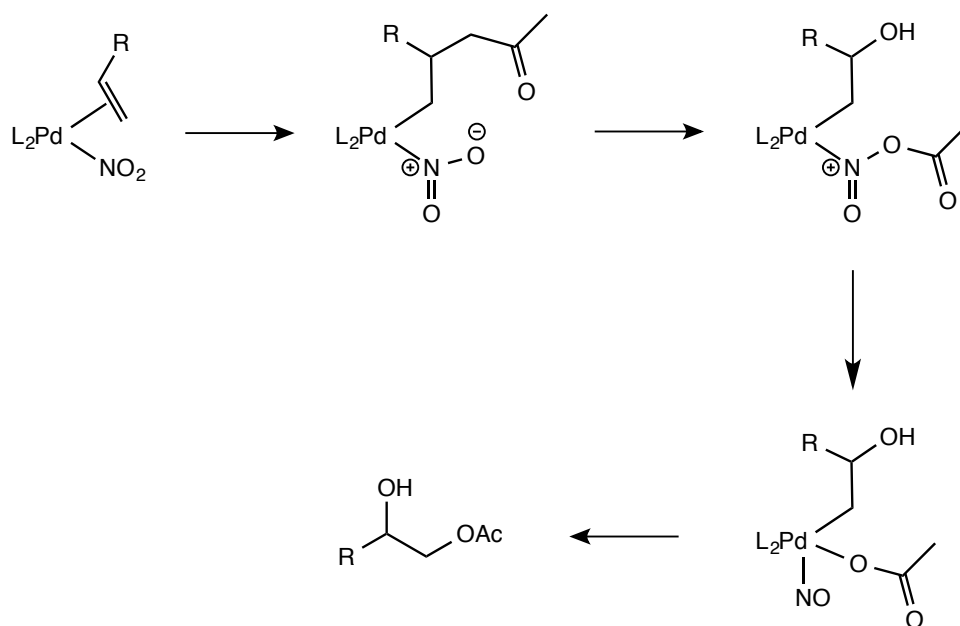
Heumann and Bäckvall reported that nitrite can play a more significant role in Pd-catalysed processes, which was not highlighted in Sanford's study.<sup>38</sup> Work conducted by Mares and co-workers in 1985 had shown that the complex [Pd(Cl)NO<sub>2</sub>(CH<sub>3</sub>CN)<sub>2</sub>], containing a nitrite ligand, could be used to catalyse the acetoxylation of alkenes (Scheme 17).<sup>39</sup>



**Scheme 17:** Alkene Acetoxylation Catalysed by a Pd-Nitrite Complex

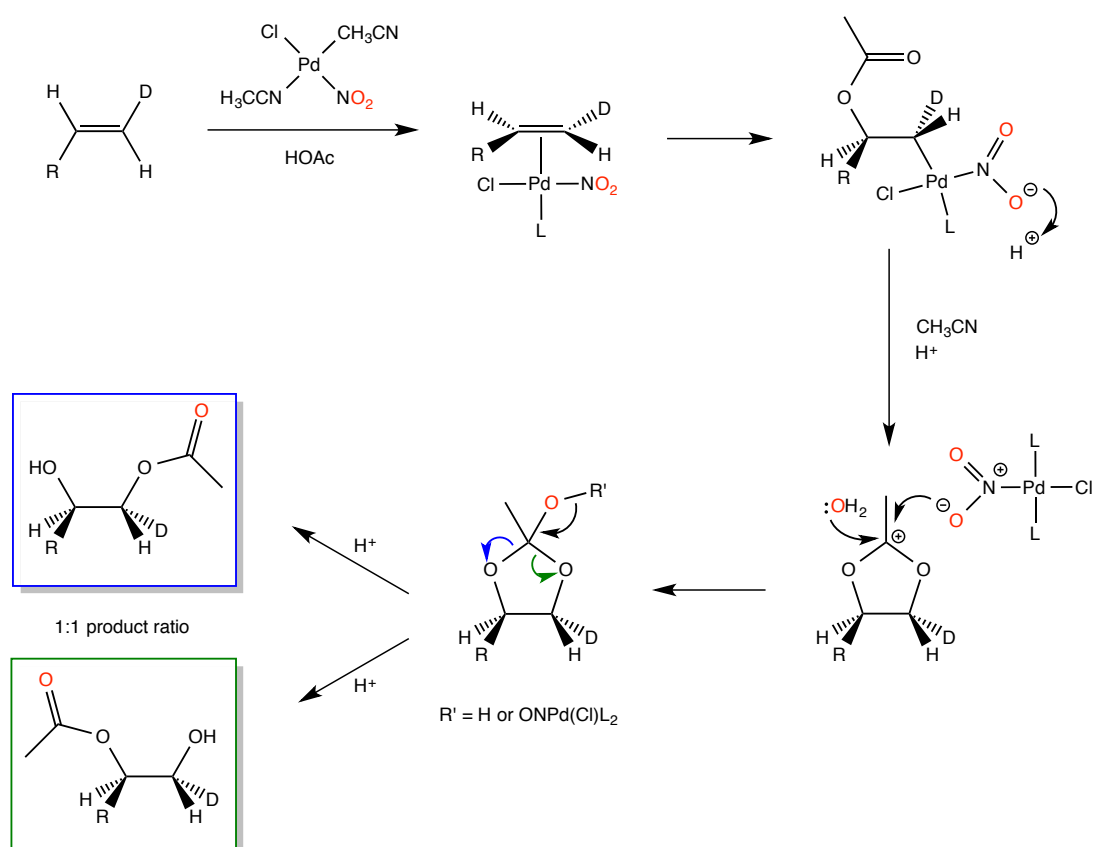
When the NO<sub>2</sub> group in the catalyst was labelled with <sup>18</sup>O, it was found to be the source of the carbonyl oxygen in the acetate group of the product. The mechanism that had been proposed by Mares initially involved an acetoxy-palladation step; the acetyl group would then migrate to the NO<sub>2</sub> group coordinated nearby, before an acetate migration to the Pd atom and reductive elimination of the acetoxyated product (Scheme 18).





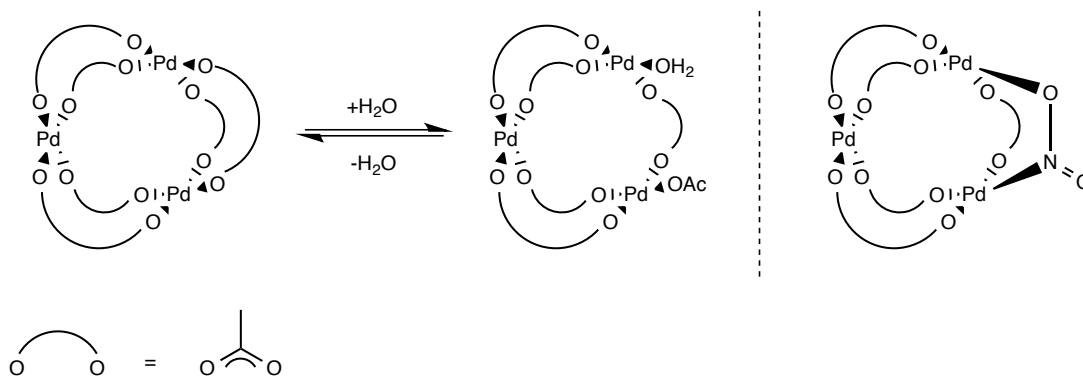
**Scheme 18:** Mechanism as Proposed by Mares for Pd-Catalysed Alkene Acetoxylation<sup>39</sup>

In a paper published shortly after Mares', Heumann and Bäckvall commented on several flaws in this mechanism, most notably the fact that a 1:1 ratio of Markovnikov and anti-Markovnikov acetoxylation would be required for the proposed mechanism, whereas the reaction conditions used would be expected to favour the formation of the Markovnikov intermediate. On the basis of results obtained from isotopic labelling studies, Heumann and Bäckvall instead proposed the mechanism shown in Scheme 19. After an initial acetoxylation step, cleavage of the oxygen-carbon bond proceeds with an inversion of configuration at the D-labelled carbon. Simultaneous neighbouring group attack forms the five-membered cyclic cationic intermediate, which can then be attacked either by  $^{18}O$ -labelled water, generated during the previous step, or an  $^{18}O$  atom from the neighbouring nitrite ligand. Rearrangement of the cyclic intermediate gives a 1:1 mixture of the two acetoxylation products.



**Scheme 19:** Mechanism as Proposed by Heumann and Bäckvall for Alkene Acetoxylation<sup>38</sup>

Previous work within the Fairlamb group has focused on Pd<sup>II</sup> nitrite species and their role in catalytic reactions.<sup>40</sup> Attempts to synthesize the complex Pd(OAc)<sub>2</sub>(pip)<sub>2</sub> (where pip = piperidine), a useful catalyst for Suzuki-Miyaura cross-couplings,<sup>41</sup> resulted in the unexpected formation of Pd(OAc)(NO<sub>2</sub>)(pip)<sub>2</sub>. The source of the NO<sub>2</sub> ligand was determined to be a nitrite impurity in commercial Pd(OAc)<sub>2</sub>, which is able to replace one of the acetate bridges in Pd<sub>3</sub>(OAc)<sub>6</sub> and form Pd<sub>3</sub>(OAc)<sub>5</sub>NO<sub>2</sub>, where the nitrite itself then becomes a bridging ligand between two Pd atoms. The nitrite here has a similar role to that often played by trace H<sub>2</sub>O in laboratory grade CDCl<sub>3</sub>, which has been shown by Murillo and co-workers to disrupt acetate bridging in Pd<sub>3</sub>(OAc)<sub>6</sub> and bring about the loss of the trimer's *D*<sub>3h</sub> symmetry (Scheme 20).<sup>42</sup>



**Scheme 20:** Disruption of Acetate Bridging in  $\text{Pd}_3(\text{OAc})_6$  by  $\text{H}_2\text{O}$  and  $\text{NO}_2$

The presence of nitrite impurities found in a range of commercial samples of  $\text{Pd}(\text{OAc})_2$  in the Department of Chemistry at York has raised the question of whether many “ $\text{Pd}(\text{OAc})_2$ -catalysed” reactions are actually influenced by nitrite, and whether  $\text{Pd}-\text{NO}_2$  species could be present as precatalytic species in such systems. The ability of the  $\text{NO}_2$  group to oxidise  $\text{Pd}^{\text{II}}$  to  $\text{Pd}^{\text{IV}}$  suggests that its presence in reactions taking place under oxidative conditions could have an effect on catalysis.<sup>36</sup>

As well as hinting at a potential role for nitrite in catalysis, the discovery of these impurities also sheds some light on the unexpected formation of  $\text{NO}_2$  adducts in palladacyclic complexes observed by Nonoyama and co-workers.<sup>43</sup> Upon reaction with  $\text{Pd}(\text{OAc})_2$  in acetonitrile, C<sup>^</sup>N ligands 1-(2-pyridyl and 2-pyrimidyl)indole (Hpyi) and 2-(2-pyridyl)benzo[*b*]furan (Hpbfb) formed monomeric complexes with  $\text{NO}_2$  and  $\text{CH}_3\text{CN}$  ligands (Figure 2). The geometries of these complexes were confirmed by X-ray crystallography.

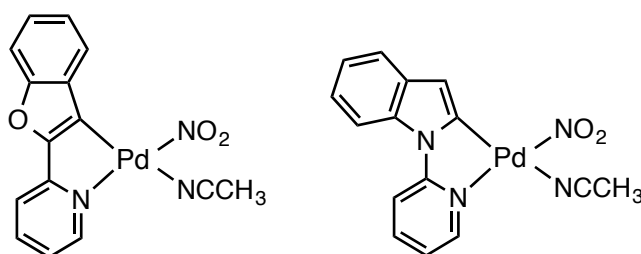


**Figure 2:** Hpyi and Hpbfb Complexes Prepared by Nonoyama

Two chemical equations were proposed by Nonoyama to account for the formation of nitrite adducts (Equations 1 and 2), involving the oxidation of acetonitrile under aerobic conditions.

Unfortunately, such a process is unprecedented in the literature under the mild conditions used; typically metallic Cu is required and the process is conducted at 600 °C.<sup>44</sup> Given the recent results published by Fairlamb and co-workers, it seems likely that impurities in the Pd(OAc)<sub>2</sub> used could well be the source of the unexpected nitrite adducts observed by Nonoyama.



One of the most notable aspects of Nonoyama's findings was the geometry of the Pd(C<sup>^</sup>N)(NO<sub>2</sub>)(NCCH<sub>3</sub>) complexes. Typically, a nitrite ligand would be expected to occupy the site *trans*- to the Pd–C bond in a square planar complex. However, re-crystallisation of the complexes from DMSO resulted in the formation of crystals of Pd(C<sup>^</sup>N)(NO<sub>2</sub>)(DMSO), and X-ray diffraction confirmed the *cis*- geometry of the NO<sub>2</sub> ligand and Pd–C bond. The geometry of square planar Pd complexes can be of great significance when such complexes are involved in catalysis. For example, a *cis*- geometry is typically required for the formation of C–NO<sub>2</sub> species *via* reductive elimination.

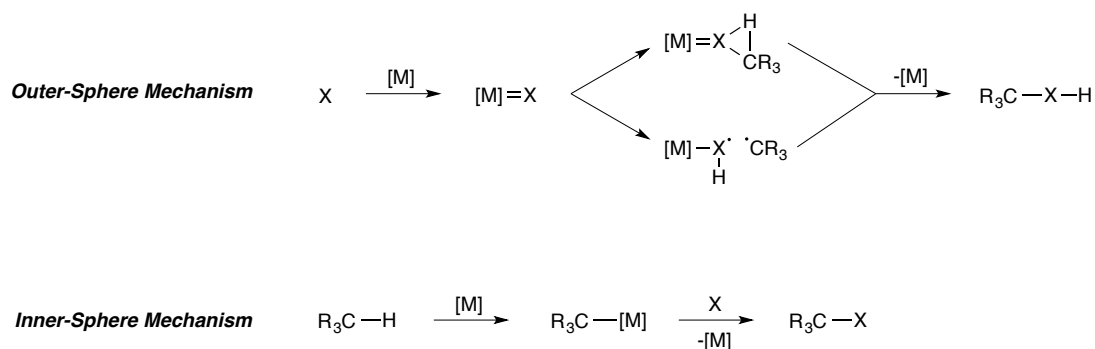
There are clear differences between the system used in Bäckvall's work and that used in Sanford's C–H functionalisation chemistry. However, the mechanism proposed for the acetoxylation of alkenes suggests that, rather than acting solely as a passive spectator ligand, nitrite could potentially have an active role in the mechanism.

## Mechanistic Aspects of Oxidative C–H Bond Functionalisation

In order to apply promising C–H bond functionalisation processes to a wide range of substrates with complex or sensitive functionalities, a comprehensive understanding of the mechanism of catalysis is essential.

The plethora of methods available for transition metal catalysis of C–H bond functionalisation means that several mechanistic pathways have been proposed. Most oxidative functionalisation processes are said to proceed by one of two general mechanisms: 1) an outer-sphere mechanism, where the metal interacts only with the approaching

functional group (X) and C–H bond cleavage follows without the formation of a formal metal–carbon bond, or 2) an inner-sphere mechanism, where C–H bond cleavage produces an “activated” organometallic species which then reacts with the relevant functional group (Scheme 21).<sup>45</sup> Since the majority of the reactions investigated in this thesis are believed to operate *via* an inner-sphere mechanism, this section will focus on mechanisms of catalysis that proceed *via* the formation of C–[M] intermediate species.

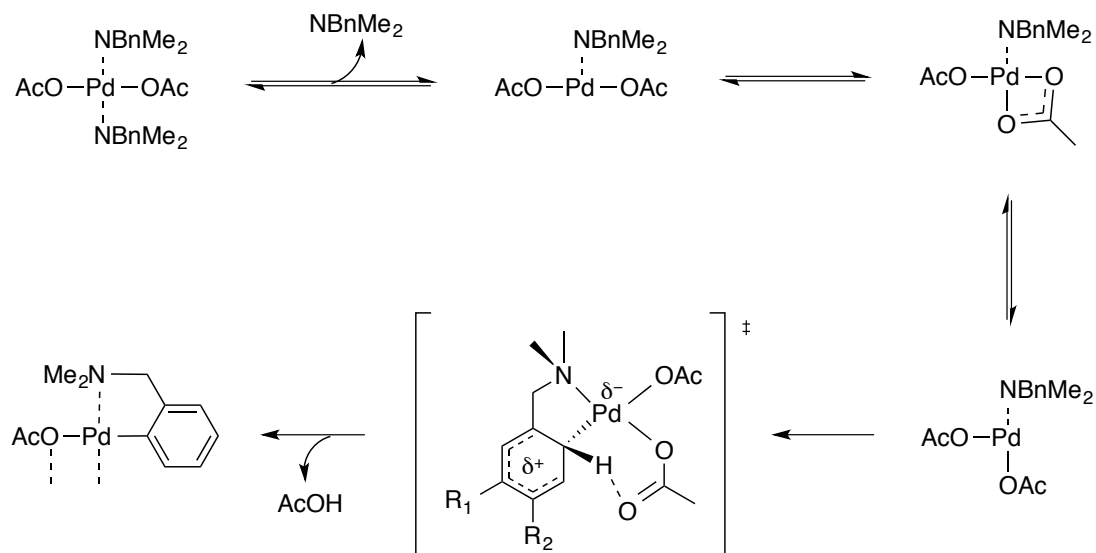


**Scheme 21:** Outer- and Inner-Sphere Mechanisms for Transition Metal Catalysis

The mechanism of C–H bond cleavage and C–[M] bond formation has been fiercely debated in the literature, and on the whole sp<sup>2</sup> C–H bond activations processes are better understood than their sp<sup>3</sup>-counterparts. Since the publication of Fagnou’s pivotal study of metal-catalysed C–H functionalisation mechanisms in 2010, it has become widely accepted that sp<sup>2</sup> “C–H activation” proceeds *via* a concerted metalation-deprotonation (CMD) mechanism.<sup>46</sup> This process relies on a base such as pivalate or carbonate, and has been described several times throughout recent years, often being referred to as internal electrophilic substitution (IES)<sup>47</sup> or ambiphilic metal–ligand substitution (AMLA).<sup>48</sup>

While early studies into C–[M] bond formation at arenes had proposed a S<sub>E</sub>Ar mechanism for the conversion of a C–H bond into a C–[M] bond,<sup>49,50</sup> studies conducted by Ryabov into the *ortho*-palladation of *N,N*-dimethylbenzylamine (DMBA-H) found that the key transition state involved concerted Pd–C bond formation and C–H bond cleavage, with the coordinated acetate ligand acting as a nucleophile for the deprotonation step (Scheme 22).<sup>51,52</sup> Computational studies by Macgregor and co-workers provided further evidence for this mechanism.<sup>53</sup> Agostic interactions were found to increase the acidity of the C–H bond, meaning that it can be easily deprotonated by a neighbouring acetate ligand, which is steered into a suitable position for attack *via* hydrogen bonding. Perutz and Eisenstein showed that

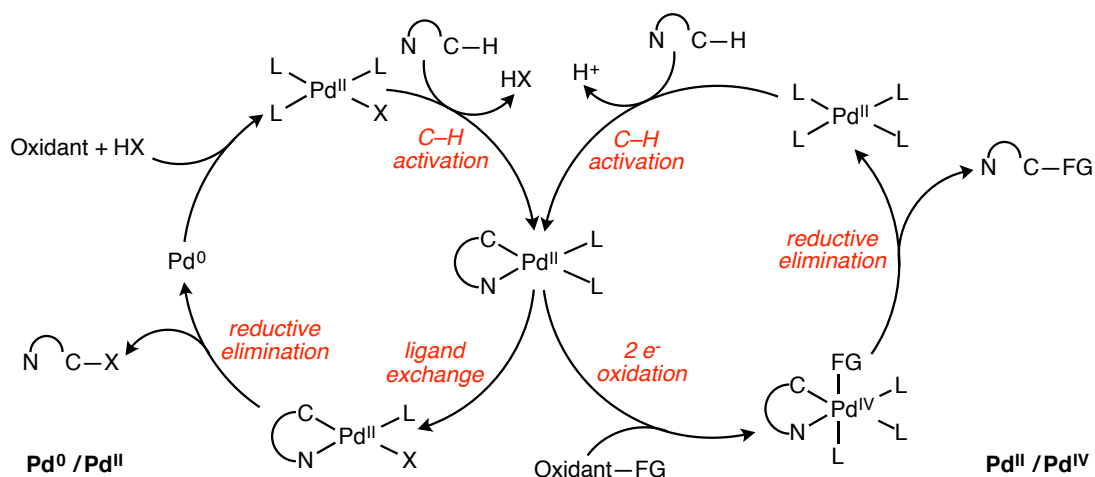
this step is also strongly dependent on the strength of the Pd–C bond, with a high bond energy creating a significant kinetic barrier.<sup>54</sup>



**Scheme 22:** Mechanism as Proposed by Ryabov for the Cyclopalladation of H-DMBA

Despite most studies into the mechanism of C–H bond cleavage focusing on the cleavage of  $sp^2$  C–H bonds, results published in 2010 by Fagnou and co-workers suggested that  $Pd^0$ -catalysed  $sp^3$  C–H functionalisation adjacent to nitrogen atoms may proceed *via* a similar mechanism.<sup>55</sup>

Baudoin has extensively reviewed several mechanistic aspects of transition-metal catalysed C–H bond functionalisation at  $sp^3$  centres.<sup>45</sup> For Pd-catalysed systems, both  $Pd^{0/II}$  and  $Pd^{II/IV}$  pathways have been proposed. Scheme 23 shows a general catalytic cycle for each of the two pathways, both proceeding *via* the key  $Pd^{II}$  intermediate  $[Pd(C^{\wedge}N)L_2]$ .

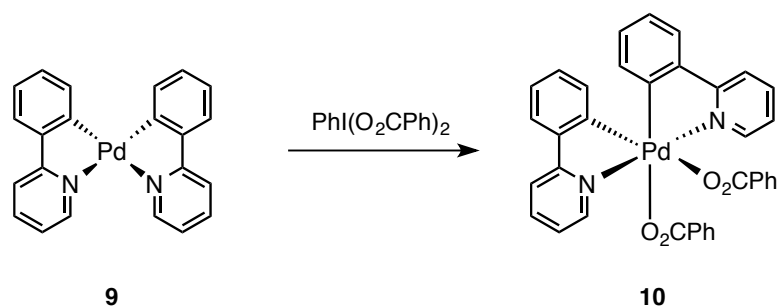


**Scheme 23:** Pd<sup>0/II</sup> and Pd<sup>II/IV</sup> Pathways for Oxidative C–H Bond Functionalisation

While both systems shown here involve the use of an oxidant, it plays different roles depending on the oxidation states of Pd involved. In a Pd<sup>0/II</sup> system, for example, the key C–FG bond-forming reductive elimination occurs from Pd<sup>II</sup>, and the role of the oxidant is to regenerate the catalyst from a Pd<sup>0</sup> to a Pd<sup>II</sup> oxidation state. In the Pd<sup>II/IV</sup> system, on the other hand, reaction of the key intermediate with the oxidant generates the Pd<sup>IV</sup> species, which can then undergo reductive elimination to form the product, whilst regenerating the Pd<sup>II</sup> catalyst.

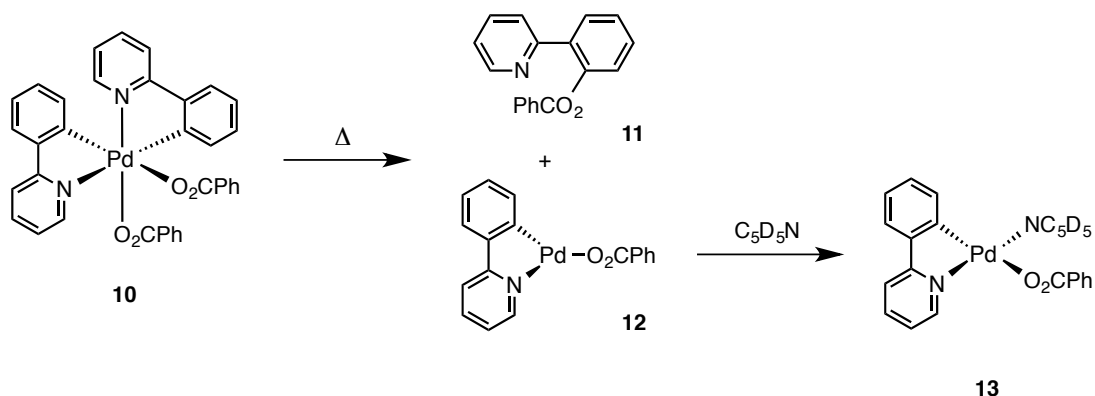
The widespread use of Pd<sup>II</sup>-catalysed processes means that their mechanisms have been extensively studied throughout recent years.<sup>56–58</sup> Comparatively little attention, however, has been paid to the mechanistic details of Pd<sup>IV</sup>-catalysed processes,<sup>59,60</sup> despite other high oxidation state systems such as those catalysed by Pt<sup>IV</sup> having been thoroughly examined.<sup>61</sup> While a number of Pd<sup>IV</sup> complexes have been known since the 1960s, there are some key difficulties faced when attempting mechanistic investigations at Pd<sup>IV</sup>; detailed reviews published by Canty and Fairlamb highlighted some of these.<sup>59,62</sup> Oxidative addition to Pd<sup>II</sup> species is often disfavoured (*e.g.* reactions with haloarenes), especially when bulky phosphine ligands are present, meaning that the formation of Pd<sup>IV</sup> species can be challenging. Additionally, the steric bulk around 5-coordinate Pd<sup>IV</sup> complexes means that they readily undergo reductive elimination, and thus are often too unstable to be isolated and characterised.

In 2005, Sanford and co-workers published a detailed investigation into C–O bond-forming reductive elimination from Pd<sup>IV</sup>. Complex **10**, which was easily prepared from the [Pd(C<sup>^</sup>N)<sub>2</sub>] complex **9** by reaction with PhI(O<sub>2</sub>CPh)<sub>2</sub> (Scheme 24), was used as a model substrate.



**Scheme 24:** Synthesis of Pd<sup>IV</sup> Complex **10**

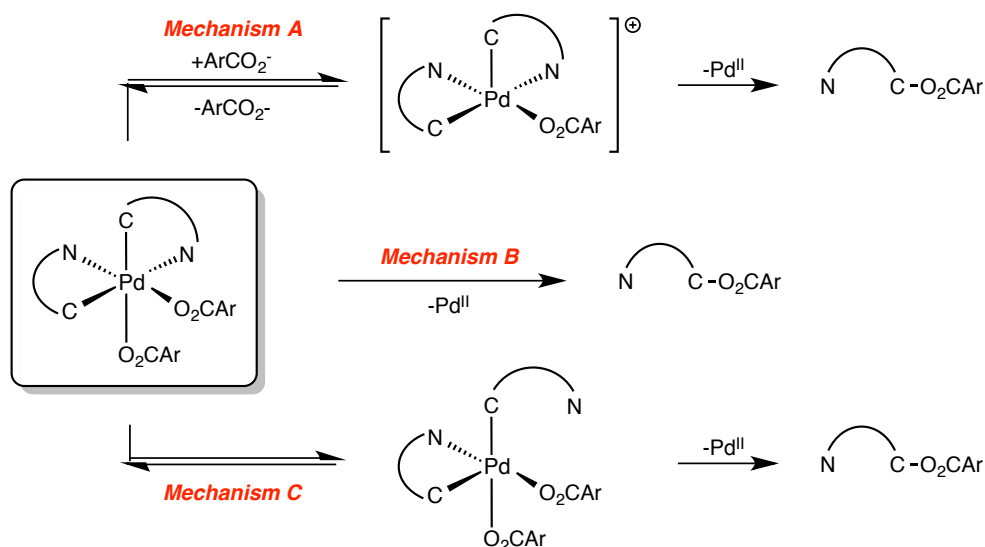
Interestingly, complex **10** was surprisingly stable in the solid-state, enabling characterisation by X-ray crystallography, whereas complexes prepared without a cyclometallating ligand are often undetectable even at  $-70\text{ }^{\circ}\text{C}$ .<sup>63</sup> When heated at  $60\text{ }^{\circ}\text{C}$  for 1 h, **10** underwent reductive elimination to form the functionalized product **11** (Scheme 25), along with three-coordinate intermediate **12** (presumably a  $\mu_2$ -bridged benzoate dinuclear Pd<sup>II</sup> complex), which was trapped with the addition of *d*<sub>5</sub>-pyridine.



**Scheme 25:** C–O Bond Forming Reductive Elimination from Pd<sup>IV</sup>

Sanford proposed three potential mechanistic pathways for the reductive elimination step (Scheme 26). Mechanism A involves the dissociation of a benzoate ligand to form a cationic five-coordinate complex before reductive elimination of the product. Mechanism B involves direct reductive elimination from the Pd<sup>IV</sup> starting material, and mechanism C involves the dissociation of one pyridyl ligand to give a five-coordinate Pd<sup>IV</sup> species, from which reductive elimination occurs.



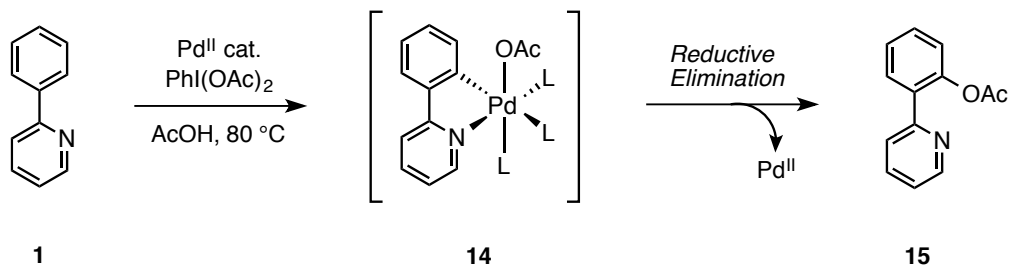


**Scheme 26:** Proposed Mechanisms for Reductive Elimination from Pd<sup>IV</sup>

C–C bond-forming reductive elimination from Pd<sup>IV</sup> and C–O bond-forming reductive elimination from Pt<sup>IV</sup> are typically believed to proceed *via* mechanism A;<sup>61,64</sup> both systems show a strong rate dependence on solvent polarity, indicating an ionic pathway. In reductive elimination from intermediate **10**, however, Sanford's detailed studies into solvent effects showed a complete lack of solvent dependence. In addition, Eyring and Hammett analysis provided further evidence that mechanism A was an unfeasible pathway. While no preference was established for either mechanism B or C, which are kinetically indistinguishable under the experiments carried out by Sanford, the fact that C–O bond forming reduction from Pd<sup>IV</sup> proceeded *via* a significantly different pathway from analogous processes at Pt<sup>IV</sup>, or those forming C–C bonds from Pd<sup>IV</sup>, was a remarkable breakthrough.

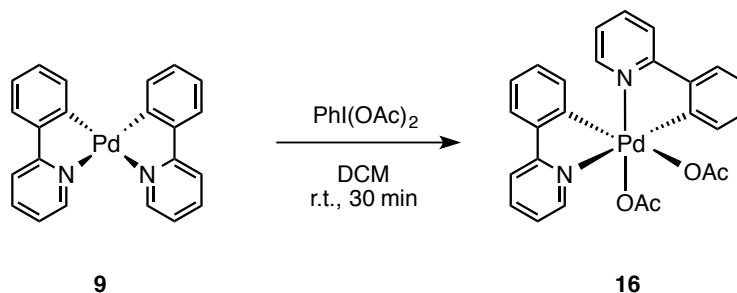
In order to further elucidate the mechanism of reductive elimination, Liu and co-workers conducted thorough computational investigations into the three proposed pathways for the formation of **11** from **10**.<sup>65</sup> Calculated rate constants in CDCl<sub>3</sub> and DMSO showed a similar ratio to that obtained experimentally by Sanford, confirming the lack of solvent dependence, and theoretical Hammett parameters provided further evidence against mechanism A. In order to differentiate between mechanisms B and C, Liu calculated the single point energies of the key transition states for each pathway, finding that reductive elimination was the rate-limiting step for all three mechanisms. It was found that the free energy barrier for pathway B was approximately 20 kcal mol<sup>-1</sup> lower for mechanism B than for mechanism C, and thus Liu proposed a pathway proceeding *via* direct reductive elimination from a six-coordinate Pd<sup>IV</sup> species.

In 2009, Sanford published another detailed mechanistic investigation into Pd<sup>IV</sup> catalysis, this time into the acetoxylation of 2-phenylpyridine with PhI(OAc)<sub>2</sub> (Scheme 27).



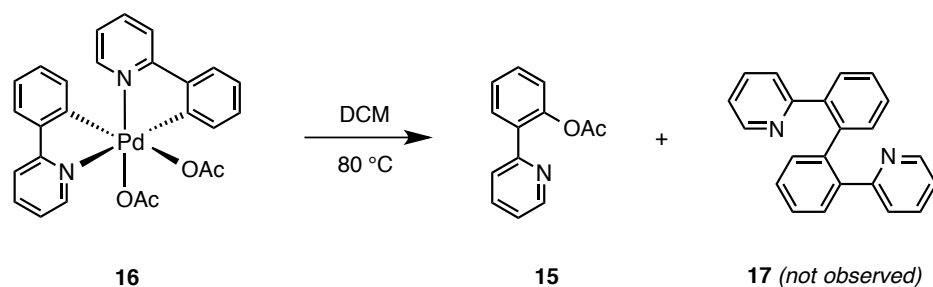
**Scheme 27:** Pd-Catalysed Acetoxylation of 2-Phenylpyridine

It was proposed that the mechanism would proceed *via* the formation of a Pd<sup>IV</sup> species such as **16**. In order to test the catalytic viability of such a complex, **16** was prepared from the [Pd(C<sup>^</sup>N)<sub>2</sub>] species **9** under mild conditions (Scheme 28).



**Scheme 28:** Preparation of Proposed Intermediate **16**

Once again, complex **16** was found to be unexpectedly stable at room temperature, and its geometry was characterised by single crystal X-ray crystallography. Upon heating in dichloromethane, **16** underwent C–O reductive elimination to form product **15**, with no formation of the competing C–C product **18** observed (Scheme 19).

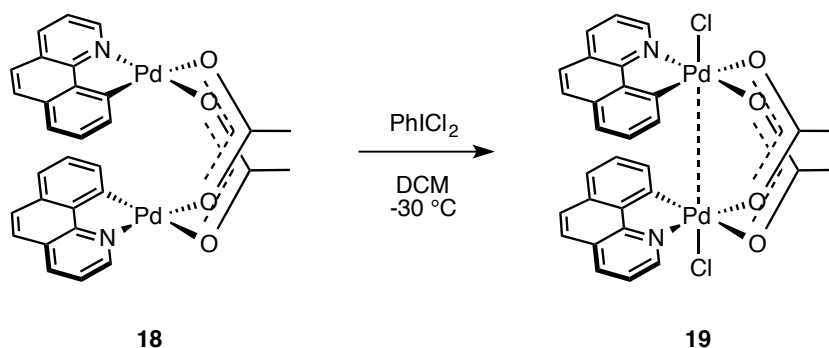


**Scheme 29:** Reductive Elimination from Pd<sup>IV</sup> Complex **16**

Detailed investigations into solvent effects and ligand exchange mechanisms, as well as competition studies, led to the conclusion that the formation of **15** proceeded *via* mechanism A, where initial dissociation of an acetate ligand is followed by reductive elimination of the product from a cationic 5-membered Pd<sup>IV</sup> complex.

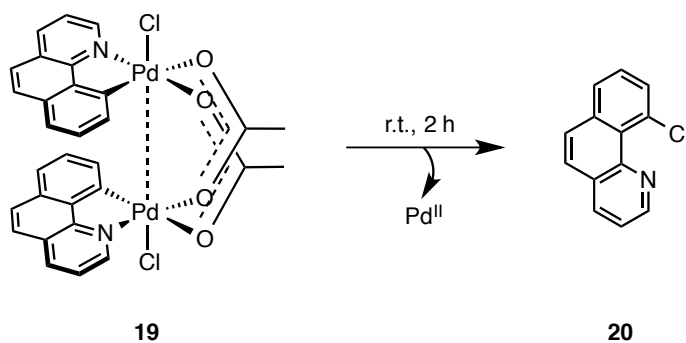
These investigations into mechanisms for Pd<sup>IV</sup> catalysis confirmed that Pd<sup>IV</sup> complexes with O-donor ligands are, in fact, isolable, and can undergo reductive elimination to form *O*-functionalised organic products. However, their role in active catalytic systems has still not been identified, and the instability of several Pd<sup>IV</sup> complexes has raised doubts about their viability as catalytic intermediates.<sup>66</sup>

In 2009, Ritter and co-workers published a key paper proposing the intermediacy of bimetallic Pd<sup>III</sup>–Pd<sup>III</sup> dimers in oxidative carbon–halogen bond forming reactions.<sup>67</sup> Complex **19** was synthesised *via* addition of PhICl<sub>2</sub> to acetato-bridged dimer **18** in a Pd–Pd bond-forming reaction (Scheme 30).



**Scheme 30:** Synthesis of Bimetallic Pd<sup>III</sup>–Pd<sup>III</sup> Complex **19**

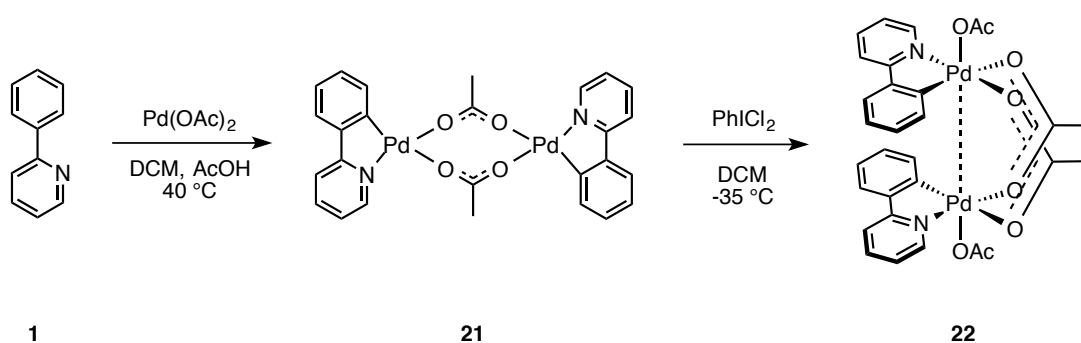
When heated to room temperature, **19** smoothly underwent reductive elimination to form chlorinated product **20**. Several in-depth mechanistic experiments concluded that C–Cl bond formation proceeded *via* two concerted reductive elimination steps from **19**.



**Scheme 31:** Reductive Elimination from Bimetallic Pd<sup>III</sup>–Pd<sup>III</sup> Complex **19**

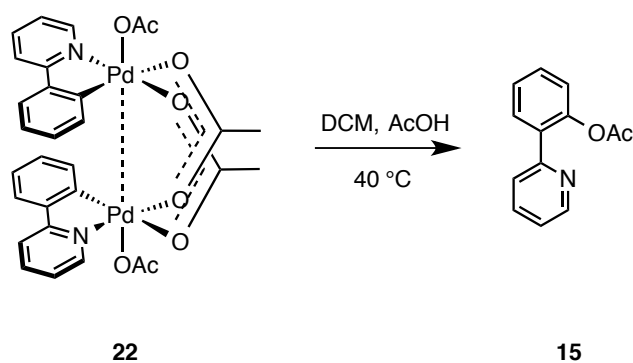
The formation of **19** was observed during catalysis of the chlorination of benzoquinoline with PhICl<sub>2</sub>, meaning that it is a viable catalytic intermediate.

In order to identify the scope for Pd<sup>III</sup> intermediates during catalysis, Ritter and co-workers conducted kinetic experiments on the acetoxylation of 2-phenylpyridine;<sup>68</sup> these results were published simultaneously with Sanford's studies on the same system. From the acetato-bridged dimer **21**, which is formed from the cyclopalladation of 2-phenylpyridine, Pd<sup>III</sup>–Pd<sup>III</sup> dimer **22** was prepared (Scheme 32).



**Scheme 32:** Formation of Bimetallic Pd<sup>III</sup>–Pd<sup>III</sup> Species **22**

**22** was found to be stable below  $-10\text{ }^{\circ}\text{C}$ , and was characterised by single crystal X-ray diffraction. When heated to  $40\text{ }^{\circ}\text{C}$ , bimetallic reductive elimination of the acetoxyated product was observed (Scheme 33).



**Scheme 33:** Bimetallic Reductive Elimination from **22**

Ritter undertook kinetic studies, comparing catalysis of the acetoxylation on 2-phenylpyridine by  $\text{Pd}(\text{OAc})_2$ , bimetallic complex **22**, and  $\text{Pd}^{\text{IV}}$  complex **16**, proposed by Sanford as an intermediate. While complex  $\text{Pd}^{\text{IV}}$  species **16** was found to catalyse the reaction at half the rate than when catalysed by  $\text{Pd}(\text{OAc})_2$ , when  $\text{Pd}^{\text{III}}\text{-Pd}^{\text{III}}$  species **22** was used the reaction proceeded faster, thus implicating it as a viable catalytic intermediate.

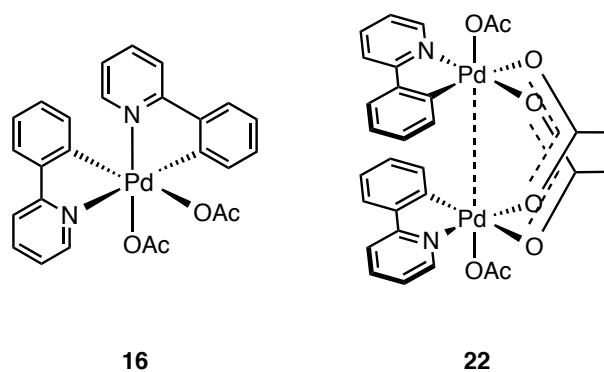
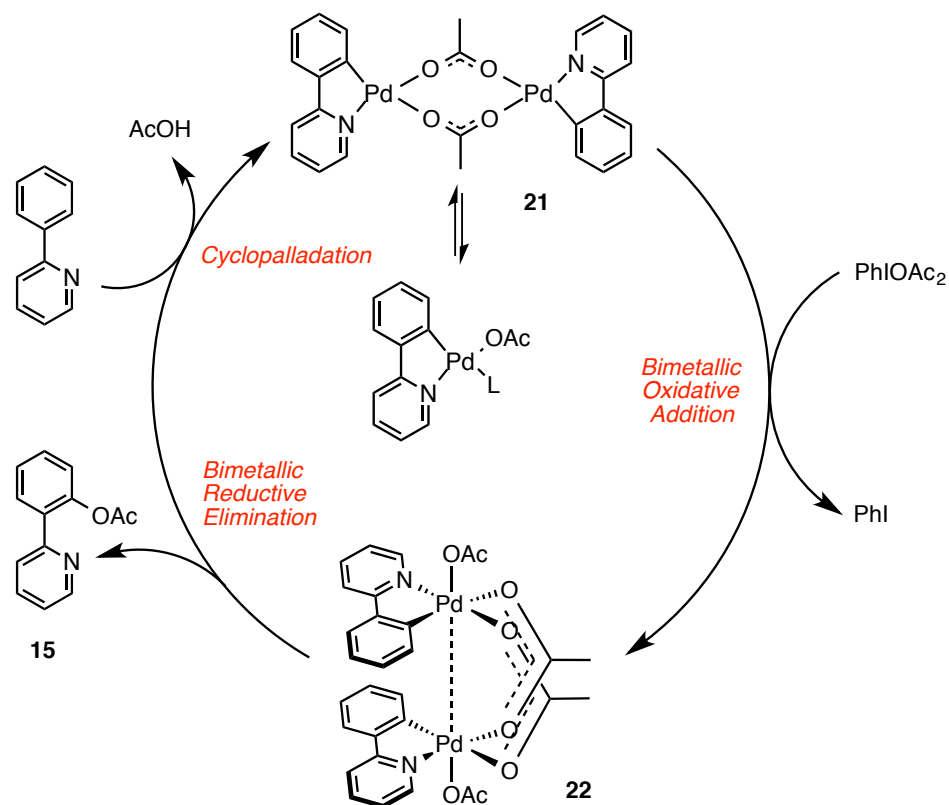


**Figure 3:**  $\text{Pd}^{\text{IV}}$  and  $\text{Pd}^{\text{III}}$  Intermediates Proposed by Sanford and Ritter

Ritter proposed the catalytic cycle shown in Scheme 34. The rate-determining step is initial cyclopalladation of 2-phenylpyridine to form acetato-bridged dimer **21**. Oxidative addition

of  $\text{PhI}(\text{OAc})_2$  generates the high oxidation state intermediate **22**, which then undergoes two simultaneous reductive elimination processes to release the product **15**.



**Scheme 34:** Mechanism for  $\text{Pd}^{\text{II}}/\text{Pd}^{\text{III}}$  Catalysis as Proposed by Ritter

While Sanford's proposed intermediate **16** was found not to be kinetically competent for catalysis, its presence in catalytic systems cannot be ruled out. Ritter's studies, however, have highlighted the fact that bimetallic  $\text{Pd}^{\text{III}}$  complexes should be considered as potential reaction intermediates, and that a range of processes previously believed to operate *via*  $\text{Pd}^{\text{II}}/\text{Pd}^{\text{IV}}$  mechanistic manifolds may actually involve  $\text{Pd}^{\text{II}}/\text{Pd}^{\text{III}}$  catalysis. The emergence of new strategies for oxidative C–H functionalisation, such as the redox co-catalysed system recently described by Sanford, provides scope for investigation of the generality of  $\text{Pd}^{\text{III}}$  catalysis, as well as for the isolation and characterisation of new  $\text{Pd}^{\text{III}}$  complexes in systems based on a range of different oxidants.

## Proposed Work

In the first instance, the project will involve the synthesis and characterisation of a range of Pd<sup>II</sup> complexes based upon a C<sup>^</sup>N ligand backbone. Following procedures recently developed within the Fairlamb group, complexes containing NO<sub>2</sub> and NO<sub>3</sub> ligands will be prepared. In order to assess their potential activity in catalytic systems, full characterisation will be carried out, with particular attention being paid to identifying the geometry of the complexes. Recent results published by Fairlamb showed that linkage isomerization between NO<sub>2</sub> and ONO-type species can occur at Pd.<sup>40</sup> The relative stabilities of the isomeric complexes could have a significant effect on the complexes' activities as catalysts. Additionally, the *cis/trans* isomerism of the NO<sub>2</sub> or NO<sub>3</sub> anionic ligand with respect to the Pd–C bond must be taken into account when assessing the likelihood of the complexes to undergo C–NO<sub>2</sub> bond forming reductive elimination. Complementary Density Functional Theory (DFT) studies will be conducted in order to gain a thorough understanding of the relative stabilities of the different isomeric species. C<sup>^</sup>N compounds containing a nitrogen atom, which can act as a directing group, will be chosen as ligands; this means that the ligand used is able to act as a C–H bond functionalisation substrate.

Since most Pd-catalysed C–H bond functionalisation processes are believed to proceed *via* cyclopalladation of the organic substrate to form a metallocyclic intermediate, we anticipate that complexes already containing the relevant C<sup>^</sup>N backbone could make excellent catalysts. With this in mind, all of the complexes prepared will be tested as precatalysts in C–H bond functionalisation reactions of organic substrates, initially under the redox co-catalysis conditions described by Sanford.<sup>30</sup> In order to investigate the potential role of nitrite or nitrate as an active ligand, complexes containing NO<sub>2</sub> or NO<sub>3</sub> ligands will be employed as catalysts both in the presence and absence of a sodium nitrate additive. The effect of varying the other ligands present will also be probed. For example, is there a significant effect on catalyst activity when changing from a phosphine ligand to a more labile acetonitrile ligand? Based on Sanford's results, which found that sp<sup>2</sup> C–H bonds were significantly less likely to undergo functionalisation reactions than sp<sup>3</sup> C–H bonds, 8-methylquinoline will be used as a model substrate; the presence of both a nitrogen directing group and a methyl group containing three sp<sup>3</sup> C–H bonds make it an ideal candidate.

Lastly, a series of thorough mechanistic investigations will be conducted, with two main aims. Firstly, we aim to elucidate the role played by nitrite in systems involving a Pd catalyst along with a source of nitrite. Is it simply acting as an oxidant, allowing access to high

oxidation state Pd intermediates, or does it have a more active role, such as that proposed for the acetoxylation of alkenes?<sup>38</sup> Isotopic labelling experiments such as those conducted by Heumann and Bäckvall will be conducted to establish whether the nitrite could in fact be the source of the carbonyl oxygen atom in the acetoxyated product. The stability of the various isomeric forms of nitrite complexes of Pd will also be probed, through the use of DFT calculations, as well as by submitting the complexes to reactions assessing their ability to undergo reductive elimination to form useful C–NO<sub>2</sub> species.

Secondly, our attention will focus on the identification of intermediate species in C–H bond functionalisation reactions catalysed by our newly-prepared complexes with the use of real time NMR spectroscopy experiments. We hope that these methods will allow for the observation and characterisation of intermediate Pd complexes. Given the oxidative conditions under which the reactions will be taking place, we believe that the mechanism of catalysis will proceed *via* high oxidation state Pd species. However, an important question is whether the key catalytic intermediates are Pd<sup>III</sup> or Pd<sup>IV</sup> species. Attempts will be made to isolate such complexes *via* procedures described by Ritter and Sanford.<sup>68,69</sup> All the experimental results of our mechanistic investigations will be supported by DFT studies.

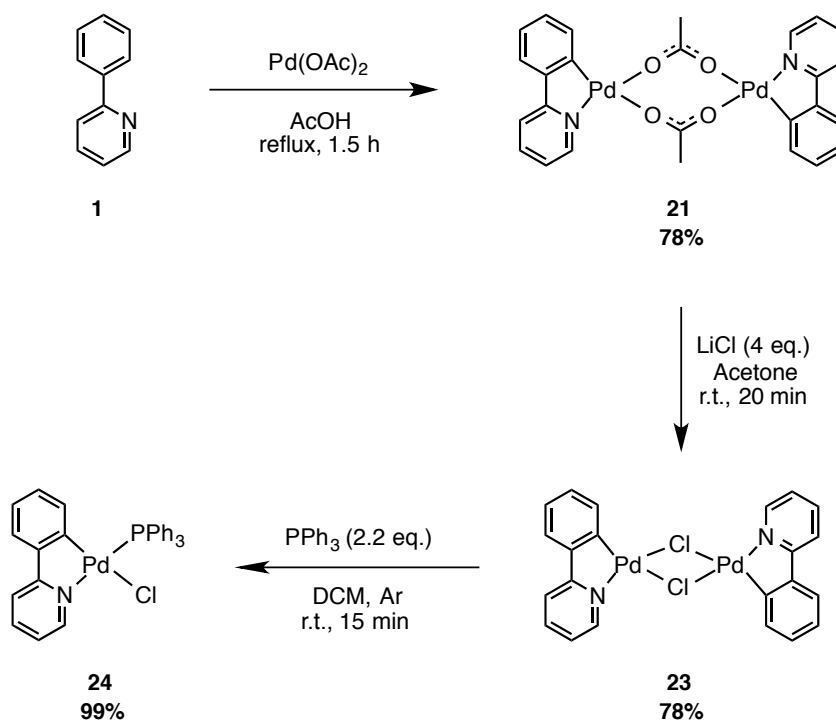


## Chapter 2: Synthesis and Characterisation of Cyclopalladated C<sup>N</sup> Complexes

The first aim of the project was the synthesis of Pd complexes containing nitrite or nitrate ligands, which could later be used as catalysts, *via* the cyclopalladation of C<sup>N</sup> organic compounds.

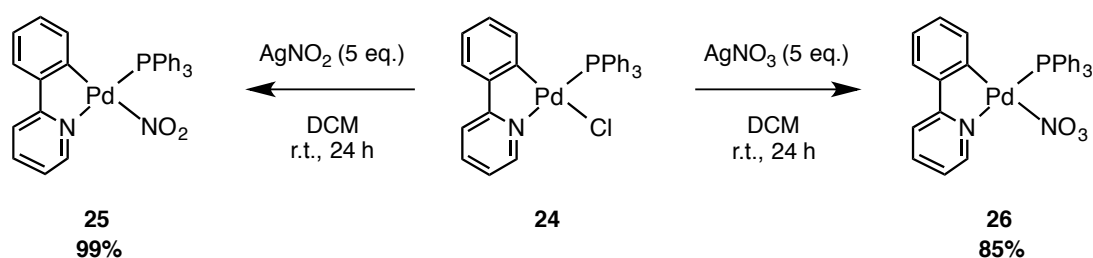
### C<sup>N</sup> Palladacyclic Complexes of 2-Phenylpyridine

Initially, a series of complexes were prepared using 2-phenylpyridine (**1**) as the C<sup>N</sup> ligand, since ongoing work within the Fairlamb group, and indeed several other groups,<sup>70-72</sup> has shown that the synthesis of several of its cyclopalladated derivatives proceeds in good to excellent yields *via* the reaction pathway shown in Scheme 35. The acetato-bridged dimer **21** was prepared by the reaction of 2-phenylpyridine with Pd(OAc)<sub>2</sub> in acetic acid, following a procedure described by Hiraki and co-workers.<sup>70</sup> Treatment with an excess of lithium chloride afforded the insoluble chlorido-bridged dimer **23**, which was then converted to the phosphine monomer **24** *via* addition of triphenylphosphine.<sup>72</sup>



**Scheme 35:** Synthesis of Palladacyclic Complexes of 2-Phenylpyridine

One of the key project aims was to identify whether any Pd–NO<sub>2</sub> or Pd–NO<sub>3</sub> species are present in oxidative C–H bond functionalisation processes and to investigate the role that they play at Pd in the catalytic chemistry. If C<sup>∧</sup>N complexes with nitrite and nitrate ligands do influence the reactivity of intermediates within the catalytic cycle, then their independent synthesis and characterisation could be important in defining a more specific role to the active ligands. Additionally, such complexes may be catalytically competent species in their own right. With this in mind, novel complexes **25** and **26** were prepared in excellent yield from the reaction of **24** with either silver nitrite or silver nitrate (Scheme 36).



**Scheme 36:** Synthesis of Novel Complexes of 2-Phenylpyridine

Selected examples have been characterised by single crystal X-ray diffraction, and the structures of all complexes prepared have been confirmed by LIFDI-MS and IR and NMR spectroscopic analysis. For **25** and **26**, LIFDI-MS showed peaks for the complexes without the NO<sub>2</sub> or NO<sub>3</sub> anionic ligands. The infrared spectra, however, allow us to confirm the presence of the ligands. The NO<sub>2</sub> anionic ligand gives rise to a peak at 1335 cm<sup>-1</sup>, and a characteristic Pd–NO<sub>2</sub> stretch is observed between 325 cm<sup>-1</sup> and 375 cm<sup>-1</sup>. These values are in keeping with those reported by Nonoyama and co-workers.<sup>43</sup> The Pd–NO<sub>3</sub> stretch in **26** appears at a slightly higher frequency, producing a peak at around 370 cm<sup>-1</sup>, compared to 347 cm<sup>-1</sup> in **25**.

For compounds where single crystal growth was difficult to achieve, the <sup>1</sup>H NMR chemical shift of the proton α- to the nitrogen atom of the pyridine ring proved a useful diagnostic tool when following the transformations between complexes. For example, the shielding/deshielding effects of the ligand *cis*- to the Pd–N bond can be seen in Figure 4, where changing a chloride ligand to a nitrate ligand causes an upfield shift of over 1 ppm, from 9.62 ppm to 8.51 ppm.

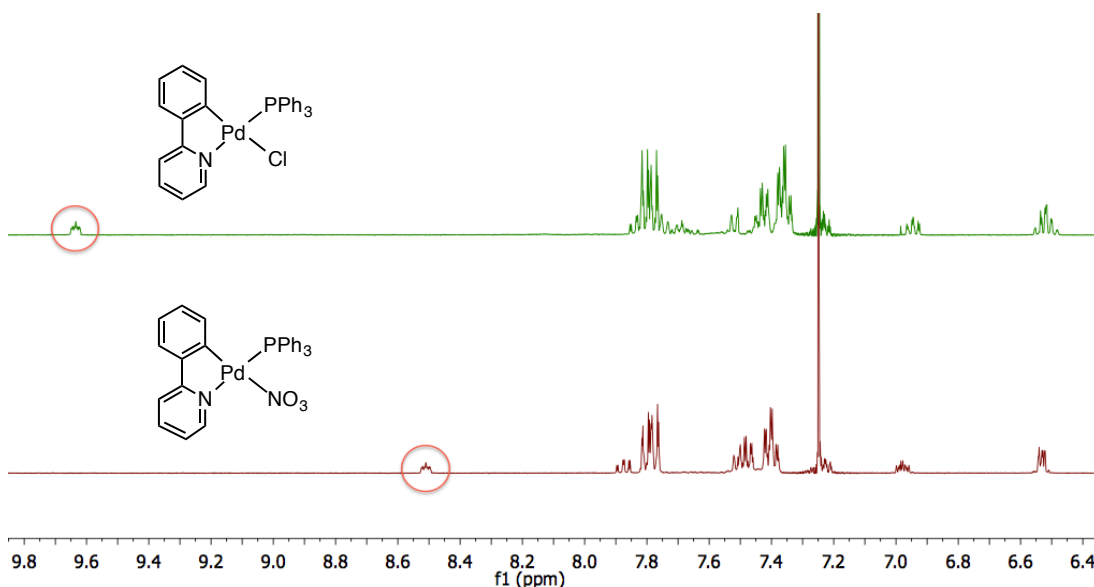


**Figure 4:** Comparison of the  $^1\text{H}$  NMR spectra of **24** and **26**

Kleinpeter and co-workers have used *ab initio* calculations to explain the origin of the shielding effect.<sup>73</sup> Calculating the shielding surface of the planar  $\text{NO}_3^-$  anion showed that the regions above and below the plane of the nitrate anion are exposed to an upfield shift, whereas the area in the plane of the anion is deshielded. The structures of  $\text{Pd}^{\text{II}}$  complexes containing mutually *cis*  $\text{NO}_3$  and pyridine ligands were calculated and the shielding surface plotted (Figure 5, right), which showed that the proton  $\alpha$ - to the pyridyl nitrogen atom is within the shielding region of the  $\text{NO}_3$  ligand. These theoretical results explain the upfield chemical shift observed in the experimentally prepared complexes containing  $\text{NO}_3$  ligands.

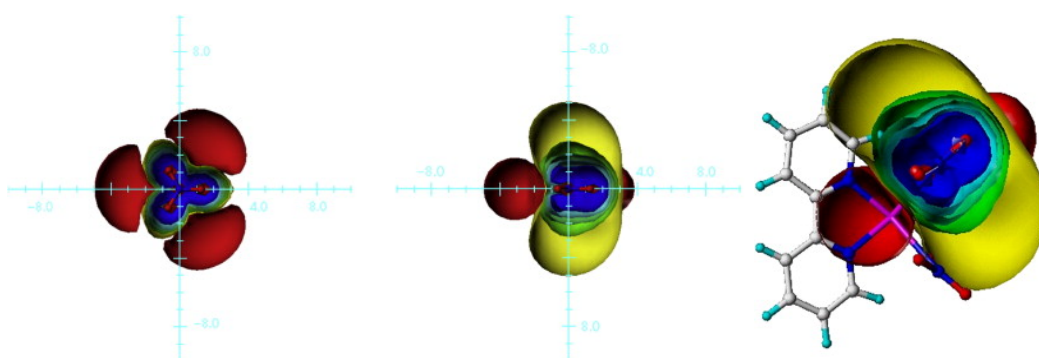


**Figure 5:** Visualisation of the shielding surface of the nitrate anion. Blue, green and yellow represent shielding regions; red represents deshielding regions.

Reprinted from *Tetrahedron*, 64, Kleinpeter et al., ‘Anisotropic effect of the nitrate anion-manifestation of diamagnetic proton chemical shifts in the  $^1\text{H}$  NMR spectra of  $\text{NO}_3^-$ -coordinated complexes’, 5044–5050, Copyright (2008), with permission from Elsevier.

## Geometry and Linkage Isomerism in Pd–NO<sub>2</sub> and Pd–ONO Species

For novel compounds **25** and **26**, crystals suitable for X-ray diffraction were grown from layering a solution of dichloromethane with cyclohexene (anti-solvent); the single crystal structures obtained are displayed in Figure 6. These confirmed that both nitrite and nitrate anionic ligands occupy the coordination site *trans*- to the Pd–C bond. In the crystal structure of **25**, a mixture of Pd–NO<sub>2</sub> and Pd–ONO isomers of the nitrite ligand is observed.

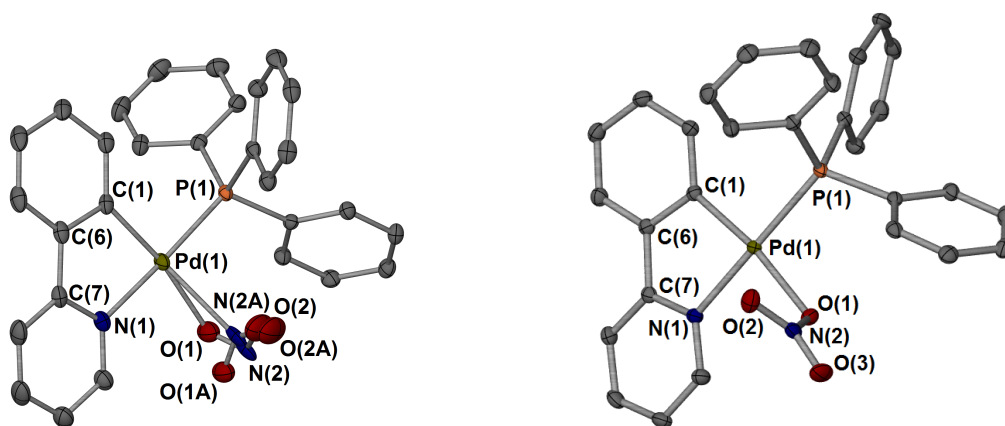


**Figure 6:** Crystal Structures of Complexes **25** and **26**

**Selected bond lengths for 25 (Å):** Pd(1)–C(1) 1.9900 (18), Pd(1)–N(1) 2.0818 (14), Pd(1)–O(1) 2.1250 (13), Pd(1)–P(1) 2.2725 (4)

**Selected bond lengths for 26 (Å):** Pd(1)–C(1) 2.003 (2), Pd(1)–N(1) 2.0653 (19), Pd(1)–N(2A) 2.39 (3), Pd(1)–O(1) 2.112 (2), Pd(1)–P(1) 2.2473 (6)

There is already a precedent for nitro/nitrito linkage isomerization in transition metal complexes; Raithby and co-workers have reported photocatalysed linkage isomerization of the nitrite ligand in [Ni(dppe)( $\eta^1$ -ONO)Cl].<sup>74,75</sup> The first nitro/nitrito linkage isomerization at Pd<sup>II</sup> was reported recently by Fairlamb and co-workers.<sup>40</sup> Upon excitation from 400 nm light at 150 K, a 1:3 mixture of Pd– $\eta^1$ -NO<sub>2</sub> and Pd– $\eta^1$ -ONO linkage isomers of Pd( $\eta^1$ -ONO)(C<sup>N</sup>)PPh<sub>3</sub> (C<sup>N</sup> = papaverine) converted fully to the Pd– $\eta^1$ -ONO species (Figure 7). Determination of the crystal structure after irradiation confirmed that this was the only isomer present, and in fact that it was stable at the conditions described.

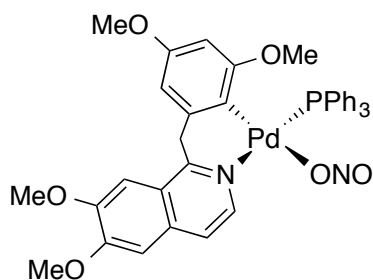


**Figure 7:** Crystallographically-determined structure of  $\text{Pd}(\eta^1\text{-ONO})(\text{C}^{\wedge}\text{N})\text{PPh}_3$  ( $\text{C}^{\wedge}\text{N}$  = papaverine) after UV irradiation (1 h) of a mixture of  $\text{NO}_2$ - and  $\text{ONO}$ -bound linkage isomers.<sup>40</sup>

Since complexes **25** and **26** were prepared for their use as precatalytic species, their *cis/trans* geometry and the preferred linkage isomerism of the nitrite ligand could be of great significance. In a catalytic system, the likelihood of the nitrite ligand to undergo reductive elimination, along with an organic substrate, to form  $\text{C-NO}_2$  or  $\text{C-ONO}$  products, could be determined by the relative geometry of the  $\text{Pd-C}$  and  $\text{Pd-NO}_2/\text{ONO}$  bonds; typically the two anionic ligands would need to be *cis*- to each other in order for reductive elimination to occur. Additionally, the stability of  $\text{Pd-NO}_2$  or  $\text{Pd-ONO}$  species could determine whether the ligand is likely to become involved in reductive elimination or will act solely as a spectator ligand.

In order to probe the anticipated stability of the  $\text{Pd-NO}_2$  or  $\text{Pd-ONO}$  forms of the nitrite ligand, it was decided to compare our observations with theoretically-determined values. Density functional theory (DFT) calculations were conducted by Dr. Jason Lynam to deduce single point energies at 298 K for the *O*-bound and *N*-bound isomers of  $[\text{Pd}(\text{C}^{\wedge}\text{N})(\text{NO}_2)\text{PPh}_3]$ , where  $\text{C}^{\wedge}\text{N}$  = 2-phenylpyridine, 2-benzylpyridine or 2-phenylethylpyridine; previous work within the Fairlamb group has involved the preparation of  $\text{C}^{\wedge}\text{N}$  complexes of 2-benzylpyridine, which contains a 6-membered palladacycle, and it was thought that varying the length of the alkyl chain between the two rings would facilitate examination of analogues of the 2-phenylpyridine complexes which possess similar electronic properties but vary in their steric bulk. Calculations were also performed on *cis*- and *trans*- isomers. The Gibbs free energies of each complex at the pbe0/TZVPP level of theory are shown in Figure 8.

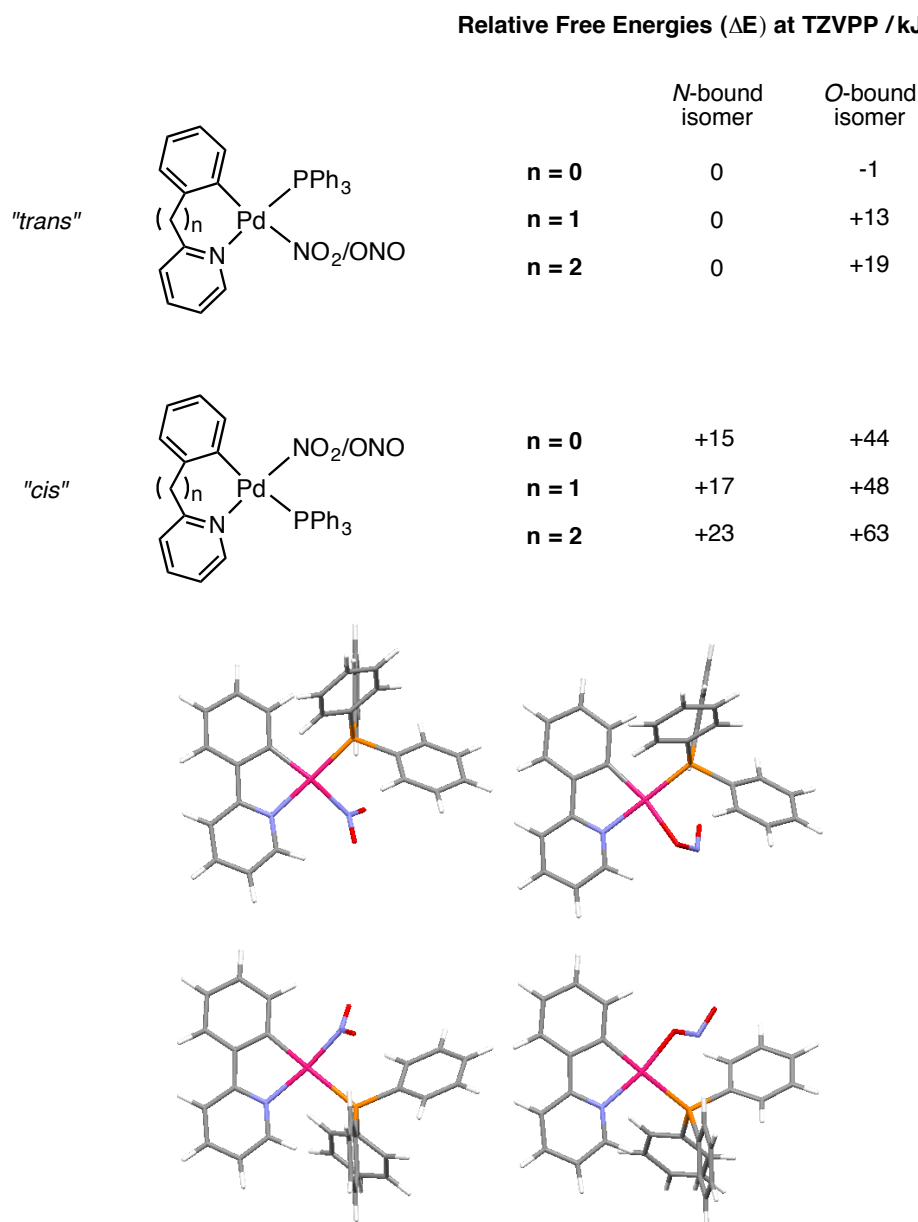


**Figure 8:** Single point energies of complexes of the type  $[\text{Pd}(\text{C}^{\wedge}\text{N})(\text{NO}_2)\text{PPh}_3]$  performed at the TZVPP level of theory, along with optimised geometries for complexes of 2-phenylpyridine.

For complexes of 2-phenylpyridine, DFT results showed that when the nitrite ligand occupies a position *cis*- to the Pd–C bond, the *O*-bound isomer is 29 kJ mol<sup>-1</sup> higher in energy than the *N*-bound isomer. Since a *cis*-geometry is typically required for reductive elimination, these values suggest that in any species that is set-up for reductive elimination, the nitrite ligand would be likely to be bound through the nitrogen atom. However, the crystal structure of **25** showed that the nitrite ligand is in fact *trans*- to the Pd–C bond. For this geometry, the DFT results showed that the difference in free energy between *O*- and *N*-

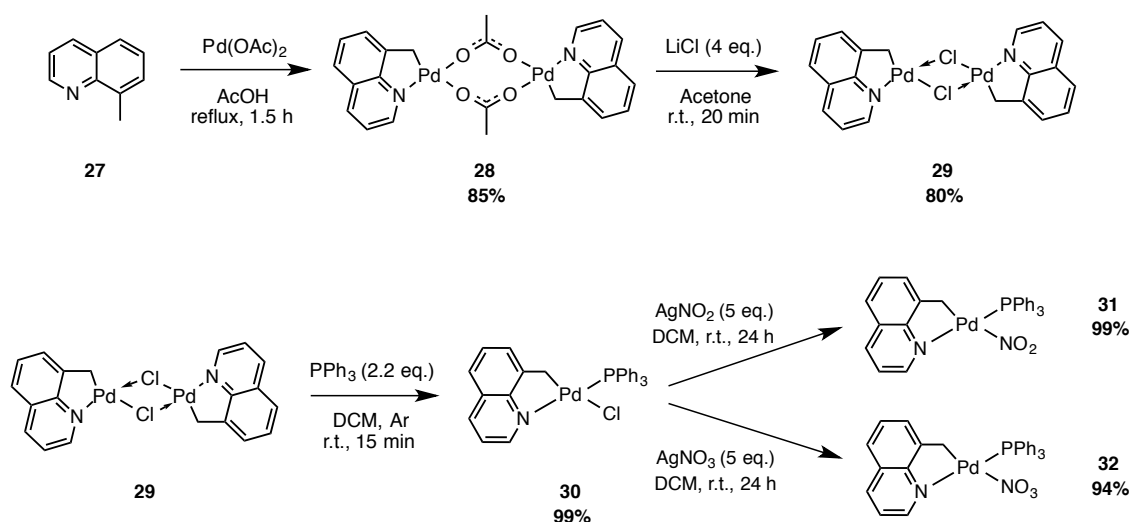
bound forms of the complex is negligible. This outcome is consistent with the mixture of isomers observed in the X-ray single crystal structure.

For the *trans*- isomer, as the length of the alkyl linker, and therefore the steric bulk of the C<sup>^</sup>N ligand, increases, the *O*-bound isomer was found to increase in energy, whereas the Gibbs free energy of the *N*-bound isomer remained constant. This may suggest that the *N*-bound form of the nitrite ligand has less steric clash with the neighbouring ligands, and therefore is preferred over the *O*-bound form when a bulky C<sup>^</sup>N ligand is present. A similar effect is observed for the *cis*- geometric isomer. Both *N*- and *O*-bound isomers were found to increase in energy with increasingly bulky C<sup>^</sup>N ligands, but the *O*-bound isomer is destabilised to a greater extent; when C<sup>^</sup>N = 2-phenylpyridine, the difference in free energy of the two linkage isomers is 29 kJ mol<sup>-1</sup>, but this Gibbs free energy difference increases to 40 kJ mol<sup>-1</sup> when the C<sup>^</sup>N ligand is the bulky 2-phenylethylpyridine.

### **C<sup>^</sup>N Palladacyclic Complexes of 8-Methylquinoline**

2-Phenylpyridine has previously been shown to be a good model substrate for Pd-catalysed oxidative C–H bond functionalisation processes, probably due to its excellent ability to form 5-membered palladacyclic complexes which can act as important reaction intermediates.<sup>21,68</sup> However, when subjected to Sanford's redox co-catalytic conditions, 2-phenylpyridine was found to remain unreacted.<sup>30</sup> This was an interesting result, since the functionalisation of sp<sup>2</sup> C–H bonds is generally viewed as less challenging than the functionalisation of unactivated sp<sup>3</sup> C–H bonds using conventional co-catalysts such as Pd(OAc)<sub>2</sub>.<sup>10</sup> In order to fully elucidate the mechanism of systems where nitrate is acting as a co-catalyst, it was decided to prepare a range of cyclopalladated complexes, analogous to those prepared with 2-phenylpyridine, with C<sup>^</sup>N ligands that could undergo C–H bond functionalisation reactions under such conditions. With this in mind, many of the other substrates used in Sanford's study were considered.

One substrate that had successfully undergone C–H bond functionalisation in the presence of NaNO<sub>3</sub> was 8-methylquinoline (**27**), which is commercially available and relatively inexpensive. Several palladacycles were therefore prepared with 8-methylquinoline as the C<sup>^</sup>N backbone (Scheme 37).



**Scheme 37:** Synthesis of Palladacyclic Complexes of 8-Methylquinoline

The  $sp^3$  C–H acetoxylation of organic substrates has been proposed to proceed *via* a  $Pd^{II}/Pd^{IV}$  catalytic cycle,<sup>21,23,76</sup> and previous work into  $Pd^{IV}$  chemistry has suggested that the presence of a phosphine ligand in oxidative processes can slow down catalysis.<sup>59</sup> Canty and co-workers isolated and characterised a range of unstable  $Pd^{IV}$  complexes containing phosphine ligands, and demonstrated that their stability decreases in the order  $PMe_2Ph > PMePh_2 > PPh_3$  (Figure 9).<sup>77</sup> This suggests that although  $Pd^{IV}$  complexes of triphenylphosphine may be well set up for reductive elimination, their formation *via* oxidative addition to a  $Pd^{II}$  species may be highly disfavoured, providing a large energy barrier in the catalytic cycle.

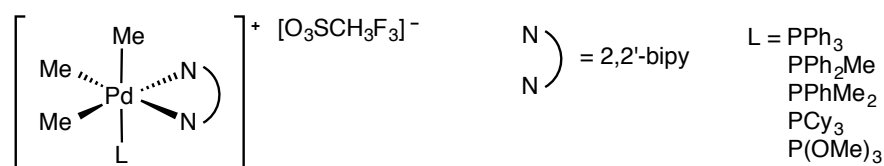
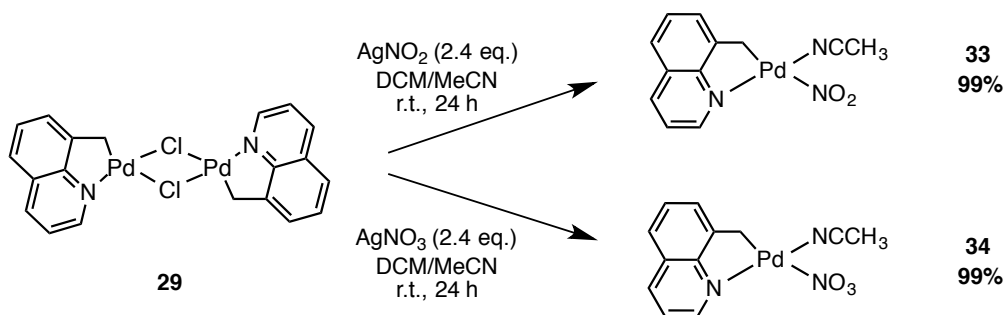


**Figure 9:**  $Pd^{IV}$  Complexes Prepared by Canty

One of the key incentives for the preparation of C<sup>^</sup>N complexes based on 8-methylquinoline was the investigation of their use as precatalysts, so the design of species which could be catalytically viable was an important requirement. It was thought that the use of an alternative coordinating ligand might accelerate catalysis. For this reason, novel  $Pd^{II}$  complexes **33** and **34**, analogues of the monomeric phosphine complexes, were prepared from the chloride-bridged dimer **29** (Scheme 38); it was thought that the increased lability of



the acetonitrile ligand compared to triphenylphosphine could lead to complexes having higher catalytic efficacy.



**Scheme 38:** Synthesis of Novel Acetonitrile Complexes

Analogues of compounds **33** and **34** had previously been prepared by Nonoyama and co-workers, who used 2-(2-pyridyl)benzo[*b*]furan (Hpbf) or 1-(2-pyridyl)indole (Hpyi) as the C<sup>^</sup>N backbone for complexes of the type [Pd(C<sup>^</sup>N)(NCCH<sub>3</sub>)NO<sub>2</sub>] or [Pd(C<sup>^</sup>N)(DMSO)NO<sub>2</sub>] (Figure 10).<sup>43</sup>

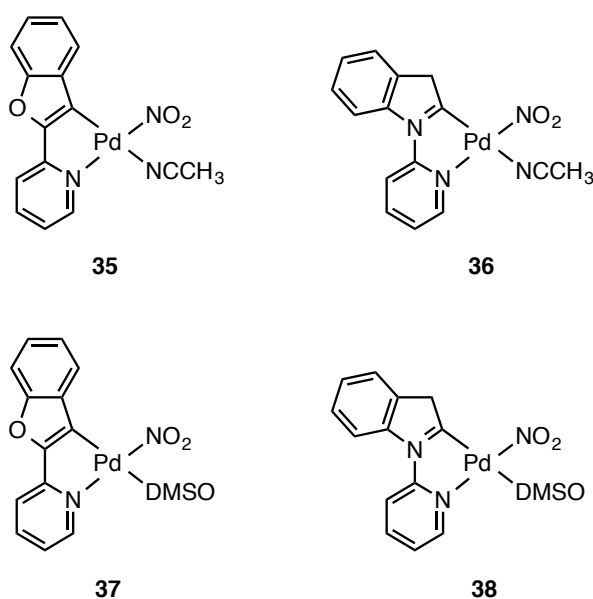


**Figure 10:** Complexes of Hpbf and Hpyi prepared by Nonoyama and co-workers

While their synthesis was unintentional and likely to have been due to the unexpected presence of nitrite in the reaction system, as indicated by Fairlamb's study with papaverine,<sup>40</sup> X-ray diffraction studies showed DMSO adducts of the complexes to have a geometry where the NO<sub>2</sub> ligand is *cis*- to the Pd–C bond. This was an interesting result; in a

square planar Pd<sup>II</sup> complex, an anionic NO<sub>2</sub> ligand would often be expected to occupy the position *trans*- to the Pd–C bond. However, the isolation of a complex with *cis*- geometry could have important implications. As well as achieving C–H functionalisation *via* acetoxylation of sp<sup>3</sup> substrates, another aim was to assess the potential for the synthesis of nitrated products *via* reductive elimination from square planar Pd complexes. Liu and co-workers have recently demonstrated that aromatic nitration is possible in Pd-catalysed systems proceeding *via* either a Pd<sup>II/III</sup> or Pd<sup>II/IV</sup> pathway.<sup>78</sup> A global aim for the project was to examine the possibility of C–N bond-forming reductive elimination from Pd<sup>II</sup>. This sort of process will occur when the two ligands to be eliminated are *cis*- to one another. However, *cis/trans* isomerization processes are often too slow or energetically disfavoured to occur readily, meaning that other techniques, such as the introduction of a sterically-bulky phosphine, to form a 3-coordinate Pd<sup>II</sup> species,<sup>79</sup> need to be employed in order to make reductive elimination from Pd<sup>II</sup> feasible. The preparation of complexes where the two relevant ligands are already arranged in the *cis*-geometry may allow reductive elimination to occur under milder conditions.

Since crystal growth of complexes **33** and **34** proved difficult, DFT calculations were used again, in order to gain an idea of the likely *cis/trans* geometry of the two complexes, as well as the nitrite linkage isomerism in **33**. Figure 11 shows the free energies in kJ mol<sup>-1</sup> at the TZVPP level of theory for the different isomeric forms of complexes **33** and **34**.

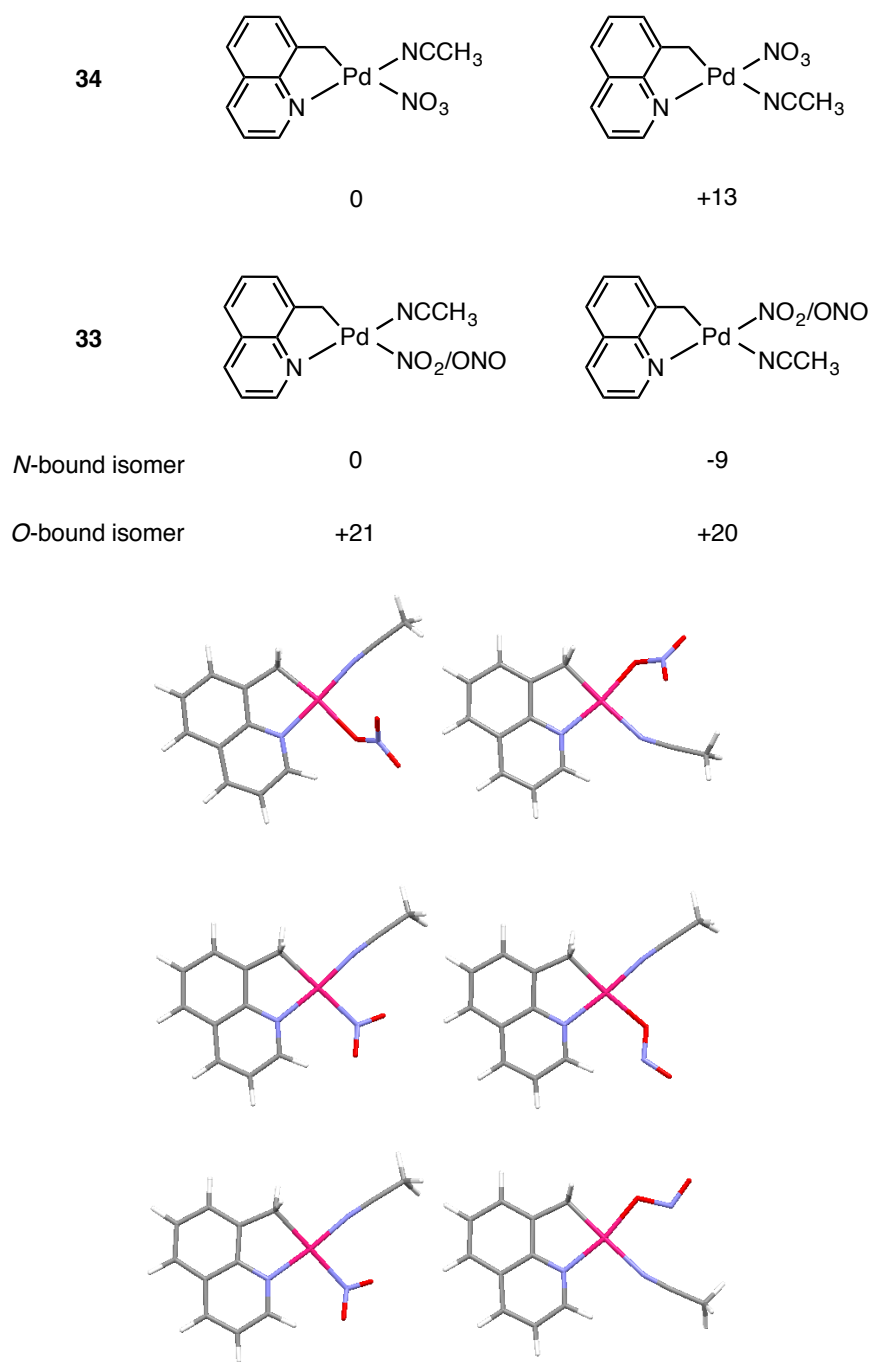


**Figure 11:** Single Point Energies for Isomeric Forms of Novel Complexes **33** and **34**, and their Optimised Geometries

For the nitrate complex **34**, the “*trans*” geometric isomer is again the more stable complex. For complex **33**, calculations showed the complex to be more stable when the nitrite ligand is bound through the nitrogen atom. Interestingly, for the *N*-bound linkage isomer, the “*cis*” geometric isomer is more stable by 9 kJ mol<sup>-1</sup>, whereas for the phosphine complexes of 2-phenylpyridine, it was found to be higher in energy. This could have important implications in our planned investigations into reductive elimination from Pd<sup>II</sup> species. While 9 kJ mol<sup>-1</sup>

still represents a relatively small change in free energy, and therefore is unlikely to indicate that the complex exists with exclusively this geometry rather than as a mixture of isomers, the increased stability of the “*cis*” bound isomer could make the complex a good candidate for inducing useful C–NO<sub>2</sub> bond-forming reductive elimination. One key question is whether this can occur with a small, labile ligand such as acetonitrile, or whether the addition of a phosphine ligand is required to introduce sufficient steric bulk to the complex.

### C<sup>^</sup>N Palladacyclic Complexes of 2-(2-Pyridyl)benzo[*b*]furan

Complexes **35** and **36**, prepared by Nonoyama and co-workers, were of great interest to this project, not just because of their unusual geometry but because of the unexpected formation of the nitrite ligands observed.<sup>43</sup> The balanced full and half equations proposed by Nonoyama for the complexes' formation were correct. However, it is unlikely that CH<sub>3</sub>CN can be oxidized to NO<sub>2</sub> anion under the conditions described (heating to 600 °C with a Cu metal surface is needed for this kind of transformation). Moreover, the recent results from the Fairlamb group suggested that they could be accounted for by the presence of nitrite contaminants in commercial Pd(OAc)<sub>2</sub>.<sup>40</sup> It was proposed that attempts to repeat the reported procedure could shed light on the source of the nitrite ligand.

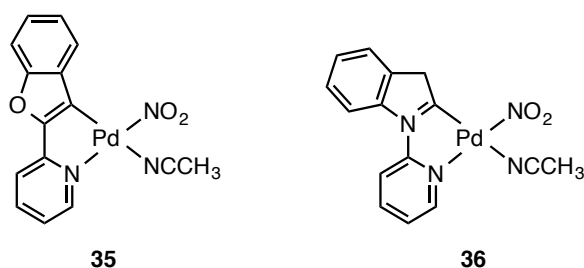
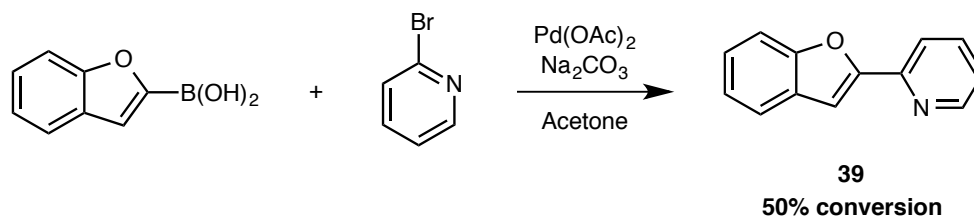


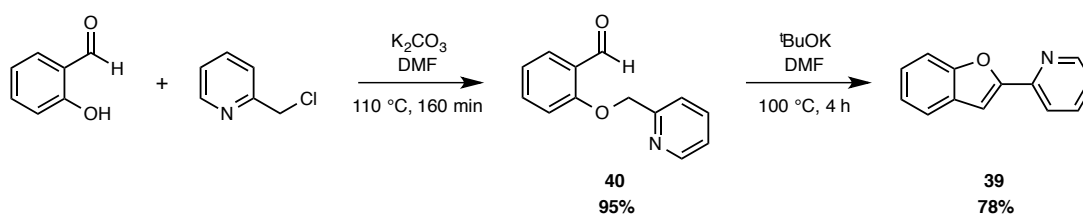
**Figure 12:** “*cis*” Pd–NO<sub>2</sub> Complexes Prepared by Nonoyama and co-workers.

For this endeavor, the C<sup>^</sup>N ligands needed to be prepared first. Initial attempts to prepare the 2-(2-pyridyl)benzo[*b*]furan ligand **39** *via* the Suzuki coupling of 2-bromopyridine and 2-phenylbenzo[*b*]furan (Scheme 39) met with limited success.<sup>80</sup> While quantitative mass recovery was achieved, the reaction proceeded with 50% conversion, with purification by column chromatography proving difficult.



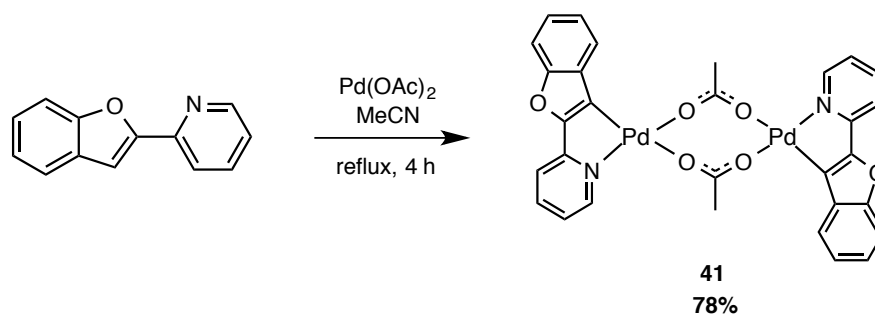
**Scheme 39:** Synthesis of Hpbf *via* Suzuki Coupling

The synthesis described by Nonoyama and co-workers, a two-step procedure involving a Williamson ether synthesis to form the benzaldehyde intermediate followed by a base-assisted ring closure, proceeded in overall 75% yield and the product was easily purified by flash column chromatography on silica gel (Scheme 40).



**Scheme 40:** Two-Step Synthesis of Hpbf Ligand

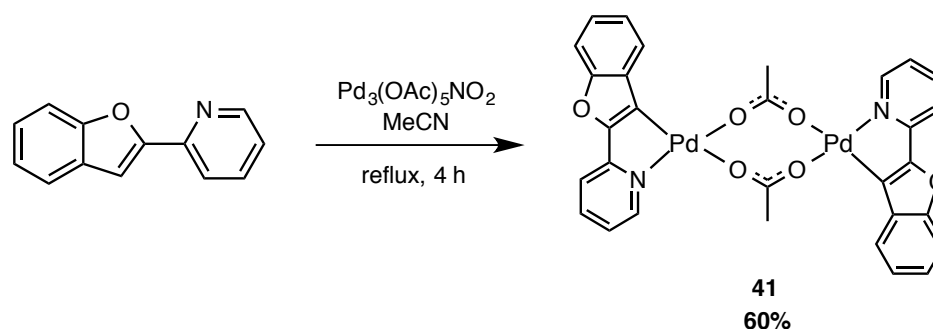
With one of the relevant ligands prepared in good yield, it was decided to attempt to repeat the synthesis of one of Nonoyama's complexes. The  $[(C^{\wedge}N)Pd(NO_2)(NCCH_3)]$  complex **35** had been prepared by Nonoyama through reaction of the  $C^{\wedge}N$  ligand with ultra-pure  $Pd(OAc)_2$  (>99.9 % purity from Precious Metals Online, Monash, Australia) in acetonitrile. This procedure was repeated but, as expected, yielded only the acetato-bridged dimer **41** (Scheme 41).



**Scheme 41:** Synthesis of the Acetato-Bridged Dimer of Hpbfb

Prior to the reaction taking place,  $^1\text{H}$  NMR spectroscopic analysis of the  $\text{Pd}(\text{OAc})_2$  showed that the sample was free of nitrite contaminants.  $^1\text{H}$  NMR spectroscopic analysis of the product showed only one methyl resonance, whereas the loss of symmetry upon formation of  $\text{Pd}_3(\text{OAc})_5(\text{NO}_2)$  causes five methyl environments to be observed. Additionally, the infrared spectrum did not show a  $\text{Pd}-\text{NO}_2$  stretch; Nonoyama reported a stretching frequency at  $325\text{ cm}^{-1}$ , which was not observed here.

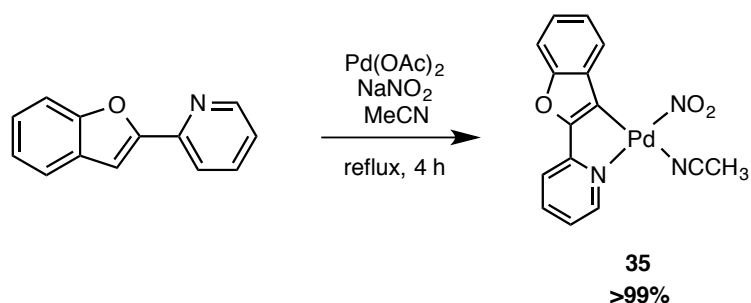
The lack of any nitrite group in the product of a reaction taking place under Nonoyama's conditions pointed towards the idea that complexes **35** and **37** had been formed due to some sort of impurity. In order to test this theory, the reaction was repeated using a batch of  $\text{Pd}(\text{OAc})_2$  that was known to contain nitrite impurities. Through  $^1\text{H}$  NMR spectroscopic analysis, the sample was calculated to contain approximately 81%  $\text{Pd}_3(\text{OAc})_5\text{NO}_2$ .<sup>40</sup> Interestingly, when subjected to the same reaction conditions as described above, once again only formation of the acetato-bridged dimer **41** was observed (Scheme 42).



**Scheme 42:** Reaction of Hpbfb Ligand with  $\text{Pd}_3(\text{OAc})_5\text{NO}_2$

While  $^1\text{H}$  NMR spectroscopic analysis of the product showed a more complicated spectrum than that of the product isolated from the reaction with spectroscopically pure  $\text{Pd}(\text{OAc})_2$  (>99.9% purity), only one set of peaks corresponding to the Hpbf ligand was observed; these corresponded to those present in the authentic sample of **41**, and thus the impurity peaks in the spectrum were attributed to unreacted  $\text{Pd}_3(\text{OAc})_5\text{NO}_2$ . Moreover, LIFDI-MS analysis showed only the presence of **41** ( $m/z$  719.96 [ $\text{M}^+$ ]).

In order to confirm that none of Nonoyama's  $[(\text{C}^{\wedge}\text{N})\text{Pd}(\text{NO}_2)(\text{NCCH}_3)]$  complex **35** had been formed, an authentic sample of the complex was prepared for comparison. Addition of sodium nitrite to the reaction conditions specified in Scheme 43 resulted in the formation of **35** in quantitative yield.



**Scheme 43:** Synthesis of an Authentic Sample of **35**

The structure of **35** was confirmed by  $^1\text{H}$  NMR spectroscopic analysis and as such it was confirmed that the reaction of Hpbf with a contaminated sample of  $\text{Pd}(\text{OAc})_2$  did not lead to the formation of **35**; the characteristic  $\text{Pd}-\text{NO}_2$  stretch at  $327\text{ cm}^{-1}$  observed in the infrared spectrum of an authentic sample was not observed. Despite this result, the idea that the formation of **35** observed by Nonoyama and co-workers was due to the presence of nitrite cannot be ruled out. For example, the ratio of  $\text{NO}_2$  to  $\text{OAc}$  ligands in Nonoyama's sample could have been much higher than the 1:5 ratio found in Fairlamb's study. The successful preparation of an authentic sample of **35** upon addition of a nitrite source suggests that its formation in a system containing free nitrite ligands is feasible. In this study, only one contaminated sample was tested; in the future, investigations involving the use of an authentic sample of  $\text{Pd}_3(\text{OAc})_n(\text{NO}_2)_x$ , where  $x = 6-n$ , could provide further clarification. For example, when exposed to a contaminated sample of " $\text{Pd}(\text{OAc})_2$ ", the dimeric compound **41** was formed in only moderate yield. The mixture of Pd species present in the complex used could introduce an element of competition, meaning that the possibility remains that the Hpbf ligand reacts preferentially with  $\text{Pd}(\text{OAc})_2$  over  $\text{Pd}_3(\text{OAc})_5\text{NO}_2$ .

In the same study by Fairlamb and co-workers,  $\text{Pd}_3(\text{OAc})_5\text{NO}_2$  has been shown to exhibit catalytic activity comparable to that of  $\text{Pd}(\text{OAc})_2$  in the C2-arylation of indole. With this in mind, the newly-prepared complexes **41** and **35** make excellent candidates for screening as potential precatalysts. Moreover, the nitrite ligand in  $\text{Pd}_3(\text{OAc})_5\text{NO}_2$  has been proposed to act as a spectator ligand, *i.e.* it will not undergo reductive elimination to form C–NO<sub>2</sub> species; this has not been proven, however, and stoichiometric reductive elimination experiments from complex **35** may provide further elucidation of the role played by the nitrite ligand.

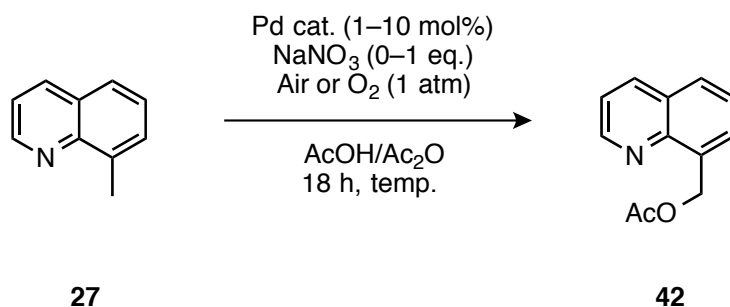


## Chapter 3: C<sup>N</sup> Palladacyclic Complexes as Precatalysts for Oxidative C–H Bond Functionalisation Processes

Having successfully prepared a series of Pd<sup>II</sup> complexes with C<sup>N</sup> backbones, attention was turned to employing them as catalytic Pd sources for oxidative C–H functionalisation processes, similar to those reported by Sanford.<sup>30</sup> Since 8-methylquinoline had been successfully used as a ligand in the preparation of C<sup>N</sup> palladacyclic complexes, it made an ideal substrate choice for screening purposes.

### C–H Acetoxylation of 8-Methylquinoline

Using 8-methylquinoline as a model substrate, and the C–H acetoxylation reaction outlined in Scheme 44, the catalytic efficacy of the precatalysts **28** and **31–34** was examined.



**Scheme 44:** Acetoxylation of 8-Methylquinoline

The structures of the five palladacyclic complexes of 8-methylquinoline are shown overleaf (Figure 13). The acetato-bridged dimer **28** was used, since it seemed likely that it could form monomeric intermediate species similar to those formed in the Pd(OAc)<sub>2</sub>-catalysed system. Complexes **31–34**, containing either NO<sub>2</sub> or NO<sub>3</sub> anionic ligands, were also screened in order to assess the viability of Pd–NO<sub>2</sub> species as catalytic intermediates.

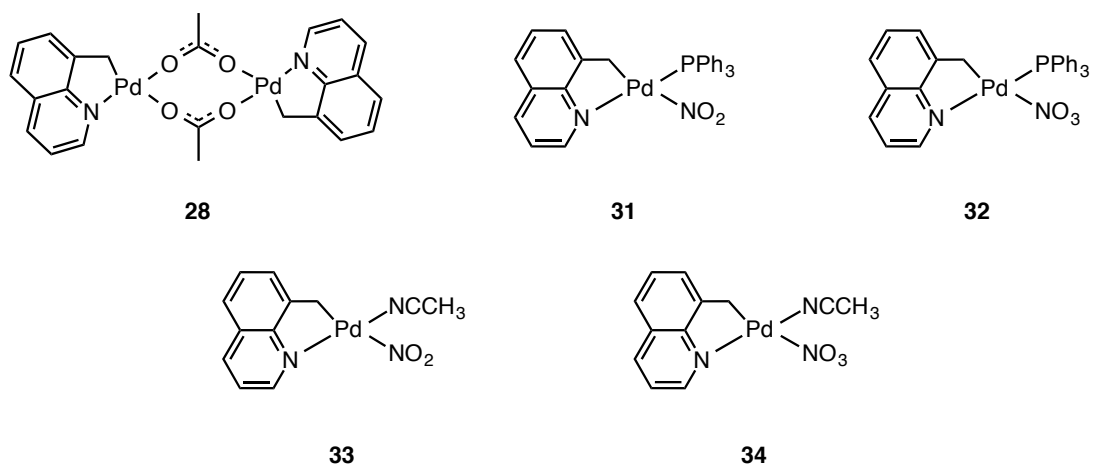


**Figure 13:** Complexes of 8-Methylquinoline Used as Precatalysts

Using the literature conditions of 5 mol% Pd catalyst (the variable),<sup>30</sup> 1 equivalent of NaNO<sub>3</sub> (with respect to the substrate), and a temperature of 110 °C, all complexes examined catalysed the reaction in good to excellent yields (Table 1).

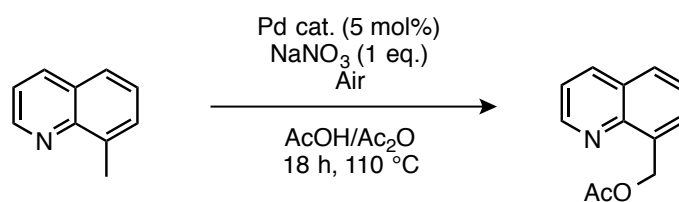
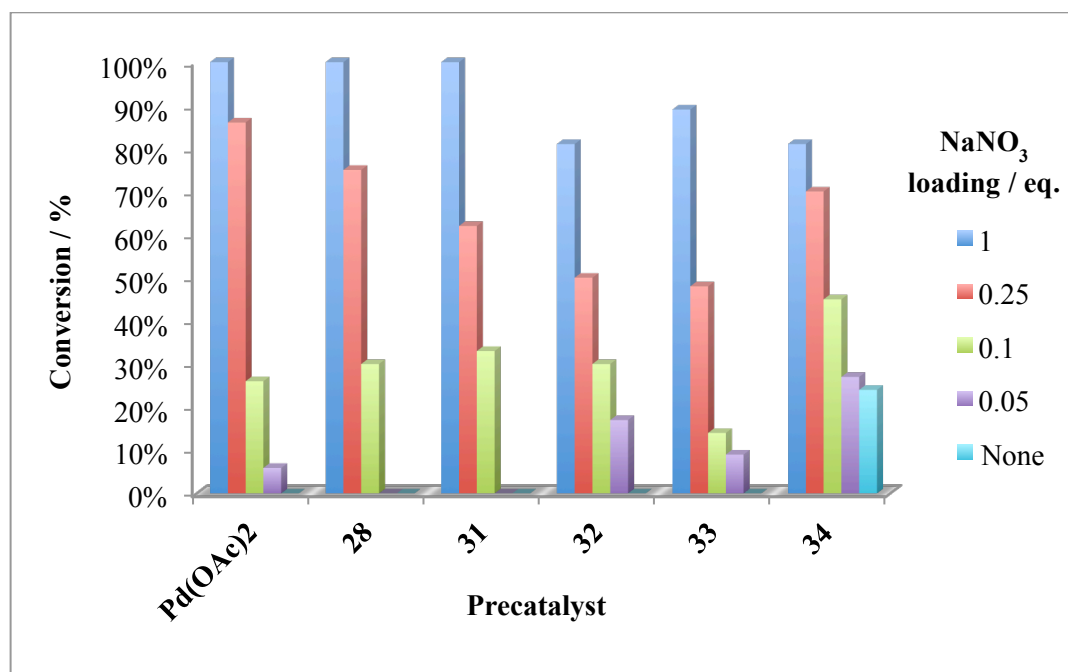
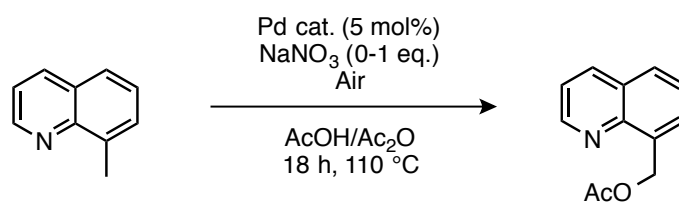


**Table 1:** Screening of 8-Methylquinoline Complexes as Precatalysts<sup>a</sup>

Entry	Precatalyst	Conversion / %
1	Pd(OAc) <sub>2</sub>	>99
2		>99
3		>99
4		81
5		89
6		81

<sup>a</sup>Conversions were calculated through <sup>1</sup>H NMR integration of the singlet corresponding to the methylene protons in the product (at  $\delta = 5.89$  ppm, 2H) against the singlet corresponding to the methyl protons in residual starting material (at  $\delta = 2.88$  ppm, 3H).

In order to further elucidate the role that the sodium nitrate additive plays in the catalytic cycle, all of the palladacyclic complexes were examined at varying loadings of the sodium nitrate co-catalyst (Graph 1; See Appendix A for a full table of data).



Graph 1: Screening of Precatalysts with Varying Co-Catalyst Loading

When the loading of sodium nitrate was lowered to 25 mol% (0.25 equiv.), which is the lowest loading used in Sanford's study, all the complexes were successful catalysts, with the reaction proceeding in moderate to good yields that are comparable to those achieved with Pd(OAc)<sub>2</sub>. When the co-catalyst loading was lowered further, a remarkable difference was observed between the reactions catalysed by the C<sup>N</sup> cyclopalladated species and those using Pd(OAc)<sub>2</sub> under the literature conditions.

At a loading of 0.05 equiv. NaNO<sub>3</sub> it can be seen that the complexes **32** and **34**, containing NO<sub>3</sub> ligands, are more effective at mediating the reaction than the reported conditions, with Pd(OAc)<sub>2</sub> affording only 6% conversion versus the 27% obtained when using **34** as a catalyst. NO<sub>2</sub>-containing palladacyclic complex **33** was also a successful catalyst under these conditions.

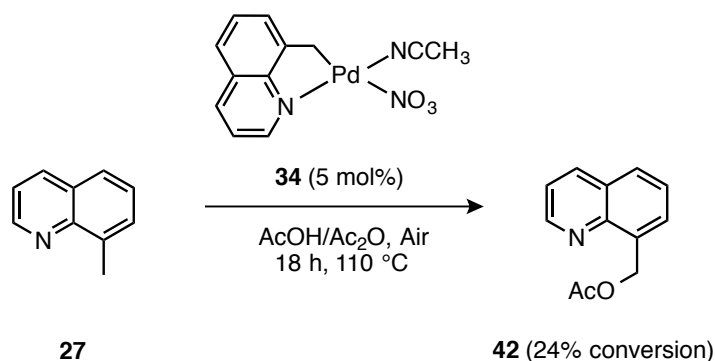
There are two key possible reasons for the higher efficacy of complexes **32** and **34** compared to Pd(OAc)<sub>2</sub>. If 'NO<sub>2</sub>' is acting as a redox co-oxidant, as proposed by Sanford, then Pd complexes containing nitrite or nitrate as a ligand could simply be a source of free nitrite;

the reduction of nitrite to form NO is responsible for the formation of the proposed Pd<sup>IV</sup> intermediate, and as such the formation of nitrite is an essential part of the catalytic cycle. If the nitrite or nitrate ligands in **32** and **34** are sufficiently labile, their dissociation in the catalytic system could liberate additional NO<sub>2</sub>, thus effectively increasing the co-catalyst loading.

Additionally, the possibility remains that complexes containing 'Pd-NO<sub>3</sub>' or 'Pd-NO<sub>2</sub>' groups are important intermediate species. If this is the case, then using complexes already containing the relevant ligands as precatalysts could mean that any key intermediates are present at the start of the reaction, offering significant kinetic advantages if their formation in the catalytic system is rate-limiting.

While no obvious explanation presents itself for the increased efficiency of 'Pd-NO<sub>3</sub>' complexes **32** and **34** compared to their NO<sub>2</sub> counterparts, it is worth noting that Sanford also found higher yields when sodium nitrate was used as a co-catalyst than when sodium nitrite was used, and it was thought that this could be due to a slower activation step from NO<sub>3</sub> for the key reduction step of NO<sub>2</sub> to NO. If 'Pd-NO<sub>2</sub>' species are implicated in catalysis, then they are likely to exhibit linkage isomerism, existing as either *N*- or *O*- bound isomers.<sup>40</sup> While our DFT calculations (Chapter 2) on the palladacyclic complexes suggested that for **31** and **33**, the *N*-bound isomers were preferred, this might not be the case for intermediate species with higher coordination. If a linkage isomerisation step is required for the formation of any key intermediate species, then a difference in energy between the *N*- and *O*- bound isomers could add a significant energy barrier and thus slow down catalysis. 'Pd-NO<sub>3</sub>' complexes, on the other hand, are only able to coordinate to Pd through an oxygen atom.

As expected, when the reaction was conducted without NaNO<sub>3</sub>, the Pd(OAc)<sub>2</sub>-catalysed reaction did not proceed. This was also the case for precatalysts **28** and **31–33**. Remarkably, when catalysed by **34** (5 mol%) in the absence of sodium nitrate, the reaction proceeded to 24% conversion with ~5 catalytic turnovers (Scheme 45).



**Scheme 45:** Catalysis of 8-Methylquinoline Acetoxylation Without NaNO<sub>3</sub>

Initially, this result appeared to confirm that the complex is able to act as a source of essential NO<sub>3</sub>, whereas Pd(OAc)<sub>2</sub> or the acetate dimer **28** are not. Interestingly, however, compound **34** was the only complex able to catalyse the reaction to any extent in the absence of sodium nitrate, despite **31**, **32** and **33** all containing either NO<sub>2</sub> or NO<sub>3</sub> ligands. Moreover, carrying out the reaction with Pd(OAc)<sub>2</sub> or acetate dimer **28** and 5 mol% of NaNO<sub>3</sub>, *i.e.* an equivalent amount of nitrate to that present in systems catalysed by complexes **31–34**, resulted in no more than 6% conversion to the acetoxyated product.

These results suggest that the role that nitrate and nitrite play could be highly dependent not only on their presence in the reaction mixture, but also on their source. The lack of conversion when Pd(OAc) or **28** was used along with 5 mol% of NaNO<sub>3</sub> indicates that coordination of a nitrate (or nitrite) ligand to Pd is essential for turnover of the acetoxyated product to occur. Furthermore, it appears that a ‘Pd–NO<sub>3</sub>’ bond is required for catalysis in the absence of sodium nitrate, highlighting a key role for nitrate at Pd<sup>II</sup>.

It was also observed that for entries with co-catalyst loadings, Pd<sup>II</sup> complexes containing an acetonitrile ligand proved more effective catalysts than those containing phosphine ligands. This is most likely due to the increased lability of the acetonitrile ligand relative to the phosphine, which allows expedient access to potential intermediate complexes. Also, phosphines are soft ligands, which are unlikely to be able to stabilize harder Pd<sup>II</sup> species, and especially not higher oxidation state Pd species. If Pd<sup>IV</sup> species are implicated in catalysis, then the presence of a phosphine could be a hindrance to the reaction kinetics; a phosphine ligand slowing down catalysis in oxidation reactions is in keeping with other Pd<sup>IV</sup> chemistry.<sup>59</sup> The increased activity of **34** could therefore be due to a combination of factors; the NO<sub>3</sub> ligand acting as a superior source of nitrite at Pd, with the labile acetonitrile ligand helping with the formation of key intermediates.

In order to gain a better picture of the catalytic activity of **34**, it was decided to conduct further investigations. All reactions discussed up until this point were conducted under air; the system was flushed with compressed air at regular intervals to ensure saturation of the reaction mixture (see experimental section for a full description of the setup). Whilst the development of methodology requiring only air as the oxidant remains highly desirable for industrial applications, many of the oxidative C–H bond functionalisation processes described in recent years have conducted reactions under an O<sub>2</sub> atmosphere, which can provide a relatively inexpensive alternative to some of the harsh oxidants commonly used.<sup>28–30</sup> Sanford's study involved reactions carried out under both air and dioxygen, and found that the use of an O<sub>2</sub> atmosphere offered increased yield, especially with substrates that proved harder to functionalise. With this in mind, a thorough screening of the acetoxylation reaction catalysed by **34** was also conducted under an oxygen atmosphere (Table 2).

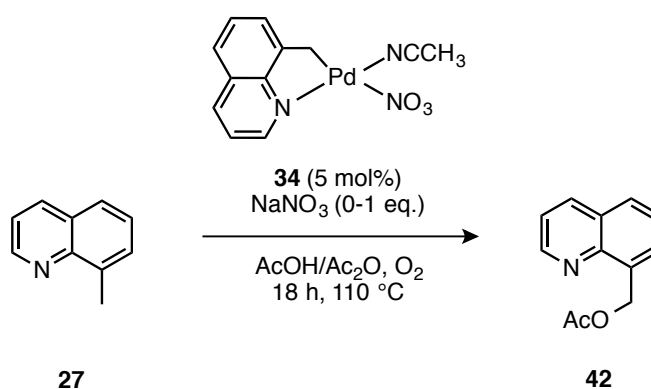


**Table 2** – Screening of **34** as a Catalyst Under 1 atm O<sub>2</sub>

Entry	NaNO <sub>3</sub> / mol%	Conversion / % (air)	Conversion / % (1 atm O <sub>2</sub> )
1	100	81	>99
2	25	70	83
3	10	45	82
4	5	38	66
5	0	24	36

The reaction is seen to proceed with good to excellent product conversions at co-catalyst loadings as low as 5 mol%. Pleasingly, the use of an oxygen atmosphere increased conversion from 24% to 36% in the absence of sodium nitrate (Table 2, Entry 5). As a control, all the reactions conducted in the absence of NaNO<sub>3</sub> were repeated under O<sub>2</sub>, which confirmed that even in an enriched oxygen atmosphere, **34** remains the only complex able to catalyse the reaction in the absence of sodium nitrate.

In an attempt to improve on the results obtained so far, it was decided to vary the loadings of catalyst **34** used. Typically, the effect of catalyst loading in Pd-catalysed processes is highly dependent upon the mechanism of catalysis. For example, in processes that operate *via* a Pd<sup>0/II</sup> pathway, it has been shown that a lower catalyst loading can sometimes dramatically increase catalytic efficiency.<sup>81,82</sup> This is largely thought to be due to increased aggregation of Pd<sup>0</sup> species at higher loadings leading to less active catalysis. On the other hand, for Pd<sup>II/IV</sup> processes, a larger amount of catalyst is often required, with loadings of 2–20 mol% being commonplace.<sup>59</sup>

The acetoxylation reaction with **34** was tested at varying catalyst loadings, from 0.5–10 mol% (Table 3). Results obtained with 100 mol% NaNO<sub>3</sub> (Entries 1–4) confirmed the expected trend for a system operating *via* high oxidation state Pd intermediates. When the reactions were repeated in the absence of NaNO<sub>3</sub>, the same trend was observed; gratifyingly, an increase in Pd catalyst loading to 10 mol% provided 45% conversion to the acetoxyated product (Entry 5). The same reactions conducted with Pd(OAc)<sub>2</sub> followed a similar trend (Entries 9–16). As expected, an increase in catalyst loading still did not lead to any formation of the acetoxyated product without the presence of sodium nitrate.



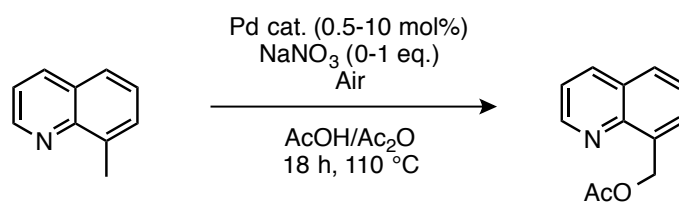
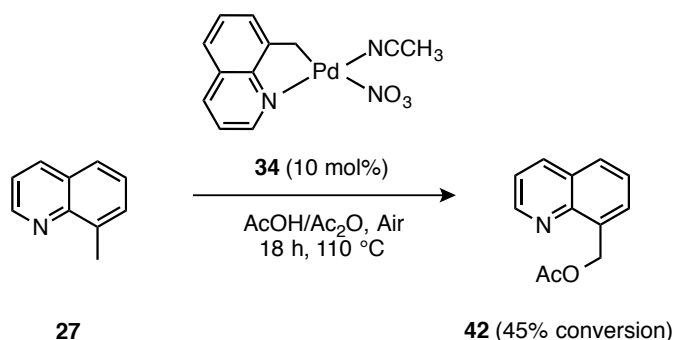


**Table 3:** Catalyst Activity at Varying Pd/NaNO<sub>3</sub> Loadings

Entry	Catalyst	Pd Catalyst / mol%	Co-catalyst / mol%	Conversion / %
1		10	100	>99
2		5	100	81
3		2	100	61
4	<b>34</b>	0.5	100	48
5		10	0	45
6		5	0	24
7		2	0	8
8		0.5	0	6
9		10	100	>99
10		5	100	>99
11		2	100	43
12		0.5	100	22
13	Pd(OAc) <sub>2</sub>	10	0	0
14		5	0	0
15		2	0	0
16		0.5	0	0

The thorough screening conducted has proved that all palladacyclic complexes of 8-methylquinoline effect catalytic acetoxylation in good to excellent yield. Additionally, the C–H acetoxylation of 8-methylquinoline can be achieved in up to 45% yield in the absence of a sodium nitrate co-catalyst (Scheme 46).



**Scheme 46:** Acetoxylation of 8-Methylquinoline in the Absence of  $\text{NaNO}_3$

These results represent an important breakthrough: an oxidative Pd-catalysed C–H bond functionalisation process that proceeds without the addition of an exogenous co-catalyst. A role for nitrate at  $\text{Pd}^{\text{II}}$  has been confirmed for Sanford’s acetoxylation reaction.

### Substrate Scope

With the promising results from the acetoxylation of 8-methylquinoline in hand, it was decided to employ the methodology in the functionalisation of other organic substrates. Initially, the substrates used in Sanford’s work were investigated.<sup>30</sup>

The reaction conditions described by Sanford had been optimized using the functionalisation of camphor *O*-methyl oxime **2** as a model reaction. Initial plans to subject it to our acetoxylation conditions, however, were hampered by the difficulty in preparing the substrate according to the literature conditions.<sup>23</sup> Despite the use of several different sets of conditions (Table 4), conversions did not exceed 40% and it was thought that this could be due to the *O*-methyl hydroxylamine hydrochloride being in salt form and thus requiring deprotonation before being able to react. This hypothesis was supported by an observed lack of solubility in solvents suggested by the literature. However, attempts to form the free base of the amine, *via* the use of a basic ion exchange resin, were unsuccessful. Attempts to carry out the reaction on cyclohexanone instead of camphor only resulted in trace product formation,<sup>83</sup> suggesting that the problem did indeed lie with the amine and could have been due to the quality of the commercial sample used.

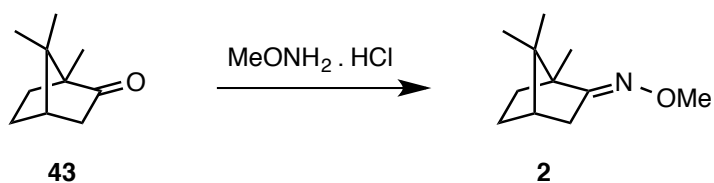
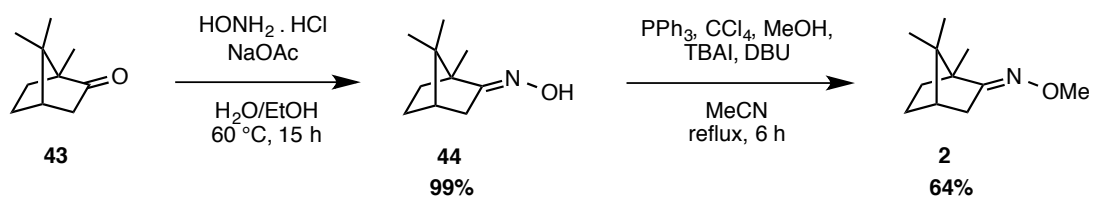


**Table 4:** Attempted Synthesis of Camphor O-Methyl Oxime (**2**)

Entry	Equivalents MeONH <sub>2</sub> · HCl	Solvent	Conditions	Conversion <sup>a</sup> / %
1	1.5	Pyridine	r.t., 24 h aqueous work-up	40
2	1.2	H <sub>2</sub> O	r.t., 24 h NaOH work-up	0
3	1.2	MeOH	r.t., 24 h NaOH work-up	0
4	1.2	MeOH	r.t., 24 h cat. TsOH	0
5	1.2	DCM	60 °C, 2 h NaOH work-up	10

<sup>a</sup> Conversions calculated by <sup>1</sup>H NMR spectroscopy

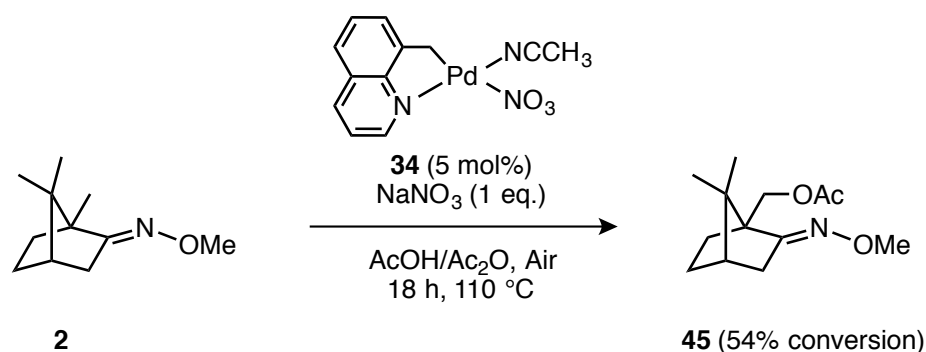
**2** was instead prepared *via* an alternative two-step route (Scheme 47), involving the formation of camphor oxime **44**,<sup>84</sup> followed by an *O*-alkylation using triphenylphosphine and carbon tetrachloride.<sup>85</sup>



**Scheme 47:** Synthesis of Camphor *O*-Methyl Oxime

Having prepared camphor *O*-methyl oxime **2** in good yield, it was tested as a substrate for C–H bond functionalisation using complex **34**, which had been found to exhibit the high catalytic activity of the complexes prepared, as a catalyst. Using the literature conditions of

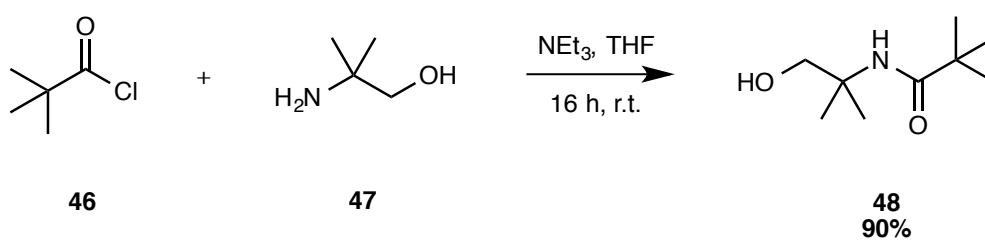
5 mol% Pd catalyst, 1 equivalent of NaNO<sub>3</sub>, and a temperature of 110 °C, **2** was acetoxylation in good yield (Scheme 48).



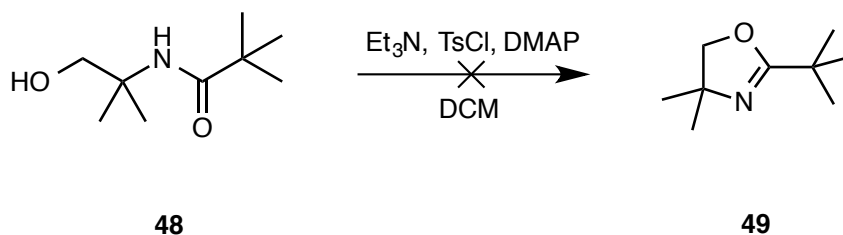
**Scheme 48:** Acetoxylation of Camphor *O*-Methyl Oxime with **34**

While Sanford's methodology had been applied to a range of sp<sup>3</sup> C–H compounds, there remained several organic substrates that did not undergo acetoxylation under the optimised conditions. One example is 2-*tert*-butyl-4,4-dimethyl-4,5-dihydrooxazole **49**. It was thought that the use of a catalyst with increased activity over Pd(OAc)<sub>2</sub> might have an effect on the reaction. Attempts to make **49** *via* the literature procedures,<sup>86</sup> however, proved challenging.

While amide precursor **48** was formed in excellent yield (Scheme 49), subsequent cyclisation attempts proved unsuccessful (Scheme 50), with no isolation of the desired product.

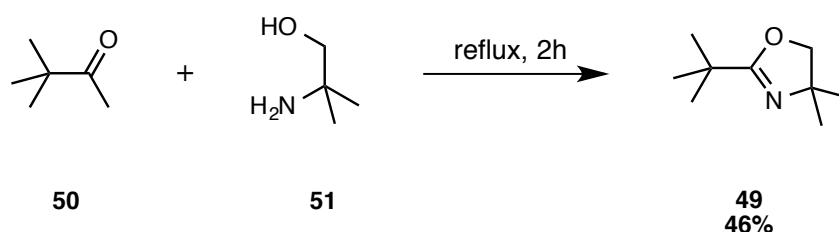


**Scheme 49:** Preparation of Amide Precursor **48**



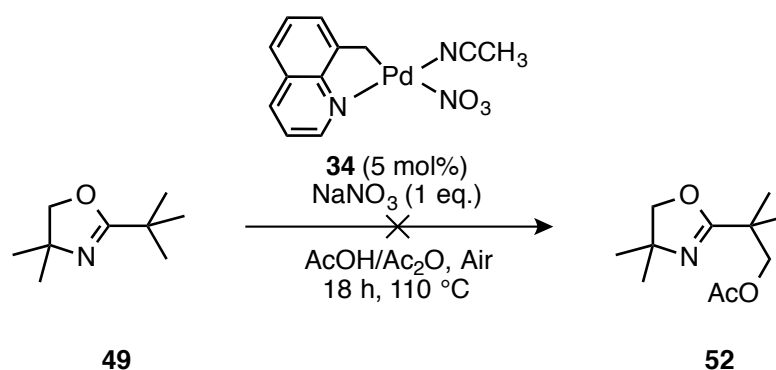
**Scheme 50:** Attempted Preparation of Oxazoline Substrate **49** from Amide **48**

The solvent-free reaction of distilled 2,2-dimethylaminopropanol **51** with pivalic acid (Scheme 51) was more successful, affording substrate **49** in a workable yield.<sup>87</sup>



**Scheme 51:** One-Step Synthesis of **49**

Unfortunately, when subjected to the same conditions of catalysis as oxime substrate **2**, no formation of the acetoxyated product was observed by <sup>1</sup>H NMR spectroscopic analysis, and work-up only isolated unreacted starting material (Scheme 52).

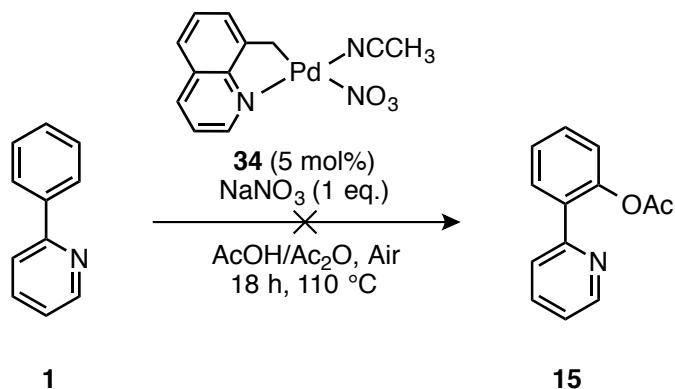


**Scheme 52:** Attempted Acetoxylation of Oxazoline **49**

Undeterred by this result, C–H acetoxylation at sp<sup>2</sup> centres was assessed. Despite the fact that these are more acidic than sp<sup>3</sup> C–H bonds and therefore typically easier to

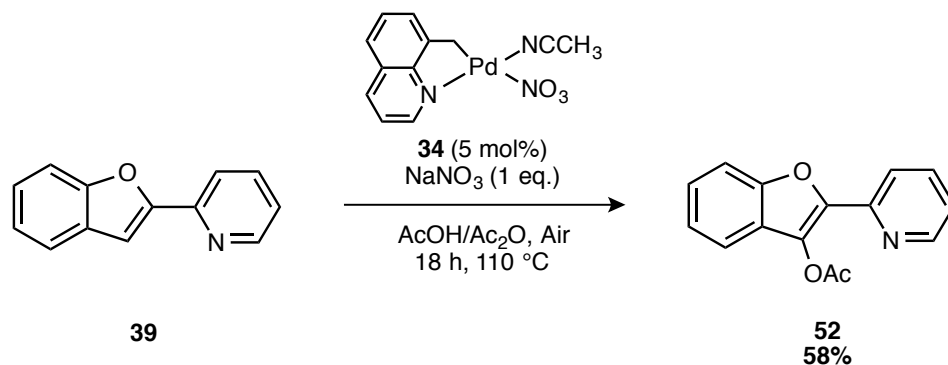
functionalise,<sup>10</sup> Sanford's methodology had failed to convert simple  $sp^2$  substrates to the acetoxyated products in any reasonable yield.

The acetoxylation of 2-phenylpyridine **1** was first attempted (Scheme 53), but resulted only in the recovery of starting material (94%).



**Scheme 53:** Attempted Acetoxylation of 2-Phenylpyridine

Having successfully prepared palladacyclic complexes of the 2-(2-pyridyl)benzo[*b*]furan **39** (see Chapter 2), it was decided to use the ligand as a substrate for C–H bond functionalisation. Pleasingly, when reacted with 5 mol% of catalyst **34** and 100 mol% sodium nitrate, the acetoxyated product **52** was isolated in 58% yield.

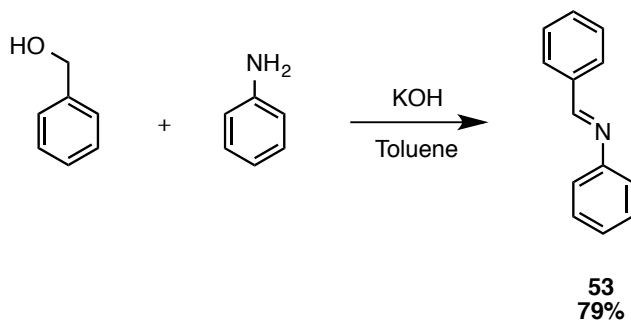


**Scheme 54:** Acetoxylation of Hpbf

Another  $sp^2$  substrate that has been of interest to the group is *N*-phenylbenzaldimine (bza) **53**.  $C^{\wedge}N$  palladacyclic complexes of bza containing imidate ligands have previously been

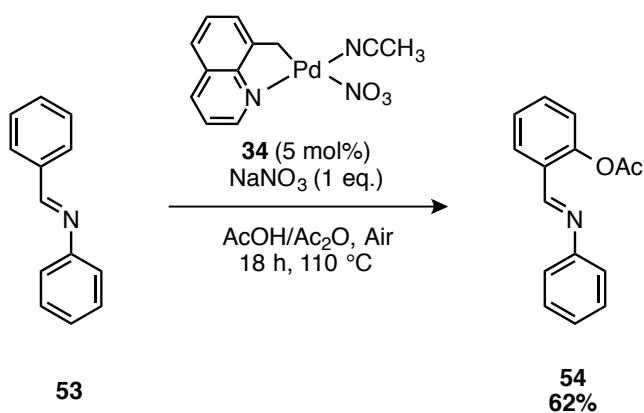
prepared and employed as efficient precatalysts in Suzuki-Miyaura cross-coupling reactions.<sup>88</sup>

The *N*-phenylbenzaldimine substrate was prepared *via* a simple reaction of benzyl alcohol and aniline to afford 79% isolated yield of the desired product (Scheme 55).<sup>89</sup>



**Scheme 55:** Preparation of *N*-Phenylbenzaldimine

When subjected to the same catalysis conditions, the acetoxyated product **54** was isolated in moderate yield (Scheme 56).



**Scheme 56:** Acetoxylation of *N*-Phenylbenzaldimine

Table 5 summarises our investigations into substrate scope. As preliminary studies, all reactions were carried out using the optimal catalyst **34** at 5 mol%, along with 100 mol% sodium nitrate.

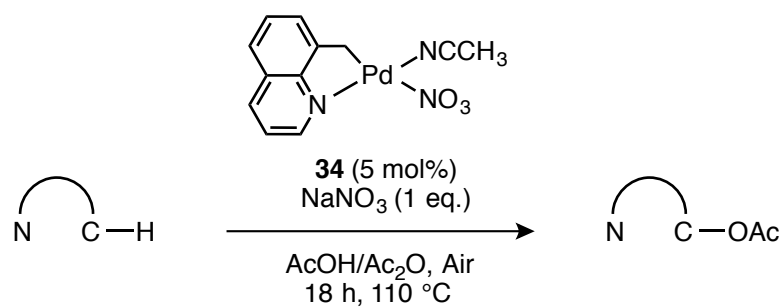


**Table 5:** Substrate Scope of Catalysis with **34**

Entry	Substrate	Product	Conversion <sup>a</sup> / %
1			81
2			54
3			0
4			0
5			58
6			62

<sup>a</sup> Conversions were calculated by <sup>1</sup>H NMR integration of the singlet corresponding to the acetate CH<sub>3</sub> group in each product compared to a reference signal from the spectrum of the starting material. See Experimental section for more detail.



Further optimisation studies, including the use of an O<sub>2</sub> atmosphere and a screening of all newly prepared catalysts, are necessary in order to gain a full idea of the scope of our catalysts. However, the successful functionalisation of sp<sup>2</sup> substrates **39** and **53** with the optimised catalyst represents a significant breakthrough, with sp<sup>2</sup> C–H bond functionalisation being achieved for the first time using nitrate co-catalysis. The results from our thorough screening investigations for the functionalisation of 8-methylquinoline suggest that with further optimisation, the functionalisation of **39** and **53**, as well as other sp<sup>2</sup> substrates, could be achieved in higher yields.

## Chapter 4: Mechanistic Studies into Pd-catalysed C–H Bond Functionalisation Processes

Having prepared a range of novel Pd complexes containing NO<sub>2</sub> or NO<sub>3</sub> anionic ligands that have been shown to be excellent precatalysts for C–H bond functionalisation, attention was turned to elucidating the mechanism of catalysis in sp<sup>3</sup> C–H bond acetoxylation, and in particular the role played by the ligands present at Pd. Several mechanistic investigations have been conducted, with a view to understanding what makes the catalysts efficient and how these properties can be exploited in future C–H bond functionalisation processes.

### Reductive Elimination from Pd<sup>II</sup> Species

As some of the most widely used Pd-catalysed transformations, cross-coupling reactions have been subject to extensive mechanistic studies. Since the majority of cross-coupling processes proceed via a Pd<sup>0/II</sup> mechanistic pathway, reductive elimination from Pd<sup>II</sup> is well understood and has been shown through several elegant studies to be affected by electronic and steric effects of the ligands involved,<sup>90–92</sup> as well as the relative bond dissociation energies of the atoms involved; the higher bond dissociation energies of metal–heteroatom bonds compared to metal–carbon bonds can provide some insight into why carbon–heteroatom bond-forming reductive elimination at transition metal centres is less well documented than carbon–carbon bond forming processes.<sup>93,94</sup>

Nitroaromatic compounds are of great importance to the pharmaceutical industry,<sup>95</sup> and are currently prepared via electrophilic aromatic substitution using HNO<sub>3</sub>, a process known to suffer from poor functional group tolerance.<sup>96</sup> More recent methods have involved copper catalysis, described by Saito and co-workers in their formation of nitroaromatic compounds from aryl iodides.<sup>97</sup> Buchwald and co-workers have also described the Pd<sub>2</sub>(dba)<sub>3</sub>-catalysed conversion of aryl chlorides, nonaflates and triflates to nitroaromatics, where the Ar–NO<sub>2</sub> bond is most likely formed by reductive elimination from Pd<sup>II</sup>.<sup>98</sup>

The acetoxylation reaction that has been studied in this thesis is believed to proceed *via* a Pd<sup>II/III</sup> or Pd<sup>II/IV</sup> pathway,<sup>68,99</sup> and some of the mechanistic aspects relating to reductive elimination from potential high oxidation state intermediates, resulting in C–O bond

formation, will be discussed later in this chapter. However, another potential application arising from the preparation of Pd–NO<sub>2</sub> complexes is the possibility of their use in the formation of C–N bonds *via* reductive elimination. One particularly attractive use is the nitration of sp<sup>2</sup> C–H bonds to form useful nitroaromatic compounds.

Reductive elimination as part of a catalytic cycle is the basis of key carbon–carbon and carbon–heteroatom bond forming steps in the majority of metal-catalysed transformations, and reductive elimination processes from both Pd<sup>II</sup> and Pd<sup>IV</sup> are well precedented in the literature.<sup>58,79,90,100</sup>

Reductive elimination from high oxidation state Pd intermediates (Pd<sup>III</sup> or Pd<sup>IV</sup>) has been shown by Liu and co-workers to occur in catalytic C–H bond nitration processes involving [Pd(C<sup>^</sup>N)L<sub>2</sub>] intermediate species.<sup>78</sup> A key question that we sought to answer was whether this could also occur from stable Pd<sup>II</sup> complexes of C<sup>^</sup>N ligands, resulting in the formation of nitroaromatic compounds and Pd<sup>0</sup>.

An initial factor to consider in reductive elimination to form C–NO<sub>2</sub> bonds is the relative geometry of the ligands at Pd; typically, reductive elimination requires the Pd–C bond to be *cis*- to the NO<sub>2</sub> ligand. DFT calculations (reported in Chapter 2) of the single point energies of 2-phenylpyridine complex **25**, containing a nitrite ligand, showed the relative stabilities of the *cis*- and *trans*- isomers as well as the NO<sub>2</sub>/ONO linkage isomers (Figure 14).

Relative Free Energies ( $\Delta G$ ) at 298 K of **25** /kJ mol<sup>-1</sup>

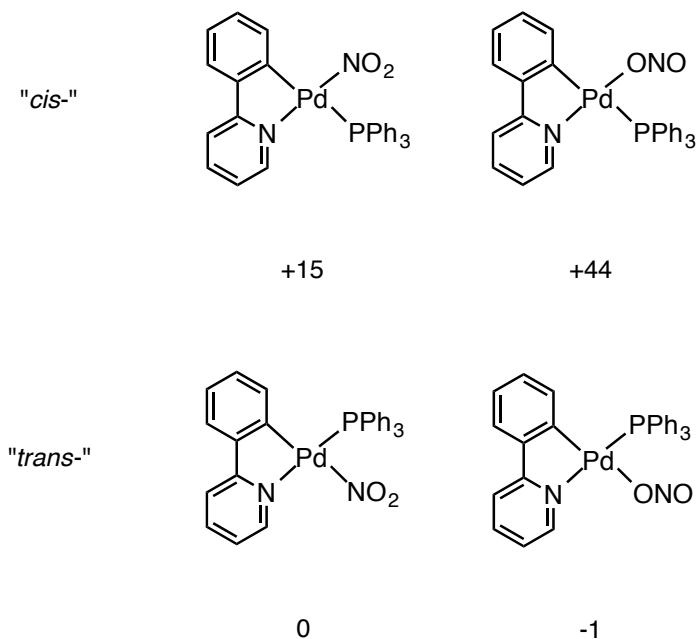
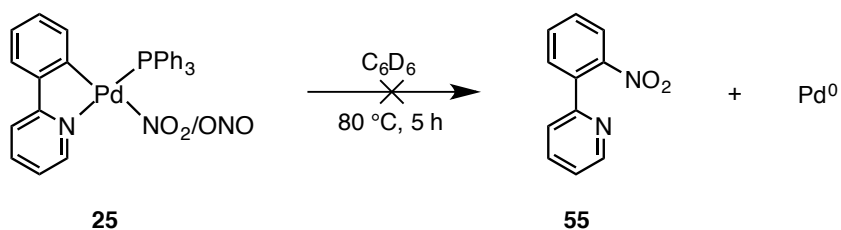


**Figure 14:** Calculated Free Energies of Isomers of **25** at the TZVPP Level of Theory

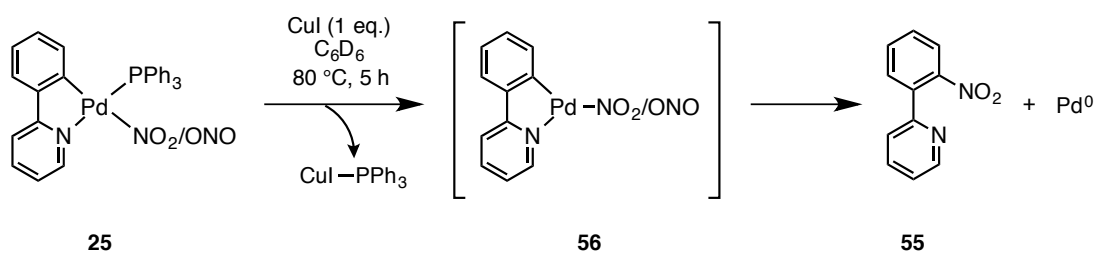
While *cis*- isomers are both higher in energy than their corresponding *trans*- isomers, a difference of 15 kJ mol<sup>-1</sup> between the *N*-bound linkage isomeric forms suggested that the kinetic (*cis*-) isomer may be accessible with heating. Since the *O*-bound *cis*-isomer was the highest in energy of all isomeric forms of the complex, we reasoned that it would not be formed by heating a mixture of isomers of the *trans*- complex, meaning that any subsequent reductive elimination would most likely result in the formation of the C–NO<sub>2</sub> product rather than the C–ONO product.

To test this hypothesis, complex **25** was heated for 5 h in benzene-*d*<sub>6</sub>, which would allow any changes to be monitored by <sup>1</sup>H and <sup>31</sup>P NMR spectroscopy (Scheme 57).



**Scheme 57:** Attempted Reductive Elimination from **25**

Unfortunately, no formation of nitrated product **55** was observed upon heating, which could suggest that the *cis*- isomer could not be accessed under the conditions used. The reaction was therefore repeated with the addition of CuI, which it was hoped would act as a phosphine scavenger, promoting the loss of the PPh<sub>3</sub> ligand to form 14-electron Pd<sup>II</sup> intermediate and setting up the complex for reductive elimination of nitrated product **55** (Scheme 58).



**Scheme 58:** Attempted Reductive Elimination from **25** with CuI

While <sup>31</sup>P NMR spectroscopic analysis of the reaction mixture showed degradation of complex **25** to form a mixture of three unidentified phosphorus species, no formation of **55** was observed by either NMR or mass spectrometry analysis. With reductive elimination experiments from complex **25** proving unsuccessful, attention turned to the use of complex **33**, which our DFT calculations had shown to prefer a geometry with Pd-C and Pd-NO<sub>2</sub> bonds mutually *cis* (Figure 15).

Relative Free Energies ( $\Delta G$ ) of **33** /kJ mol<sup>-1</sup>

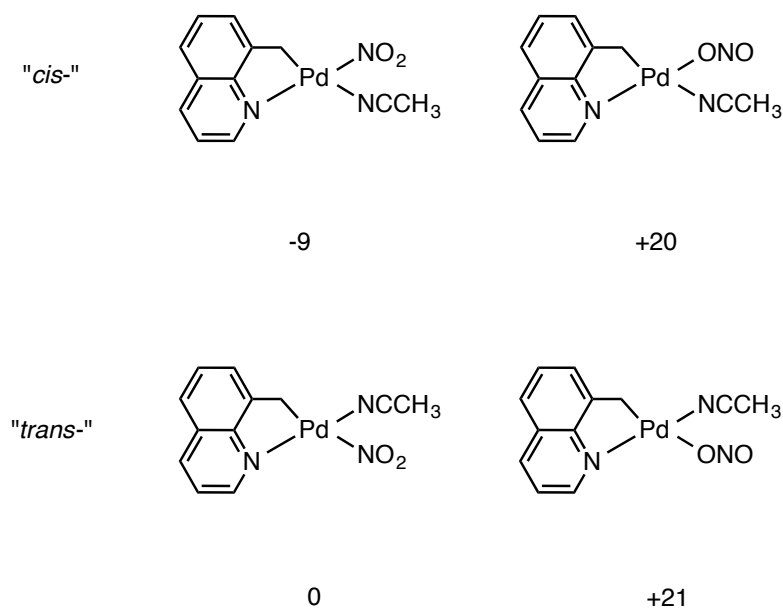
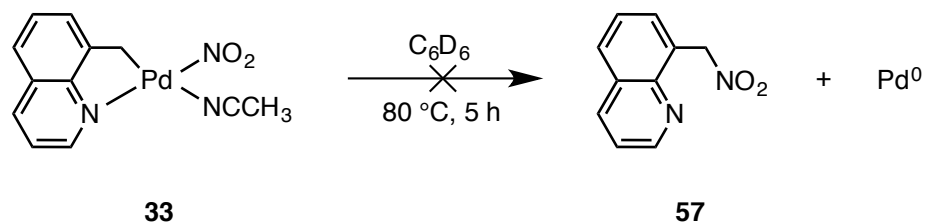


**Figure 15:** Calculated Free Energies of Isomers of **33** and **34** at the TZVPP Level of Theory

In this case, the DFT calculations suggested that the *N*-bound isomer of the nitrite ligand with a *cis* geometry was the lowest energy conformation of the complex, allowing for C–NO<sub>2</sub> formation. However, attempts to access nitrated product **57** were also unsuccessful (Scheme 59). <sup>1</sup>H NMR spectroscopic analysis showed degradation of complex **33**, no formation of product **57** was observed. Additionally, ESI-MS did not show the expected peak at *m/z* 118.06, and no NO<sub>2</sub> stretch was visible in the infrared spectrum.

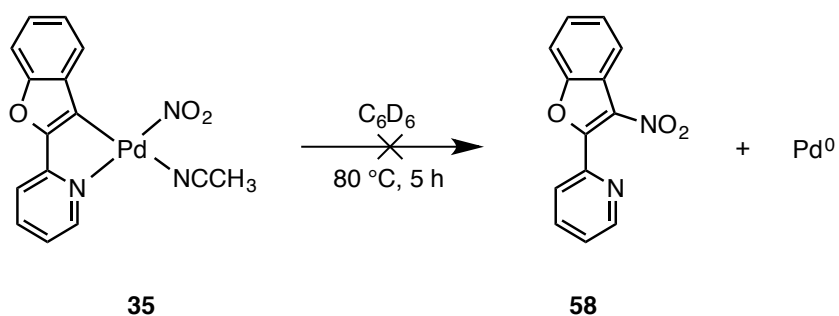


**Scheme 59:** Attempted Reductive Elimination from **33**

To explain these results one may consider that the formation of nitrated product **57** would require the formation of an sp<sup>3</sup> C–NO<sub>2</sub> bond, which is unprecedented at Pd. Secondly, it is likely that the presence of a small acetonitrile ligand in **33**, as opposed to the

triphenylphosphine ligand in **25**, means that the steric bulk around the metal centre is not significant enough to promote reductive elimination; Buchwald has previously reported that the presence of a bulky phosphine ligand is important in C–F bond-forming reductive elimination from Pd<sup>II</sup>, and it is likely that a similar effect could be required here.<sup>79</sup>

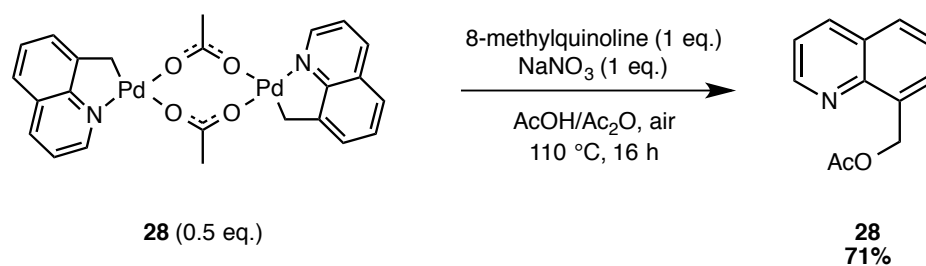
This theory was supported by the lack of formation of nitrated product **58** through reductive elimination from **35** (Scheme 60), which had been shown by Nonoyama to occupy a geometry where the Pd–NO<sub>2</sub> and Pd–C bonds are mutually *cis*.<sup>43</sup>



**Scheme 60:** Attempted Reductive Elimination from **35**

Since the geometry of **35** had been confirmed crystallographically, it is likely that the steric bulk that a phosphine ligand would provide is insufficient to promote reductive elimination.

With the palladacyclic Pd<sup>II</sup> complexes seemingly unable to undergo reductive elimination upon heating, it was decided to assess the potential of the complexes to undergo stoichiometric C–H functionalisation reactions under the conditions for acetoxylation. Gratifyingly, when acetate-bridged dimer **28** was heated with 1 equivalent sodium nitrate as well as 1 equivalent of 8-methylquinoline, the acetoxyated product **42** was formed in 71% yield (Scheme 61).



**Scheme 61:** Stoichiometric C–H Bond Functionalisation of 8-Methylquinoline

Interestingly, the reaction did not proceed without the addition of an additional equivalent of the C<sup>^</sup>N ligand 8-methylquinoline; this could suggest that reductive elimination is unable to occur unless there is a ligand present to coordinate to the Pd centre as the product is eliminated.

The ability of **28** to undergo stoichiometric C–O bond formation under oxidative conditions suggests that reductive elimination is likely to occur from a high Pd oxidation state, where either acetate or nitrite/nitrate ligands present will oxidise the Pd<sup>II</sup> centre to either Pd<sup>III</sup> or Pd<sup>IV</sup>. No formation of the nitrated product **57** was observed, which could suggest that it is in fact acetate ligands that are present in the high oxidation state species and thus involved in the reductive elimination step. However, the preference for acetoxylation over nitration could be due to the preferred geometry of any high oxidation state Pd species, and the exact role of the anionic ligands cannot be confirmed without further mechanistic investigations. A key question is whether the high oxidation state species formed *via* addition to Pd<sup>II</sup> under stoichiometric reaction conditions mirrors the formation of intermediate species when the same Pd<sup>II</sup> complexes are used in catalysis.

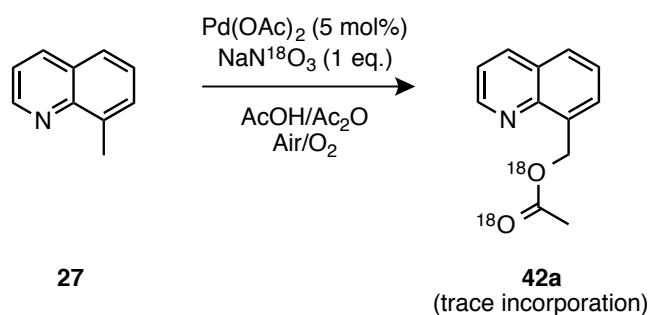


## Isotopic Labelling Studies

Having established that Pd complexes containing NO<sub>2</sub> or NO<sub>3</sub> anionic ligands are highly active catalysts in C–H functionalisation processes, one of the key objectives was to establish the exact role that the ligands play in the mechanism of catalysis. While Sanford's proposed mechanism suggested that the nitrite acted solely as an oxidant,<sup>30</sup> enabling the formation of Pd<sup>IV</sup> intermediates, this conclusion could be contradicted by Heumann and Bäckvall's findings that NO<sub>2</sub> anion can play an active role in catalysis, attacking a carbonyl group and acting as the source of oxygen in the acetoxyated product.<sup>38</sup>

Sanford's study involved conducting the acetoxylation of camphor *O*-methyl oxime under an atmosphere of <sup>18</sup>O<sub>2</sub>, finding less than 5% incorporation of the <sup>18</sup>O label in the acetoxyated product. Since no experiments had been conducted with the use of <sup>18</sup>O-labelled acetic acid, it was not confirmed that the acid was the source of O in the final product. We therefore decided to conduct experiments using <sup>18</sup>O-labelled sodium nitrate, which would allow us to identify whether the oxygen in the product derives from the nitrite, as proposed by Heumann and Bäckvall.

Initially, the acetoxylation of 8-methylquinoline was conducted under the literature conditions, with Pd(OAc)<sub>2</sub> as catalyst, and the addition of 1 equivalent of NaN<sup>18</sup>O<sub>3</sub> (Scheme 62).

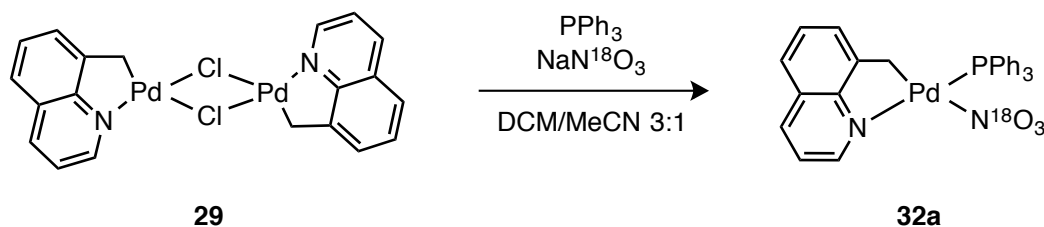


**Scheme 62:** Acetoxylation of 8-Methylquinoline with NaN<sup>18</sup>O<sub>3</sub>

While quantitative yield of the acetoxyated product was obtained when the reaction was conducted both under air and under 1 atm O<sub>2</sub>, HRMS (ESI<sup>+</sup>) analysis of the product showed only trace incorporation of the <sup>18</sup>O label. Compound **42a**, containing two <sup>18</sup>O labels, has an exact mass of 205.23, which was not observed by ESI-MS. A small peak was observed at

203.23, the exact mass for an acetoxyated product containing one  $^{18}\text{O}$  label, but the ratio of peak intensity for non-labelled:labelled products was approximately 98:2, confirming only trace incorporation. This result taken together with Sanford's data, which showed that  $^{18}\text{O}_2$  was not a source of oxygen in the product, would suggest that the product oxygen does derive from the acetic acid (by process of elimination).

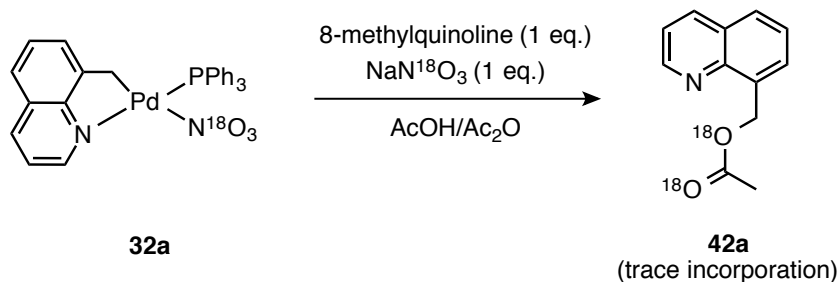
In order to establish whether there was any difference in mechanism between the literature conditions, and reactions catalysed by our  $\text{Pd-NO}_2/\text{NO}_3$  complexes, it was decided to incorporate an  $^{18}\text{O}$  label into one of the catalysts. Complex **32a** was therefore prepared from the chloride-bridged dimer **29** in good yield, *via* the addition of triphenylphosphine and  $^{18}\text{O}$ -labelled sodium nitrate (Scheme 63).



**Scheme 63:** Synthesis of  $^{18}\text{O}$ -Labelled Complex **29**

Previous studies (Chapter 3) showed that **32**, the non-isotopically labelled analogue of **32a**, was unable to catalyse the acetoxylation of 8-methylquinoline in the absence of  $\text{NaNO}_3$ . Therefore, any C–H functionalisation reaction with **32a** would still require the addition of sodium nitrate. The addition of non-isotopically labelled  $\text{NaNO}_3$  would mean that a lack of  $^{18}\text{O}$  incorporation in the product would not provide any clarity on the effect of the presence of an  $^{18}\text{O}$ -labelled nitrate group in the catalyst.

With this in mind, it was decided to conduct a stoichiometric experiment with 1 equivalent of  $^{18}\text{O}$ -labelled sodium nitrate, to see whether reductive elimination from catalyst **32a** would form a product containing the  $^{18}\text{O}$ -label. The complex was treated with an additional equivalent of 8-methylquinoline, acting as the coordinative ligand and favouring reductive elimination of the acetoxyated product (Scheme 64).



**Scheme 64:** Stoichiometric Formation of Acetoxyated Product from Labelled Catalyst **32a**

Again, while quantitative recovery of the organic product **42** was achieved, no incorporation of  $^{18}\text{O}$  was observed in the product. The results of these isotopic labelling experiments appear to confirm that the nitrate or nitrite anions present are not a source of oxygen in the final product. Their role is most likely to act as a redox co-catalyst, *vide infra*.

While these results appear to confirm Sanford's proposed mechanism, questions still remain as to what makes complexes containing nitrite or nitrate ligands more active catalysts than  $\text{Pd}(\text{OAc})_2$ . In particular, why is complex **34** able to catalyse the reaction in the absence of sodium nitrate, when its phosphine or nitrite analogues are not? In order to fully understand the differences in catalytic activity, more thorough mechanistic investigations needed to be carried out. Further experiments could, for example, involve subjecting the  $^{18}\text{O}$ -labelled analogue of complex **34**, which was found to be the most effective catalyst, to stoichiometric acetoxylation conditions.

## Direct Observation of High Oxidation State Pd Intermediates

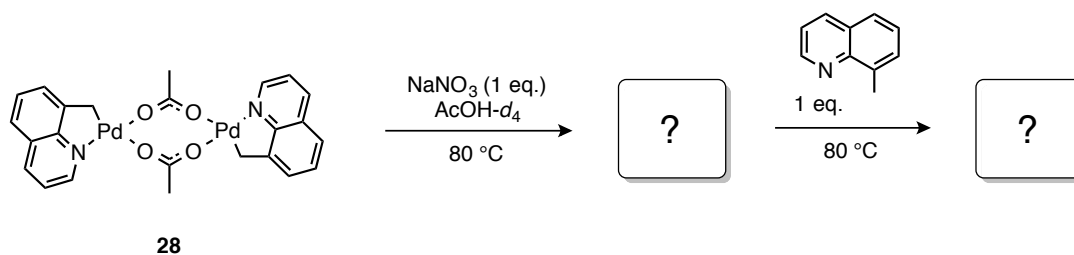
Given the successful isolation of potential high oxidation state Pd intermediates reported by both Sanford and Ritter,<sup>68,99</sup> efforts were made to identify similar complexes that could be present in the catalytic system. One key incentive was to establish whether  $\text{Pd}^{\text{III}}$  or  $\text{Pd}^{\text{IV}}$  species, or a mixture of both, are implicated in the catalytic cycle.

Both the  $\text{PhI}(\text{OAc})_2$ -mediated and nitrate co-catalysed acetoxylation processes reported by Sanford involve the use of a  $\text{Pd}(\text{OAc})_2$  catalyst and an oxidant, and are carried out in acetic acid in the presence of oxygen. There is therefore a strong likelihood that similar high oxidation state species to those observed by Sanford and Ritter are present in the acetoxylation reaction investigated in this thesis. It was thought that conducting similar

experiments to those conducted by Ritter would allow us to observe any high oxidation state intermediates present by NMR spectroscopic analysis. Moreover, characterisation of any isolated species would allow identification of any nitrite or nitrate ligands present in such species.

Both Sanford and Ritter had described their proposed intermediates as having low stability at ambient temperatures, but stable when stored at  $-35\text{ }^{\circ}\text{C}$ . For this reason, the independent syntheses of the complexes were conducted at significantly lower temperatures than the reaction conditions; while the catalytic acetoxylation reaction takes place at  $80\text{ }^{\circ}\text{C}$ , Sanford's  $\text{Pd}^{\text{IV}}$  species was prepared at  $25\text{ }^{\circ}\text{C}$  and Ritter's  $\text{Pd}^{\text{III}}\text{-Pd}^{\text{III}}$  dimer was prepared a number of ways at temperatures between  $-35\text{ }^{\circ}\text{C}$  and  $25\text{ }^{\circ}\text{C}$ . Despite the obvious advantages of low temperature synthesis, it was essential to ensure that any analogous complexes prepared were viable for catalysis under the real reaction conditions. For this reason, initial experiments were conducted at  $80\text{ }^{\circ}\text{C}$ .

Complex **28**, which is prepared in good yield from 8-methylquinoline and  $\text{Pd}(\text{OAc})_2$ , and has been used successfully as a precatalyst in the acetoxylation of 8-methylquinoline, was heated to  $80\text{ }^{\circ}\text{C}$  with 1 eq.  $\text{NaNO}_3$  in acetic acid- $d_4$  (Scheme 65). After heating for 3 h, 1 equivalent 8-methylquinoline was added and the reaction mixture was heated overnight.



**Scheme 65:** Proposed Strategy for Identification of Intermediate Species

The reaction of **28** (1 equiv.) was conducted in an NMR tube and monitored by  $^1\text{H}$  NMR spectroscopic analysis (Figure 16). After addition of sodium nitrate (1 equiv.) and subsequent heating with the reaction mixture open to air, the results show clear degradation of the dinuclear Pd starting material **28**, which has a broad spectrum in  $\text{AcOH-}d_4$  (Figure 16, Spectrum A). Instead, formation of at least two new species is observed, as depicted in Spectrum B. After heating the reaction overnight (20 hours) with 8-methylquinoline (1 equiv.), these new species appear to have degraded (Spectrum C). Interestingly, no

acetoxyated product was observed in any of these NMR spectra, despite earlier experiments having shown the formation of the product in 71% yield under similar conditions (*i.e.* stoichiometric C–H acetoxylation from a cyclopalladated complex with addition of 1 equiv. 8-methylquinoline).

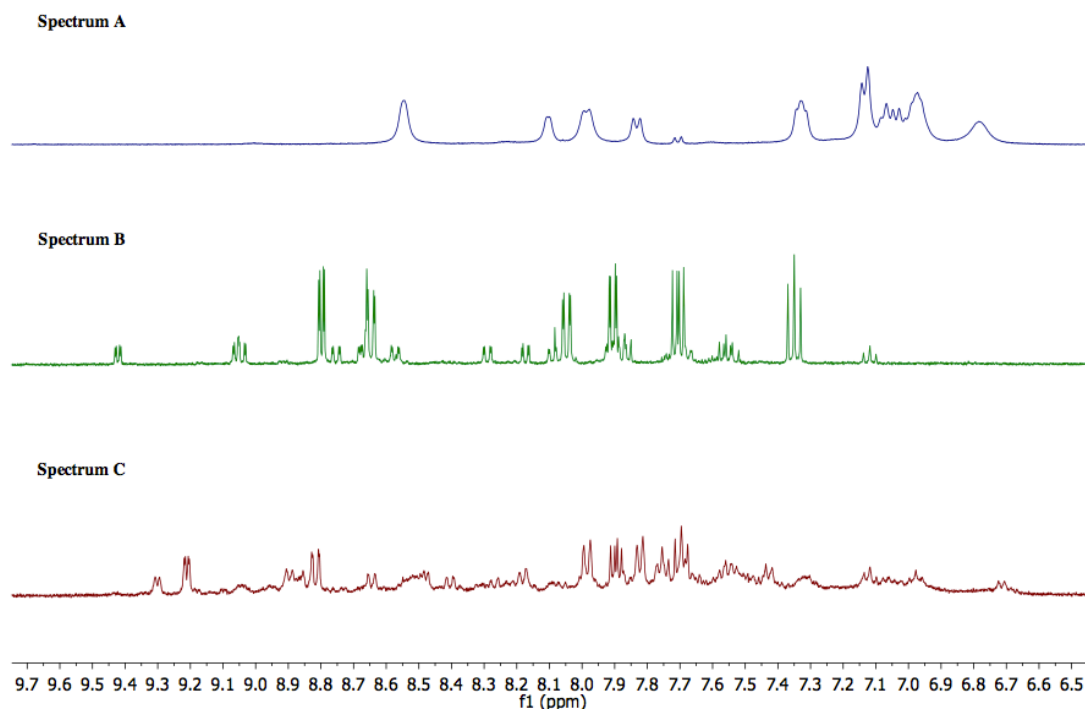


**Figure 16:**  $^1\text{H}$  NMR Spectrum of Dimer **28** (700 MHz, 298 K)

**Spectrum A)** In Acetic Acid- $d_4$

**Spectrum B)** After 3 h Heating with  $\text{NaNO}_3$  in Acetic Acid- $d_4$

**Spectrum C)** After 20 h Heating with  $\text{NaNO}_3$  and 8-Methylquinoline in Acetic Acid- $d_4$

Spectrum B, obtained after heating **28** for 3 h with sodium nitrate and no additional 8-methylquinoline, was remarkably clear, so it made an excellent basis for identification of the Pd intermediates present. Comparison of Spectrum B with the spectra of both the free 8-methylquinoline ligand and the acetoxyated product **42** in acetic acid- $d_4$  showed that neither was present (Figure 17). Interestingly, no signal corresponding to the methylene protons was observed in Spectrum B.

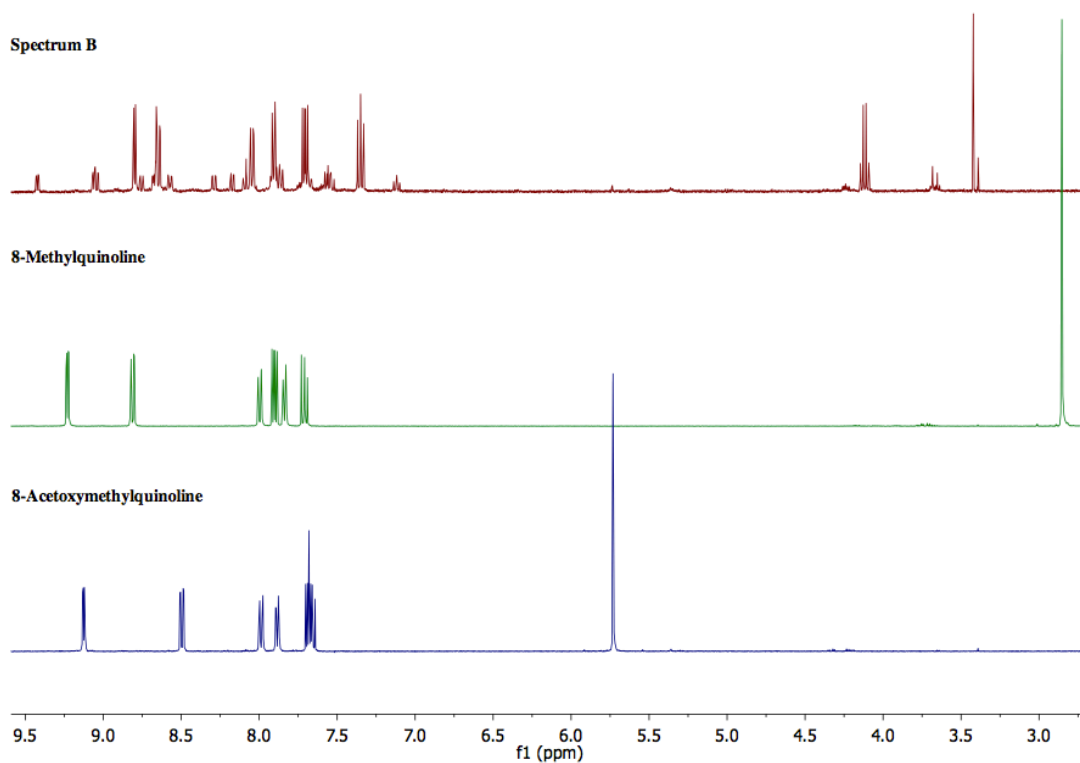


**Figure 17:** Comparison of Spectrum B with the Spectra (700 MHz, 298 K) of 8-Methylquinoline (**27**) and 8-Acetoxymethylquinoline (**42**) in Acetic Acid- $d_4$

Upon inspection of the aromatic region of Spectrum B, one major species is observed, containing six aromatic proton environments labelled “ $\alpha$ ” (Figure 18).

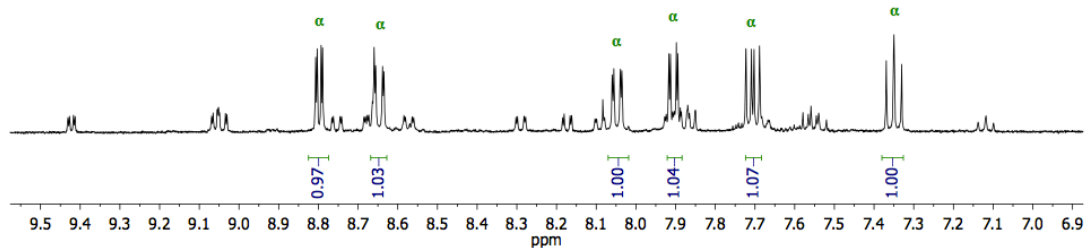


**Figure 18:** Aromatic Region of Spectrum B with Species  $\alpha$  Protons Labelled

Integration of the spectrum shows all six “ $\alpha$ ” peaks to be roughly equal in intensity, and the splitting patterns observed appear consistent with those expected for an 8-methylquinoline ligand, which contains six aromatic protons. Thus, the observation of only six proton

environments suggests that the major intermediate species contains either one 8-methylquinoline ligand, or two ligands that are identical.

Ritter described the observation of a mixture of “head-to-head” and “head-to-tail” isomers of the bimetallic Pd<sup>III</sup>-Pd<sup>III</sup> complexes of 2-phenylpyridine (Figure 19). Both isomers contain two 2-phenylpyridine ligands, which are in identical environments and therefore each have 8 corresponding aromatic proton environments.

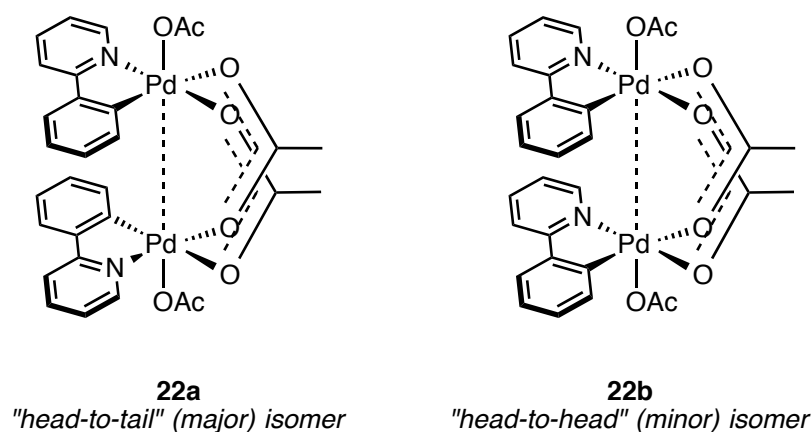


**Figure 19:** Major and Minor Isomers of Ritter's Pd<sup>III</sup>-Pd<sup>III</sup> Dimer<sup>68</sup>

Based on comparison of Spectrum B to the results obtained by Ritter, it was reasoned that the six major ( $\alpha$ ) aromatic proton environments observed could arise from a similar dinuclear Pd species, *i.e.* a [Pd(C<sup>^</sup>N)(OAc)<sub>2</sub>]<sub>2</sub> complex where the C<sup>^</sup>N ligand is 8-methylquinoline instead of 2-phenylpyridine. “Head-to-tail” and “head-to-head” isomers of this proposed intermediate are shown in Figure 20.

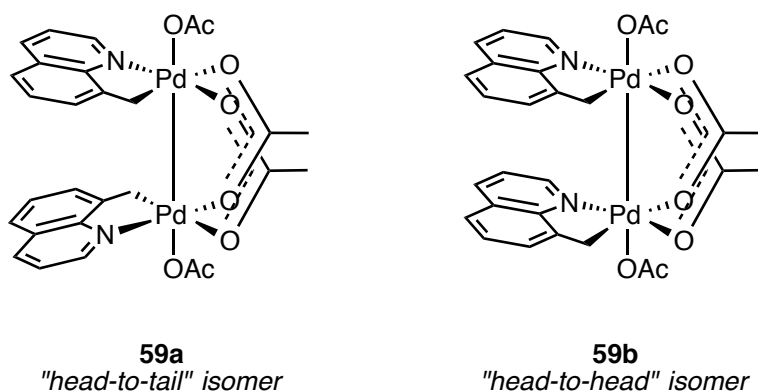


**Figure 20:** Isomers of Proposed Pd<sup>III</sup>-Pd<sup>III</sup> Intermediate **59**

In order to establish which isomer would be present as the major species, DFT calculations were carried out by Dr Jason Lynam (project co-supervisor) to calculate the single point energies of the two isomers. The results showed that the “head-to-tail” isomer **59a** is only 2 kJ mol<sup>-1</sup> lower in energy than the “head-to-head” isomer **59b**; a difference of this size is within the error of the calculations and therefore cannot provide any clarity on the relative stabilities of the two isomers. Based on Ritter’s observation that the “head-to-tail” isomer of 2-phenylpyridine complex **22a** is the major isomer (major:minor ratio of 70:1, as determined by <sup>1</sup>H NMR spectroscopic analysis), it can be proposed that the “head-to-tail” isomer **59a** is likely to be the major species in this system, but X-ray crystallography of a pure sample would be necessary for structural confirmation.

To confirm that the six proton signals assigned to the major species present were, in fact, part of the same compound, several 2D NMR experiments were run on the sample. Analysis of the COSY spectrum confirmed the presence of two sets of three spin-coupled proton environments (Figure 21), which correspond to the protons on each aromatic ring of the quinoline group. While a <sup>13</sup>C spectrum was not obtainable, the <sup>1</sup>H-<sup>13</sup>C HSQC spectrum confirmed coupling to six individual aromatic carbon signals.



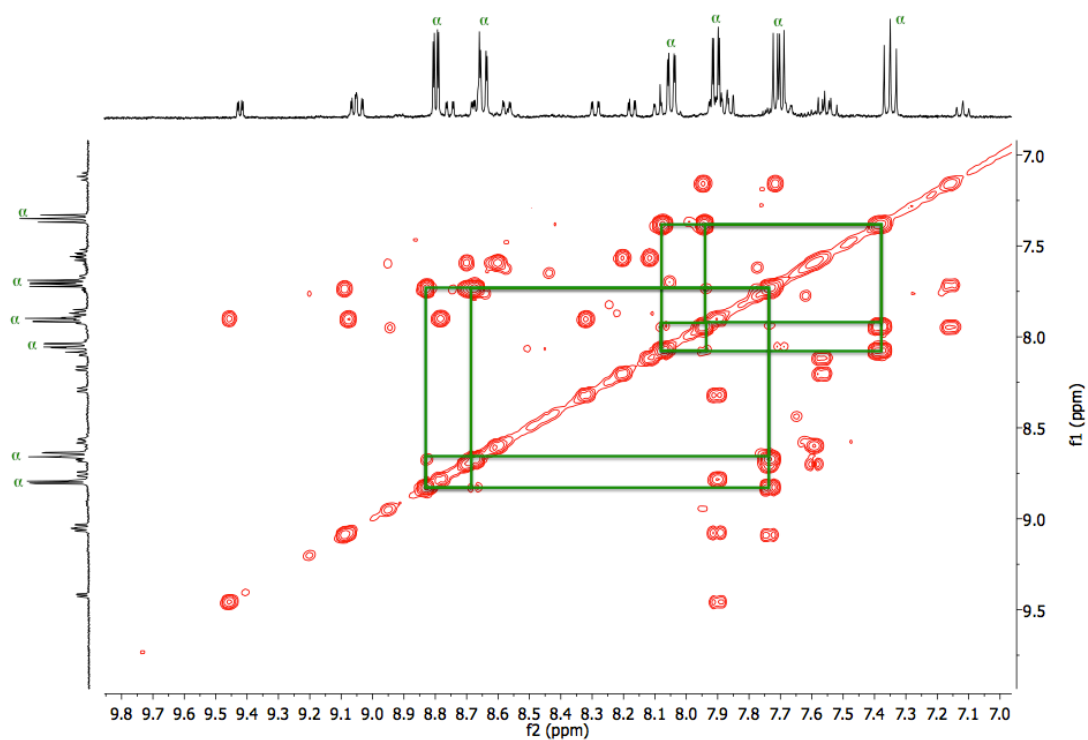


**Figure 21:** COSY  $^1\text{H}$  NMR Spectrum (700 MHz, 298 K, Acetic Acid- $d_4$ ) Showing Coupling Between Aromatic Protons in Species  $\alpha$

Having proposed a structure of the major compound observed by  $^1\text{H}$  NMR spectroscopy, attention was turned to identifying the other species present. Careful analysis of the COSY spectrum was used to identify twelve aromatic protons, connected *via* spin-spin coupling (Figure 22).

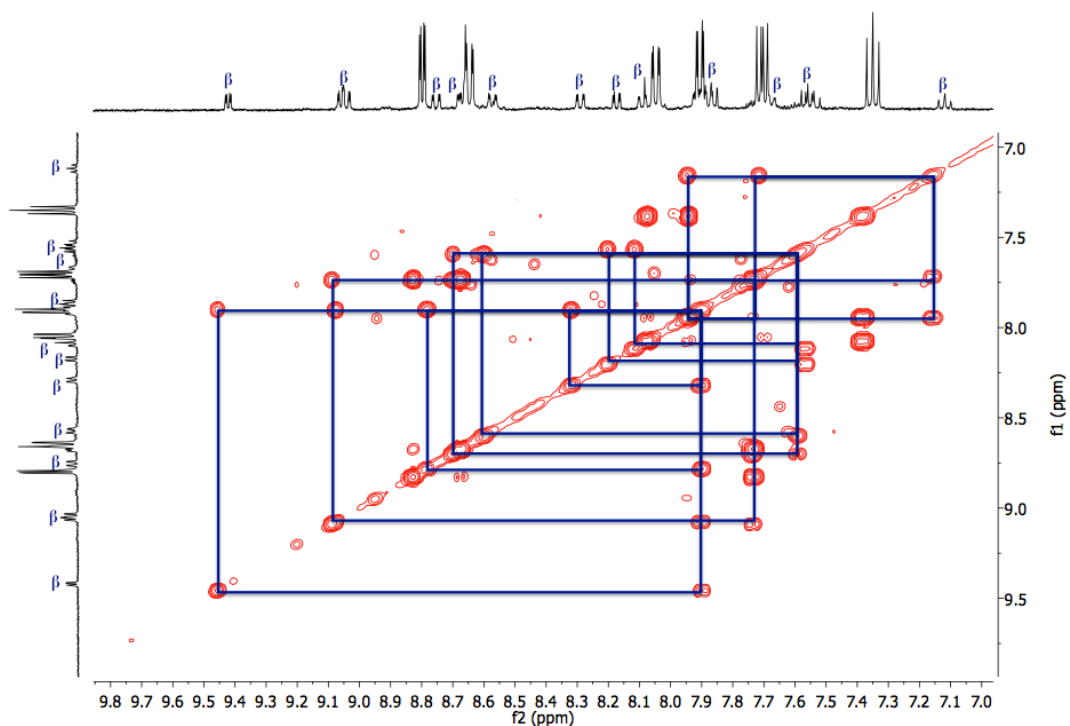
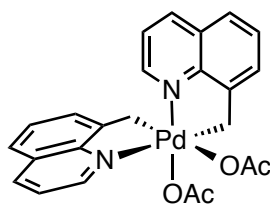


**Figure 22:** COSY Spectrum (700 MHz, 298 K, Acetic Acid- $d_4$ ) Showing Coupling Between Aromatic Protons In Species  $\beta$

The presence of twelve aromatic proton signals indicates that this compound contains two 8-methylquinoline ligands in non-identical environments. Since both isomers of proposed Pd<sup>III</sup> dimer **59** contain only one set of aromatic proton environments, complex **60**, an analogue of Sanford's proposed Pd<sup>IV</sup> complex of 2-phenylpyridine, is proposed as a minor intermediate species (Figure 23).

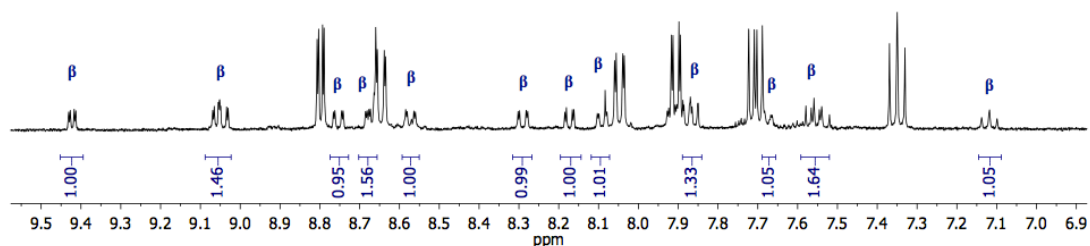


**60**

**Figure 23:** Proposed Minor Pd<sup>IV</sup> Complex of 8-Methylquinoline

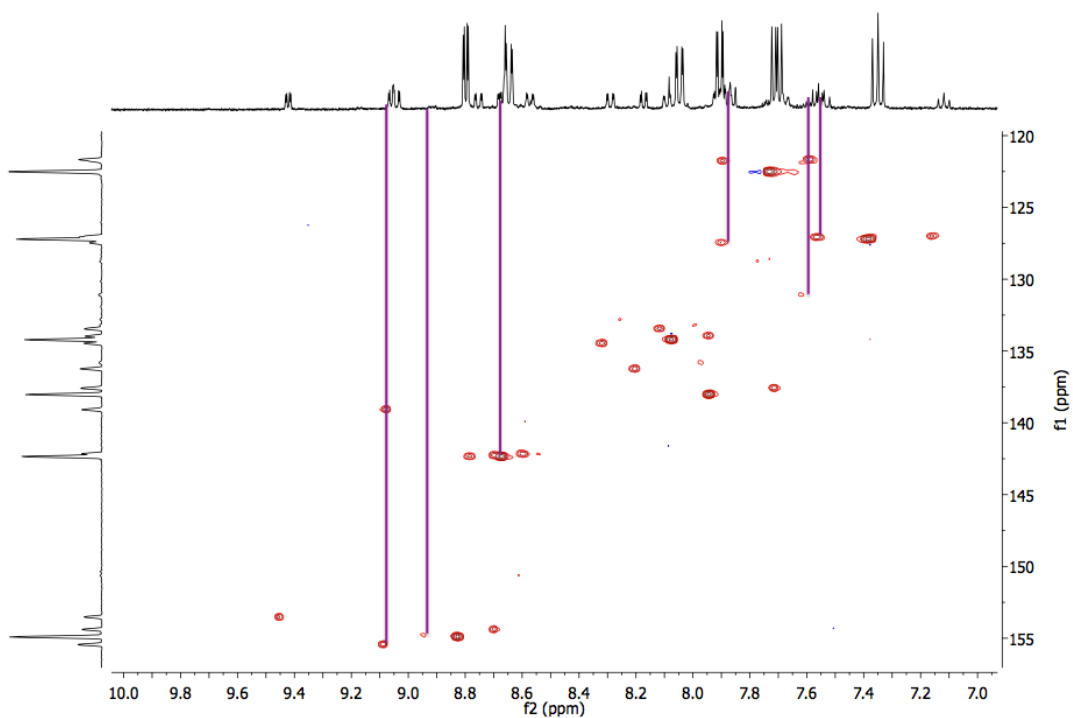
The aromatic <sup>1</sup>H NMR signals corresponding to the proposed structure for **60** are labelled “ $\beta$ ” in Figure 24. Integration of the 1H peak at 9.42 ppm versus the 1H peak at 7.34 ppm corresponding to the major species **59a/b** confirmed that the ratio of major:minor ( $\alpha$ : $\beta$ )

species is approximately 5:1. While the COSY spectrum confirmed spin-spin coupling between the twelve “ $\beta$ ” protons and thus confirmed that they were present in the same compound, integration of the peaks did not give the 1:1:1... ratio expected. Relative integrals are shown in Figure 24.



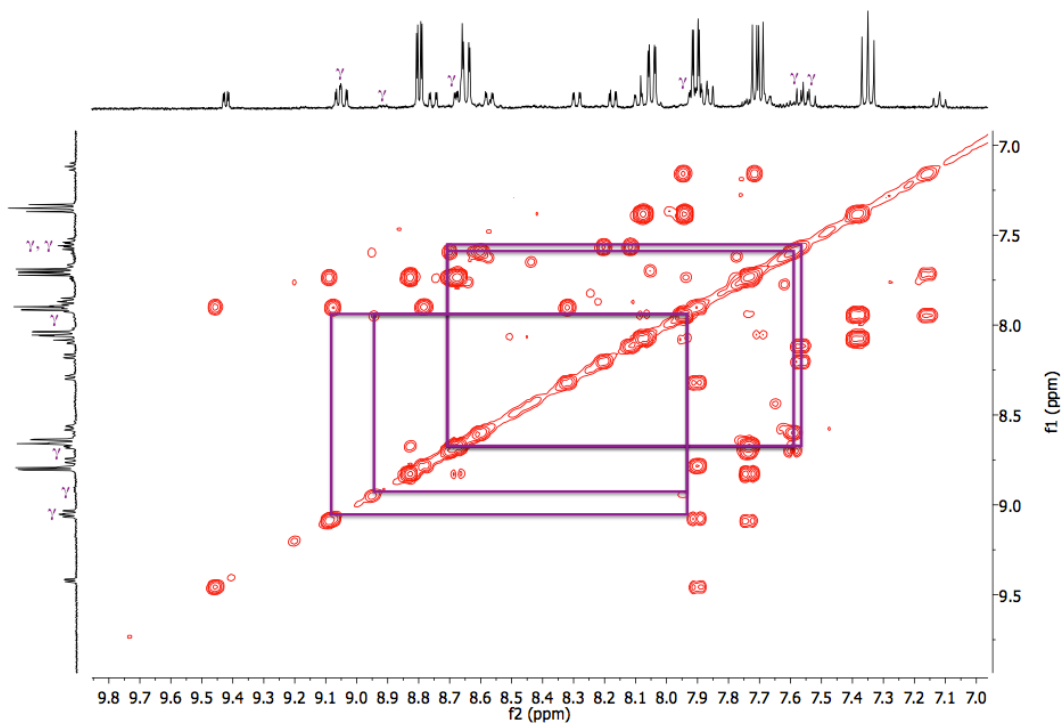
**Figure 24:** Aromatic Region of Spectrum B with Species  $\beta$  Signals Labelled

The peaks at 9.05, 8.68, 7.86, and 7.55 ppm were noted to have higher integrals than expected based upon the 1H peak at 9.42 ppm. This observation led us to believe that there was yet another species present, with aromatic protons whose signals were coincident with those in proposed complex **60**. This hypothesis was further supported by examination of the aromatic region of the <sup>1</sup>H-<sup>13</sup>C HSQC spectrum (Figure 25).



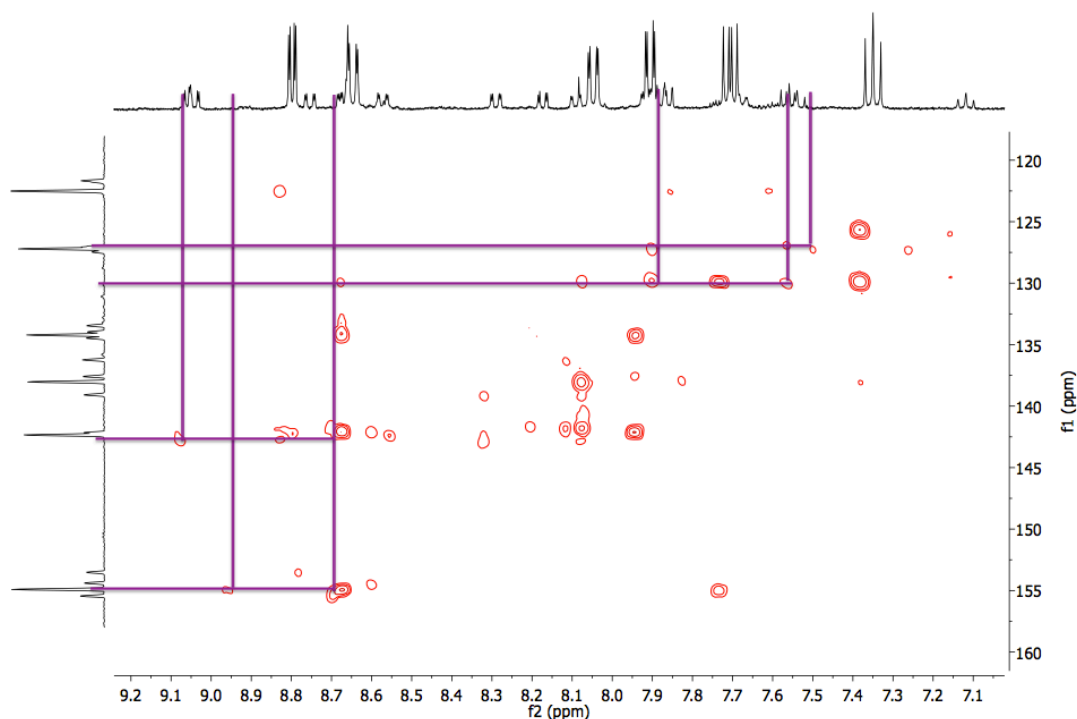
**Figure 25:**  $^1\text{H}$ - $^{13}\text{C}$  HSQC Spectrum (700 MHz, 298 K, Acetic Acid- $d_4$ ). Proton environments showing more coupling than expected are highlighted

The  $^1\text{H}$  signals at 9.07, 8.68 and 7.86 ppm each showed a direct correlation to two carbon environments, and the signal at 7.55 ppm showed a correlation to three carbon environments. Additionally, a correlation was observed between a  $^1\text{H}$  peak at 8.92 ppm, which had not yet been assigned, and a carbon environment at 155 ppm. Based on the relative integrals of the signals and the crosspeaks observed in the HSQC spectrum, we reasoned that the signals at 9.07, 8.68 and 7.86 ppm could each be assigned to one proton in the minor ( $\beta$ ) species and one proton in a third ( $\gamma$ ) complex, which contains 6 aromatic proton environments. The signal at 7.55 ppm corresponded to one proton in the “ $\beta$ ” species and two protons in the “ $\gamma$ ” species. Finally, the  $^1\text{H}$  peak at 8.92 ppm, which is spin-coupled to the peaks at 9.07 and 8.68 ppm, can also be assigned to the third intermediate compound. Figure 26 shows the spin-spin coupling between “ $\gamma$ ” protons in the COSY spectrum.



**Figure 26:** COSY Spectrum (700 MHz, 298 K, Acetic Acid- $d_4$ ) Showing Coupling Between Aromatic Protons in Species  $\gamma$

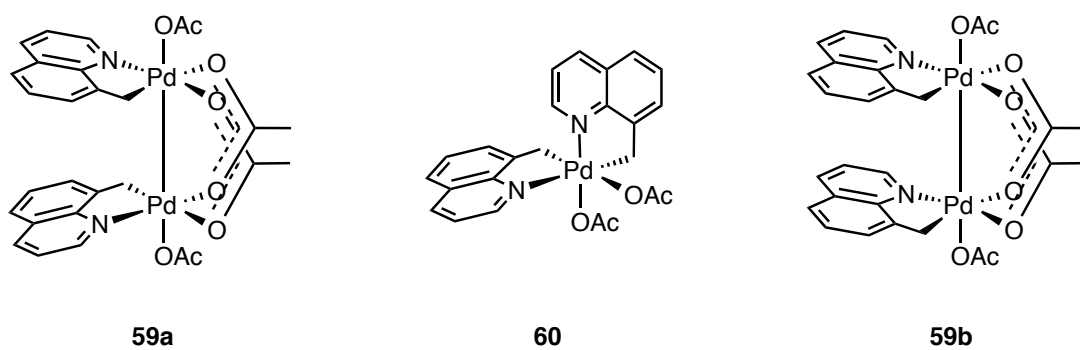
Further confirmation for the assignment of protons in the “ $\gamma$ ” intermediate complex came from careful inspection of the HMBC spectrum, which displayed coupling between two sets of three proton/carbon environments, corresponding to the two aromatic rings of an 8-methylquinoline ligand. The HMBC signals from two-bond proton-carbon coupling in the third ( $\gamma$ ) intermediate complex are displayed in Figure 27.



**Figure 27:** HMBC Spectrum (700 MHz, 298 K, Acetic Acid- $d_4$ ) Showing  $^1\text{H}$ - $^{13}\text{C}$  Two-Bond Coupling for Species  $\gamma$

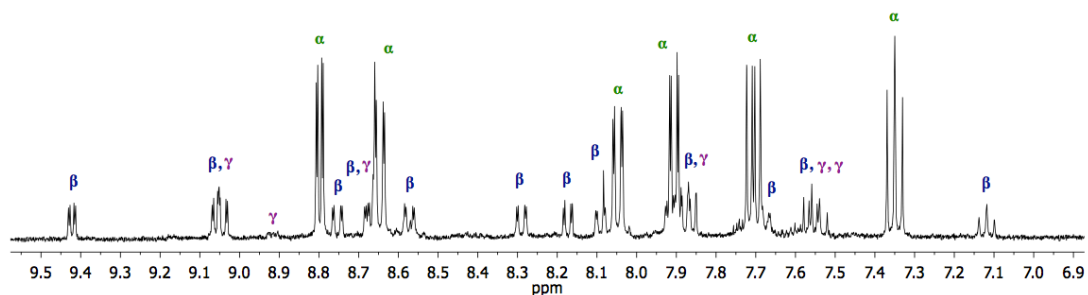
Based on these thorough NMR investigations, it is possible to tentatively propose structures for three high oxidation state Pd complexes (Figure 28). The major ( $\alpha$ ) species contains two 8-methylquinoline ligands in identical environments, and thus is believed to be a bimetallic  $\text{Pd}^{\text{III}}\text{-Pd}^{\text{III}}$  dimer. Based on observations by Ritter, “head-to-tail” isomer **59a** is currently believed to be the more likely major species, although this cannot be confirmed without single crystal diffraction and cross-check of the resultant single crystal with  $^1\text{H}$  NMR spectroscopic analysis.<sup>†</sup> The  $\text{Pd}^{\text{IV}}$  intermediate **60**, containing two non-identical 8-methylquinoline ligands and thus giving rise to 12 aromatic proton environments, is proposed as a minor ( $\beta$ ) intermediate complex. Lastly, the “head-to-head” isomer **59b**, also containing two 8-methylquinoline ligands in identical environments, is believed to be present in small quantities as the minor ( $\delta$ )  $\text{Pd}^{\text{III}}$  isomer.

<sup>†</sup> Since the initial submission of this thesis, further crystallographic studies conducted within the Fairlamb group have confirmed the acetato-bridged dimer of a bidentate 8-methylquinolinecarboxylic acid ligand to be the major species present (species  $\alpha$ ). Further details of these results are given in the Future Work section.



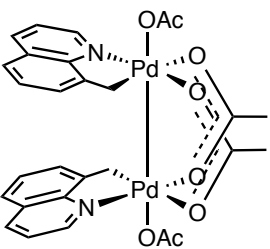
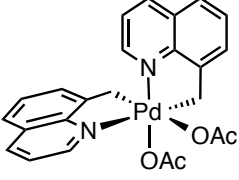
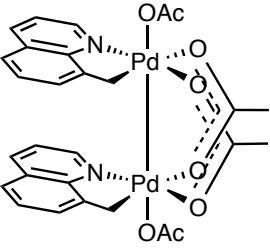
**Figure 28:** Proposed High Oxidation State Pd Complexes formed under Acetoxylation Conditions

Integration of  $^1\text{H}$  signals showed the  $\alpha:\beta:\gamma$  ratio to be approximately 10:2:1. The assignments of aromatic proton signals for all three proposed complexes are displayed in Figure 29 and Table 6.



**Figure 29:**  $^1\text{H}$  NMR Assignments for Proposed Intermediate Complexes

**Table 6:**  $^1\text{H}$  NMR Assignments for Proposed Intermediate Complexes

Proposed Species	Chemical Shift / ppm	Splitting Pattern and Coupling Constants	Relative Integration
 <p><math>\alpha</math> <b>59a</b></p>	8.82–8.78	dd, $J = 5.5, 1.5$ Hz	1H
	8.63–8.58	dd, $J = 8.3, 1.5$ Hz	1H
	8.02–7.99	dd, $J = 8.2, 1.5$ Hz	1H
	7.87–7.83	dd, $J = 7.5, 1.6$ Hz	1H
	7.69–7.64	dd, $J = 8.2, 5.5$ Hz	1H
	7.34–7.27	t, $J = 7.7$ Hz	1H
 <p><math>\beta</math> <b>60</b></p>	9.43–9.41	dd, $J = 5.5, 1.6$ Hz	1H
	9.08–9.02	m	1H <sup>a</sup>
	8.77–8.73	dd, $J = 8.3, 1.6$ Hz	1H
	8.69–8.67	dd, $J = 3.3, 1.6$ Hz	1H <sup>a</sup>
	8.58–8.55	dd, $J = 8.4, 1.6$ Hz	1H
	8.31–8.27	dd, $J = 8.2, 1.6$ Hz	1H
	8.19–8.15	dd, $J = 7.5, 1.6$ Hz	1H
	8.11–8.08	m	1H
	7.88–7.85	m	1H <sup>a</sup>
	7.67–7.66	m	1H
 <p><math>\gamma</math> <b>59b</b></p>	9.08–9.02	m	1H <sup>b</sup>
	8.94–8.89	m	1H
	8.69–8.67	dd, $J = 3.3, 1.6$ Hz	1H <sup>b</sup>
	7.88–7.85	m	1H <sup>b</sup>
	7.58–7.51	m	2H <sup>b</sup>

<sup>a</sup> Coincident with signal from species  $\gamma$

<sup>b</sup> Coincident with signal from species  $\beta$



In order to gather further clarification on the structures compounds present, ESI and LIFDI mass spectrometric analysis was conducted on the sample. Both methods have been used to characterise organometallic complexes, especially ESI-MS. In York, LIFDI has been found particularly useful for the characterisation of ‘neutral’ organometallic complexes.<sup>101</sup> No peaks were observed corresponding to the exact masses of the three structures proposed above, but LIFDI-MS showed a peak at  $m/z$  449.88, which corresponds to the radical cation of  $[\text{Pd}(\text{C}^{\wedge}\text{N})_2(\text{OAc})]$  fragment **61** (Figure 30). Additionally, a peak was observed in the ESI-MS spectrum at  $m/z$  481.0592, for which the isotope pattern corresponds to the calculated isotope pattern for the same fragment containing methanol, which was used as the solvent (with acetonitrile) for the ESI-MS LC injection (Figure 30, Fragment **62**).

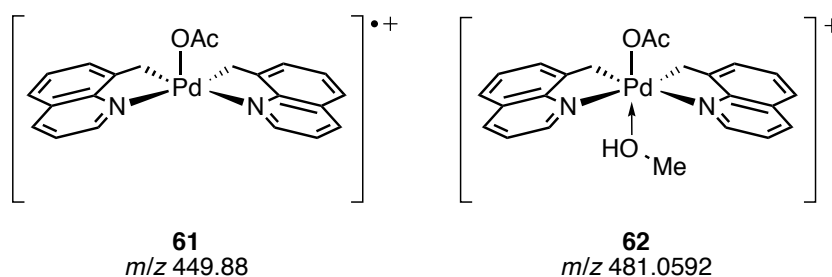
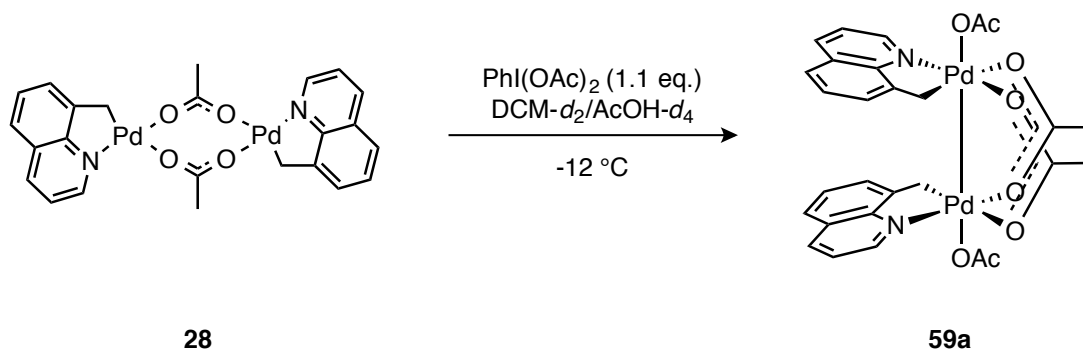


**Figure 30:** Proposed Fragments Observed by Mass Spectrometry

Both of these fragments contain two 8-methylquinoline ligands at one Pd centre; this is only seen in proposed complex **60**, providing further indication for the presence of a higher oxidation state complex in the system.

In order to gain confirmation of the presence of  $\text{Pd}^{\text{III}}$  complexes **59a** and **59b**, it was decided to prepare an authentic sample of the complex, as described by Ritter for the 2-phenylpyridine species. Therefore, a sample of acetato-bridged dimer **28** in a mixture of dichloromethane- $d_2$  and acetic acid- $d_4$  at  $-12$  °C was treated with 1.1 equivalents of  $\text{PhI}(\text{OAc})_2$  (Scheme 66).



**Scheme 66:** Preparation of an Authentic Sample of Pd<sup>III</sup> Dimer **59a**

The <sup>1</sup>H NMR spectrum of the mixture at -12 °C was taken four minutes after mixing, and as well as the presence of what is likely to be the dinuclear Pd complex, formation of the acetoxyated product **42** was also observed. Figure 31 shows the <sup>1</sup>H spectrum, with signals for the acetoxyated product marked with an asterisk. The peaks labelled “α” are believed to belong to the major isomer of bimetallic dimer **59a**. Evidence for a proton which is engaging in extensive hydrogen bonding was observed around 10 ppm, which could be caused by a monomeric complex, where acetate bridging is disrupted and instead AcOH is acting as a neutral ligand.

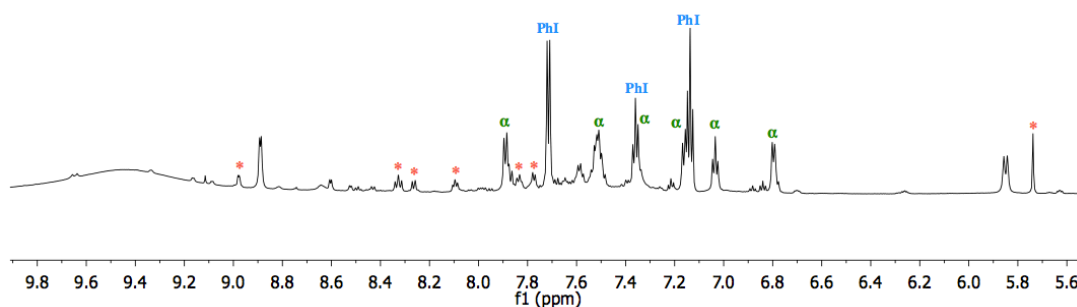


**Figure 31:** <sup>1</sup>H NMR spectrum (700 MHz, 261 K, Acetic Acid-*d*<sub>4</sub>) at *t* = 24 min, showing peaks assigned to dimer **59a**, acetoxyated product **42** and PhI (formed from reduction of PhI(OAc)<sub>2</sub>)

Further spectra were taken of the sample over 2 hours, and the intensity of the signals for the dimeric complex gradually decreases, with the hydrogen bonding observed disappearing rapidly (Figure 32). At 2 h 8 mins, all of the complex **59a** is seen to have turned over to the acetoxyated product **42**. The sample was warmed to room temperature, but no further change was observed.

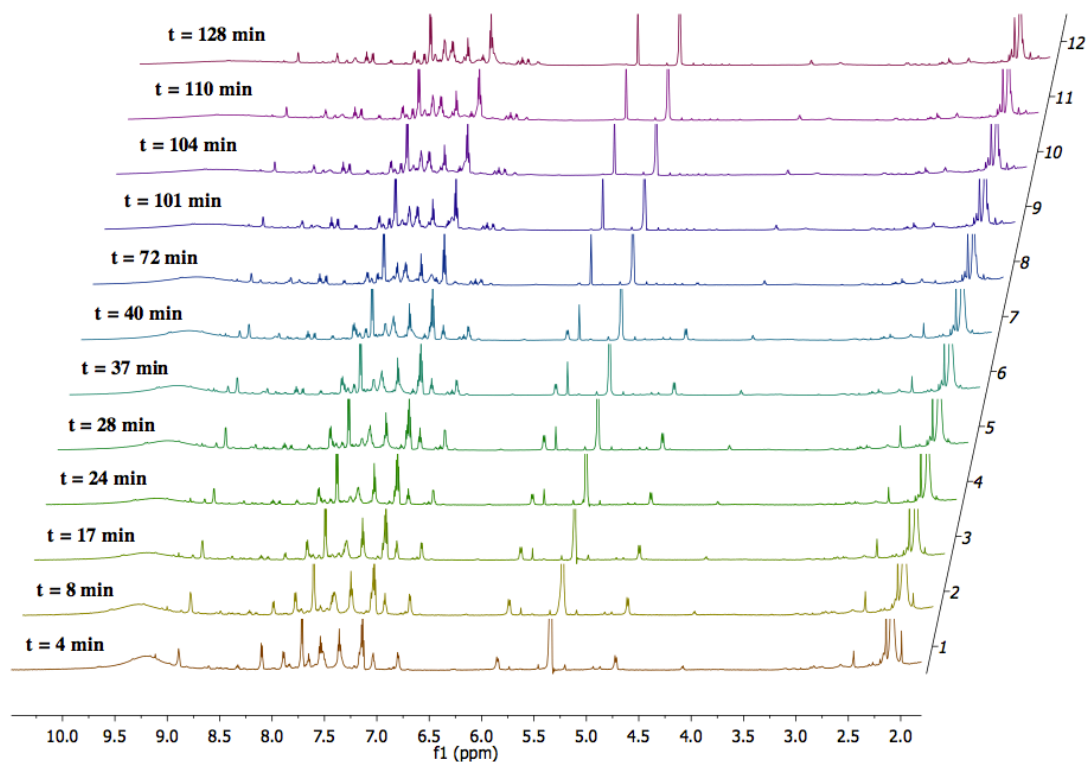
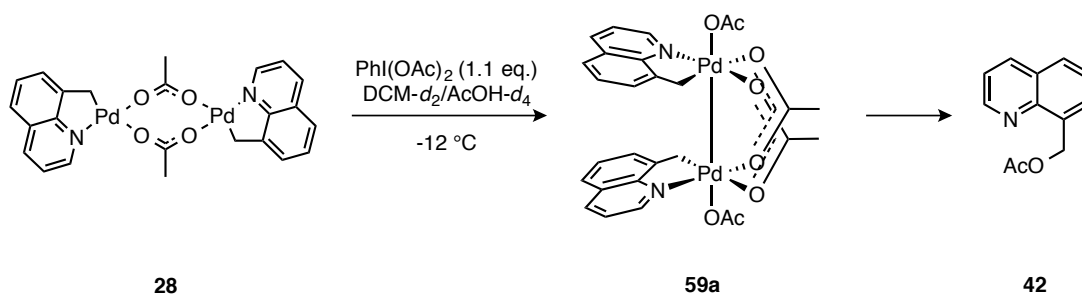


**Figure 32:**  $^1\text{H}$  NMR Spectra (700 MHz, 261 K, Acetic Acid- $d_4$ ) of a Mixture of Dimer **59a** and  $\text{PhI}(\text{OAc})_2$

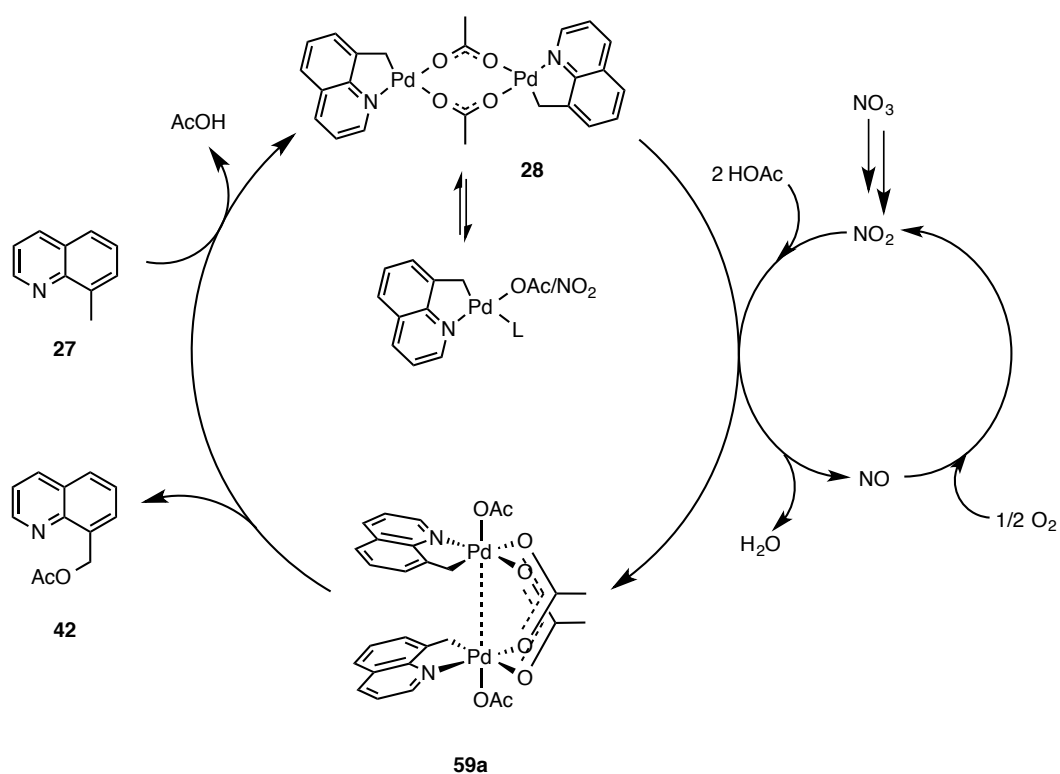
These results were unexpected; in Ritter's study the 2-phenylpyridine  $\text{Pd}^{\text{III}}$  dimer had been prepared at  $-10\text{ }^\circ\text{C}$  and was stable enough to be thoroughly characterised. The increased propensity of the complex prepared here to eliminate the functionalised product may give an indication of why our 8-methylquinoline complexes have such high catalytic activity. Nevertheless, the rapid decomposition of proposed  $\text{Pd}^{\text{III}}\text{-Pd}^{\text{III}}$  dimer **59a** to form product **42** (Scheme 67) confirms that it is a viable intermediate in the functionalisation of 8-methylquinoline.



**Scheme 67:** Decomposition of Proposed Intermediate **59a** to form **42**

In order to confirm the structures of the three proposed high oxidation state Pd complexes, further studies are necessary, and current work within the Fairlamb group is focusing on crystallographic identification of the species present. Further work is ongoing to determine the intermediacy of the proposed Pd<sup>III/IV</sup> species and whether they are kinetically competent.

With the results of all of our mechanistic investigations in hand, a tentative catalytic cycle can be proposed for the acetoxylation of 8-methylquinoline co-catalysed by sodium nitrate (Scheme 68). Cyclopalladation of the substrate **27** to form acetate-bridged dimer **28**, which is in equilibrium with a monomeric Pd<sup>II</sup> complex containing either acetate or nitrite ligands, is followed by oxidative addition of two acetate ligands to form Pd<sup>III</sup>-Pd<sup>III</sup> intermediate **59a**. This is assisted by the simultaneous reduction of free NO<sub>2</sub> to NO, as described by Sanford.<sup>30</sup> From **59a**, bimetallic reductive elimination results in the formation of acetoxyated product, **42** and regeneration of the active Pd<sup>II</sup> species.



**Scheme 68:** Proposed Catalytic Cycle for the Aerobic Acetoxylation of 8-Methylquinoline with NaNO<sub>3</sub>

While further evidence is required to confirm such a mechanism, this catalytic cycle is consistent with Ritter's proposed pathway for the acetoxylation of 2-phenylpyridine with  $\text{PhI}(\text{OAc})_2$ . The proposed mechanism also takes into account the observations from our isotopic labelling studies, which suggest that the nitrite is not responsible for providing an oxygen atom in the product. Instead, it is expected that the  $\text{NO}_3/\text{NO}_2/\text{NO}$  redox cycle described by Sanford is active and responsible for the formation of the major  $\text{Pd}^{\text{III}}$  intermediate. Preliminary work within the Fairlamb group is underway to isolate single crystals of the major intermediate species, and should provide confirmation of their structure, geometry, and potential catalytic competence.

## Chapter 5: Conclusions and Future Work

### Conclusions

Nitrite and nitrate anions have recently been implicated in the catalysis of oxidative C–H bond functionalisation. Their behaviour as ligands at Pd, however, remains underexplored and as such their role in the catalytic cycle has not been established. This thesis presents discussion of their geometry at Pd, the use of Pd–NO<sub>2</sub> and Pd–NO<sub>3</sub> complexes as highly active catalysts, and a thorough investigation into the mechanism of Pd-catalysed C–H bond functionalisation.

The preparation of a range of complexes with differing C<sup>^</sup>N ligands has allowed us to gain a greater understanding of the cyclopalladation behaviour of several organic substrates. Moreover, the successful synthesis and characterisation of a range of C<sup>^</sup>N palladacyclic complexes containing nitrite and nitrate ligands has provided further insight into how NO<sub>2</sub> or NO<sub>3</sub> bond to Pd. When assessing the role that such ligands can play in catalysis, and in particular the potential for reductive elimination of useful “C–NO<sub>2</sub>” type products, the geometry and linkage isomerism of the complexes is of significant importance.<sup>40</sup> This was shown to have implications in attempted reductive elimination experiments, where elimination of C–NO<sub>2</sub> type products, which would normally require the two ligands being eliminated to be mutually *cis*, was not observed. Complementary Density Functional Theory calculations were in agreement with our experimental observations that the *trans* geometric isomer is preferred for both [Pd(2-*phpy*)(PPh<sub>3</sub>)(NO<sub>2</sub>)] and [Pd(2-*phpy*)(PPh<sub>3</sub>)(NO<sub>3</sub>)]. Calculated free energy values suggest that the energy difference between *cis* and *trans* geometric isomers increases with increasing steric bulk of the C<sup>^</sup>N ligand. The crystal structure of [Pd(2-*phpy*)(PPh<sub>3</sub>)(NO<sub>2</sub>)] showed a mixture of *N*- and *O*- bound linkage isomers. This finding was again consistent with DFT calculations, which showed only a 1 kJ mol<sup>-1</sup> difference in the free energies of the two linkage isomers.

Reductive elimination experiments appeared to confirm the *trans*- geometry of the complexes, with elimination of nitrated products not achievable under a range of sets of conditions. This could also be due to the phosphine ligand present. Triphenylphosphine is relatively small, and may not provide enough steric hindrance for reductive elimination to be favoured. Attempted reductive elimination from the acetonitrile complex [Pd(H*pb*f)(NCCH<sub>3</sub>)(NO<sub>2</sub>)], which was shown by Nonoyama to have a *cis*- geometry, was

also unsuccessful,<sup>43</sup> suggesting that the geometry is not the only factor to have an effect on the complexes' ability to undergo reductive elimination, and that the bulk of the other coordinating ligands present should also be considered.

Five palladacyclic complexes of 8-methylquinoline were tested in the nitrate-co-catalysed acetoxylation of 8-methylquinoline reported by Sanford and found to be highly effective precatalysts, giving yields comparable to Pd(OAc)<sub>2</sub> under the literature conditions.<sup>30</sup> At low loadings of the NaNO<sub>3</sub> co-catalyst, the novel complexes **32** and **34** were shown to have increased activity. Remarkably, complex **34** is able to catalyse the reaction to 45% conversion in the absence of NaNO<sub>3</sub>. These results represent a Pd-catalysed oxidative functionalisation process that proceeds without the addition of any external oxidants or co-catalysts. Moreover, the superior activity of **34** over other catalysts used in conjunction with an equivalent quantity of NaNO<sub>3</sub> shows that the source of the nitrite can have a significant impact on the outcome of the reaction. The presence of a labile acetonitrile ligand is thought to accelerate catalysis when compared to the triphenylphosphine ligand.



**Figure 33:** Highly Active C–H Bond Functionalisation Catalysts

The catalyst **34** has been used in preliminary substrate scope investigations, and found to catalyse the reaction in moderate to good yields, without any optimisation having been carried out. Importantly, **34** was able to catalyse the C–H acetoxylation of sp<sup>2</sup> substrates where the Pd(OAc)<sub>2</sub> and NaNO<sub>3</sub> system was not.

The mechanism of catalysis at Pd has been extensively studied. Isotopic labelling experiments conducted with NaN<sup>18</sup>O<sub>3</sub> appeared to confirm Sanford's proposal that the acetate oxygen in the product derives from acetic acid, and that the nitrite is not acting as a source of oxygen. Stoichiometric experiments involving the reaction of acetate-bridged dimer **28** with NaNO<sub>3</sub> have allowed observation of several high oxidation state Pd intermediates. Through detailed analysis of the reaction by NMR spectroscopy, three

potential intermediate species have been proposed: two bimetallic Pd<sup>III</sup>-Pd<sup>III</sup> complexes, and one octahedral Pd<sup>IV</sup> complex (Figure 35).

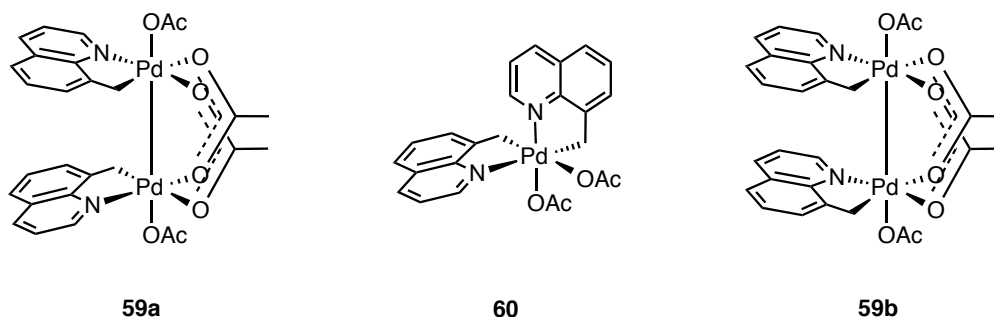


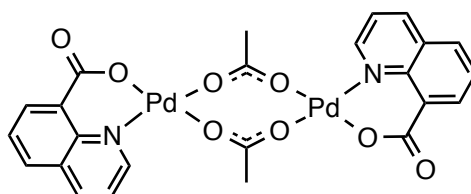
**Figure 34:** Proposed High Oxidation State Intermediates

Attempts to isolate an authentic sample of the proposed major species **59a** through reaction with  $\text{PhI}(\text{OAc})_2$  met with the rapid turnover of the intermediate complex to form the acetoxyated product. While this was a setback for confirmation of the structure of the intermediate, it confirms that such a complex is viable as a catalytic intermediate, since reductive elimination occurred rapidly at  $-12\text{ }^\circ\text{C}$ . With these results and comparison to the observations made by Ritter,<sup>68</sup> it has been possible to propose a Pd<sup>II</sup>/Pd<sup>III</sup> catalytic cycle for the acetoxylation of 8-methylquinoline, which could offer a competing pathway to the Pd<sup>II</sup>/Pd<sup>IV</sup> cycle proposed by Sanford.



## Future Work

While the studies detailed in this thesis provided strong evidence for the observation of the three intermediate species proposed, their independent isolation and subsequent characterisation remains a priority. This will be attempted using low temperature techniques as described by Sanford and Ritter, which aim to achieve single crystal growth of the complexes.<sup>30,68</sup> Since the initial submission of this thesis, ongoing studies conducted within the Fairlamb group have shown that the major intermediate species present is the acetato-bridged dimer of 8-methylquinoline carboxylic acid (**63**). An authentic sample of **63** has been isolated and its structure confirmed by X-ray crystallography.



**63**

**Figure 35:** Crystallographically Determined Structure of Major Intermediate Species **63**

NMR spectroscopic analysis of an authentic sample has now confirmed that **63** is the major ( $\alpha$ ) species observed in Spectrum B (see Chapter 4, page 78) and is therefore responsible for the peaks previously attributed to dimeric complex **59a**.

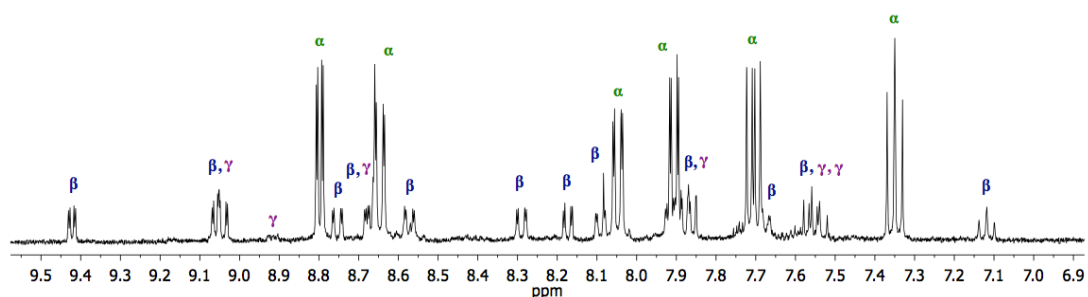


**Figure 36:** Spectrum B with Assignments for Proposed Intermediate Complexes

The successful isolation and characterisation of **63** has proven that in the presence of sodium nitrate, the oxidation of an  $sp^3$  C–H bond in 8-methylquinoline to the carboxylic acid can occur at Pd. Additionally, preliminary kinetic studies have shown that this complex could be involved in an important activation step; when an authentic sample of **63** is exposed to the typical acetoxylation reaction conditions, turnover to the acetoxyated product **42** is observed.

It remains a priority to establish the intermediacy of all complexes present during catalysis; further studies are ongoing within the Fairlamb group to determine the exact mechanism of oxidation at Pd, as well as the kinetics of the formation of 8-acetoxymethylquinoline from key dimeric complexes **28** and **63**.

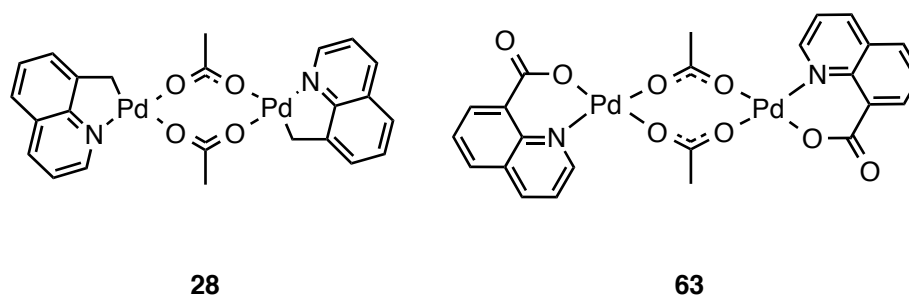


**Figure 37:** Dimeric Complexes of 8-Methylquinoline and 8-Methylquinoline Carboxylic Acid

The isolation and identification of intermediates in C–H functionalisation reactions catalysed by Pd–NO<sub>2</sub> or Pd–NO<sub>3</sub> complexes is another key aim. One important question is whether NO<sub>2</sub> or NO<sub>3</sub> ligands can act as ligands at high oxidation state Pd species in the same way that acetate ligands can. The work in this thesis has suggested that both Pd<sup>III</sup> and Pd<sup>IV</sup> species are present, and thus that there could be two competing mechanistic pathways. A comparison of the intermediates observed in systems with different catalysts could offer an understanding of which conditions favour a Pd<sup>III/III</sup> pathway and which favour a Pd<sup>II/IV</sup> pathway. In order for the mild conditions of catalysis developed within this thesis to be widely adopted and applied in the synthesis of more complex molecules, a thorough understanding of the catalytic cycle is crucial, and can provide information that is invaluable when designing novel C–H bond functionalisation catalysts.

Further investigations into the mechanism of acetoxylation are also underway within the Fairlamb group. The results presented in this thesis showed that under an O<sub>2</sub> atmosphere, no incorporation of <sup>18</sup>O into the acetoxyated product was observed when reactions were conducted in the presence of a NaN<sup>18</sup>O<sub>3</sub> co-catalyst. However, recent work conducted since the initial submission of this thesis has shown that <sup>18</sup>O incorporation is, in fact, observed when reactions are carried out in the presence of air. This result offers key new insights into the mechanism of sp<sup>3</sup> C–H acetoxylation. Firstly, it confirms that nitrite/nitrate anions present in catalysis are able to act as a source of oxygen in the final product, and thus that their role could be more significant than that of a redox co-oxidant. Additionally, it suggests that some sort of exchange process is occurring between dioxygen and the oxygen atoms in nitrate/nitrite, which end up in the acetoxyated product. O<sub>2</sub> is known to participate in the NO<sub>3</sub>/NO<sub>2</sub>/NO redox cycle, and is currently believed to be essential for the regeneration of nitrite in the proposed catalytic cycle for acetoxylation. Since it has now been confirmed that nitrate or nitrite is able to provide the oxygen atom in the acetate group of the product, the lack of incorporation for reactions carried out at higher concentrations of O<sub>2</sub> is indicative of exchange between <sup>18</sup>O in the co-catalyst and <sup>16</sup>O in dioxygen, which results in any <sup>18</sup>O label present in the product being “washed out” and therefore not being transferred to the acetoxyated product. We currently propose that this exchange process is fast in an O<sub>2</sub> atmosphere, but slower under air (*i.e.* at a lower concentration of O<sub>2</sub>), meaning that the <sup>18</sup>O label is able to incorporate into the acetate group before exchange takes place, and thus can be detected by mass spectrometry. Ongoing kinetics experiments aim to elucidate the exact mechanism of oxygen incorporation and exchange; these results, combined with the results of our investigations into reaction intermediates, should provide significant insight into the overall mechanism of catalysis.

Further studies on the scope of the newly developed catalysts in C–H bond functionalisation processes should be conducted. One of the key reasons for exploring the role of new species in oxidative C–H bond functionalisation is to be able to apply this methodology in the modification of compounds that have significant biological relevance. Examples of such complexes are tryptophan **64**, and amino acids L-histidine **65** and 3-(3'-pyridyl)-L-alanine **66**.

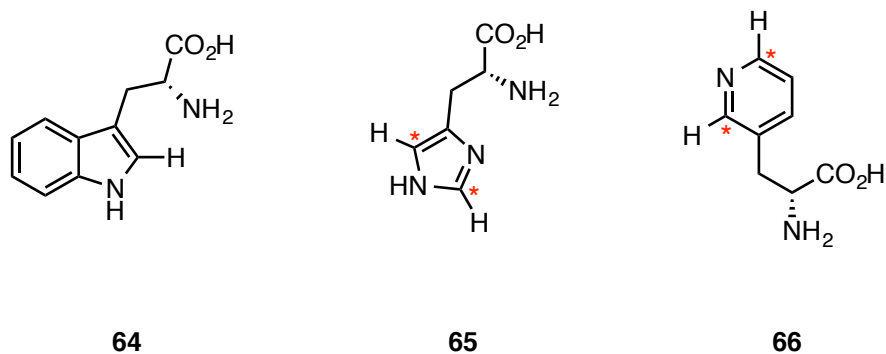
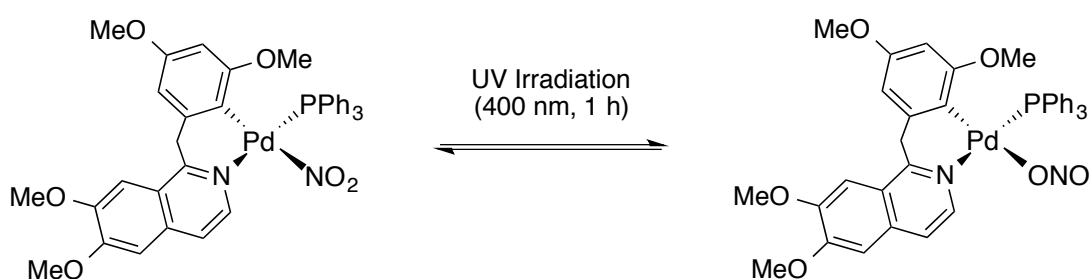


**Figure 38:** Biologically Relevant C–H Functionalisation Substrates

Typically,  $\text{Cu}^{\text{II}}$  salts are required for the functionalisation of tryptophan, but Cu binding to amino acid residues means that the functionalisation of peptides is not possible.<sup>102</sup> The catalysts developed within this thesis could be employed in the functionalisation of important biological substrates, with further development of catalysts based upon the use of these substrates as C<sup>^</sup>N ligands also a possibility.

One key reason for our interest in the behaviour of the nitrite anion at Pd was its ability to undergo photochemical linkage isomerization (Scheme 69).<sup>40</sup> Previous work within the Fairlamb group has focused on the development of an LED system, which allows reactions to be irradiated with a narrow-band 400 nm LED ( $\pm 20$  nm, 5 W).<sup>103</sup> Another potential route of exploration is the use of this system in photoredox processes catalysed by  $\text{Pd}^{\text{II}}$ , where the LED system could be used to selectively induce linkage isomerisation of Pd–NO<sub>2</sub>, which avoiding excitation of the substrate. It is proposed that this methodology could be employed in the oxidative functionalisation of organic substrates to form R–NO<sub>2</sub> or R–OAc type products.



**Scheme 69:** Linkage Isomerisation of Pd–NO<sub>2</sub> Complexes Reported by Fairlamb<sup>40</sup>

## Chapter 6: Experimental

### General Experimental Details

Reagents were purchased from Sigma-Aldrich, Alfa Aesar, Acros Organics or Fluorochem and used as received unless otherwise stated. Isotopically labelled chemicals were purchased from Icon Isotopes Ltd. and used as received. Pd(OAc)<sub>2</sub> was obtained from Precious Metals Online. Dry THF, CH<sub>2</sub>Cl<sub>2</sub> and acetonitrile were obtained from a Pure Solv MD-7 solvent system and stored under nitrogen. THF was also degassed by bubbling nitrogen through the solvent with sonication. Triethylamine was dried over and distilled from KOH. Dry methanol was obtained by drying over 3 Å molecular sieves. Petroleum ether refers to the fraction of petroleum that is collected at 40–60 °C. Reactions requiring anhydrous conditions were carried out in oven-dried glassware under an argon or nitrogen atmosphere.

Thin layer chromatography (TLC) was carried out using Merck 5554 aluminium backed silica plates and spots were visualized using UV light. Where necessary, plates were stained and heated with one of potassium permanganate, anisaldehyde or vanillin as appropriate. Retention factors (*R<sub>f</sub>*) are reported in parentheses along with the solvent system used. Flash column chromatography was performed using Merck 60 silica gel (particle size 40–63 μm) and a solvent system as reported in the text.

Melting points were recorded using a Stuart digital SMP3 machine.

<sup>1</sup>H, <sup>13</sup>C and <sup>31</sup>P NMR spectra were recorded on either a Jeol ECX400 or ECS400 MHz spectrometer at 400, 100 or 162 MHz respectively. Alternatively and where specified, <sup>1</sup>H spectra were recorded on a Bruker AV700 at 700 MHz. Chemical shifts are reported in parts per million (ppm) of tetramethylsilane and were referenced to residual undeuterated solvent. Unless otherwise stated, spectra were recorded at 298 K. <sup>13</sup>C and <sup>31</sup>P spectra were obtained with <sup>1</sup>H decoupling. <sup>1</sup>H and <sup>13</sup>C chemical shifts are given to 2 decimal places. Coupling constants (*J*) are quoted to the nearest 0.1 Hz. Spectra were processed using MestreNova.

Mass spectrometry was performed using a Bruker Daltronics micrOTOF spectrometer using electrospray ionisation (ESI). Liquid induction field desorption ionisation (LIFDI) mass spectrometry was performed using a Waters GCT Premier mass spectrometer. Mass to charge ratios (*m/z*) are reported in Daltons. High resolution mass spectra are reported with

<5 ppm error (ESI) or <20 ppm error (LIFDI). For clarity, LIFDI data are reported for  $^{106}\text{Pd}$ , the most abundant natural isotope of Pd.

Infrared spectra were obtained using either a Unicam Research Series FTIR (KBr IR) or a Bruker ALPHA-Platinum FTIR Spectrometer with a platinum-diamond ATR sampling module.

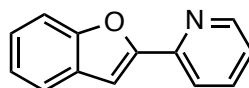
Elemental analysis was carried out on an Exeter Analytical CE-440 Elemental Analyser.

Gas chromatographic analysis was carried out using a Varian CP-3800 GC equipped with a CP-8400 autosampler. Separation was achieved using a DB-1 column (30 m  $\times$  0.32 mm, 0.25  $\mu\text{m}$  film thickness) with carrier gas flow rate of 2 mL  $\text{min}^{-1}$  and a temperature ramp from 50 to 250  $^{\circ}\text{C}$  at 20  $^{\circ}\text{C}$   $\text{min}^{-1}$ . The injection volume was 1  $\mu\text{L}$  with a split ratio of 10.

All DFT calculations were performed by Dr Jason Lynam using the TURBOMOLE V5.10 package using the resolution of identity (RI) approximation.<sup>109</sup> Initial optimisations were performed at the (RI-)BP86/SV(P) level, followed by frequency calculations at the same level. All minima were confirmed as such by the absence of imaginary frequencies, energies, geometries and vibrational frequencies are presented. Single-point calculations on the (RI-)BP86/SV(P) optimised geometries were performed using the hybrid PBE0 functional and the flexible def2-TZVPP basis set. The (RI-)PBE0/def2-TZVPP SCF energies were corrected for their zero point energies, thermal energies (DE) and entropies (obtained from the (RI-)BP86/SV(P)-level frequency calculations at 298.15 K,  $\text{DG}_{298.15}$ ). In all calculations, a 28 electron quasi-relativistic ECP replaced the core electrons of Pd. No symmetry constraints were applied during optimisations. Calculated XYZ coordinates, single point energies and vibrational spectra are reported in Appendix D.

## Synthesis of C<sup>N</sup> Ligands

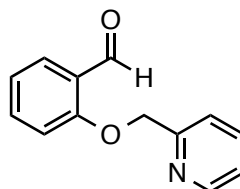
### 2(2-pyridyl)benzo[*b*]furan (39)<sup>43</sup>



In a 35 mL pressure tube, **40** (1 g, 4.7 mmol) was dissolved in dimethylformamide (8 mL). Potassium *tert*-butoxide (592 mg, 5.28 mmol) was added with stirring. The reaction mixture was heated at 100 °C for 4 h, after which the solvent was removed under reduced pressure. Brine (0.5 mL) was added to the resulting residue, and the organic products were extracted into diethyl ether. The organic extracts were filtered through a plug of silica gel and concentrated *in vacuo* to yield **39** as a white crystalline solid (712 mg, 78% yield).

MP 84–86 °C (lit.<sup>104</sup> mp 86–87 °C); <sup>1</sup>H NMR (400 MHz, CDCl<sub>3</sub>) δ 8.69 (ddd, *J* = 4.8, 1.8, 1.0 Hz, 1H), 7.91 (dt, *J* = 8.0, 1.1 Hz, 1H), 7.79 (ddd, *J* = 7.5, 1.8 Hz, 1H), 7.65 (ddd, *J* = 7.7, 1.4, 0.7 Hz, 1H), 7.57 (dq, *J* = 8.2, 1.0 Hz, 1H), 7.44 (d, *J* = 1.0 Hz, 1H), 7.37 – 7.31 (m, 1H), 7.29 – 7.22 (m, 2H); <sup>13</sup>C NMR (100 MHz, CDCl<sub>3</sub>) δ 155.38, 155.10, 149.99, 149.32, 136.89, 128.91, 125.31, 123.29, 123.02, 121.80, 119.94, 111.63, 104.91; HRMS (ESI<sup>+</sup>) *m/z* 196.0757 [M+H] (calc. for C<sub>13</sub>H<sub>10</sub>NO 196.0757); IR (ATR, cm<sup>-1</sup>) 3052, 3005, 1605, 1555, 1467, 1422, 1255, 1165, 1106, 1054, 921, 775, 750, 623.

### 2(2-pyridylmethoxy)benzaldehyde (40)<sup>43</sup>



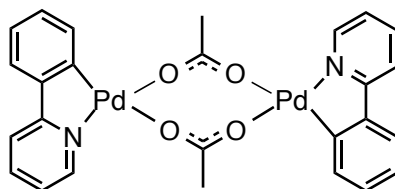
In a 35 mL pressure tube, salicylaldehyde (626 μL, 6.4 mmol) and 2-picolyl chloride hydrochloride (1.076 g, 6.56 mmol) were dissolved in dimethylformamide (8 mL). Potassium carbonate (1.769 g, 12.8 mmol) was added with stirring. The reaction mixture

was heated at 110 °C for 160 min, after which the solvent was removed *in vacuo*. The resulting residue was dissolved in acetonitrile (12 mL) and filtered under gravity. The filtrate was concentrated *in vacuo* to yield **40** as fine light brown crystals (1.271 g, 95% yield).

MP 68–70 °C (lit.<sup>104</sup> mp 69–71 °C); <sup>1</sup>H NMR (400 MHz, CDCl<sub>3</sub>) δ 10.62 (s, 1H), 8.62 (ddd, *J* = 4.9, 1.8, 0.9 Hz, 1H), 7.87 (ddd, *J* = 7.6, 1.9, 0.4 Hz, 1H), 7.76 (td, *J* = 7.7, 1.8 Hz, 1H), 7.57 – 7.50 (m, 2H), 7.32 – 7.26 (m, 1H), 7.09 – 7.03 (m, 2H), 5.33 (s, 2H); <sup>13</sup>C NMR (100 MHz, CDCl<sub>3</sub>) δ 189.73, 160.72, 156.46, 149.52, 137.20, 136.17, 129.00, 125.25, 123.12, 121.40, 113.4, 71.20 (only 12 carbon environments observed); HRMS (ESI<sup>+</sup>) *m/z* 214.0860 [M+H] (calc. for C<sub>13</sub>H<sub>12</sub>NO<sub>2</sub> 214.0863), 236.0679 [M+Na] (calc. for C<sub>13</sub>H<sub>11</sub>NNaO<sub>2</sub> 236.0682); IR (ATR, cm<sup>-1</sup>) 3073, 2865, 1682, 1591, 1486, 1457, 1433, 1375, 1243, 1171, 1105, 1031, 850, 750, 665, 626, 523.

## Synthesis of C<sup>N</sup> Palladacyclic Complexes

### [Pd<sub>2</sub>(μ-OAc)<sub>2</sub>(2-Phpy)<sub>2</sub>] (**21**)<sup>70</sup>

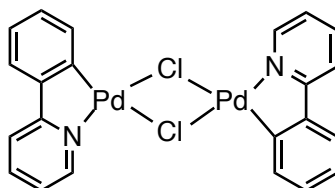


A suspension of 2-phenyl pyridine (201 mg, 1.3 mmol) and Pd(OAc)<sub>2</sub> (291 mg, 1.3 mmol) in glacial acetic acid (20 mL) was heated to reflux for 1.5 h and filtered. Water (150 mL) was added to the filtrate and the mixture was left overnight. The precipitate was collected by filtration and recrystallised from dichloromethane and hexane to yield **21** as fine yellow-orange crystals (332 mg, 78% yield).

MP 273–276 °C (lit. mp 294–296 °C); <sup>1</sup>H NMR (400 MHz, CDCl<sub>3</sub>) δ 7.88 (dd, *J* = 5.7, 1.6, 0.8 Hz, 2H), 7.38 (ddd, *J* = 8.1, 7.5, 1.6 Hz, 2H), 7.09 (ddd, *J* = 8.2, 1.4, 0.7 Hz, 2H), 6.87 (m, 8H), 6.45 (ddd, *J* = 7.5, 5.7, 1.4 Hz, 2H), 2.26 (m, 6H); <sup>13</sup>C NMR (100 MHz, CDCl<sub>3</sub>) δ 181.80, 150.22, 137.56, 131.95, 128.55, 123.97, 122.42, 121.11, 117.18, 25.00, ; HRMS (ESI<sup>+</sup>) *m/z* 638.9567 [M+H] (calc. for C<sub>26</sub>H<sub>23</sub>N<sub>2</sub>O<sub>2</sub>Pd<sub>2</sub> 638.9724); IR (KBr, cm<sup>-1</sup>) 3047, 2361, 2339, 1605, 1584, 1567, 1484, 1415, 1343, 1276, 1159, 1024, 752, 733, 685; Anal. calc. for C<sub>26</sub>H<sub>22</sub>N<sub>2</sub>O<sub>2</sub>Pd<sub>2</sub> C 48.85, H 3.47, N 4.38, observed C 48.72, H 3.40, N 4.19.



**[Pd<sub>2</sub>(μ-Cl)<sub>2</sub>(2-Phpy)<sub>2</sub>] (23)**<sup>70</sup>

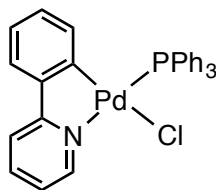


To a suspension of **21** (220 mg, 0.34 mmol) in acetone (15 mL) was added lithium chloride (57 mg, 1.36 mmol) in water (7.5 mL). The mixture was stirred at room temperature until the formation of a yellow-green precipitate, which was collected by filtration. The residue was washed with methanol and water (1:1 v/v) to yield **23** as a pale yellow solid (172 mg, 86% yield).

Pyridine-*d*<sub>5</sub> was added to an NMR tube containing a sample of complex **23** in CDCl<sub>3</sub>, in order to increase its solubility in common NMR solvents. Upon addition of pyridine-*d*<sub>5</sub>, a yellow solution was formed, presumably due to the formation of the monomeric complex [PdCl(2-Phpy)(py-*d*<sub>5</sub>)]. Residual pyridine signals have been omitted from the reported NMR data for clarity. <sup>13</sup>C NMR data are not reported because only pyridine signals are observed.

MP >310 °C (lit.<sup>71</sup> mp 327 °C); <sup>1</sup>H NMR (400 MHz, CDCl<sub>3</sub>) δ 9.39 (d, *J* = 5.7 Hz, 1H) 7.71 (ddd, *J* = 8.1, 7.5, 1.7 Hz, 1H), 7.56 (m, 1H), 7.39 (dd, *J* = 7.7, 1.5 Hz, 1H), 7.03 (m, 2H), 6.86 (td, *J* = 7.5, 1.5 Hz, 1H), 6.13 (d, *J* = 7.8 Hz, 1H); LIFDI-MS *m/z* 591.90 (calc. for C<sub>22</sub>H<sub>16</sub>N<sub>2</sub>Cl<sub>2</sub>Pd<sub>2</sub> 591.88); IR (KBr, cm<sup>-1</sup>) 3063, 2362, 2340, 1605, 1580, 1487, 1439, 1422, 1277, 1161, 10623, 1019, 741, 722; Anal. calc. for C<sub>22</sub>H<sub>16</sub>Cl<sub>2</sub>N<sub>2</sub>Pd<sub>2</sub> C 44.63, H 2.72, N 4.73, observed C 44.38, H 2.61, N 4.61.

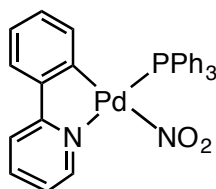
**[PdCl(2-Phpy)(PPh<sub>3</sub>)] (24)**<sup>72</sup>



A solution of chlorido-bridged dimer **23** (117 mg, 0.2 mmol) and triphenylphosphine (115 mg, 0.44 mmol) in dichloromethane (10 mL) was stirred at room temperature for 15 min under argon. The reaction mixture was filtered through Celite and hexane was added to induce precipitation. The product was collected by filtration and recrystallised from dichloromethane/hexane to yield **24** as a fine yellow powder (202 mg, 93% yield).

MP 218–220 °C (Lit.<sup>105</sup> mp 211–214 °C); <sup>1</sup>H NMR (400 MHz, CDCl<sub>3</sub>) δ 9.65 (dddd, *J* = 5.6, 3.6, 1.7, 0.8 Hz, 1H), 7.80 (m, 8H), 7.53 (m, 1H), 7.39 (m, 9H), 7.23 (m, 1H), 6.95 (m, 1H), 6.53 (m, 2H); <sup>13</sup>C NMR (100 MHz, CDCl<sub>3</sub>) δ 193.89, 193.65, 155.32, 150.85, 147.48, 139.51, 139.39, 139.37, 135.68, 131.79, 131.29, 130.85, 130.83, 128.97, 128.91, 128.81, 128.27, 128.16, 124.46, 123.87, 122.31, 122.28, 118.32, 118.30, 103.04, 101.05; <sup>31</sup>P NMR (162 MHz, CDCl<sub>3</sub>) δ 43.99; LIFDI-MS *m/z* 559.03 (calc. for C<sub>29</sub>H<sub>23</sub>NCIPPd 559.03); IR (KBr, cm<sup>-1</sup>) 3056, 2963, 1600, 1578, 1480, 1434, 1311, 1261, 1097, 1016, 802, 745, 729, 531; Anal. calc. for C<sub>29</sub>H<sub>23</sub>NCIPPd C 62.38, H 4.15, N 2.51, observed C 61.83, H 4.15, N 2.23.

**[Pd(NO<sub>2</sub>)(2-Phpy)(PPh<sub>3</sub>)] (25)**



A solution of **24** (135 mg, 0.24 mmol) and silver nitrite (186 mg, 1.20 mmol) in dichloromethane (18 mL) was stirred at room temperature for 48 h. The reaction mixture was filtered and the filtrate concentrated *in vacuo* to yield **25** as fine pale yellow crystals in quantitative yield.

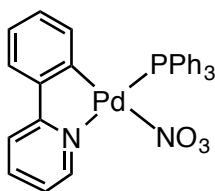
MP 206–209 °C; <sup>1</sup>H NMR (400 MHz, CDCl<sub>3</sub>) δ 7.89–7.73 (m, 8H), 7.59–7.31 (m, 11H), 7.18–7.13 (m, 1H), 7.00–6.94 (m, 1H), 6.56–6.50 (m, 2H); <sup>13</sup>C NMR (100 MHz, CDCl<sub>3</sub>) δ 193.86, 192.14, 170.55, 168.57, 135.33, 135.30, 135.21, 135.18, 131.23, 128.47, 128.37, 128.21, 101.11, 101.00, 99.00 (only 15 carbon signals observed); <sup>31</sup>P NMR (162 MHz, CDCl<sub>3</sub>) δ 32.74; LIFDI-MS *m/z* 522.00 [M–NO<sub>2</sub>] (Calc. for C<sub>29</sub>H<sub>23</sub>NPPd 522.06); IR (KBr, cm<sup>-1</sup>) 3049, 2962, 2361, 2338, 1603, 1486, 1435, 1362, 1335, 1263, 1099, 1019, 745, 691, 533, 347.

Crystals suitable for X-ray diffraction were grown by layering of a dichloromethane solution with cyclohexane.

### Summary of X-ray data for 25

Empirical formula	C <sub>32</sub> H <sub>29</sub> N <sub>2</sub> O <sub>2</sub> PPd
Formula weight	610.94
Temperature/K	110.00(10)
Crystal system	monoclinic
Space group	P2 <sub>1</sub> /c
<i>a</i> /Å	17.0574(7)
<i>b</i> /Å	9.4203(3)
<i>c</i> /Å	17.4240(6)
<i>α</i> /°	90.00
<i>β</i> /°	109.393(4)
<i>γ</i> /°	90.00
Volume/Å <sup>3</sup>	2640.94(17)
<i>Z</i>	4
<i>ρ</i> <sub>calc</sub> /mg/mm <sup>3</sup>	1.537
<i>m</i> /mm <sup>-1</sup>	0.797
F(000)	1248.0
Crystal size/mm <sup>3</sup>	0.2239 × 0.173 × 0.0852
2 $\Theta$ range for data collection	5.8 to 64.32°
Index ranges	-25 ≤ <i>h</i> ≤ 24, -11 ≤ <i>k</i> ≤ 13, -25 ≤ <i>l</i> ≤ 12
Reflections collected	14958
Independent reflections	8322[R(int) = 0.0237]
Data/restraints/parameters	8322/0/353
Goodness-of-fit on F <sup>2</sup>	1.047
Final R indexes [ <i>I</i> ≥ 2 $\sigma$ ( <i>I</i> )]	R <sub>1</sub> = 0.0393, wR <sub>2</sub> = 0.0821
Final R indexes [all data]	R <sub>1</sub> = 0.0490, wR <sub>2</sub> = 0.0871
Largest diff. peak/hole / e Å <sup>-3</sup>	1.56/-1.68

[Pd(NO<sub>3</sub>)(2-Phpy)(PPh<sub>3</sub>)] (**26**)



A solution of **24** (90 mg, 0.16 mmol) and silver nitrate (135 mg, 0.8 mmol) in dichloromethane (12 mL) was stirred at room temperature for 48 h. The reaction mixture was filtered and the filtrate concentrated *in vacuo* to yield **26** as fine light brown crystals (79 mg, 85% yield).

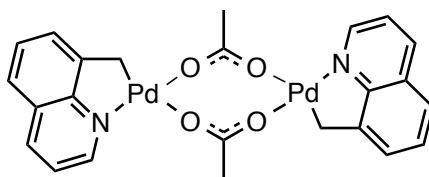
MP 204–209 °C; <sup>1</sup>H NMR (400 MHz, CDCl<sub>3</sub>) δ 8.52 (m, 1H), 7.92–7.85 (m, 1H), 7.84–7.76 (m, 7H), 7.54–7.46 (m, 4H), 7.44–7.37 (m, 6H), 7.23 (m, 1H), 6.99 (m, 1H), 6.56–6.52 (m, 2H); <sup>13</sup>C NMR (100 MHz, CDCl<sub>3</sub>) δ 193.86, 193.85, 163.81, 149.41, 148.54, 147.15, 140.12, 140.00, 139.72, 135.30, 135.18, 132.50, 131.20, 129.79, 129.29, 129.24, 129.18, 128.65, 128.54, 124.94, 124.17, 122.86, 118.71; <sup>31</sup>P NMR (162 MHz, CDCl<sub>3</sub>) δ 41.41; LIFDI-MS *m/z* 522.00 [M–NO<sub>3</sub>] (Calc. for C<sub>29</sub>H<sub>23</sub>NPPd 522.06); IR (KBr, cm<sup>-1</sup>) 3055, 2921, 2851, 2360, 2340, 1601, 1485, 1451, 1433, 1384, 1289, 1099, 1018, 752, 703, 534, 370; Anal. calc. for C<sub>29</sub>H<sub>23</sub>N<sub>2</sub>O<sub>3</sub>PPd C 59.55, H 3.96, N 4.79, observed C 59.05, H 4.78, N 3.83.

Crystals suitable for X-ray diffraction were grown by layering of a dichloromethane solution with cyclohexane.

### Summary of X-ray data for 26

Empirical formula	C <sub>29</sub> H <sub>23</sub> N <sub>2</sub> O <sub>3</sub> PPd
Formula weight	584.86
Temperature/K	110.00(14)
Crystal system	monoclinic
Space group	P2 <sub>1</sub> /c
a/Å	9.43313(15)
b/Å	15.07499(18)
c/Å	17.3486(2)
α/°	90.00
β/°	90.1549(13)
γ/°	90.00
Volume/Å <sup>3</sup>	2467.04(6)
Z	4
ρ <sub>calc</sub> /mg/mm <sup>3</sup>	1.575
m/mm <sup>-1</sup>	0.852
F(000)	1184.0
Crystal size/mm <sup>3</sup>	0.4233 × 0.154 × 0.1148
2θ range for data collection	5.62 to 64.46°
Index ranges	-14 ≤ h ≤ 14, -22 ≤ k ≤ 21, -25 ≤ l ≤ 22
Reflections collected	18360
Independent reflections	7871[R(int) = 0.0274]
Data/restraints/parameters	7871/0/325
Goodness-of-fit on F <sup>2</sup>	1.061
Final R indexes [I ≥ 2σ (I)]	R <sub>1</sub> = 0.0303, wR <sub>2</sub> = 0.0672
Final R indexes [all data]	R <sub>1</sub> = 0.0381, wR <sub>2</sub> = 0.0716
Largest diff. peak/hole / e Å <sup>-3</sup>	0.68/-0.73

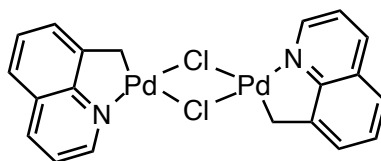
**[Pd<sub>2</sub>(μ-OAc)<sub>2</sub>(8-Mequin)<sub>2</sub>] (28)**<sup>70</sup>



8-Methylquinoline (186 mg, 1.3 mmol) and Pd(OAc)<sub>2</sub> (291 mg, 1.3 mmol) were suspended in glacial acetic acid (20 mL), refluxed for 1.5 h and then filtered. Water (150 mL) was added to the filtrate and the mixture left overnight. The precipitated product was collected by filtration and recrystallised from dichloromethane/hexane to yield **28** as a bright orange solid (342 mg, 85% yield).

MP 193–195 °C; <sup>1</sup>H NMR (400 MHz, CDCl<sub>3</sub>) δ 8.54 (dd, *J* = 5.0, 1.5 Hz, 2H), 7.88 (dd, *J* = 8.4, 1.5 Hz, 2H), 7.24 (dd, *J* = 8.3, 5.0 Hz, 2H), 7.11–6.99 (m, 2H), 6.91 (dd, *J* = 8.1, 7.1 Hz, 2H), 6.73 (dd, *J* = 7.1, 1.1 Hz, 2H), 3.47 (d, *J* = 14.0 Hz, 2H), 2.55 (d, *J* = 13.8 Hz, 2H), 2.14 (s, 6H); <sup>13</sup>C NMR (100 MHz, CDCl<sub>3</sub>) δ 182.83, 181.45, 152.79, 149.11, 148.97, 148.42, 148.32, 147.67, 136.52, 136.06, 128.23, 128.04, 127.86, 127.39, 127.33, 126.81, 122.85, 122.40, 121.14, 120.51, 24.53, 23.85, 22.77, 22.23; LIFDI-MS *m/z* 615.99 (Calc. for C<sub>24</sub>H<sub>22</sub>N<sub>2</sub>O<sub>4</sub>Pd<sub>2</sub> 615.97); IR (KBr, cm<sup>-1</sup>) 3390, 1566, 1504, 1408, 1050, 817, 776, 671; Anal. calc. for C<sub>24</sub>H<sub>22</sub>N<sub>2</sub>O<sub>4</sub>Pd<sub>2</sub> C 46.85, H 3.60, N 4.55, observed C 45.91, H 3.40, N 4.55.

**[Pd<sub>2</sub>(μ-Cl)<sub>2</sub>(8-Mequin)<sub>2</sub>] 29**<sup>106</sup>



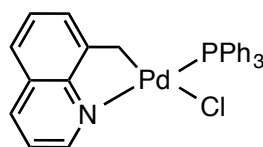
To a solution of **28** (500 mg, 0.8 mmol) in methanol (15 mL) was added lithium chloride (170 mg, 4 mmol) in methanol (10 mL), resulting in immediate precipitation of the product. The precipitate was collected by filtration and washed with methanol/water (1:1 v/v) to yield **29** as a yellow powder (455 mg, 80% yield).

Pyridine-*d*<sub>5</sub> was added to an NMR tube containing a sample of complex **29** in CDCl<sub>3</sub>, in order to increase its solubility in common NMR solvents. Upon addition of pyridine-*d*<sub>5</sub>, a

yellow solution was formed, presumably due to the formation of the monomeric complex [PdCl(8-Mequin)(pyr-*d*<sub>5</sub>)]. Residual pyridine signals have been omitted from the reported NMR data for clarity.

MP 249–251 °C; <sup>1</sup>H NMR (400 MHz, CDCl<sub>3</sub>) δ 9.57 (dd, *J* = 5.1, 1.5 Hz, 2H), 8.16 (dd, *J* = 8.3, 1.5 Hz, 2H), 7.62–7.24 (m, 8H), 3.54 (t, *J* = 1.1 Hz, 4H); <sup>13</sup>C NMR (100 MHz, CDCl<sub>3</sub>) δ 153.4, 152.2, 147.6, 137.6, 129.0, 128.2, 127.9, 123.9, 121.6, 30.1; LIFDI-MS *m/z* 567.90 (Calc. for C<sub>20</sub>H<sub>16</sub>Cl<sub>2</sub>N<sub>2</sub>Pd<sub>2</sub> 567.88); IR (KBr, cm<sup>-1</sup>) 3059, 2919, 2283, 1563, 1505, 1385, 1375, 1316, 1056, 825, 787, 762, 676, 535; Anal. calc. for C<sub>20</sub>H<sub>16</sub>Cl<sub>2</sub>N<sub>2</sub>Pd<sub>2</sub> C 42.28, H 2.84, N 4.93, observed C 41.99, H 2.65, N 4.71.

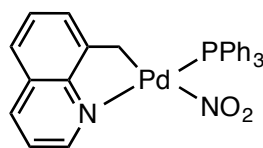
### [PdCl(8-Mequin)(PPh<sub>3</sub>)] (**30**)



A solution of chlorido-bridged dimer **29** (290 mg, 0.5 mmol) and triphenylphosphine (288 mg, 1.1 mmol) in dichloromethane (20 mL) was stirred at room temperature for 15 min under argon. The reaction mixture was filtered through Celite and hexane was added to induce precipitation. The product was collected by filtration and recrystallised from dichloromethane/hexane to yield **30** as fine yellow crystals in quantitative yield.

MP 205–209 °C (lit.<sup>107</sup> MP 148–153 °C); <sup>1</sup>H NMR (400 MHz, CDCl<sub>3</sub>) δ 9.79 (m, 1H), 8.27 (dd, *J* = 8.3, 1.6 Hz, 1H), 7.84–7.78 (m, 4H), 7.74–7.30 (m, 15H), 2.85 (d, *J* = 3.8, 2H); <sup>13</sup>C NMR (100 MHz, CDCl<sub>3</sub>) δ 150.4, 148.2, 137.9, 135.0, 131.6, 131.1, 130.5, 129.1, 128.4, 127.7, 123.8, 121.6, 100.0, 33.4; <sup>31</sup>P (162 MHz, CDCl<sub>3</sub>) δ 35.18; LIFDI-MS *m/z* 545.05 (Calc. for C<sub>28</sub>H<sub>23</sub>ClNPPd 545.03); Anal. calc. for C<sub>28</sub>H<sub>23</sub>ClNPPd C 61.56, H 4.24, N 2.56, observed C 61.70, H 4.12, N 2.21.

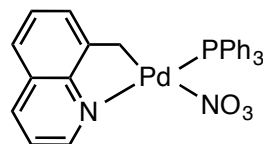
**[Pd(8-Mequin)(NO<sub>2</sub>)(PPh<sub>3</sub>)] (31)**



A solution of **30** (250 mg, 0.46 mmol) and silver nitrite (352 mg, 2.29 mmol) in dichloromethane (20 mL) was stirred at room temperature for 24 h. The reaction mixture was filtered and the filtrate concentrated *in vacuo* to yield **31** as a light brown solid in quantitative yield.

MP 178–180 °C; <sup>1</sup>H NMR (400 MHz, CDCl<sub>3</sub>) δ 8.72 (s, 1H), 8.29 (d, *J* = 8.2 Hz, 1H), 7.77–7.68 (m, 5H), 7.51–7.37 (m, 13H), 2.75 (s, 2H); LIFDI-MS *m/z* 510.03 [M–NO<sub>2</sub>] (Calc. for C<sub>28</sub>H<sub>23</sub>NPPd 510.06); IR (KBr, cm<sup>-1</sup>) 3055, 2870, 1684, 1569, 1503, 1481, 1431, 1340, 1095, 825, 752, 696, 349.

**[Pd(8-Mequin)(NO<sub>3</sub>)(PPh<sub>3</sub>)] (32)**

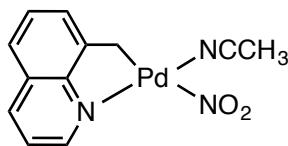


A solution of **30** (250 mg, 0.46 mmol) and silver nitrate (389 mg, 2.29 mmol) in dichloromethane (20 mL) was stirred at room temperature for 24 h. The reaction mixture was filtered and the filtrate concentrated *in vacuo* to yield **32** as a pale yellow solid in quantitative yield.

MP 180–183 °C; <sup>1</sup>H NMR (400 MHz, CDCl<sub>3</sub>) δ 8.87 – 8.79 (m, 1H), 8.32 (dd, *J* = 8.3, 1.4 Hz, 1H), 7.77 – 7.68 (m, 3H), 7.64 (d, *J* = 7.6 Hz, 1H), 7.54 – 7.37 (m, 15H), 3.04 (d, *J* = 4.2 Hz, 2H); <sup>13</sup>C NMR (100 MHz, CDCl<sub>3</sub>) δ 163.61, 162.98, 162.53, 151.92, 148.85, 147.80, 141.34, 138.45, 134.32, 134.20, 130.93, 130.40, 129.91, 129.64, 129.53, 129.20, 128.84, 128.78, 127.99, 124.14, 121.84, 120.37, 31.68; LIFDI-MS *m/z* 510.04 [M–NO<sub>3</sub>] (Calc. for C<sub>28</sub>H<sub>23</sub>NPPd 510.06); IR (KBr, cm<sup>-1</sup>) 3054, 1505, 1447, 1384, 1286, 1096, 1021, 825, 786, 751, 696, 335.



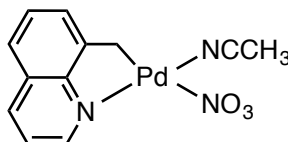
**[Pd(8-Mequin)(NO<sub>2</sub>)(NCCH<sub>3</sub>)] (33)**



**29** (140 mg, 0.25 mmol) and silver nitrite (91 mg, 0.6 mmol) were suspended in a mixture of dichloromethane and acetonitrile (8 mL, 3:1 *v/v*) and stirred at room temperature for 24 h. The reaction mixture was filtered and the filtrate concentrated *in vacuo* to yield **33** as a yellow solid in quantitative yield.

MP 236–242 °C; <sup>1</sup>H NMR (400 MHz, CDCl<sub>3</sub>) δ 8.53 (dd, *J* = 5.0, 1.5 Hz, 1H), 8.29 (dd, *J* = 8.4, 1.5 Hz, 1H), 7.66–7.57 (m, 2H), 7.53–7.38 (m, 2H), 3.94 (s, 2H), 1.53 (m, 3H); <sup>13</sup>C NMR (100 MHz, CDCl<sub>3</sub>) δ 149.55, 147.14, 138.66, 129.07, 128.78, 128.45, 124.01, 121.46, 101.99, 40.41, 1.10; LIFDI-MS *m/z* 389.06 [M–NO<sub>2</sub>+C<sup>+</sup>N] (Calc. for C<sub>20</sub>H<sub>16</sub>N<sub>2</sub>Pd 390.03); IR (KBr, cm<sup>-1</sup>) 2919, 2849, 1505, 1435, 1374, 1216, 1055, 1018, 818, 778, 348.

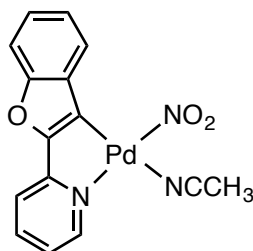
**[Pd(8-Mequin)(NO<sub>3</sub>)(NCCH<sub>3</sub>)] (34)**



**29** (140 mg, 0.25 mmol) and silver nitrate (100 mg, 0.6 mmol) were suspended in a mixture of dichloromethane and acetonitrile (8 mL, 3:1 *v/v*) and stirred at room temperature for 24 h. The reaction mixture was filtered and the filtrate concentrated *in vacuo* to yield **34** as a brown solid in quantitative yield.

MP 139–143 °C; <sup>1</sup>H NMR (400 MHz, CDCl<sub>3</sub>) δ 8.64 (dd, *J* = 5.2, 1.5 Hz, 1H), 8.26 (dd, *J* = 8.4, 1.5 Hz, 1H), 7.59 (dd, *J* = 7.9, 1.3 Hz, 1H), 7.55–7.50 (m, 1H), 7.49–7.37 (m, 1H), 3.69 (s, 2H), 2.34 (s, 3H); <sup>13</sup>C NMR (100 MHz, CDCl<sub>3</sub>) δ 152.5, 149.7, 146.5, 138.4, 129.0, 128.5, 128.3, 124.2, 31.0, 22.9, 3.6; LIFDI-MS *m/z* 309.98 [M–NCCH<sub>3</sub>] (Calc. for C<sub>10</sub>H<sub>8</sub>N<sub>2</sub>O<sub>3</sub>Pd 309.96); IR (KBr, cm<sup>-1</sup>) 2924, 2853, 2253, 1732, 1508, 1438, 1384, 1290, 1027, 824, 783, 327.

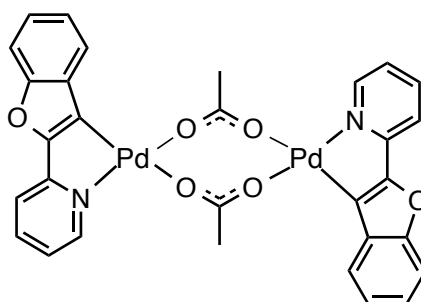
**[Pd(Hpbf)(NO<sub>2</sub>)(CH<sub>3</sub>CN)] (35)**



A solution of **39** (195 mg, 1 mmol), Pd(OAc)<sub>2</sub> (224 mg, 1 mmol) and NaNO<sub>2</sub>, (83 mg, 1.2 mmol) in acetonitrile (30 mL) was refluxed for 4 h, filtered while hot and left to cool to room temperature. The yellow precipitate formed upon cooling was collected by filtration, washed with acetonitrile and dried *in vacuo*. Recrystallisation from dichloromethane/hexane afforded product **41** as fine yellow-orange crystals in quantitative yield.

MP 110–120 °C; <sup>1</sup>H NMR (400 MHz, CDCl<sub>3</sub>) δ 8.68–8.58 (m, 1H), 8.09 (d, *J* = 7.8 Hz, 1H), 7.87–7.77 (m, 1H), 7.55–7.42 (m, 1H), 7.41–7.28 (m, 3H), 7.06 (s, 1H), 2.14 (s, 3H); LIFDI-MS *m/z* 345.98 [M–NCCH<sub>3</sub>] (Calc. for C<sub>13</sub>H<sub>8</sub>N<sub>2</sub>O<sub>3</sub>Pd 345.96); IR (KBr, cm<sup>-1</sup>) 2920, 2885, 2298, 1507, 1378, 1323, 1263, 1024, 806, 783, 325; Anal. calc. for C<sub>15</sub>H<sub>11</sub>N<sub>3</sub>O<sub>3</sub>Pd C 46.47, H 2.86, N 10.84, observed C 46.07, H 2.78, N 10.65.

**[Pd<sub>2</sub>(μ-OAc)<sub>2</sub>(Hpbf)<sub>2</sub>] (41)**<sup>43</sup>

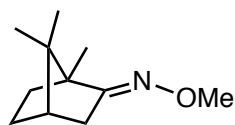


A solution of **39** (195 mg, 1 mmol) and Pd(OAc)<sub>2</sub> (224 mg, 1 mmol) in acetonitrile (30 mL) was refluxed for 4 h, filtered while hot and left to cool to room temperature. The yellow precipitate formed upon cooling was collected by filtration, washed with acetonitrile and dried *in vacuo*. Recrystallisation from dichloromethane/hexane afforded product **41** as fine orange-red crystals (281 mg, 78% yield).

MP 110–120 °C;  $^1\text{H}$  NMR (400 MHz,  $\text{CDCl}_3$ )  $\delta$  7.58 (ddd,  $J = 5.6, 1.5, 0.8$  Hz, 2H), 7.43 – 7.37 (m, 2H), 7.25 – 7.08 (m, 8H), 6.90 (ddd,  $J = 7.9, 1.3, 0.7$  Hz, 2H), 5.85 (ddd,  $J = 7.6, 5.6, 1.4$  Hz, 2H), 2.35 (s, 6H);  $^{13}\text{C}$  NMR (100 MHz,  $\text{CDCl}_3$ ) 182.76, 153.93, 153.21, 149.65, 137.78, 131.73, 125.14, 124.11, 122.86, 122.30, 118.73, 115.91, 111.20, 24.00; LIFDI-MS  $m/z$  719.96 (Calc. for  $\text{C}_{30}\text{H}_{22}\text{N}_2\text{O}_6\text{Pd}_2$  719.96).

## Synthesis and C–H Bond Functionalisation of Organic Substrates

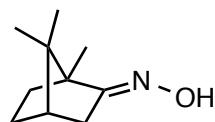
### (±)Camphor *O*-methyloxime (**2**)<sup>85</sup>



To a two-necked round bottom flask equipped with a condenser was added (±)camphoroxime **44** (200 mg, 1.2 mmol), triphenylphosphine (470 mg, 1.8 mmol), carbon tetrachloride (369 mg, 2.4 mmol), 1,8-diazabicyclo[5.4.0]undec-7-ene (183 mg, 1.2 mmol), methanol (57 mg, 1.8 mmol), and tetra-*n*-butylammonium iodide (13.2 mg, 0.036 mmol). Acetonitrile (30 mL) was added and the reaction mixture was heated at reflux until thin layer chromatography showed all (±)camphoroxime to have been consumed. The solvent was removed *in vacuo* and the residue was dissolved in chloroform and washed twice with water. The organic extracts were dried over sodium sulfate, filtered and concentrated *in vacuo*. Flash chromatography on silica gel (35% EtOAc in hexane) afforded product **2** (139 mg, 64% yield).

MP 49–53 °C (lit. mp 52–54 °C); <sup>1</sup>H NMR (400 MHz, CDCl<sub>3</sub>) δ 3.83 (s, 3H), 2.62 (dd, *J* = 18.0, 4.0 Hz, 1H), 2.46 (dd, *J* = 17.9, 4.0 Hz, 1H), 1.82 (td, *J* = 12.3, 4.2 Hz, 1H), 1.76 (ddd, *J* = 13.4, 9.0, 4.1 Hz, 1H), 1.61 (tq, *J* = 11.8, 4.0 Hz, 1H), 1.56 (m, 1H), 1.32 (ddd, *J* = 13.2, 9.3, 4.1 Hz, 1H), 1.05 (s, 3H), 0.96 (s, 3H), 0.92 (s, 3H); HRMS (ESI<sup>+</sup>) *m/z* 181.1469 [M+H] (calc. for C<sub>11</sub>H<sub>19</sub>NO 181.1467; Anal. calc. for C<sub>11</sub>H<sub>19</sub>NO C 72.88, H 10.56, N 7.73, Observed C 72.64, H 10.87, N 7.94).

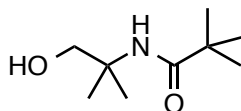
### (±)Camphoroxime (**44**)<sup>84</sup>



To a solution of hydroxylamine hydrochloride (69 mg, 0.99 mmol) and sodium acetate (65 mg, 0.79 mmol) in water (6 mL) was added ( $\pm$ )camphor (100 mg, 0.66 mmol) as a solution in ethanol (2 mL). The reaction mixture was heated at 60 °C for 16 h and the clear solution was concentrated under reduced pressure until small white crystals began to form. The residue was left overnight at 4 °C to complete crystallization. The product was collected by filtration and dried under reduced pressure to yield **44** as white crystals in quantitative yield.

MP 108–112 °C (lit. mp 118–119 °C);  $^1\text{H}$  NMR (400 MHz,  $\text{CDCl}_3$ )  $\delta$  2.56 (dt,  $J = 17.9, 4.0$  Hz, 1H), 2.06 (d,  $J = 18.0$  Hz, 1H), 1.93 (t,  $J = 4.4$  Hz, 1H), 1.85 (tq,  $J = 11.8, 4.0$  Hz, 1H), 1.72 (td,  $J = 12.3, 4.2$  Hz, 1H), 1.46 (ddd,  $J = 13.2, 9.4, 4.3$  Hz, 1H), 1.24 (ddd,  $J = 13.2, 9.3, 4.1$  Hz, 1H), 1.02 (s, 3H), 0.92 (s, 3H), 0.80 (s, 3H); HRMS (ESI $^+$ )  $m/z$  168.1379 [M+H] (calc. for  $\text{C}_{10}\text{H}_{18}\text{NO}$  168.1383); IR (ATR,  $\text{cm}^{-1}$ ) 2956, 1471, 1441, 1390, 1372, 1325, 1192, 1079, 998, 921, 826, 734, 589, 536.

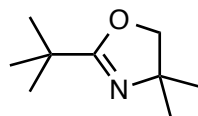
#### ***N*-(2-hydroxy-1,1-dimethyl-ethyl)-2,2-dimethyl propionamide (48)**<sup>86</sup>



In a Schlenk tube fitted with magnetic stirrer bar, 2-amino-2-methyl-1-propanol (1.337 g, 15 mmol) was dissolved in anhydrous tetrahydrofuran (100 mL). Pivaloyl chloride (1.808 g, 15 mmol) and  $\text{NEt}_3$  (15 mL) were added and the resulting white suspension was stirred at room temperature for 16 h. The solvent was removed *in vacuo*, water (50 mL) was added to the resulting white residue, and the organic products were extracted into chloroform ( $3 \times 50$  mL). The organic extracts were combined, washed with 1 M HCl, dried over magnesium sulfate, and concentrated *in vacuo* to yield **48** as white crystals (2.331 g, 90% yield).

$R_f$  0.46 (EtOAc/hexane, 1:4,  $v/v$ );  $^1\text{H}$  NMR (400 MHz,  $\text{CDCl}_3$ )  $\delta$  5.65 (s, 1H), 5.10 (s, 1H), 3.55 (s, 2H), 1.27 (s, 6H), 1.18 (s, 9H);  $^{13}\text{C}$  NMR (100 MHz,  $\text{CDCl}_3$ )  $\delta$  179.85, 71.12, 55.93, 39.08, 27.76, 24.85; HRMS (ESI $^+$ )  $m/z$  174.1489 [M+H] (calc. for  $\text{C}_9\text{H}_{20}\text{NO}_2$  174.1489), 196.1308 [M+Na] (calc. for  $\text{C}_9\text{H}_{19}\text{NNaO}_2$  196.1308); IR (ATR,  $\text{cm}^{-1}$ ) 3343, 2956, 2866, 1634, 1527, 1446, 1362, 1280, 1210, 1066, 909, 699, 671, 596.

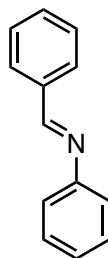
### 2-*Tert*-butyl-4,4-dimethyl-2-oxazoline (**49**)<sup>87</sup>



A pressure tube was charged with freshly distilled 2-amino-2-methylpropan-1-ol (446 mg, 5 mmol) and cooled to 0 °C. Molten pivalic acid (766 mg, 7.5 mmol) was added dropwise, and the exothermic formation of a white precipitate was observed. The reaction mixture was heated at reflux for 2 h, after which the mixture was allowed to cool to room temperature. Flash column chromatography (acetone/toluene, 1:3 v/v) afforded product **49** (357 mg, 46% yield).

<sup>1</sup>H NMR (400 MHz, CDCl<sub>3</sub>) δ 3.83 (s, 2H), 1.23 (s, 9H), 1.21 (s, 6H); <sup>13</sup>C NMR (100 MHz, CDCl<sub>3</sub>) δ 171.95, 77.92, 61.03, 31.08, 28.54, 27.64; HRMS (ESI<sup>+</sup>) *m/z* 155.1304 [M+H] (calc. for C<sub>9</sub>H<sub>18</sub>NO 155.1304); Anal. calc. for C<sub>9</sub>H<sub>17</sub>NO C 69.63, H 11.04, N 9.02, Observed C 69.64, H 10.97, N 8.94.

### *N*-phenylbenzaldimine (**53**)<sup>89</sup>



A mixture of benzyl alcohol (0.389 g, 3.6 mmol), aniline (279 mg, 3.6 mmol) and potassium hydroxide (202 mg, 3.6 mmol) in toluene (2.5 mL) was stirred at 90 °C for 24 h. The reaction mixture was filtered through a plug of silica gel, which was washed with EtOAc, and the solvent was removed under reduced pressure to yield **53** as a yellow crystalline solid (429 mg, 79% yield).

MP 49–52 °C (lit.<sup>108</sup> mp 49–51 °C); <sup>1</sup>H NMR (400 MHz, CDCl<sub>3</sub>) δ 8.49 (s, 1H), 7.97–7.91 (m, 2H), 7.51 (dd, *J* = 5.1, 1.9 Hz, 3H), 7.43 (m, 2H), 7.30–7.23 (m, 3H); <sup>13</sup>C NMR (100 MHz, CDCl<sub>3</sub>) δ 160.48, 152.16, 136.29, 131.47, 129.24, 129.08, 129.04, 126.03, 120.97;

HRMS (ESI<sup>+</sup>)  $m/z$  182.0959 [M+H] (calc. for C<sub>13</sub>H<sub>11</sub>N 182.0964); IR (ATR, cm<sup>-1</sup>) 3059, 2890, 1589, 1576, 1482, 1449, 1365, 1191, 1169, 1072, 975, 905, 754, 689, 540.

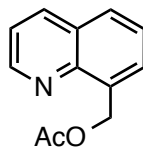
**General Procedure A: Acetoxylation of 8-Methylquinoline under Air.**

To a microwave flask containing Pd precatalyst (0.0125 mmol, 5 mol% w.r.t. substrate) and NaNO<sub>3</sub> (0.05–1 eq. relative to substrate) was added 2 mL AcOH/Ac<sub>2</sub>O (7:1). 8-Methylquinoline (34  $\mu$ L, 0.25 mmol) was added *via* syringe. The reaction mixture was heated at 110 °C, and the flask was flushed with compressed air at hourly intervals. After heating for 24 h, the reaction mixture was cooled to room temperature, filtered through a plug of Celite, and the solvent removed under reduced pressure. Sodium bicarbonate (saturated solution in water) was added to neutralise the residue, and the organic products were extracted into ethyl acetate. The organic extracts were washed with brine, dried over magnesium sulfate, and concentrated *in vacuo*. <sup>1</sup>H NMR spectroscopic and gas chromatographic analysis of the crude product was used to calculate conversion, and the acetoxyated product was then purified by flash chromatography on silica gel (35% EtOAc in hexane).

**General Procedure B: Acetoxylation of 8-Methylquinoline under O<sub>2</sub>.**

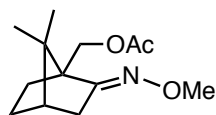
To a Schlenk tube fitted with a Young's tap and magnetic stirrer bar was added Pd precatalyst (0.0125 mmol, 5 mol% w.r.t. substrate) and NaNO<sub>3</sub> (0.05–1 eq. relative to substrate). The flask was attached to a grease-free Schlenk line fitted with Young's taps and was then evacuated (aspirator vacuum) and backfilled with oxygen three times to achieve 1 atm of O<sub>2</sub>. The flask was sealed and heated at 110 °C for 24 h. Reaction work-up followed the procedure described above.

### 8-Acetoxymethylquinoline (42)<sup>30</sup>



$R_f$  0.22 (EtOAc/hexane, 1:3, v/v);  $^1\text{H NMR}$  (400 MHz,  $\text{CDCl}_3$ )  $\delta$  8.97 (dd,  $J = 4.2, 1.8$  Hz, 1H), 8.19 (dd,  $J = 8.3, 1.7$  Hz, 1H), 7.85 – 7.74 (m, 2H), 7.55 (dd,  $J = 8.0, 7.2$  Hz, 1H), 7.45 (dd,  $J = 8.3, 4.2$  Hz, 1H), 5.86 (s, 2H), 2.16 (s, 3H);  $^{13}\text{C NMR}$  (100 MHz,  $\text{CDCl}_3$ )  $\delta$  171.14, 150.03, 146.24, 136.32, 134.27, 128.89, 128.25, 126.28, 121.40, 62.87, 21.26; HRMS (ESI<sup>+</sup>)  $m/z$  202.0872 [M+H] (calc. for  $\text{C}_{12}\text{H}_{12}\text{NO}_2$  202.0868); IR (ATR,  $\text{cm}^{-1}$ ) 3066, 2925, 1735, 1497, 1365, 1345, 1234, 1065, 1022, 827, 793, 764.

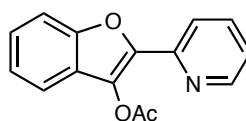
### 1-acetoxy(±)camphor *O*-methyloxime (45)



The reaction was conducted according to *General Procedure A*, with (±)camphor *O*-methyloxime (**2**) as substrate (45 mg, 0.25 mmol). Conversion was calculated by  $^1\text{H NMR}$  spectroscopic analysis of the crude product. Integration of the singlet corresponding to the acetate  $\text{CH}_3$  protons in the product (at  $\delta = 2.02$  ppm, 3H) compared to the singlet corresponding to the methyl group to be functionalised in the starting material (at  $\delta = 1.05$  ppm, 3H) gave conversion to be 54%.

$R_f$  0.34 (EtOAc/hexane, 1:9, v/v);  $^1\text{H NMR}$  (400 MHz,  $\text{CDCl}_3$ )  $\delta$  4.29 (d,  $J = 12.1$  Hz, 1H), 4.22 (d,  $J = 12.0$  Hz, 1H), 3.78 (s, 3H), 2.51 (m, 1H), 2.36 (m, 1H), 2.02 (s, 3H), 1.86–1.72 (m, 3H), 1.52 (m, 1H), 1.34 (m, 1H), 0.96 (s, 3H), 0.91 (s, 3H).

### 2(2-pyridyl)-3-acetoxybenzo[*b*]furan (52)

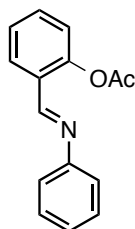




The reaction was conducted according to *General Procedure A*, with 2(2-pyridyl)benzo[*b*]furan (**39**) as substrate (49 mg, 0.25 mmol). Conversion was calculated by <sup>1</sup>H NMR spectroscopic analysis of the crude product. Integration of the singlet corresponding to the acetate CH<sub>3</sub> protons in the product (at  $\delta = 2.26$  ppm, 3H) compared to the doublet corresponding to the benzofuran C3 proton (to be functionalised) in the starting material (at  $\delta = 7.44$ ,  $J = 1.0$  Hz, 1H) gave conversion to be 58%.

$R_f$  0.30 (EtOAc/hexane, 1:3, v/v); <sup>1</sup>H NMR (400 MHz, CDCl<sub>3</sub>)  $\delta$  8.69 (dd,  $J = 4.8, 1.8$  Hz, 1H), 8.03 (dd,  $J = 7.8, 1.8$  Hz, 1H), 7.84–7.91 (m, 2H), 7.65 (dd,  $J = 7.7, 1.4$  Hz, 1H), 7.39–7.32 (m, 3H), 2.26 (s, 3H).

#### *N*-phenyl-(2-acetoxy)benzaldimine (**54**)

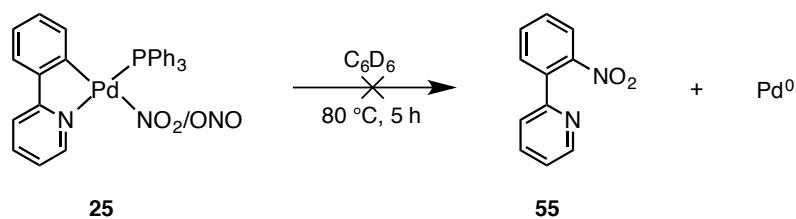


The reaction was conducted according to *General Procedure A*, with *N*-phenylbenzaldimine (**53**) as substrate (45 mg, 0.25 mmol). Conversion was calculated by <sup>1</sup>H NMR spectroscopic analysis of the crude product. Integration of the singlet corresponding to the acetate CH<sub>3</sub> protons in the product (at  $\delta = 2.32$  ppm, 3H) compared to the singlet corresponding to the imine N=CH proton in the starting material (at  $\delta = 8.52$ , 1H) gave conversion to be 62%.

$R_f$  0.26 (EtOAc/hexane, 1:3, v/v); <sup>1</sup>H NMR (400 MHz, CDCl<sub>3</sub>)  $\delta$  7.87 (dd,  $J = 4.8, 1.8$  Hz, 1H), 7.58–7.51 (m, 3H), 7.41 (dd,  $J = 4.9, 1.8$  Hz, 1H), 7.30 (m, 2H), 7.26 (m, 2H), 2.32 (s, 3H).

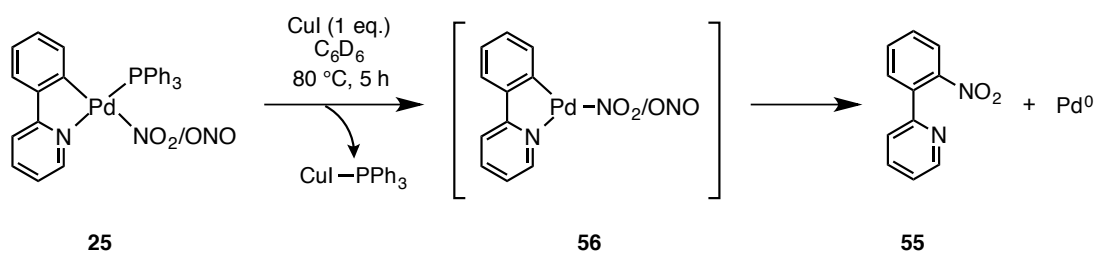
## Mechanistic Experiments

### Attempted Reductive Elimination from Pd<sup>II</sup> Complexes



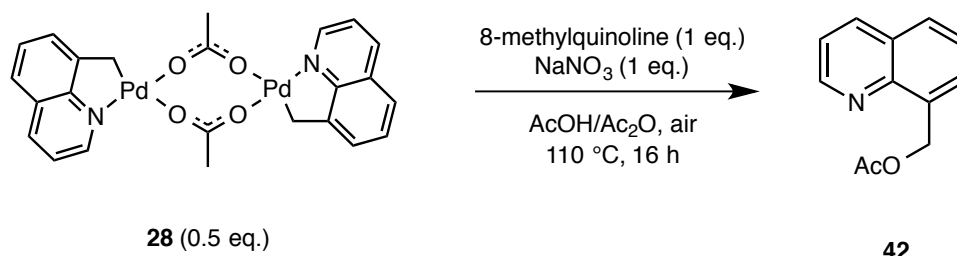
As a representative example, a sample of **25** (10 mg, 0.018 mmol) was dissolved in benzene-*d*<sub>6</sub> (1.5 mL) in an oven-dried Schlenk tube. The reaction vessel was covered in foil to exclude light, and the mixture was heated at 80 °C for 5 h before being filtered through Celite to remove any Pd<sup>0</sup>. <sup>1</sup>H and <sup>31</sup>P NMR spectra were collected for the crude filtrate, which showed no formation of the organic product. Attempted reductive elimination experiments involving other [Pd(C<sup>^</sup>N)L(NO<sub>2</sub>)] complexes followed the same procedure.

### Attempted Reductive Elimination from Pd<sup>II</sup> Complexes with CuI



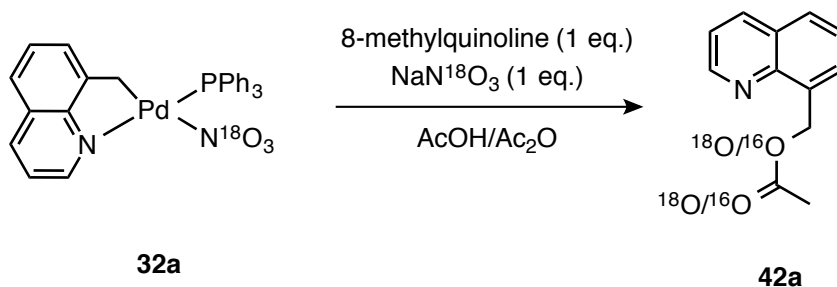
**25** (10 mg, 0.018 mmol) and CuI (3.35 mg, 0.018 mmol) were dissolved in benzene-*d*<sub>6</sub> (1.5 mL) in an oven-dried Schlenk tube. The reaction vessel was covered in foil to exclude light, and the mixture was heated at 80 °C for 5 h before being filtered through Celite to remove any Pd<sup>0</sup>. <sup>1</sup>H and <sup>31</sup>P NMR spectra were collected for the crude filtrate, which showed no formation of the organic product.

### Stoichiometric Acetoxylation of 8-Methylquinoline from **28**



The reaction was set up with **28** (32 mg, 0.05 mmol), 8-methylquinoline (15  $\mu$ L, 0.1 mmol) and NaNO<sub>3</sub> (8.9 mg, 0.1 mmol) according to *General Procedure A*. Flash column chromatography afforded product **42** (14.2 mg, 71% yield).

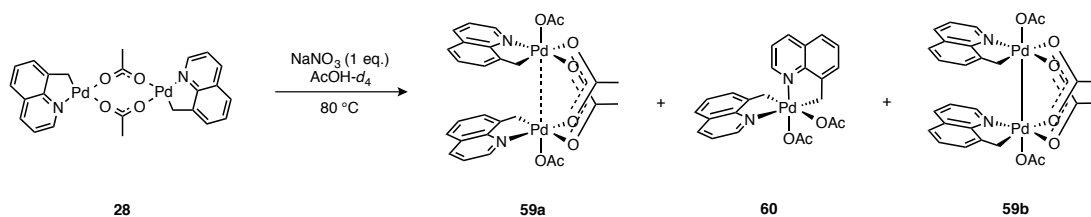
### Acetoxylation of 8-Methylquinoline with NaN<sup>18</sup>O<sub>3</sub>



The reaction was set up with 8-methylquinoline (34  $\mu$ L, 0.25 mmol) and Pd(OAc)<sub>2</sub> (2.81 mg, 0.0125 mmol) according to *General Procedure A*. NaN<sup>18</sup>O<sub>3</sub> (22.7 mg, 0.25 mmol) was used in place of NaNO<sub>3</sub>. Reaction work-up was carried out as described above, and <sup>1</sup>H NMR spectroscopy confirmed the formation of acetoxyated product **42a** (50.4 mg).

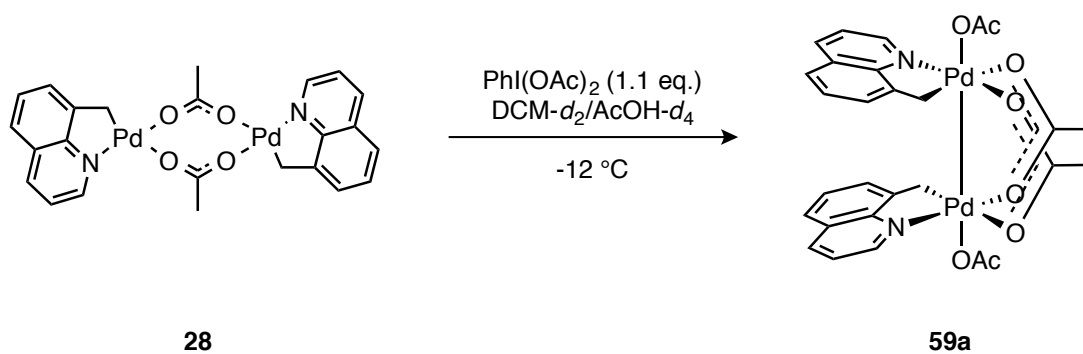
ESI-MS was used to identify any incorporation of <sup>18</sup>O into the acetoxyated product. The main molecular ion peak was observed at  $m/z$  202.0872, corresponding to [M+H]<sup>+</sup> for C<sub>12</sub>H<sub>12</sub>N<sup>16</sup>O<sub>2</sub> (**42**). A small peak was observed at  $m/z$  204.0869, suggesting only trace formation of C<sub>12</sub>H<sub>12</sub>N<sup>16</sup>O<sup>18</sup>O. No peak corresponding to C<sub>12</sub>H<sub>12</sub>N<sup>18</sup>O<sub>2</sub> was observed.

## Observation of High Oxidation State Intermediates *via* Reaction of **28** and NaNO<sub>3</sub>



In a 3-necked round-bottomed flask, **28** (80 mg, 0.13 mmol) was dissolved in acetic acid-*d*<sub>4</sub> (6 mL) to form a bright orange solution. A 0.6 mL aliquot was placed in an NMR tube and a proton NMR spectrum was taken immediately (A). NaNO<sub>3</sub> (11 mg, 0.13 mmol, 1 eq.) was added to the flask and the mixture heated at 80 °C for 3 h, after which another aliquot (0.6 mL) was taken and an NMR spectrum recorded. 8-Methylquinoline (17.7 μL, 0.13 mmol, 1 eq.) was added to the flask and heated at 80 °C for 15 h, after which the formation of a brown precipitate was observed. A 0.6 mL aliquot was taken and a third NMR spectrum recorded. The remaining reaction mixture was allowed to cool and worked up according to the general procedure for the acetoxylation of 8-methylquinoline.

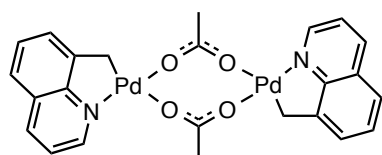
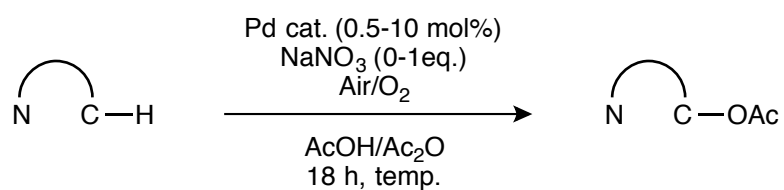
## Attempted Synthesis of **59a** from **28** and PhI(OAc)<sub>2</sub>



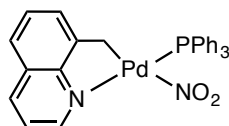
To a solution of acetato-bridged dimer **28** (5 mg,  $8.13 \times 10^{-3}$  mmol) in acetic acid-*d*<sub>4</sub> (0.15 mL) and dichloromethane-*d*<sub>2</sub> (0.15 mL) was added PhI(OAc)<sub>2</sub> (2.88 mg,  $8.94 \times 10^{-3}$  mmol) in acetic acid-*d*<sub>4</sub> (0.15 mL) and dichloromethane-*d*<sub>2</sub> (0.15 mL) at -12 °C. The sample was loaded into a spectrometer at -12 °C and spectra were taken immediately.

## Appendices

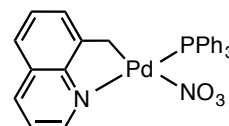
### Appendix A: Full Table of Data for the Pd-Catalysed C–H Acetoxylation of Organic Substrates



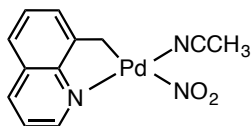
28



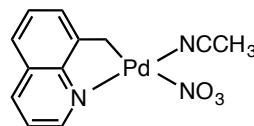
31



32



33



34

<b>Entry</b>	<b>Substrate</b>	<b>Catalyst</b>	<b>Catalyst loading / mol% Pd</b>	<b>NaNO<sub>3</sub> loading / equiv.</b>	<b>Oxidant</b>	<b>Temp. / °C</b>	<b>Conversion / %</b>
<b>1</b>	8-Methylquinoline	Pd(OAc) <sub>2</sub>	5	100	Air	80	76
<b>2</b>	8-Methylquinoline	Pd(OAc) <sub>2</sub>	5	100	Air	90	79
<b>3</b>	8-Methylquinoline	Pd(OAc) <sub>2</sub>	5	100	Air	110	>99
<b>4</b>	8-Methylquinoline	Pd(OAc) <sub>2</sub>	5	25	Air	110	86
<b>5</b>	8-Methylquinoline	Pd(OAc) <sub>2</sub>	5	10	Air	110	45
<b>6</b>	8-Methylquinoline	Pd(OAc) <sub>2</sub>	5	5	Air	110	6
<b>7</b>	8-Methylquinoline	Pd(OAc) <sub>2</sub>	5	0	Air	110	0
<b>8</b>	8-Methylquinoline	Pd(OAc) <sub>2</sub>	5	0	Air	110	0
<b>9</b>	8-Methylquinoline	Pd(OAc) <sub>2</sub>	10	100	O <sub>2</sub>	110	100
<b>10</b>	8-Methylquinoline	Pd(OAc) <sub>2</sub>	10	0	Air	110	0

Entry	Substrate	Catalyst	Catalyst loading / mol% Pd	NaNO <sub>3</sub> loading / equiv.	Oxidant	Temp.	Conversion / %
11	8-Methylquinoline	Pd(OAc) <sub>2</sub>	2	100	Air	110	43
12	8-Methylquinoline	Pd(OAc) <sub>2</sub>	2	0	Air	110	0
13	8-Methylquinoline	Pd(OAc) <sub>2</sub>	0.5	100	Air	110	22
14	8-Methylquinoline	Pd(OAc) <sub>2</sub>	0.5	0	Air	110	0
15	8-Methylquinoline	<b>28</b>	5	100	Air	110	100
16	8-Methylquinoline	<b>28</b>	5	25	Air	110	75
17	8-Methylquinoline	<b>28</b>	5	10	Air	110	30
18	8-Methylquinoline	<b>28</b>	5	5	Air	110	0
19	8-Methylquinoline	<b>28</b>	5	0	Air	110	0
20	8-Methylquinoline	<b>28</b>	5	0	O <sub>2</sub>	110	0

<b>Entry</b>	<b>Substrate</b>	<b>Catalyst</b>	<b>Catalyst loading / mol% Pd</b>	<b>NaNO<sub>3</sub> loading / equiv.</b>	<b>Oxidant</b>	<b>Temp.</b>	<b>Conversion / %</b>
<b>21</b>	8-Methylquinoline	<b>31</b>	5	100	Air	110	100
<b>22</b>	8-Methylquinoline	<b>31</b>	5	25	Air	110	62
<b>23</b>	8-Methylquinoline	<b>31</b>	5	10	Air	110	33
<b>24</b>	8-Methylquinoline	<b>31</b>	5	5	Air	110	0
<b>25</b>	8-Methylquinoline	<b>31</b>	5	0	Air	110	0
<b>26</b>	8-Methylquinoline	<b>31</b>	5	0	O <sub>2</sub>	110	0
<b>27</b>	8-Methylquinoline	<b>32</b>	5	100	Air	110	81
<b>28</b>	8-Methylquinoline	<b>32</b>	5	25	Air	110	50
<b>29</b>	8-Methylquinoline	<b>32</b>	5	10	Air	110	30
<b>30</b>	8-Methylquinoline	<b>32</b>	5	5	Air	110	17



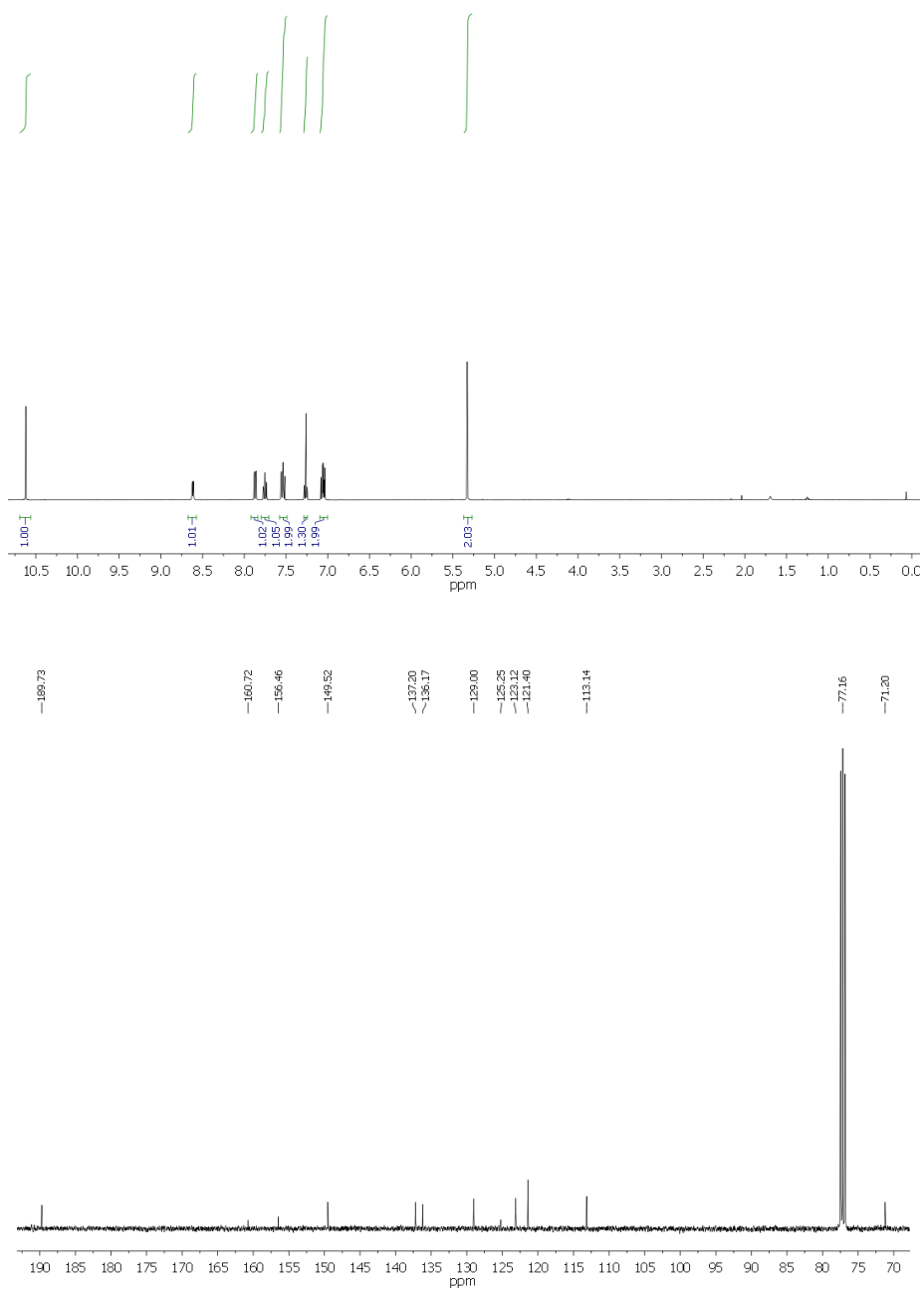
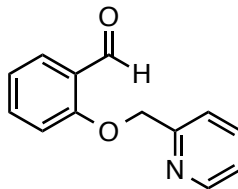
<b>Entry</b>	<b>Substrate</b>	<b>Catalyst</b>	<b>Catalyst loading / mol% Pd</b>	<b>NaNO<sub>3</sub> loading / equiv.</b>	<b>Oxidant</b>	<b>Temp.</b>	<b>Conversion / %</b>
<b>31</b>	8-Methylquinoline	<b>32</b>	5	0	Air	110	0
<b>32</b>	8-Methylquinoline	<b>32</b>	5	0	O <sub>2</sub>	110	0
<b>33</b>	8-Methylquinoline	<b>33</b>	5	100	Air	110	89
<b>34</b>	8-Methylquinoline	<b>33</b>	5	25	Air	110	48
<b>35</b>	8-Methylquinoline	<b>33</b>	5	10	Air	110	14
<b>36</b>	8-Methylquinoline	<b>33</b>	5	5	Air	110	9
<b>37</b>	8-Methylquinoline	<b>33</b>	5	0	Air	110	0
<b>38</b>	8-Methylquinoline	<b>33</b>	5	0	O <sub>2</sub>	110	0
<b>39</b>	8-Methylquinoline	<b>34</b>	5	100	Air	110	81
<b>40</b>	8-Methylquinoline	<b>34</b>	5	100	O <sub>2</sub>	110	>99

<b>Entry</b>	<b>Substrate</b>	<b>Catalyst</b>	<b>Catalyst loading / mol% Pd</b>	<b>NaNO<sub>3</sub> loading / equiv.</b>	<b>Oxidant</b>	<b>Temp.</b>	<b>Conversion / %</b>
<b>41</b>	8-Methylquinoline	<b>34</b>	5	25	Air	110	70
<b>42</b>	8-Methylquinoline	<b>34</b>	5	25	O <sub>2</sub>	110	83
<b>43</b>	8-Methylquinoline	<b>34</b>	5	10	Air	110	45
<b>44</b>	8-Methylquinoline	<b>34</b>	5	10	O <sub>2</sub>	110	82
<b>45</b>	8-Methylquinoline	<b>34</b>	5	5	Air	110	27
<b>46</b>	8-Methylquinoline	<b>34</b>	5	5	O <sub>2</sub>	110	66
<b>47</b>	8-Methylquinoline	<b>34</b>	5	0	Air	110	24
<b>48</b>	8-Methylquinoline	<b>34</b>	5	0	O <sub>2</sub>	110	36
<b>49</b>	8-Methylquinoline	<b>34</b>	10	100	Air	110	>99
<b>50</b>	8-Methylquinoline	<b>34</b>	10	0	Air	110	45

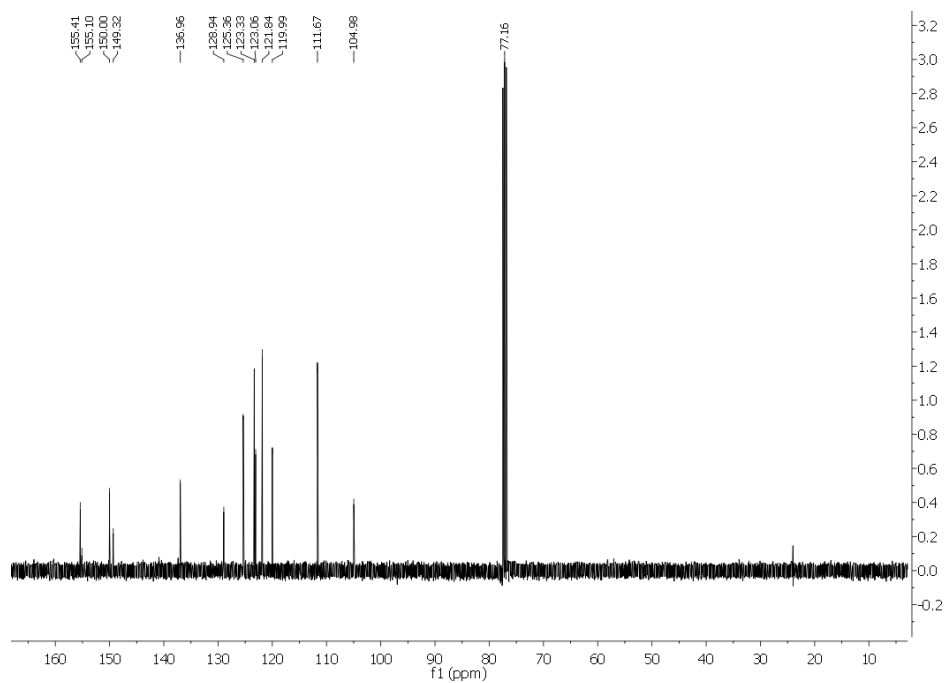
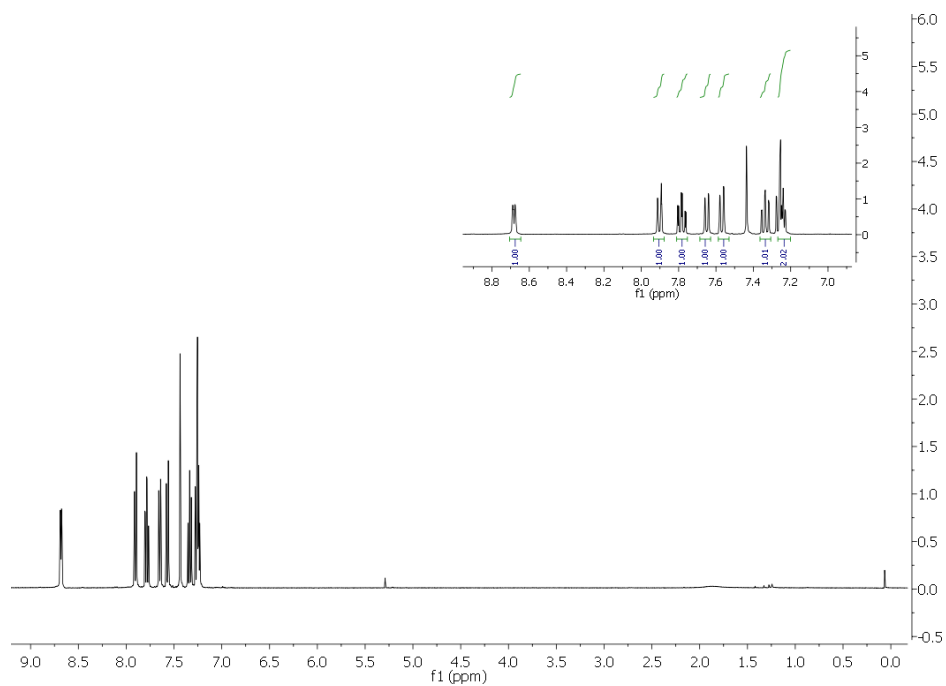
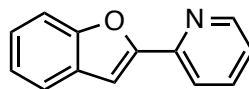
Entry	Substrate	Catalyst	Catalyst loading / mol% Pd	NaNO <sub>3</sub> loading / equiv.	Oxidant	Temp.	Conversion / %
51	8-Methylquinoline	34	2	100	Air	110	61
52	8-Methylquinoline	34	2	0	Air	110	8
53	8-Methylquinoline	34	0.5	100	Air	110	0
54	8-Methylquinoline	34	0.5	0	Air	110	0
55	Camphor <i>O</i> - Methyloxime	34	5	100	Air	110	54
56	2- <i>tert</i> -butyl-4,4- dimethyl-2-oxazoline	34	5	100	Air	110	0
57	2-Phenylpyridine	34	5	100	Air	110	0
58	2-(2- pyridyl)benzo[ <i>b</i> ]furan	34	5	100	Air	110	58
59	<i>N</i> - Phenylbenzaldimine	34	5	100	Air	110	62

## Appendix B: NMR Spectra

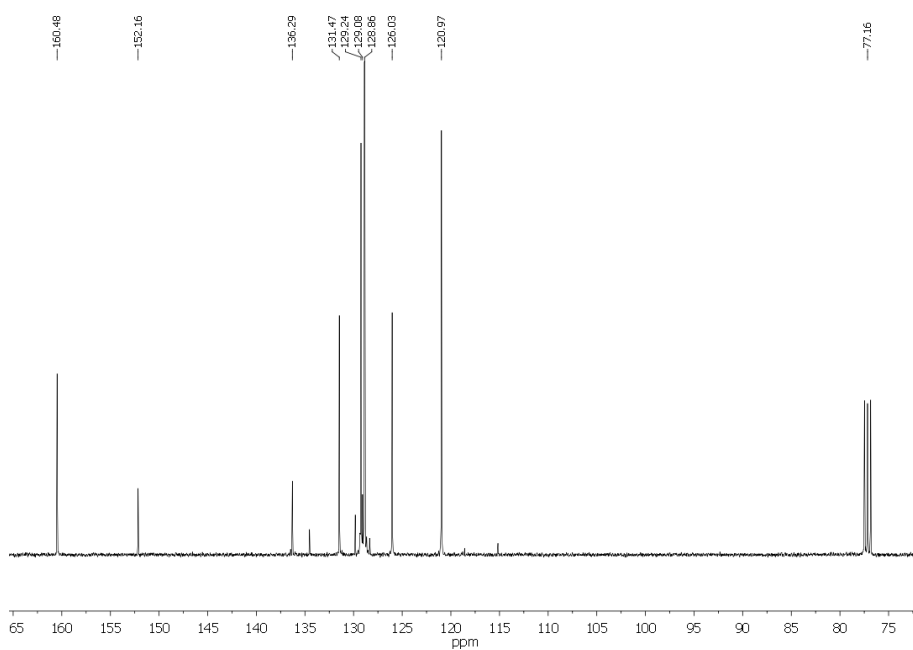
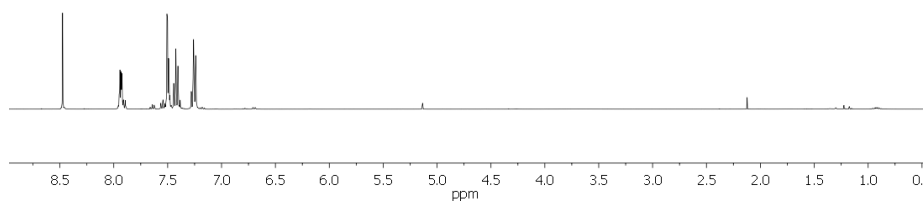
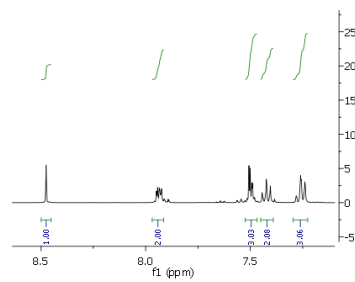
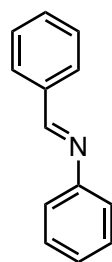
### 2(2-pyridylmethoxy)benzaldehyde (40)<sup>43</sup>



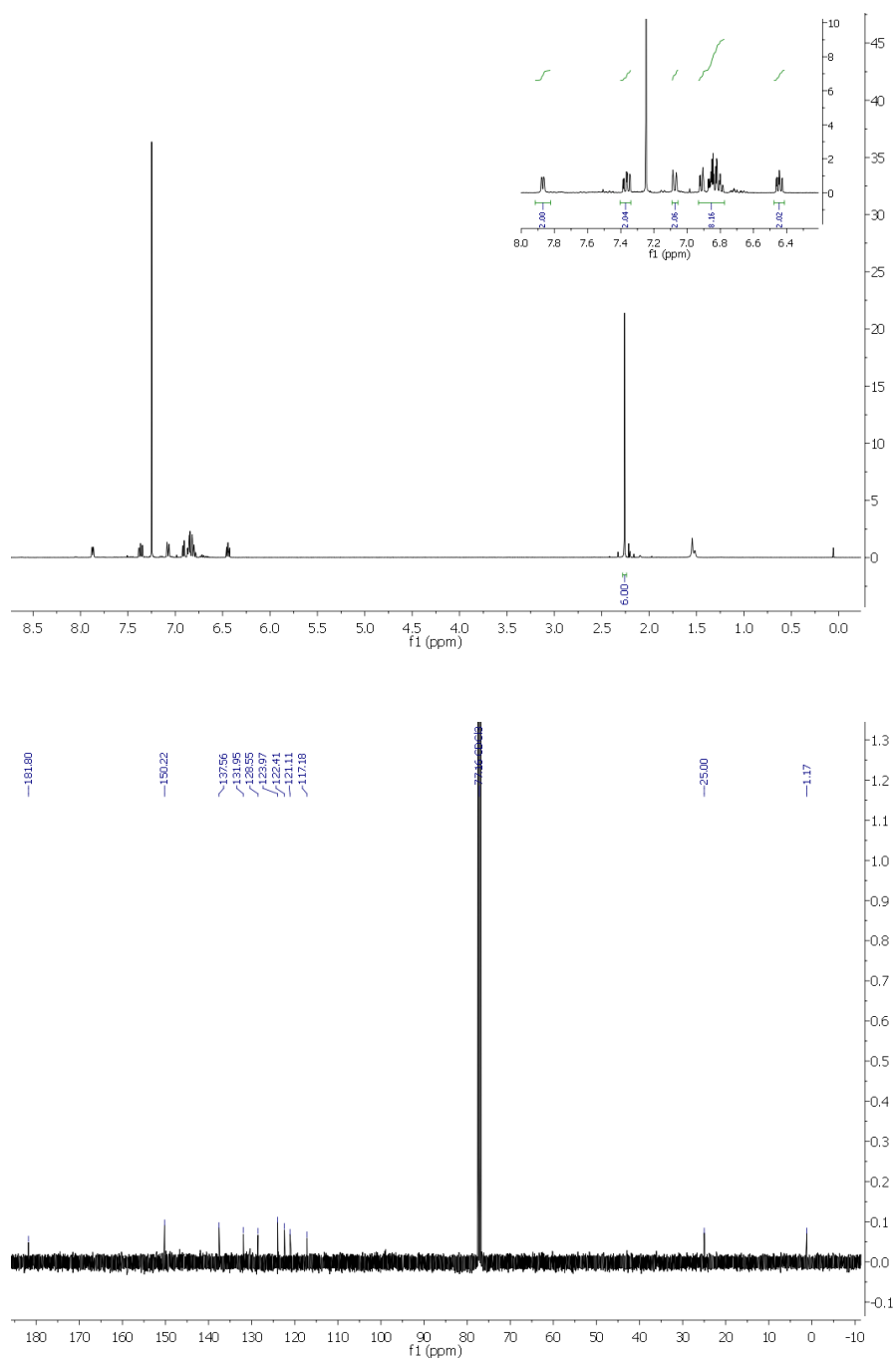
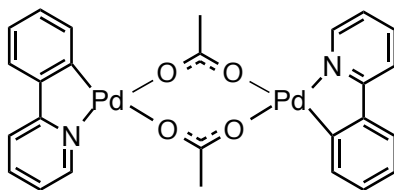
2(2-pyridyl)benzo[b]furan (39)<sup>43</sup>



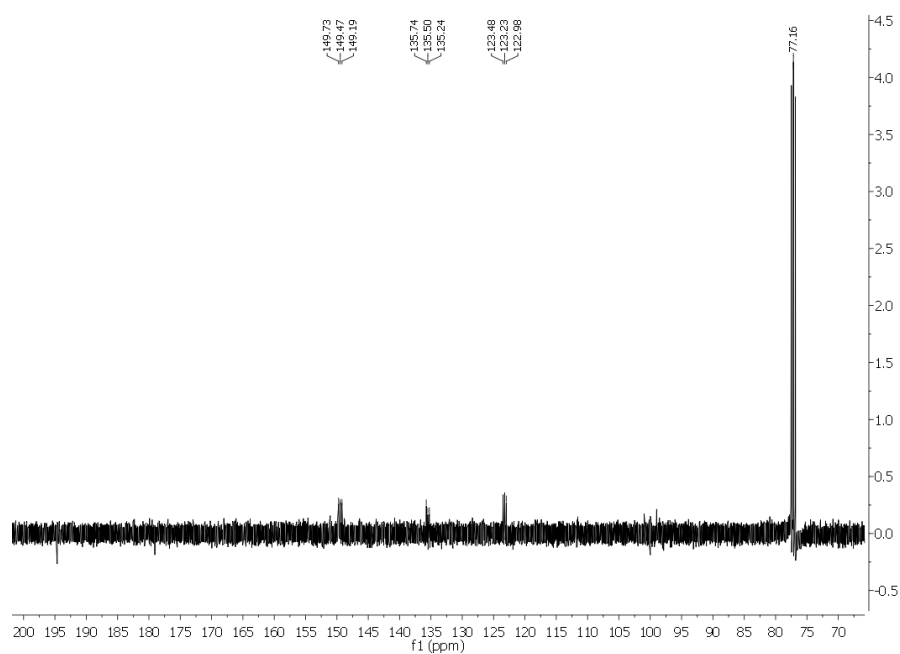
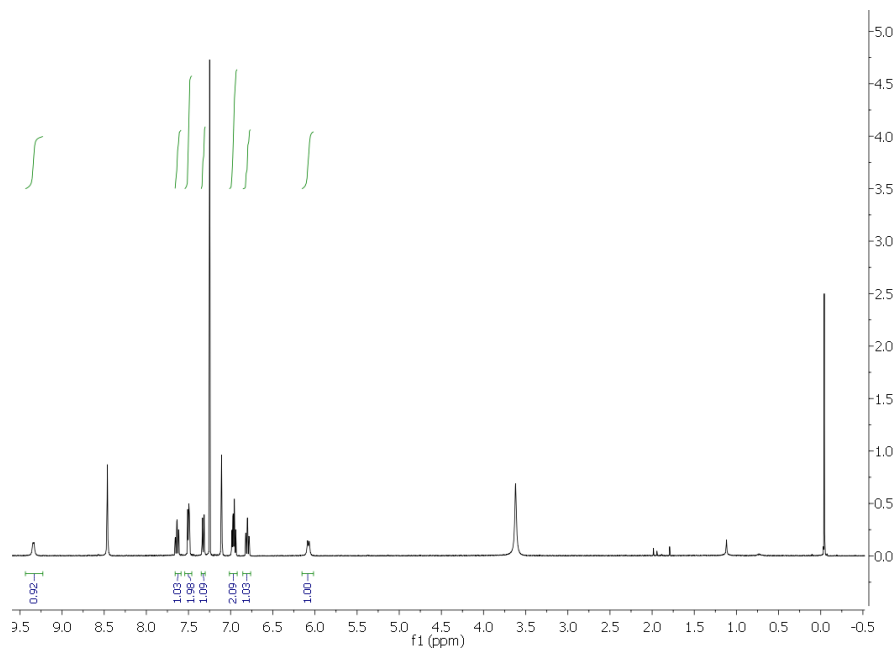
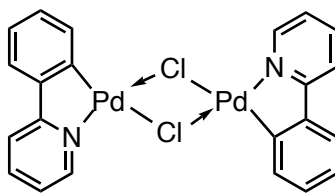
*N*-phenylbenzaldimine (53)<sup>89</sup>



$[\text{Pd}_2(\mu\text{-OAc})_2(2\text{-Phpy})_2]$  (**21**)<sup>70</sup>

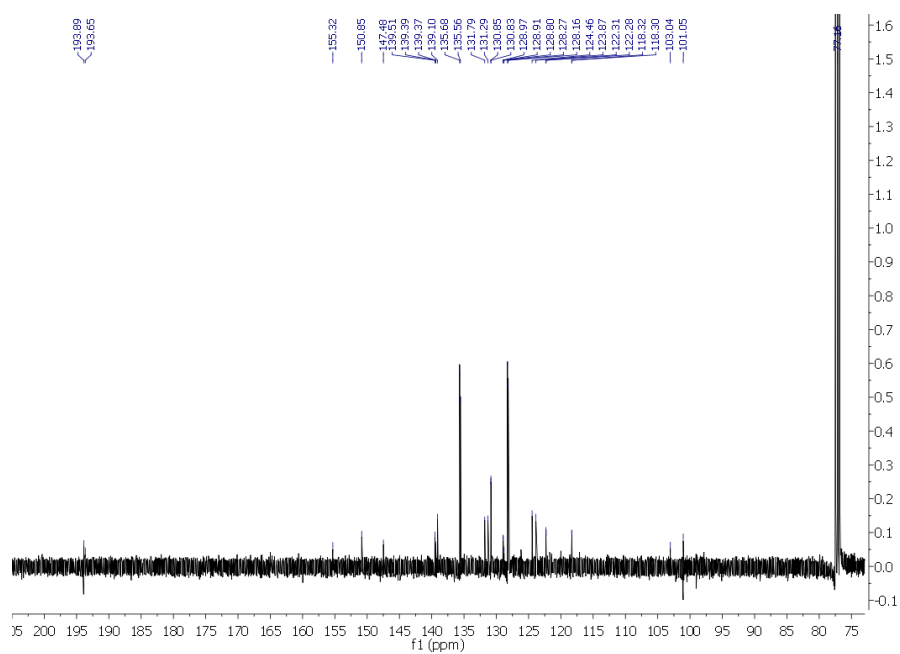
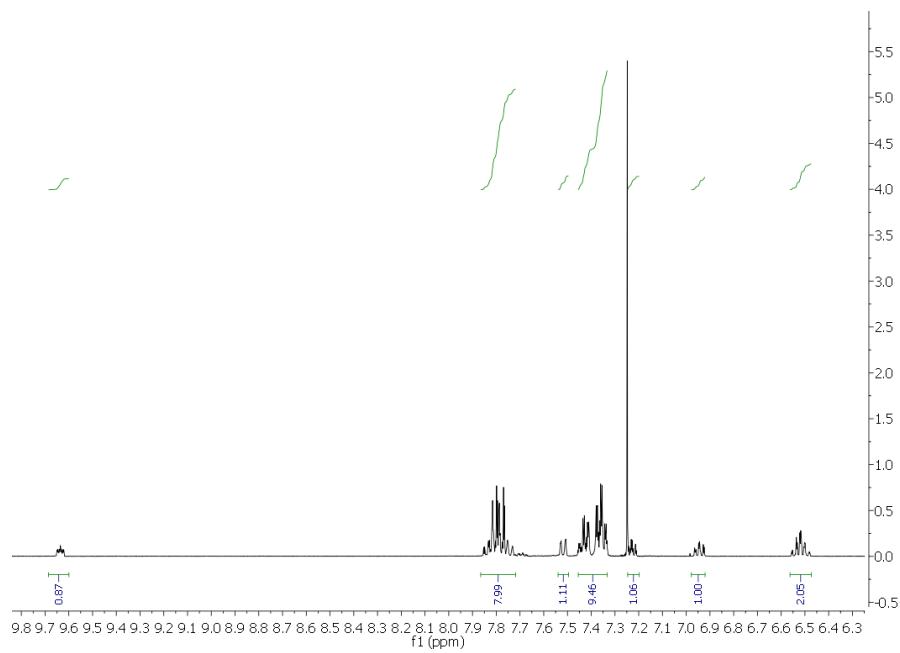
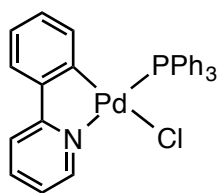


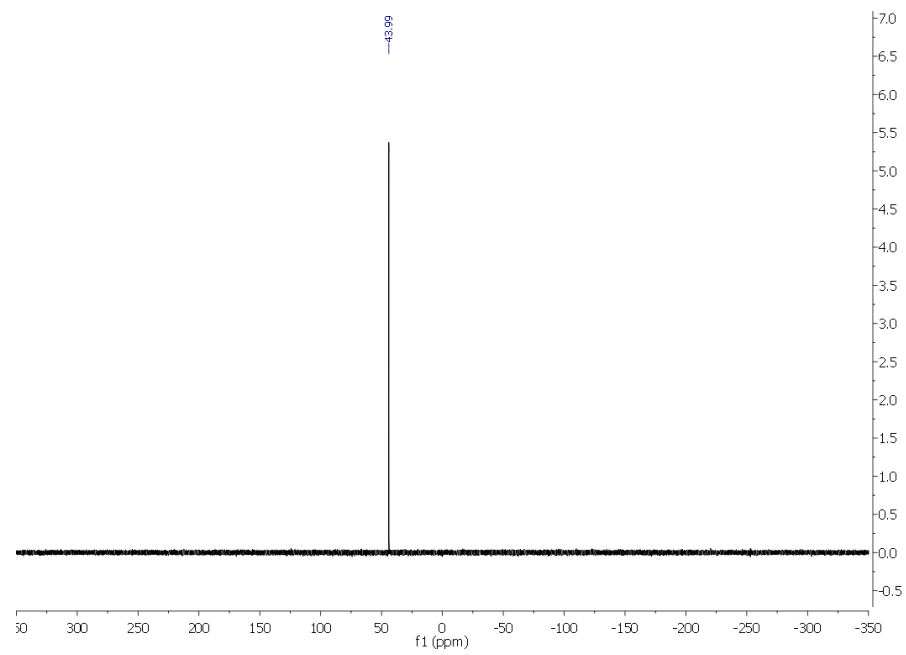
$[\text{Pd}_2(\mu\text{-Cl})_2(2\text{-Phpy})_2]$  (23)<sup>70</sup>



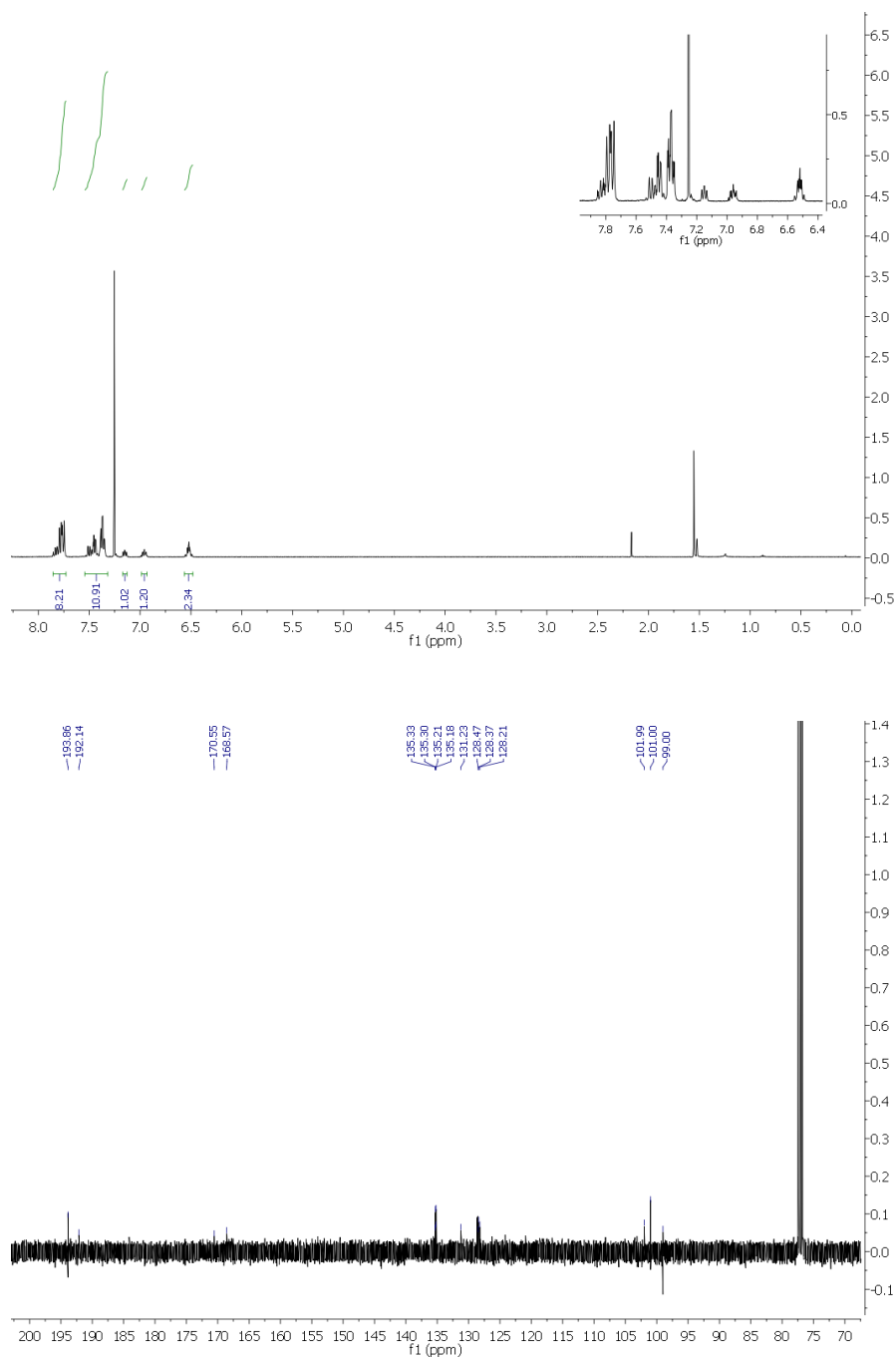
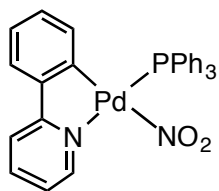


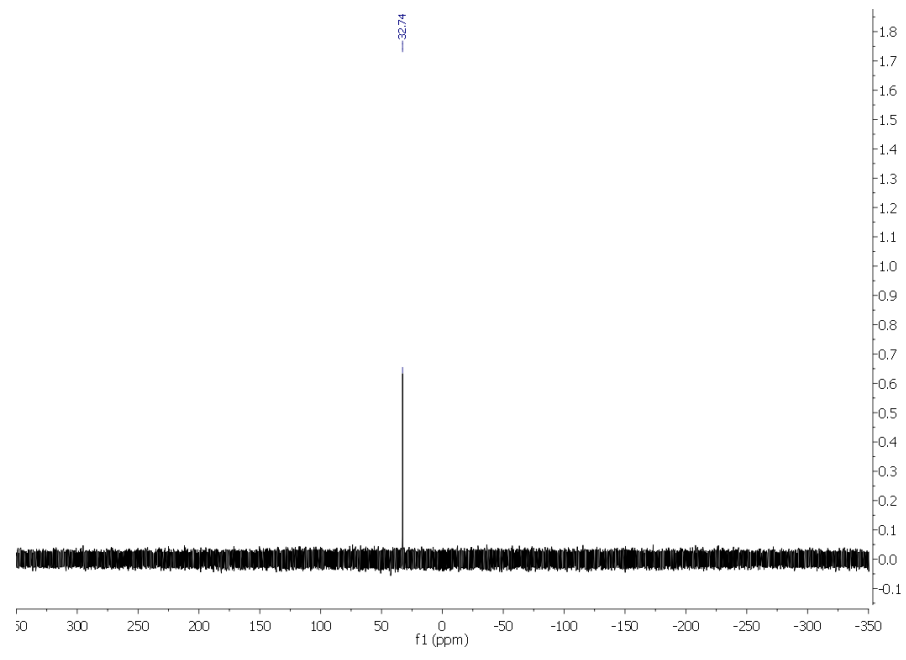
[PdCl(2-Phpy)(PPh<sub>3</sub>)] (24)<sup>72</sup>



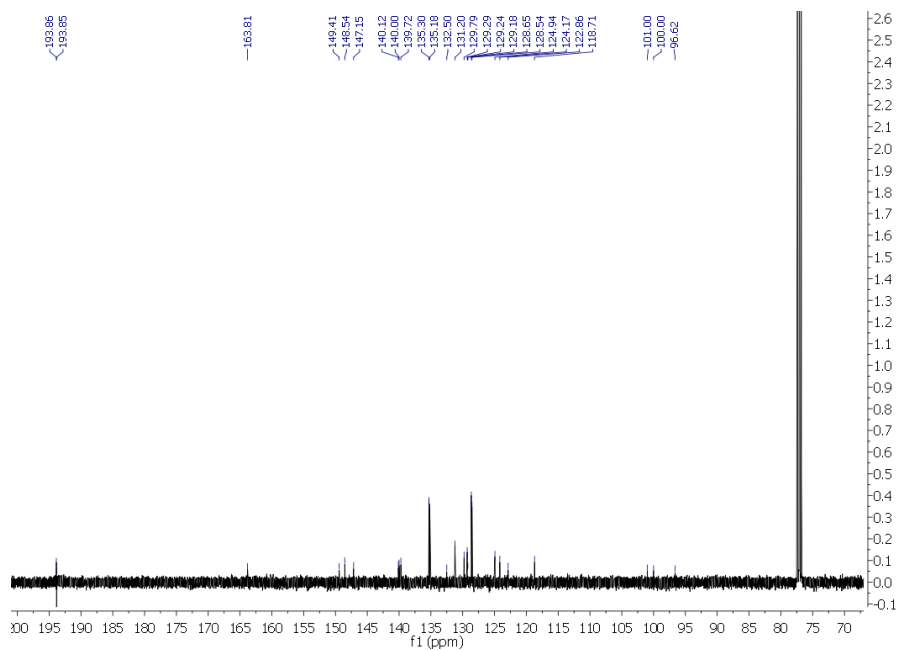
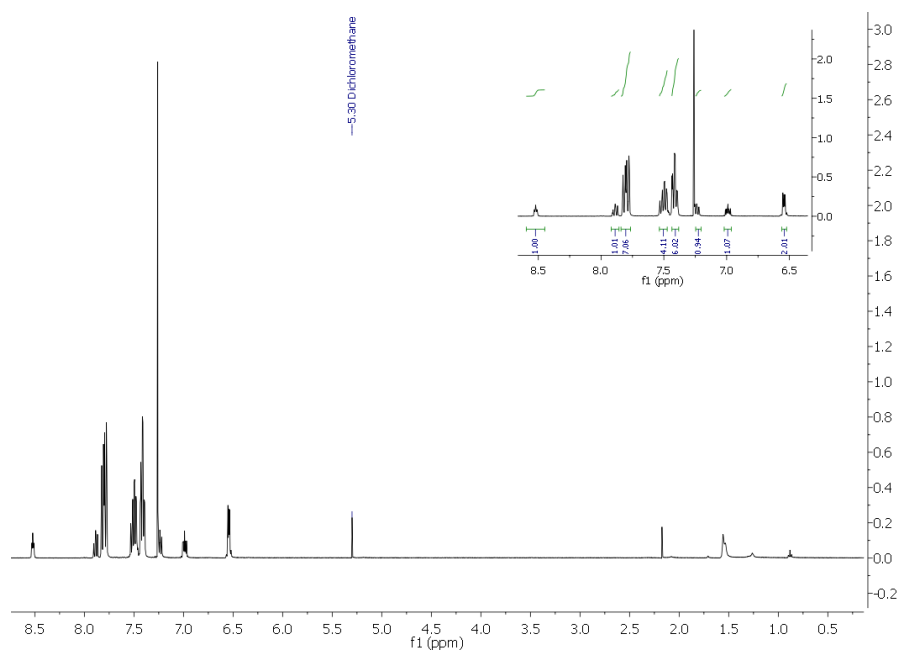
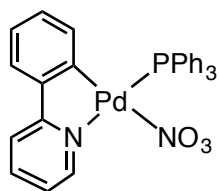


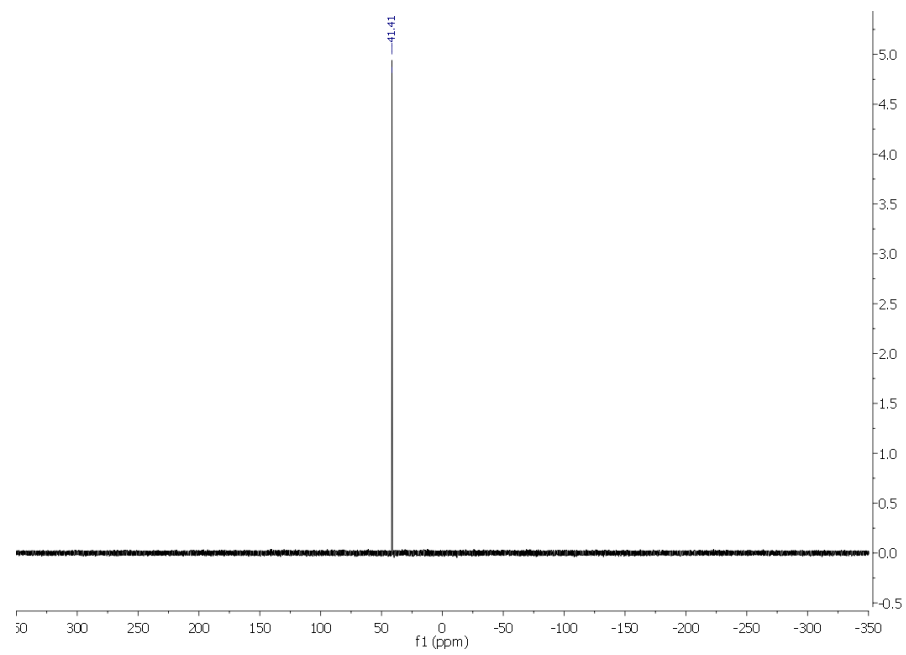
[Pd(NO<sub>2</sub>)(2-Phpy)(PPh<sub>3</sub>)] (25)



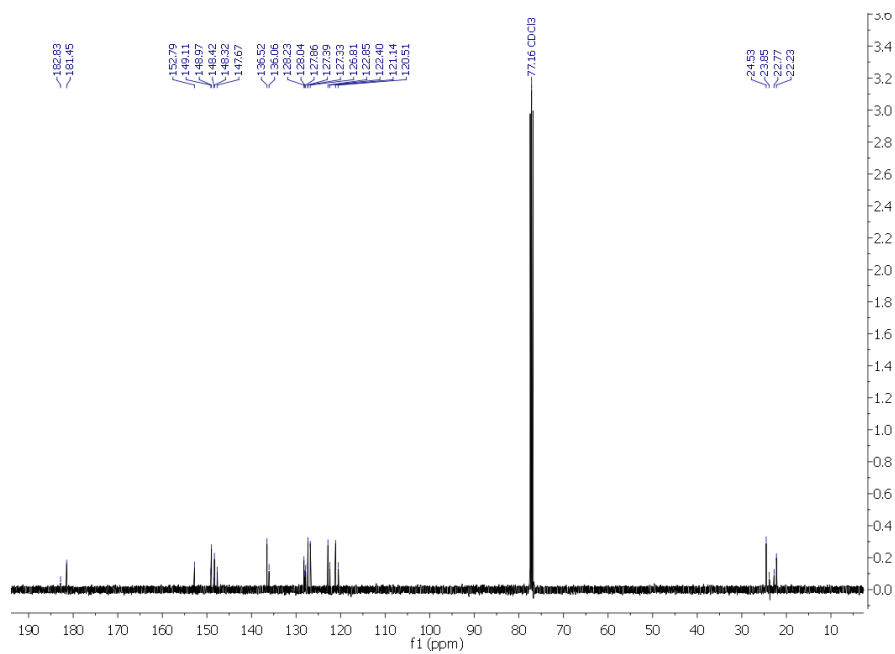
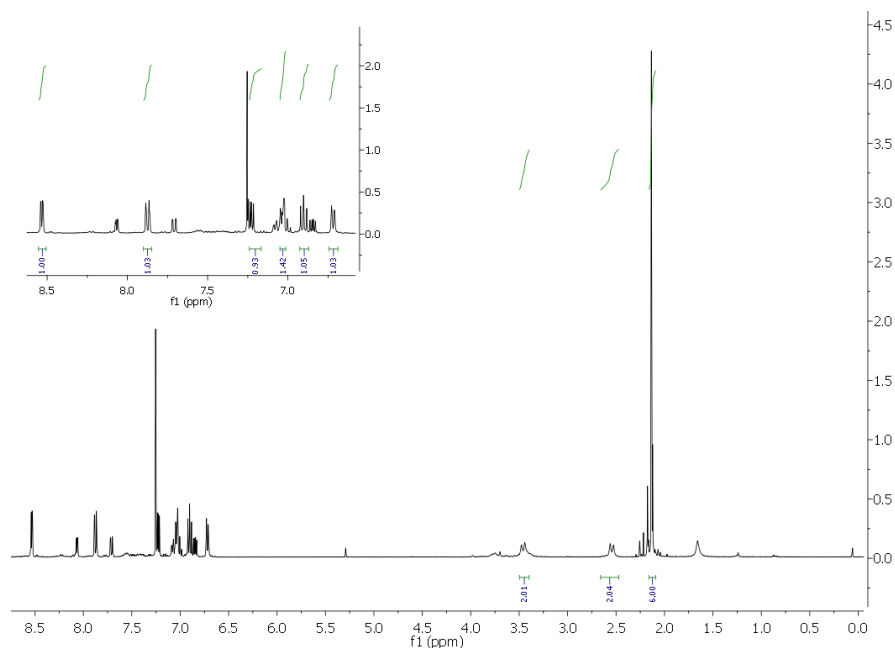
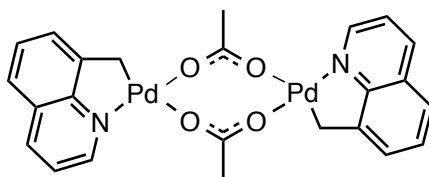


[Pd(NO<sub>3</sub>)(2-Phpy)(PPh<sub>3</sub>)] (26)

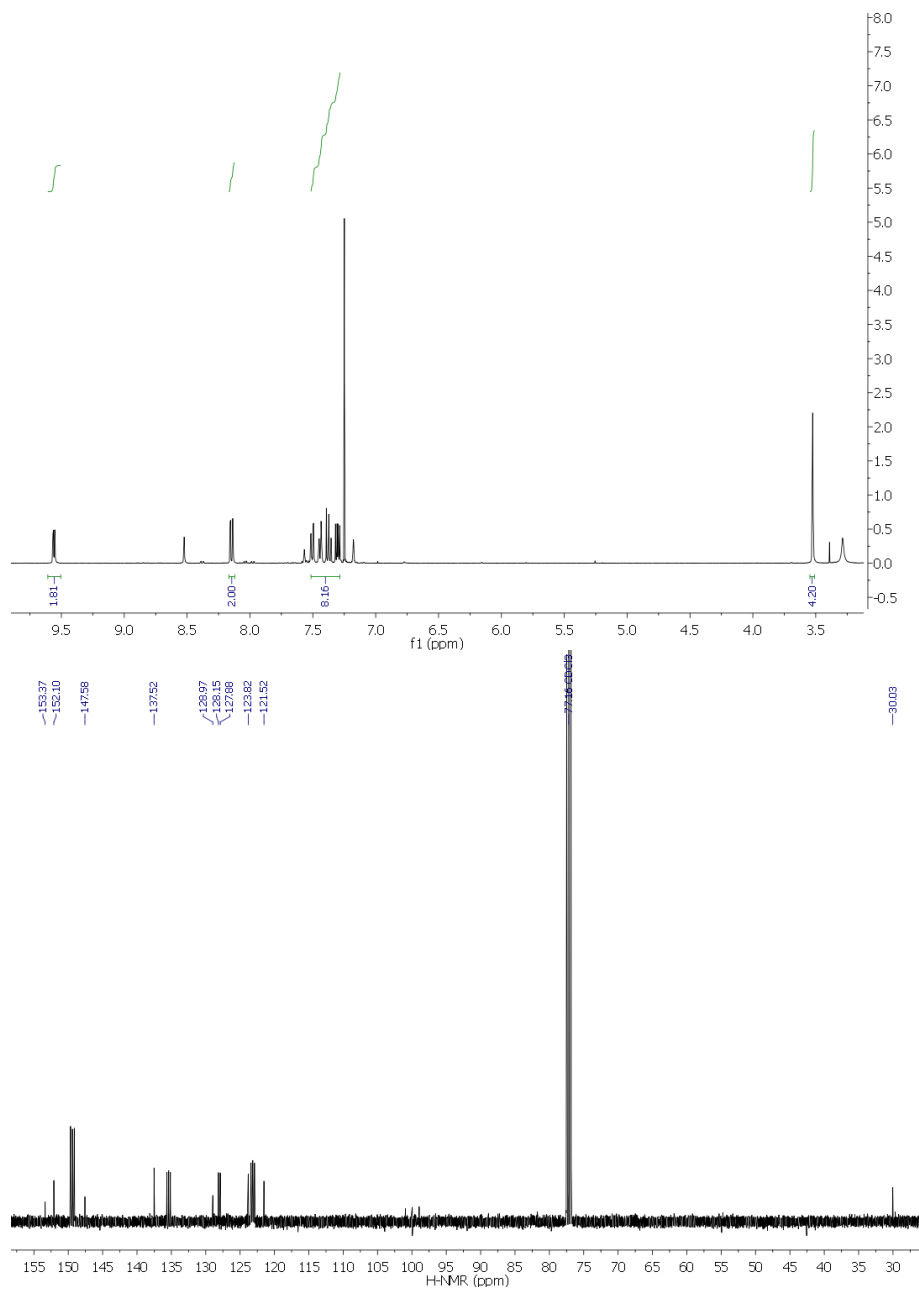
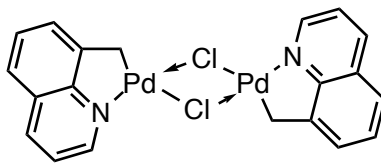




$[\text{Pd}_2(\mu\text{-OAc})_2(8\text{-Mequin})_2]$  (28)<sup>70</sup>

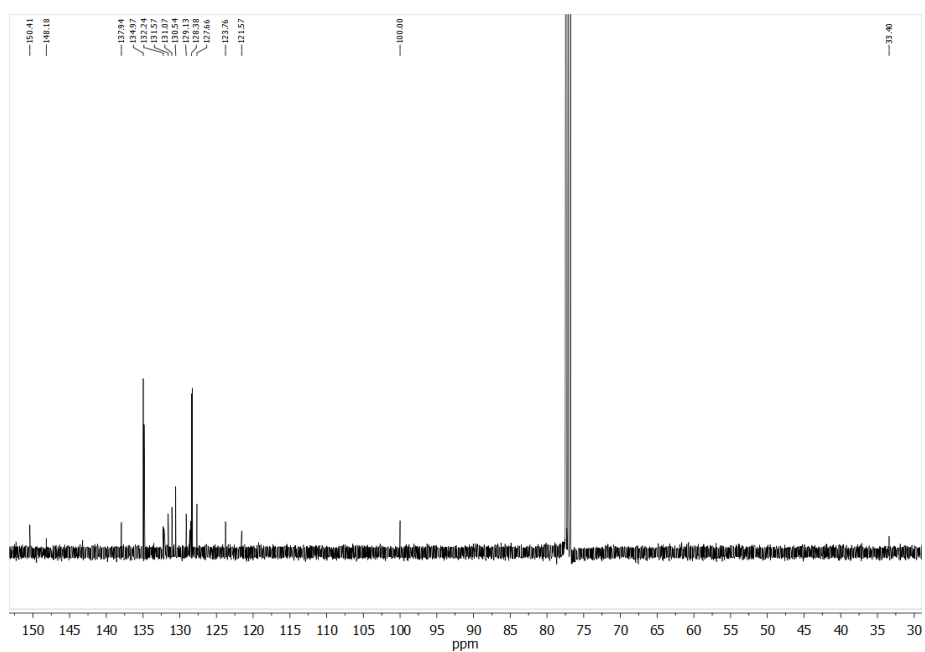
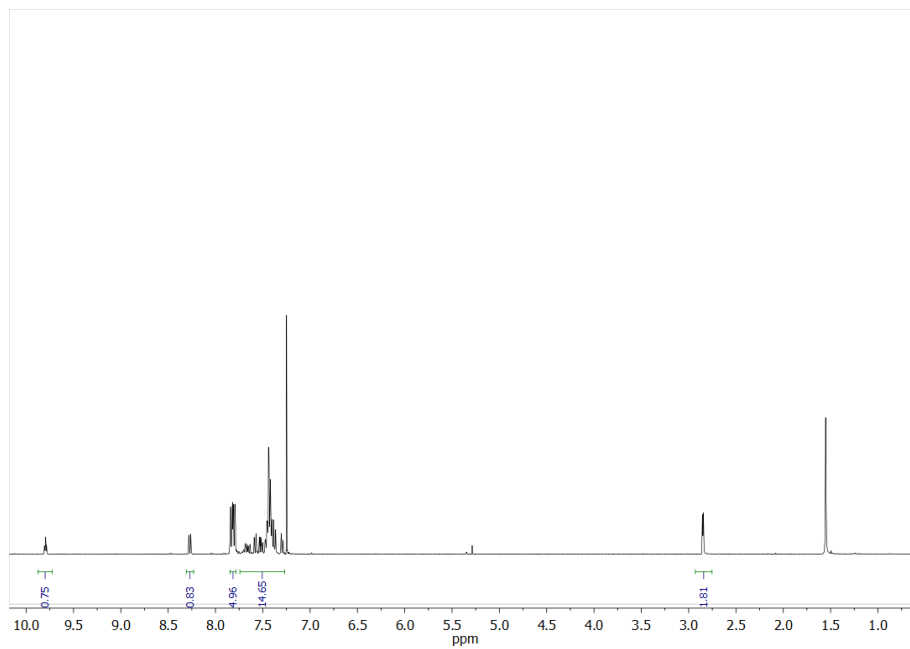
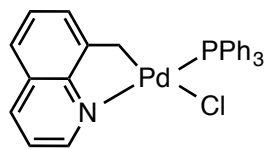


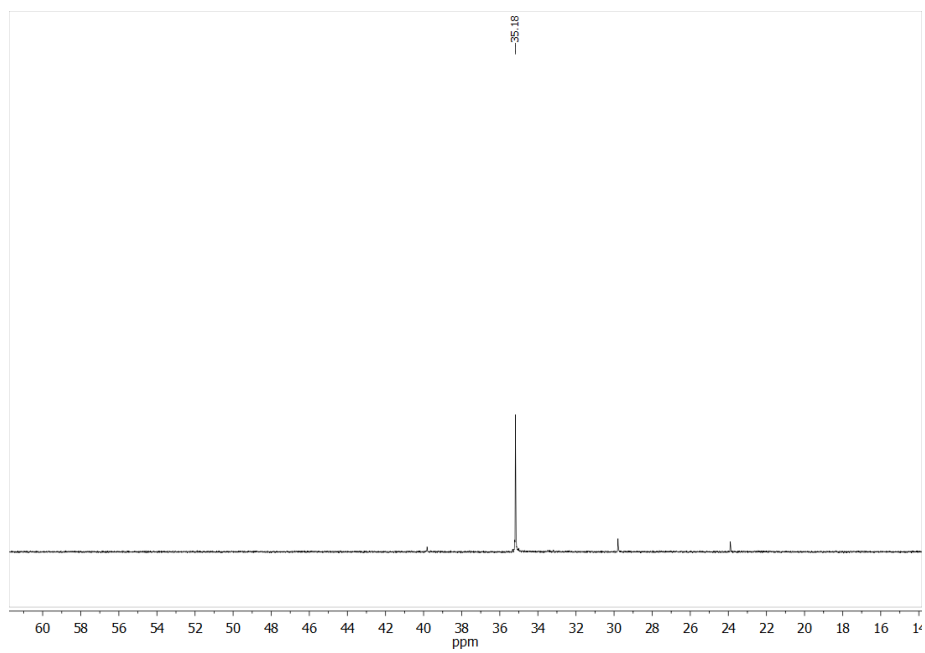
**[Pd<sub>2</sub>(μ-Cl)<sub>2</sub>(8-Mequin)<sub>2</sub>] (29)<sup>106</sup>**



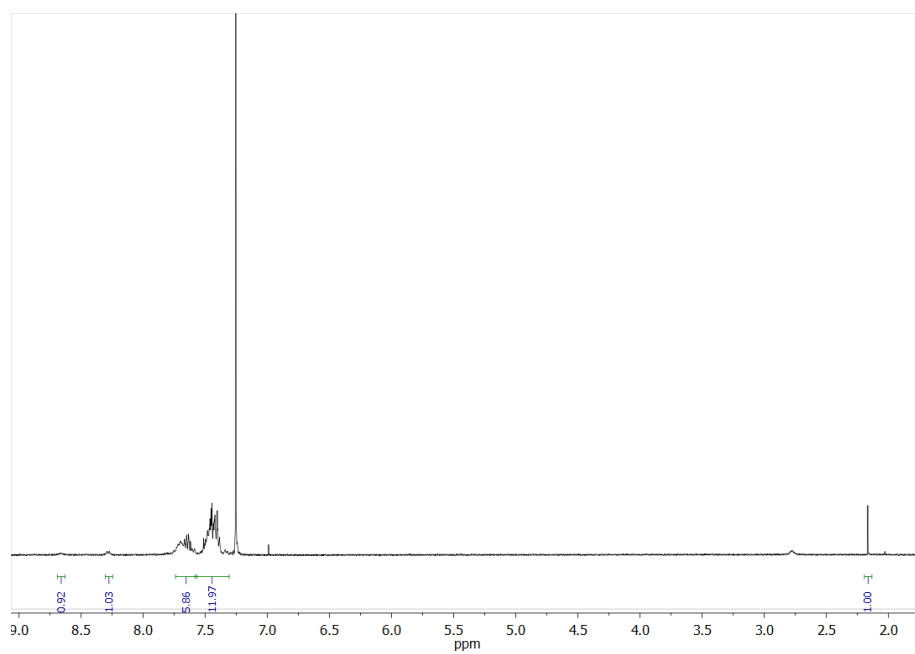
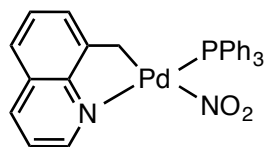


[PdCl(8-Mequin)(PPh<sub>3</sub>)] (30)

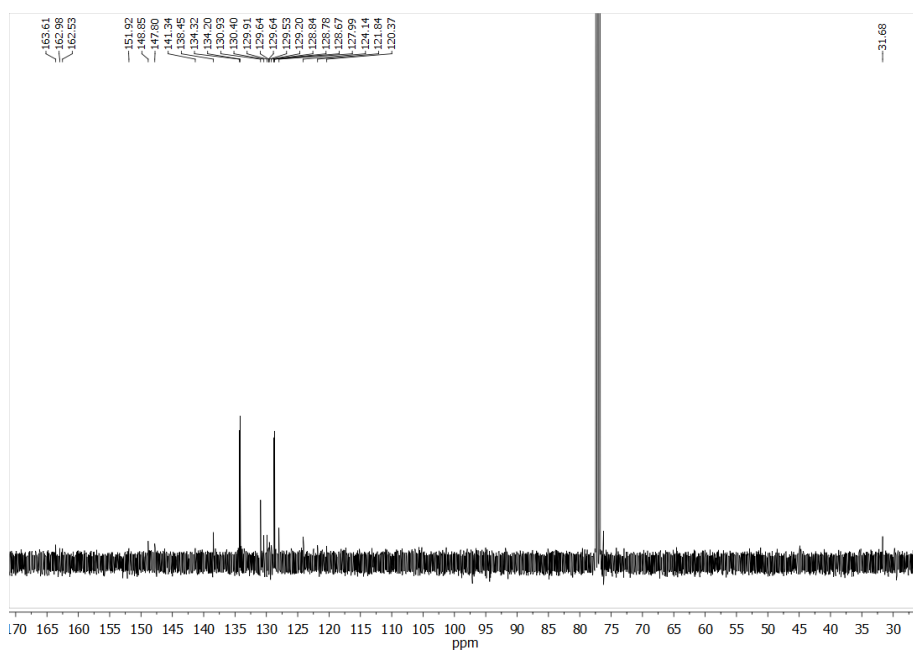
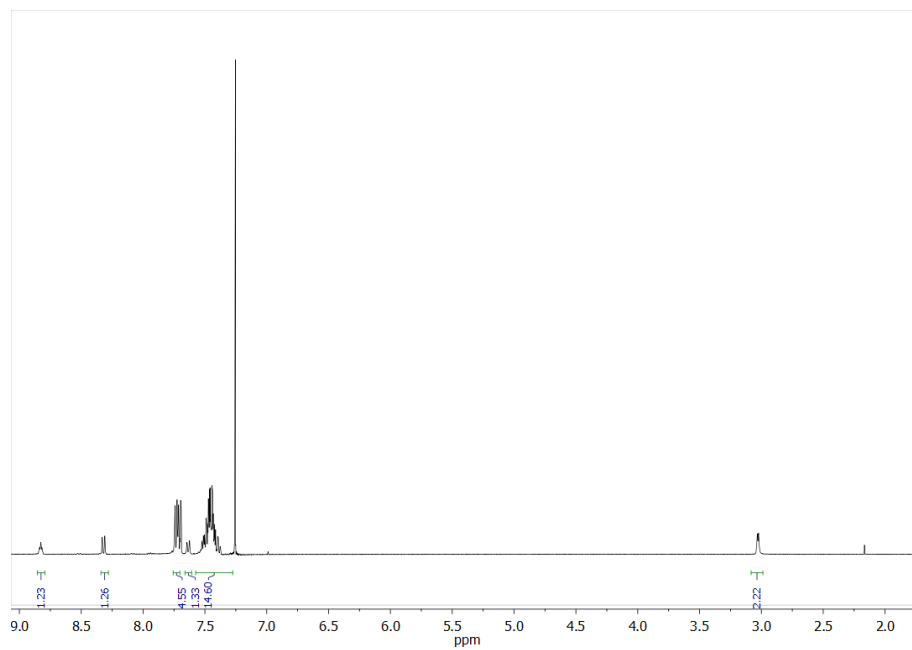
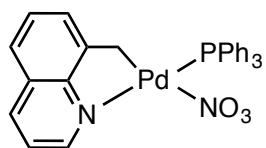




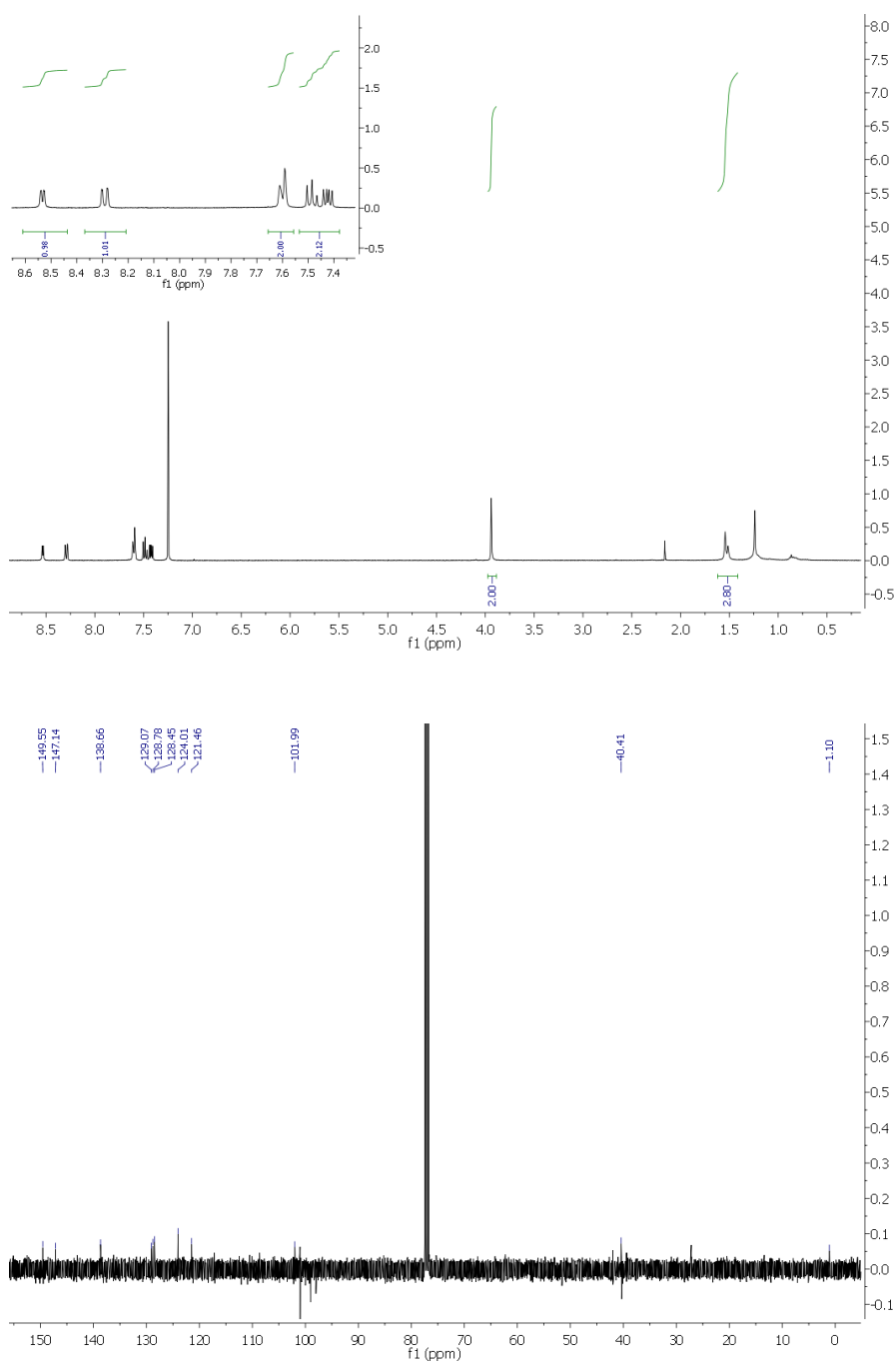
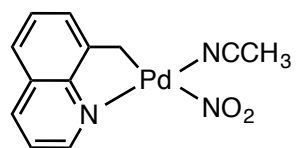
**[Pd(8-Mequin)(NO<sub>2</sub>)(PPh<sub>3</sub>)] (31)**



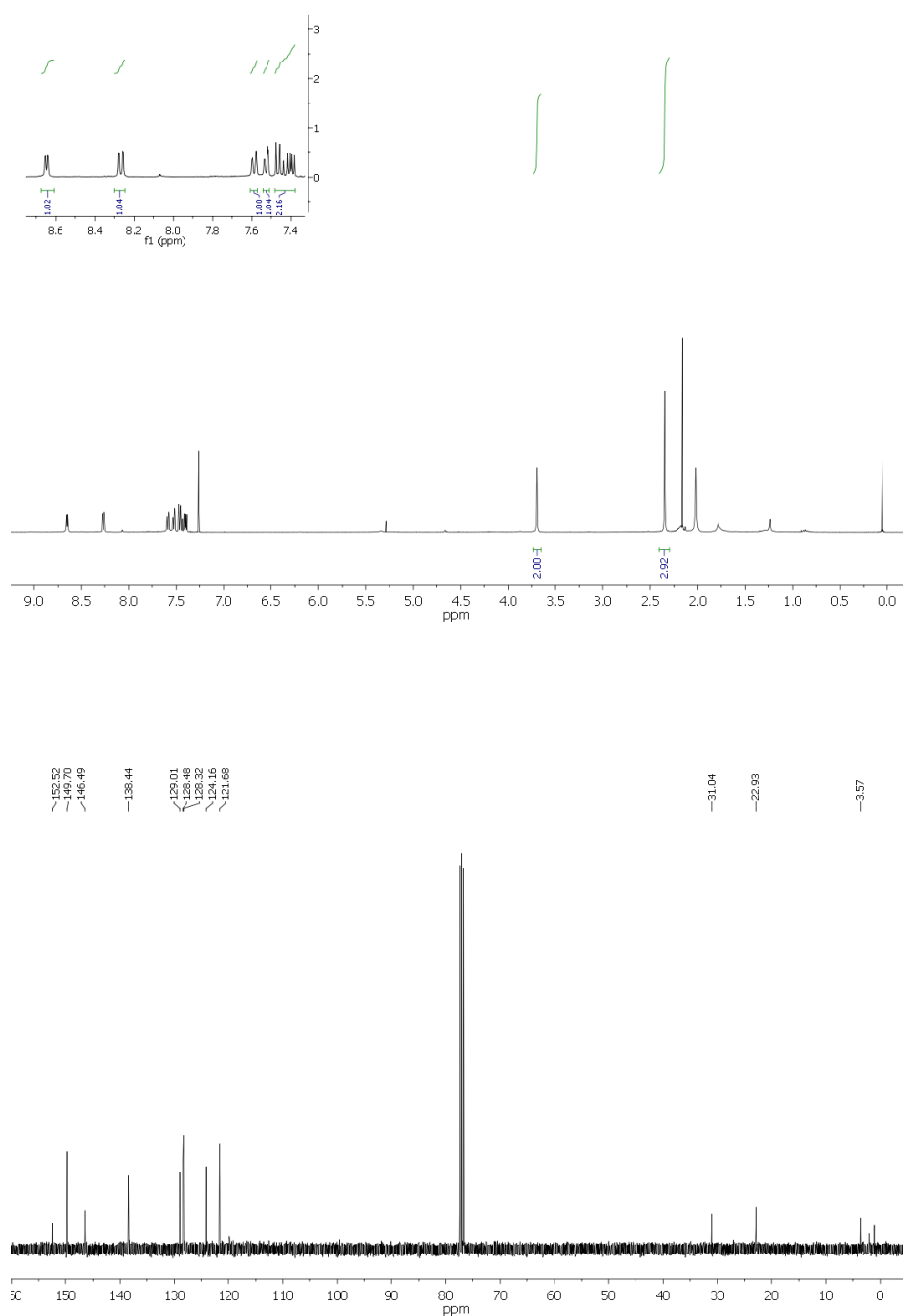
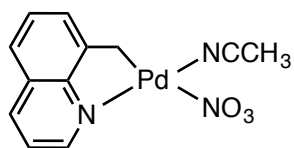
**[Pd(8-Mequin)(NO<sub>3</sub>)(PPh<sub>3</sub>)] (32)**



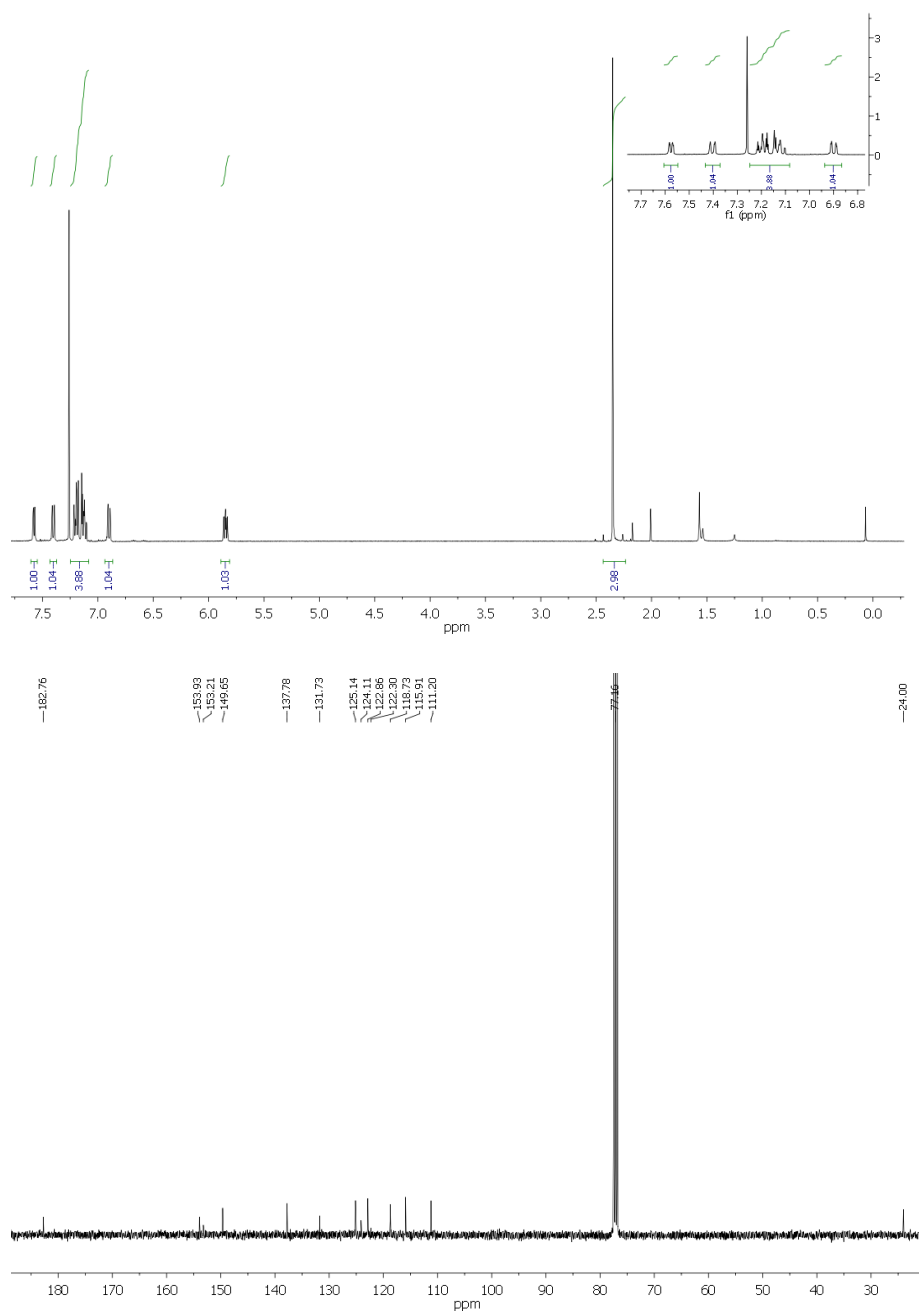
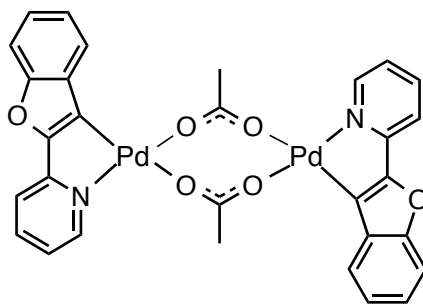
[Pd(8-Mequin)(NO<sub>2</sub>)(NCCH<sub>3</sub>)] (33)



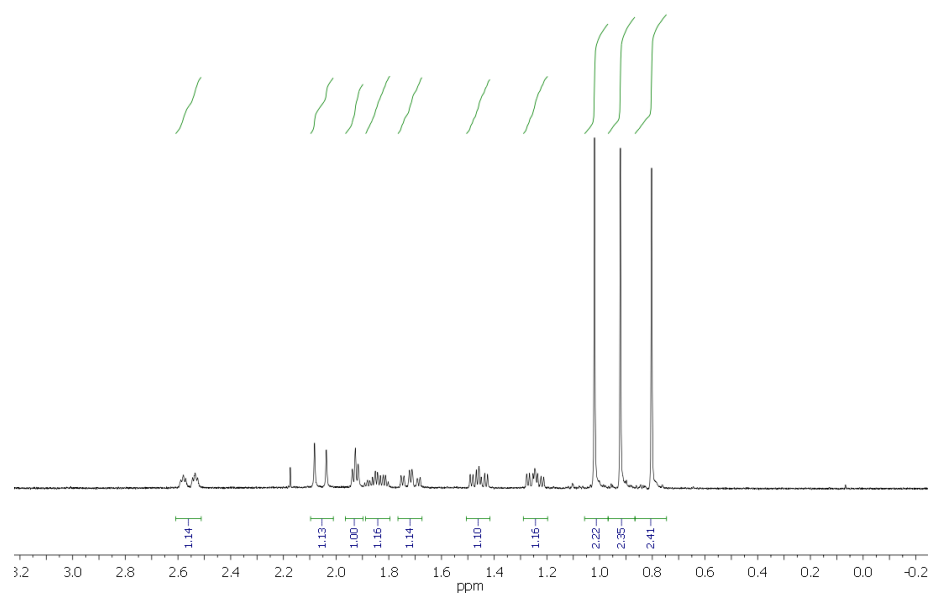
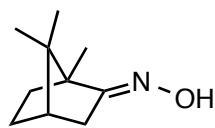
[Pd(8-Mequin)(NO<sub>3</sub>)(NCCH<sub>3</sub>)] (34)



**[Pd<sub>2</sub>(μ-OAc)<sub>2</sub>(Hpbf)<sub>2</sub>] (41)**<sup>43</sup>

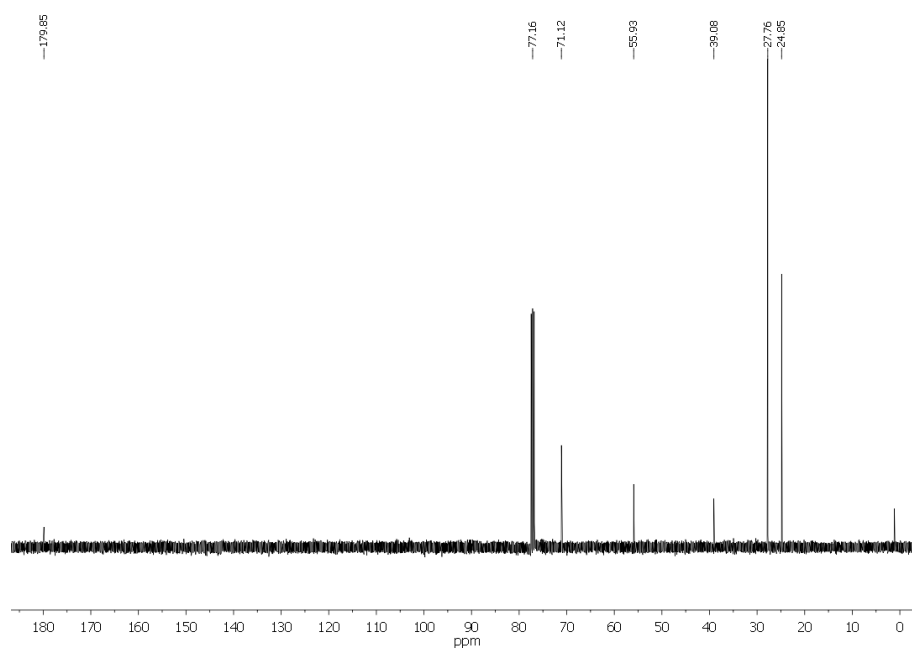
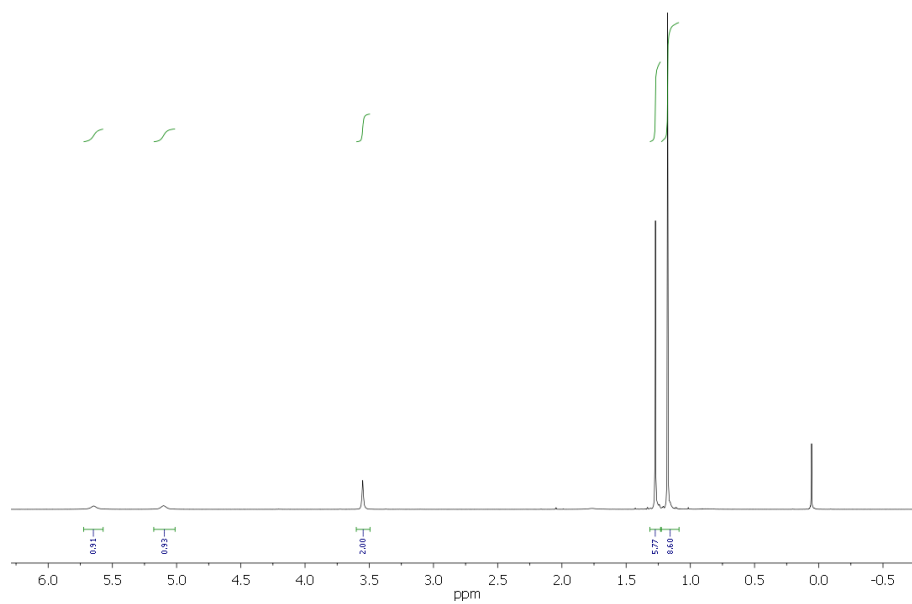
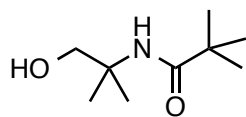


(±)Camphoroxime (2)<sup>84</sup>

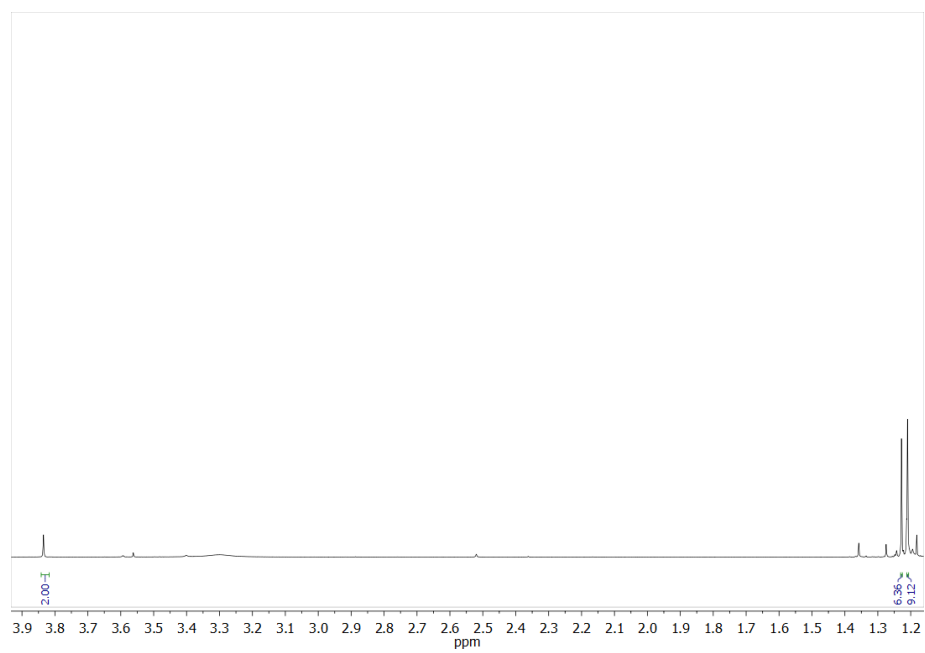
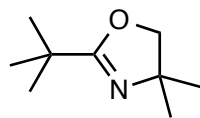




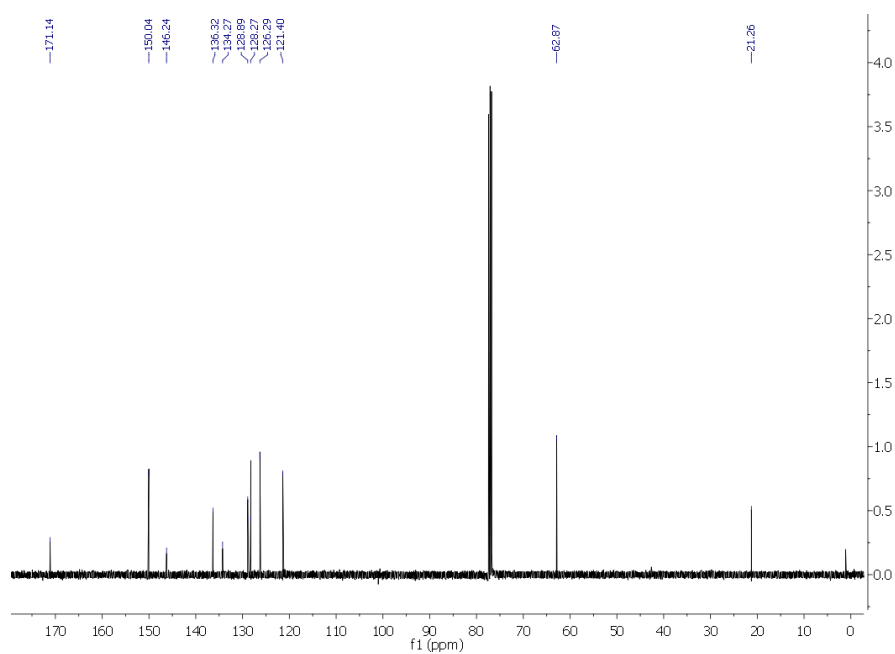
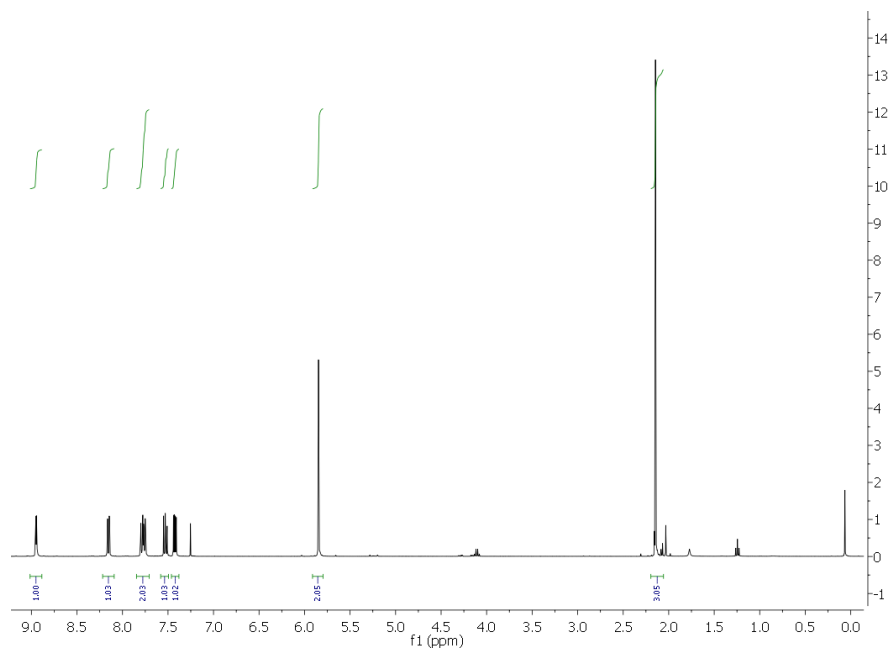
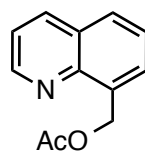
*N*-(2-hydroxy-1,1-dimethyl-ethyl)-2,2-dimethyl propionamide (48)<sup>86</sup>



**2-*tert*-butyl-4,4-dimethyl-2-oxazoline (49)**<sup>87</sup>



8-acetoxymethylquinoline (42)<sup>30</sup>



## Abbreviations

2-ppy	2-Phenylpyridine
8-mequin	8-Methylquinoline
Ac	Acetyl
acac	Acetylacetonate
AMLA	Ambiphilic metal–ligand activation
aq.	Aqueous
Ar	Aryl
ATR	Attenuated total reflectance
bipy	2,2'-Bipyridine
Boc	Di- <i>tert</i> -butyl carbonate
Bz	Benzyl
bza	<i>N</i> -Phenylbenzaldimine
cat.	Catalyst
CMD	Concerted metalation-deprotonation
COSY	Correlation spectroscopy
d (NMR)	Doublet
DBU	1,8-Diazabicyclo[5.4.0]undec-7-ene
DCE	Dichloroethane
DCM	Dichloromethane
DFT	Density functional theory
DMAP	<i>N,N</i> -Dimethylaminopyridine
DMBA	<i>N,N</i> -Dimethylbenzylamine
DMF	<i>N,N'</i> -Dimethylformamide
DMSO	Dimethylsulfoxide
ECP	Effective core potential
eq.	Equivalents
ESI	Electrospray ionisation
Et	Ethyl
FG	Functional group
FTIR	Fourier transform infrared spectroscopy
g	gram(s)
h	hour(s)
HMBC	Heteronuclear multiple-bond correlation
Hpbf	2-(2-pyridyl)benzo[ <i>b</i> ]furan

hpda	4-Hydroxypyridine-(2,6)-dicarboxylic acid
Hpyi	1-(2-pyridyl)indole
HRMS	High resolution mass spectrometry
HSQC	Heteronuclear single quantum coherence
Hz	Hertz
IES	Internal electrophilic substitution
<sup>i</sup> Pr	<i>iso</i> -Propyl
IR	Infrared
<i>J</i>	Spin-spin coupling
L	Ligand
LC	Liquid chromatography
LED	Light emitting diode
LIFDI	Liquid introduction field desorption ionisation
lit.	Literature value
m	Milli
M (concentration)	mol dm <sup>-3</sup>
m (nmr)	Multiplet
<i>m/z</i>	Mass-to-charge ratio
Me	Methyl
Mes	Mesityl
min	Minute(s)
mol	Mole(s)
MP	Melting Point
NMR	Nuclear Magnetic Resonance
OAc	Acetate
Ph	Phenyl
pip	Piperidine
ppm	Part(s) per million
Py	Pyridine
q (NMR)	Quartet
R	Substituent
r.t.	Room temperature
R <sub>f</sub>	Retention factor
s	Second(s)
t	Time
t (NMR)	Triplet
TBAI	Tetra- <i>n</i> -butylammonium iodide

<sup>t</sup> Bu	<i>tert</i> -Butyl
temp.	Temperature
THF	Tetrahydrofuran
TLC	Thin layer chromatography
TOF	Time-of-flight
Ts	4-Toluenesulfonyl
UV	Ultra-violet
Vis	Visible
X	(Pseudo)halide
δ	Chemical shift downfield from tetramethylsilane
μ	Micro

## References

- (1) Nicolaou, K. C.; Bulger, P. G.; Sarlah, D. *Angew. Chem. Int. Ed.* **2005**, *44*, 4442–4489.
- (2) Negishi, E. *Handbook of Organopalladium Chemistry for Organic Synthesis*; John Wiley & Sons, Inc., 2002.
- (3) Chen, X.; Engle, K. M.; Wang, D.-H.; Yu, J.-Q. *Angew. Chem. Int. Ed.* **2009**, *48*, 5094–5115.
- (4) Constable, D. J. C.; Dunn, P. J.; Hayler, J. D.; Humphrey, G. R.; Leazer, Jr., J. L.; Linderman, R. J.; Lorenz, K.; Manley, J.; Pearlman, B. A.; Wells, A.; Zaks, A.; Zhang, T. Y. *Green Chem.* **2007**, *9*, 411.
- (5) Daugulis, O.; Do, H.-Q.; Shabashov, D. *Acc. Chem. Res.* **2009**, *42*, 1074–1086.
- (6) Campos, K. R. *Chem. Soc. Rev.* **2007**, *36*, 1069–1084.
- (7) Alberico, D.; Scott, M. E.; Lautens, M. *Chem. Rev.* **2007**, *107*, 174–238.
- (8) Thansandote, P.; Lautens, M. *Chem.–Eur. J.* **2009**, *15*, 5874–5883.
- (9) Godula, K.; Sames, D. *Science* **2006**, *312*, 67–72.
- (10) Neufeldt, S. R.; Sanford, M. S. *Acc. Chem. Res.* **2012**, *45*, 936–46.
- (11) Giri, R.; Liang, J.; Lei, J.-G.; Li, J.-J.; Wang, D.-H.; Chen, X.; Naggar, I. C.; Guo, C.; Foxman, B. M.; Yu, J.-Q. *Angew. Chem. Int. Ed.* **2005**, *44*, 7420–7424.
- (12) Reddy, B. V. S.; Reddy, L. R.; Corey, E. J. *Org. Lett.* **2006**, *8*, 3391–3394.
- (13) Wang, G.; Yuan, T.; Wu, X. *J. Org. Chem.* **2008**, 4717–4720.
- (14) Seregin, I. V.; Gevorgyan, V. *Chem. Soc. Rev.* **2007**, *36*, 1173–1193.
- (15) Kalyani, D.; Dick, A. R.; Anani, W. Q.; Sanford, M. S. *Tetrahedron* **2006**, *62*, 11483–11498.
- (16) Chen, X.; Hao, X.; Goodhue, C. E.; Yu, J. *J. Am. Chem. Soc.* **2006**, *128*, 6790–6791.
- (17) Desai, L. V.; Stowers, K. J.; Sanford, M. S. *J. Am. Chem. Soc.* **2008**, *130*, 13285–13293.
- (18) Hickman, A. J.; Sanford, M. S. *ACS Catal.* **2011**, 170–174.
- (19) Zhang, Y.-H.; Shi, B.-F.; Yu, J.-Q. *J. Am. Chem. Soc.* **2009**, *131*, 5072–5074.
- (20) Li, H.; Li, B.-J.; Shi, Z.-J. *Catal. Sci. Tech.* **2011**, *1*, 191–206.
- (21) Dick, A. R.; Hull, K. L.; Sanford, M. S. *J. Am. Chem. Soc.* **2004**, *126*, 2300–2301.

- (22) Yoneyama, T.; Crabtree, R. H. *J. Mol. Catal. A.: Chem.* **1996**, *108*, 35–40.
- (23) Desai, L. V.; Hull, K. L.; Sanford, M. S. *J. Am. Chem. Soc.* **2004**, *126*, 9542–9543.
- (24) Wang, D.-H.; Hao, X.-S.; Wu, D.-F.; Yu, J.-Q. *Org. Lett.* **2006**, *8*, 3387–3390.
- (25) Desai, L. V.; Malik, H. A.; Sanford, M. S. *Org. Lett.* **2006**, *8*, 1141–1144.
- (26) Paavola, S.; Zetterberg, K.; Privalov, T.; Csöreg, I.; Moberg, C. *Adv. Synth. Catal.* **2004**, *346*, 237–244.
- (27) Hallman, K.; Moberg, C. *Adv. Synth. Catal.* **2001**, *343*, 260–263.
- (28) Zhang, J.; Khaskin, E.; Anderson, N. P.; Zavalij, P. Y.; Vedernikov, A. N. *Chem. Commun.* **2008**, 3625–3627.
- (29) Jiang, H.; Chen, H.; Wang, A.; Liu, X. *Chem. Commun.* **2010**, *46*, 7259–7261.
- (30) Stowers, K. J.; Kubota, A.; Sanford, M. S. *Chem. Sci.* **2012**, *3*, 3192.
- (31) Umsetzungen, K. *Angew. Chem.* **1956**, *71*, 176–182
- (32) Wickens, Z. K.; Morandi, B.; Grubbs, R. H. *Angew. Chem. Int. Ed.* **2013**, *52*, 11257–11260.
- (33) Liu, Y.; Murata, K.; Inaba, M. *J. Mol. Catal. A: Chem.* **2006**, *256*, 247–255.
- (34) Yuan, J.; Wang, L.; Wang, Y. *Ind. Eng. Chem. Res.* **2011**, *50*, 6513–6516.
- (35) An, Z.; Pan, X.; Liu, X.; Han, X.; Bao, X. *J. Am. Chem. Soc.* **2006**, *128*, 16028–16029.
- (36) Campora, J.; Palma, P.; Rı, D.; Carmona, E.; Graiff, C.; Tiripicchio, A. *Organometallics* **2003**, *22*, 3345–3347.
- (37) Janzen, E. G.; Wilcox, A. L.; Manoharan, V. *J. Org. Chem.* **1993**, *58*, 3597–3599.
- (38) Backvall, J.-E.; Heumann, A. *J. Am. Chem. Soc.* **1986**, *108*, 7107–7108.
- (39) Mares, F.; Diamond, S. E.; Regina, F. J.; Solar, J. P. *J. Am. Chem. Soc.* **1985**, *107*, 3545–3552.
- (40) Bajwa, S. E.; Storr, T. E.; Hatcher, L. E.; Williams, T. J.; Baumann, C. G.; Whitwood, A. C.; Allan, D. R.; Teat, S. J.; Raithby, P. R.; Fairlamb, I. J. S. *Chem. Sci.* **2012**, *3*, 1656.
- (41) Tao, B.; Boykin, D. W. *J. Org. Chem.* **2004**, *69*, 4330–4335.
- (42) Bakhmutov, V. I.; Berry, J. F.; Cotton, F. A.; Murillo, C. A.; Box, P. O.; Station, C. *Dalton Trans.* **2005**, 1989–1992.
- (43) Nonoyama, M.; Nakajima, K. *Polyhedron* **1999**, *18*, 533–543.



- (44) Susharina, T. L.; Kerzhentsev, M. A.; Pod'yacheva, O. Y.; Smagilov, Z. R. I. *React. Kinet. Catal. Lett.* **1986**, *31*, 27–33.
- (45) Jazzar, R.; Hitce, J.; Renaudat, A.; Sofack-Kreutzer, J.; Baudoin, O. *Chem.–Eur. J.* **2010**, *16*, 2654–2672.
- (46) Fagnou, K.; Lapointe, D. *Chem. Lett.* **2010**, *39*, 1118–1126.
- (47) Oxgaard, J.; Tenn, W. J.; Nielsen, R. J.; Periana, R. A.; Goddard, W. A. *Organometallics* **2007**, *26*, 1565–1567.
- (48) Siegbahn, P. E. M.; Blomberg, M. R. A. *Dalton Trans.* **2009**, 5832–5840.
- (49) Naylor, M. A.; Corwin, A. H. *J. Am. Chem. Soc.* **1947**, *69*, 1004.
- (50) McGary Jr., C. W.; Brown, H. C. *J. Am. Chem. Soc.* **1955**, *77*, 2300–2305.
- (51) Ryabov, A. D.; Sakodinskaya, I. K.; Yatsimirsky, A. K. *J. Chem. Soc., Dalton Trans.* **1985**, 2629–2638.
- (52) Kurzeev, S. A.; Kazankov, G. M.; Ryabov, A. D. *Inorg. Chim. Acta* **2002**, *340*, 192–196.
- (53) Davies, D. L.; Donald, S. M. A.; Macgregor, S. A. *J. Am. Chem. Soc.* **2005**, *127*, 13754–13755.
- (54) Guihaume, J.; Clot, E.; Eisenstein, O.; Perutz, R. N. *Dalton Trans.* **2010**, *39*, 10510–10519.
- (55) Rousseaux, S.; Gorelsky, S. I.; Chung, B. K. W.; Fagnou, K. *J. Am. Chem. Soc.* **2010**, *132*, 10692–10705.
- (56) Mann, G.; Shelby, Q.; Roy, A. H.; Hartwig, J. F. *Organometallics* **2003**, *22*, 2775–2789.
- (57) Widenhofer, R. A.; Zhong, H. A.; Buchwald, S. L. *J. Am. Chem. Soc.* **1997**, *119*, 6787–6795.
- (58) Widenhofer, R. A.; Buchwald, S. L. *J. Am. Chem. Soc.* **1998**, *120*, 6504–6511.
- (59) Sehnal, P.; Taylor, R. J. K.; Fairlamb, I. J. S. *Chem. Rev.* **2010**, *110*, 824–889.
- (60) Xu, L.-M.; Li, B.-J.; Yang, Z.; Shi, Z.-J. *Chem. Soc. Rev.* **2010**, *39*, 712–733.
- (61) Williams, B. S.; Goldberg, K. I. *J. Am. Chem. Soc.* **2001**, *123*, 2576–2587.
- (62) Canty, A. J. *Acc. Chem. Res.* **1992**, *25*, 83–90.
- (63) Canty, A. J.; Denney, M. C.; Skelton, B. W.; White, A. H. *Organometallics* **2004**, *23*, 1122–1131.
- (64) Byers, P. K.; Canty, A. J.; Crespo, M.; Puddephatt, R. J.; Scott, J. D. *Organometallics* **1988**, *7*, 1363–1367.

- (65) Fu, Y.; Li, Z.; Liang, S.; Guo, Q.; Liu, L. *Organometallics*. **2008**, *27*, 3736–3742.
- (66) Hull, K. L.; Lanni, E. L.; Sanford, M. S. *J. Am. Chem. Soc.* **2006**, *128*, 14047–14049.
- (67) Powers, D. C.; Ritter, T. *Nature Chem.* **2009**, *1*, 302–309.
- (68) Powers, D. C.; Geibel, M. a L.; Klein, J. E. M. N.; Ritter, T. *J. Am. Chem. Soc.* **2009**, *131*, 17050–17051.
- (69) Racowski, J. M.; Dick, A. R.; Sanford, M. S. *J. Am. Chem. Soc.* **2009**, *131*, 10974–10983.
- (70) Hiraki, K.; Fuchita, Y.; Takechi, K. *Inorg. Chem.* **1981**, 4316–4320.
- (71) Selbin, J.; Gutierrez, M. A.; Newkome, G. R. *J. Organomet. Chem.* **1980**, *202*, 341–350.
- (72) Atla, S. B.; Kelkar, A. a.; Puranik, V. G.; Bensch, W.; Chaudhari, R. V. *J. Organomet. Chem.* **2009**, *694*, 683–690.
- (73) Kleinpeter, E.; Koch, A.; Sahoo, H. S.; Chand, D. K. *Tetrahedron* **2008**, *64*, 5044–5050.
- (74) Warren, M. R.; Brayshaw, S. K.; Johnson, A. L.; Schiffers, S.; Raithby, P. R.; Easun, T. L.; George, M. W.; Warren, J. E.; Teat, S. J. *Angew. Chem. Int. Ed.* **2009**, *48*, 5711–5714.
- (75) Hatcher, L. E.; Warren, M. R.; Allan, D. R.; Brayshaw, S. K.; Johnson, A. L.; Fuertes, S.; Schiffers, S.; Stevenson, A. J.; Teat, S. J.; Woodall, C. H.; Raithby, P. R. *Angew. Chem. Int. Ed.* **2011**, *50*, 8371–8374.
- (76) Stowers, K. J.; Kubota, A.; Sanford, M. S. *Chem. Sci.* **2012**, 1–33.
- (77) Bayler, A.; Canty, A. J.; Edwards, P. G.; Skelton, B. W.; White, A. H. *J. Chem. Soc., Dalton Trans.* **2000**, 3325–3330.
- (78) Zhang, W.; Lou, S.; Liu, Y.; Xu, Z. *J. Org. Chem.* **2013**, *78*, 5932–5948.
- (79) Watson, D. a; Su, M.; Teverovskiy, G.; Zhang, Y.; García-Fortanet, J.; Kinzel, T.; Buchwald, S. L. *Science* **2009**, *325*, 1661–1664.
- (80) Ortega, N.; Urban, S.; Beiring, B.; Glorius, F. *Angew. Chem. Int. Ed.* **2012**, *51*, 1710–1713.
- (81) Fairlamb, I. J. S.; Kapdi, A. R.; Lee, A. F.; Sánchez, G.; López, G.; Serrano, J. L.; García, L.; Pérez, J.; Pérez, E. *Dalton Trans.* **2004**, 3970 – 3981.
- (82) De Vries, A. H. M.; Mulders, J. M. C. a; Mommers, J. H. M.; Henderickx, H. J. W.; de Vries, J. G. *Org. Lett.* **2003**, *5*, 3285–3288.
- (83) Booth, S. E.; Jenkins, P. R.; Swain, C. J.; Sweeney, J. B. *J. Chem. Soc., Perkin Trans I* **1994**, 3499–3508.

- (84) Gamble, D. L.; Hems, W. P.; Ridge, B. *J. Chem. Soc., Perkin Trans 1* **2001**, 248–260.
- (85) Soltani Rad, M.; Khalafi-Nezhad, A.; Karimitabar, F.; Behrouz, S. *Synthesis* **2010**, 2010, 1724–1730.
- (86) Zhang, X.-M.; Zhang, H.-L.; Lin, W.-Q.; Gong, L.-Z.; Mi, A.-Q.; Cui, X.; Jiang, Y.-Z.; Yu, K.-B. *J. Org. Chem.* **2003**, 68, 4322–4329.
- (87) Stepanova, V. A.; Kukowski, J. E.; Smoliakova, I. P. *Inorg. Chem. Commun.* **2010**, 13, 653–655.
- (88) Serrano, J. L.; García, L.; Pérez, J.; Pérez, E.; García, J.; Sánchez, G.; Sehnal, P.; De Ornellas, S.; Williams, T. J.; Fairlamb, I. J. S. *Organometallics* **2011**, 30, 5095–5109.
- (89) Xu, J.; Zhuang, R.; Bao, L.; Tang, G.; Zhao, Y. *Green Chem.* **2012**, 14, 2384.
- (90) Culkin, D. A.; Hartwig, J. F. *Organometallics* **2004**, 23, 3398–3416.
- (91) Marquard, S. L.; Rosenfeld, D. C.; Hartwig, J. F. *Angew. Chem. Int. Ed.* **2010**, 49, 793–796.
- (92) Hartwig, J. F. *Acc. Chem. Res.* **1998**, 31, 852–860.
- (93) Bryndza, H. E.; Fong, L. K.; Paciello, R. A.; Tam, W.; Bercaw, J. E. *J. Am. Chem. Soc.* **1987**, 109, 1444–1456.
- (94) Macgregor, S. A.; Neave, G. W.; Smith, C. *Faraday Discuss.* **2003**, 124, 111–127.
- (95) Belciug, M.-P.; Ananthanarayanan, V. S. *J. Med. Chem.* **1994**, 37, 4392–4399.
- (96) Ono, N. *The Nitro Group in Organic Synthesis*; John Wiley & Sons, Inc., 2001.
- (97) Saito, S.; Koizumi, Y. *Tetrahedron Lett.* **2005**, 46, 4715–4717.
- (98) Fors, B. P.; Buchwald, S. L. *J. Am. Chem. Soc.* **2009**, 131, 12898–12899.
- (99) Racowski, J. M.; Dick, A. R.; Sanford, M. S. *J. Am. Chem. Soc.* **2009**, 131, 10974–10983.
- (100) Dick, A. R.; Kampf, J. W.; Sanford, M. S. *J. Am. Chem. Soc.* **2005**, 127, 12790–12791.
- (101) Dransfield, T. a.; Nazir, R.; Perutz, R. N.; Whitwood, A. C. *J. Fluorine Chem.* **2010**, 131, 1213–1217.
- (102) Williams, T. J., “Understanding C–H Bond Functionalisation at Heterocycles and Biomolecules: A Synthetic and Mechanistic Study”, *PhD Thesis*, **2013** (York).
- (103) Ward, J. S.; Lynam, J. M.; Moir, J. W. B.; Sanin, D. E.; Mountford, A. P.; Fairlamb, I. J. S. *Dalton Trans.* **2012**, 41, 10514–10517.
- (104) Schenker, K.; Bernasconi, R. *Chem. Abstr.* **1974**, 82, 43186.

- (105) Edwards, G. L.; Black, D. S. C.; Deacon, G. B.; Wakelin, L. P. G. *Can. J. Chem.* **2005**, *83*, 980–989.
- (106) Deeming, A. J.; Rothwell, I. P. *J. Organomet. Chem.* **1981**, *205*, 117–131.
- (107) Lamb, J. R.; Stepanova, V. A.; Smoliakova, I. P. *Polyhedron* **2013**, *53*, 202–207.
- (108) Fujii, H.; Nagamatsu, K.; Abe, N.; Gunji, T.; Murafuji, T. *Heterocycles* **2010**, *81*, 2625–2633.
- (109) (a) Csaszar, P.; Pulay, P., *J. Mol. Struct.* **1984**, *114*, 31–34.  
(b) Ahlrichs, R.; Bar, M.; Haser, M.; Horn, H.; Kolmel, C., *Chem. Phys. Lett.* **1989**, *162*, 165–169.  
(c) Eichkorn, K.; Treutler, O.; Ohm, H.; Haser, M.; Ahlrichs, R., *Chem. Phys. Lett.* **1995**, *240*, 283–289.  
(d) Treutler, O.; Ahlrichs, R., *J. Chem. Phys.* **1995**, *102*, 346–354.  
(e) Eichkorn, K.; Weigend, F.; Treutler, O.; Ahlrichs, R., *Theor. Chem. Acc.* **1997**, *97*, 119–124.  
(f) Arnim, M. v.; Ahlrichs, R., *J. Chem. Phys.* **1999**, *111*, 9183–9190.  
(g) Deglmann, P.; Furche, F., *J. Chem. Phys.* **2002**, *117*, 9535–9538.  
(h) Deglmann, P.; Furche, F.; Ahlrichs, R., *Chem. Phys. Lett.* **2002**, *362*, 511–518.  
(i) Deglmann, P.; May, K.; Furche, F.; Ahlrichs, R., *Chem. Phys. Lett.* **2004**, *384*, 103–107.